PATH PLANNING, ESTIMATION, AND CONTROL IN THE PRESENCE OF INTERMITTENT STATE FEEDBACK

By

SAGE CHRISTIAN EDWARDS

A DISSERTATION PRESENTED TO THE GRADUATE SCHOOL
OF THE UNIVERSITY OF FLORIDA IN PARTIAL FULFILLMENT
OF THE REQUIREMENTS FOR THE DEGREE OF
DOCTOR OF PHILOSOPHY

UNIVERSITY OF FLORIDA

2024

To the triune God, the maker of heaven and earth, of all things visible and invisible; who is the paradigm and locus of all truth.

ACKNOWLEDGMENTS

Firstly, I would like to give thanks to God, who without, none of this would be possible or meaningful. May all of the glory be accredited to him. I would also like to thank my adviser, Dr. Warren E. Dixon for his constant support, and invaluable guidance throughout my time as his student. Next, I would like to thank my co-adviser, Dr. Dan P. Guarlnik, who instilled in me the importance of mathematical rigor and the constant need to sufficiently challenge any claim I make. I would also like to thank my committee members: Dr. John M. Shea, Dr. Amor A. Menezes, and Dr. Jane J. Shin for their oversight and instruction throughout the Ph.D. program. Additionally, I would like to thank everyone that I interacted with through the SMART Scholarship program, specifically those at my sponsoring facility. A special acknowledgment goes out to my parents, Richard Edwards and Monica Edwards, my brother, Hayden Edwards, and my beloved Claire for their constant support and encouragement. Lastly, I would like to thank the rest of my family, my friends, and my lab mates for their constant support and memories that I have made during this time.

“It is God who is the ultimate reason of things, and the Knowledge of God is no less the beginning of science than his essence and will are the beginning of beings”
– Gottfried Leibniz

TABLE OF CONTENTS

page

LIST OF FIGURES

LIST OF ABBREVIATIONS

A2/AD	anti-access and area-denial environments
DNN	deep neural network
DoD	Department of Defense
ETE	estimated tracking error
FoV	field of view
HBC	hybrid basic conditions
HDI	hybrid differential inclusion
IBC	Inscribed Ball Criterion
JNWC	Joint Navigation Warfare Center
Lb-DNN	Lyapunov-based deep neural network
LEO	low Earth orbit
MAS	multi agent system
MAUR	maximum allowed uncertainty radius
MIMO	multi-input and multi-output
NAVWAR	Navigational Warfare
PNT	pointing, navigation, and timing
ReLU	rectified linear unit
RHS	right-hand-side
SEE	state estimation error
SLAM	simultaneous localization and mapping
tanh	hyperbolic tangent activation function
TTE	true tracking error

Abstract of Dissertation Presented to the Graduate School
of the University of Florida in Partial Fulfillment of the
Requirements for the Degree of Doctor of Philosophy

PATH PLANNING, ESTIMATION, AND CONTROL IN THE PRESENCE OF INTERMITTENT STATE FEEDBACK

By

Sage Christian Edwards

May 2024

Chair: Warren E. Dixon
Cochair: Dan P. Guarlnik
Major: Mechanical Engineering

Mobile agents are often forced to follow paths in environments where state feedback may not always be available, such as in GPS denied environments, and more broadly, anti-access and area-denial environments. This has given rise to a class of Relay-Explorer problems, where an agent is tasked with switching between multiple operation modes, primarily depending on the availability of state feedback.

Past work on these problems established a framework for developing dwell-time conditions for stable tracking using these methods. However, existing work only applies to a limited class of reference paths and feedback region geometries. Chapter 2 advances a topologically inspired method for guaranteeing re-acquisition of feedback for nearly arbitrary geometries in arbitrary dimensions, all while relaxing the dwell-time conditions and retaining the uniformly ultimately bounded stability result from preceding work. Numerical experiments in the plane demonstrate an increase of hundreds of percentage points—even for fairly generic geometries—in the tracking error budget the agent could afford, using the proposed method, without sacrificing stability.

Chapter 3 extends the study of relay-explorer problems to multi-agent systems so that the idea of cooperative localization can be used to enhance the path tracking performance of each agent and to extend the duration the ensemble of agents can spend operating without state feedback. To accomplish these goals, a new cooperative

localization method is developed that uses the agents' dynamics and the distance measurements between them. Hybrid system theory is used to model and analyze the proposed localization method and path planning strategy.

Chapter 4 extends the the topological methods from Chapter 2 to time varying feedback regions. Specifically, this work introduces a novel framework for image-based tracking systems, addressing scenarios where the tracking agent needs to discontinue tracking the target agent either due to the need to fulfill other tasks or the target agent becoming obscured. The proposed approach deploys a Lyapunov-based Deep Neural Network (Lb-DNN) to learn the dynamics of the target agent when visible, and to predict its future trajectory when not visible. To ensure that target tracking resumes, the topologically method from Chapter 2 is extended, using the predicted trajectory of the target agent. This method informs the tracker agent about the duration it can suspend tracking the target agent and specifies a pose for the camera for guaranteeing that tracking resumes at some later time. Simulation results are provided to demonstrate the performance of the proposed framework.

CHAPTER 1
INTRODUCTION

1.1 Motivation

State feedback is a critical component in designing path-planning methods used for guidance, navigation, and control of autonomous vehicles. Factors such as task definition, operating environment, sensor modality, and adversarial effects may result in intermittent state feedback, inhibiting a system's ability to achieve its task. More specifically mobile agents are often forced to follow paths in environments where state feedback may not always be available, such as in GPS denied environments (Figure 1-1), and more broadly, anti-access and area-denial environments (A2/AD).

The need to overcome A2/AD environments to obtain state information for the assurance of mission success has been a critical point of discussion and research in military, space, exploration, and commercial endeavors. In response to this growing need in military operations, the Joint Navigation Warfare Center (JNWC) was activated on October 1st, 2004 to integrate Navigational Warfare (NAVWAR) throughout the Department of Defense (DoD), with the mission to enable positioning, navigation, and timing (PNT) superiority to the DoD [3]. One of the main approaches to the defense against PNT attacks in NAVWAR is to actively neutralize these attacks or reestablish information flow by creating new lanes of uncorrupted information [4]– [6]. This reliance on information is emphasized by the Chief of Naval Operations, Admiral Mike Gilday: *"Information has become the cornerstone for how the Navy functions in the 21st century. Nothing the Navy does, or will do, can exist without it"*. [7]

In space-based missions, the utilization of GPS is limited, especially when the operations extend beyond low Earth orbit (LEO) into deeper space where GPS is essentially unusable with the current infrastructure [8]. To overcome these limitations, spacecraft use precisely timed radio signals between the spacecraft and antenna stations on Earth to determine where the spacecraft is located [9]. However, due to

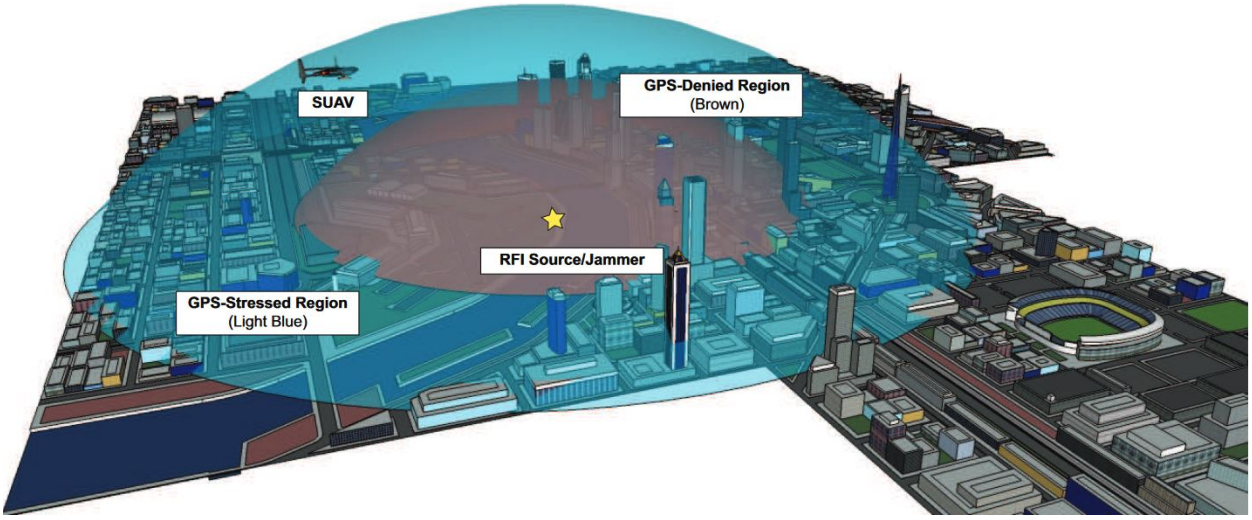

Figure 1-1. Example of a GPS denied environment due to a single jammer [2].

the substantial time delay in receiving this state information, the spacecraft is forced to make decisions intermittently since state information coming from the antenna station is intermittent. Further, this method also constrains the spacecraft's trajectory due to the need for a line of sight between the antenna stations on Earth and the spacecraft when large celestial-objects are in the way. Even though there are significant problems with navigation in military and space missions, they are not limited to just these domains and can be found throughout many commercial systems. For example, GPS requires line-of-sight between the user and the satellites; however, in environments where obstructions prevent line of sight (e.g., tall buildings, walls, foliage, etc), GPS communication may be limited or totally lost (Figure 1-2).

1.2 Literature Review

To overcome the lack of GPS communication, many navigation and control solutions utilize vision-based systems for localization by using landmarks in the environment [11–16]. These solutions typically require the landmark to always be in the vision sensor's field-of-view, constraining the trajectories an autonomous agent may take. To relax the requirement of always having a landmark in the field-of-view of a vision sensor, Simultaneous Localization and Mapping (SLAM) algorithms have been developed which

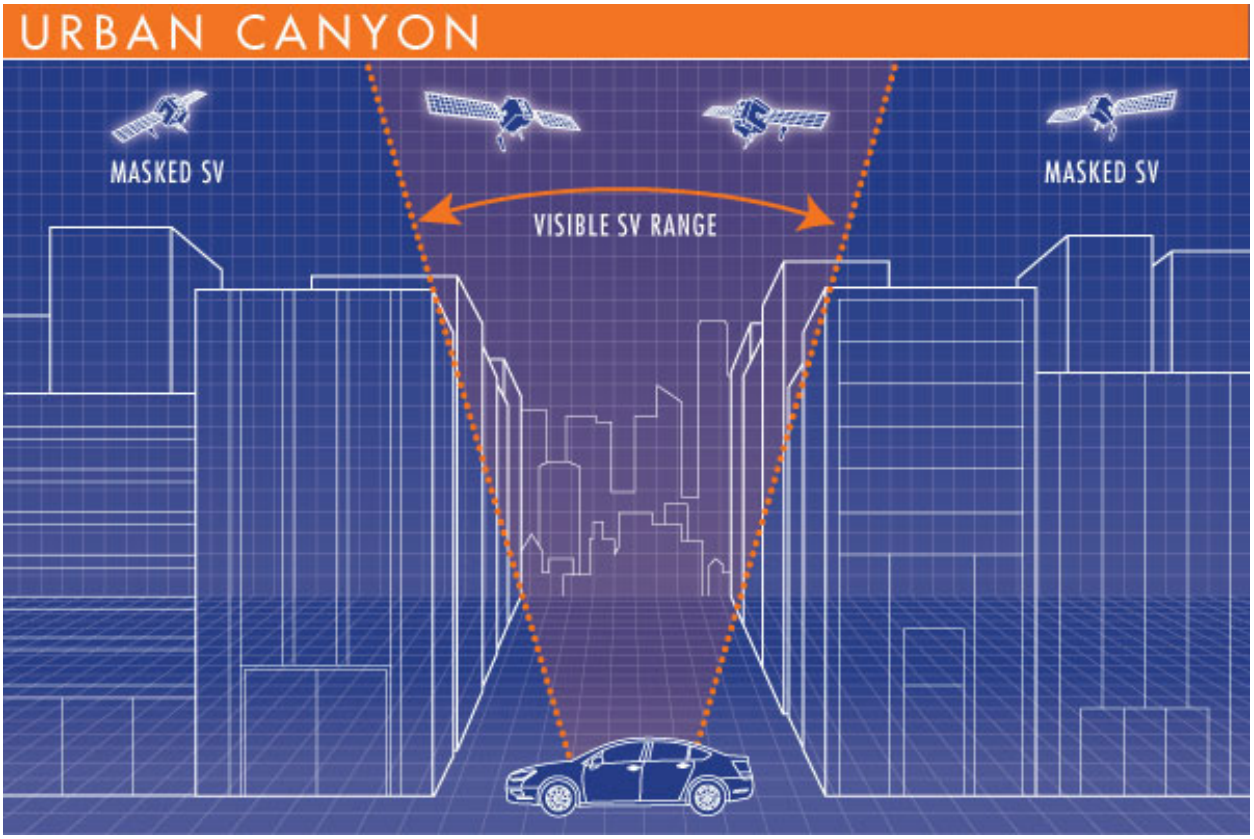

Figure 1-2. Illustrative example of an urban canyon with a loss of GPS satellite communication resulting in the deterioration of positioning accuracy or total loss of communication [10].

use relationships between features or landmarks to estimate pose (i.e., position and orientation) [17–19]. However, SLAM algorithms typically require environments that are rich with features, which limits their scope of implementation. Further, it is widely known that SLAM algorithms without proper loop closures result in pose estimation drift due to the accumulation of measurement noise (c.f, [20] and [21]).

In response to the issues in environments where state information is intermittent, a body of work has emerged [22]– [27] that embraces these difficulties by considering them as a class of Relay-Explorer problems. Typically using a switched system approach, control laws are constructed which use state feedback for navigation when available (stabilizable mode), and open-loop state estimates otherwise (unstable mode). For example, in a single agent setting [22], to ensure stability, the agent has to repeatedly reacquire feedback by entering a fixed region where feedback is available. A time-varying feedback region may naturally arise in multi-agent settings. For example in [28], some agents may have the capability of relaying feedback information to feedback-denied members of their team by moving into each other's communication radius.

Another method of overcoming the intermittency of state feedback is to deploy cooperative multi agent systems (MAS) that actively assist each other with localization by sharing information [29]– [32]. In such results, onboard sensing is shared and used to collectively assist in the localization of every agent in the MAS. Typically, individual agents are limited to relative distance measurements. Such measurements have been used in different ways to help localize each agent in a global coordinate system. For example, in [32], a Multidimensional Scaling algorithm is used to localize each agent while considering distance measurement noise found in wireless transceivers but requires stationary anchors that have perfect state information, which is a common theme in many cooperative localization techniques. In [29], the closest work in the literature to the work in Chapter 3, range sensors are used to take relative distance

measurements between agents, where the measurements have an unknown but bounded error. These errors prevent the agent from being perfectly localized, but the bound on the errors allows for feasible regions to be computed where each agent may reside. This is done by intersecting the geometric constraints imposed by the bounds on the errors of the distance measurements made by each agent. Although [29] does not require an anchor node, the result is applied to static nodes, leaving the dynamical case to future research.

Autonomous mobile agents often require optical sensors, such as a camera, to accomplish their tasks. Specifically, a tracking agent may be tasked with using a camera to measure state information of a target agent, such as the pose. These pose measurements are then used by the tracking agent's controller to maintain tracking of the target, i.e., keep its camera pointed at the target. However, cameras have sensing limitations, such as a finite field of view (FoV). This finite FoV has motivated several control schemes that force the target to remain in the FoV (cf., [11] and [33]), which may not be sufficient for maintaining a constant flow of state information. For example, environmental factors, such as debris [34], noncooperative agents, lens flare, etc, may act as momentary obstructions that occlude the scene, thus preventing the target from being seen by the tracking agent, despite being in the FoV of the camera. Further, the target may be adversarial, intentionally taking advantage of opportunities to elude tracking by causing occlusions, e.g. by maneuvering behind a building. The task definition may also hinder tracking. For example, if multiple targets need to be tracked at the same time, the tracking agent will be required to suspend tracking of one target to keep information about other targets current. Regardless of the cause, intermittent feedback presents a number of challenges for estimating the pose and velocities of agents and targets alike [35].

Traditionally, the estimation challenge resulting from the intermittency of state feedback has been addressed by probabilistic estimators, such as Kalman and particle

filters (cf., [36]– [39]). In such results, the filters are used to estimate the target motion and then a predictor propagates the target pose estimate forward in time when the target is not visible. However, these methods typically rely on a linearization of the target's dynamics (e.g., [36] and [40]). Furthermore, these probabilistic observers typically require that the probability distributions that model the system's uncertainties are known.

Several deterministic estimators have been developed (e.g., [41]– [47]) for stable target tracking, despite the indeterminacy in feedback. In these works, two subsystems are defined: a stable subsystem, where feedback is available; and an unstable subsystem, where feedback is unavailable (e.g., the target is occluded or the tracking agent suspended tracking to execute another task). This change in subsystems motivates the use of switched/hybrid analysis techniques (cf., [48] and [49]) to develop dwell time conditions that typically yield uniformly ultimately bounded stability results. In [41], a switched-systems framework is proposed yielding a dwell-time condition to inform the tracking agent, while in its unstable mode, how long it can afford to proceed in this mode before the estimation error grows too large for reacquisition to remain feasible. However, this work assumes exact model knowledge of the target. To relax the model knowledge requirement, motion model learning methods have been proposed. In [42], an integral concurrent learning method is proposed which learns the motion model of the target when feedback is available and then uses this learned model to predict the motion of a target when feedback is unavailable. Similarly, in [47], a deep neural network (DNN) was deployed to learn the motion model of the target, where an update law was constructed for both the state estimate and the weight estimate of the DNN. Specifically, the update law for the state estimator used the learned DNN model and a robust compensator term to aid in the estimation while the weight estimates converged to the ideal weights for the

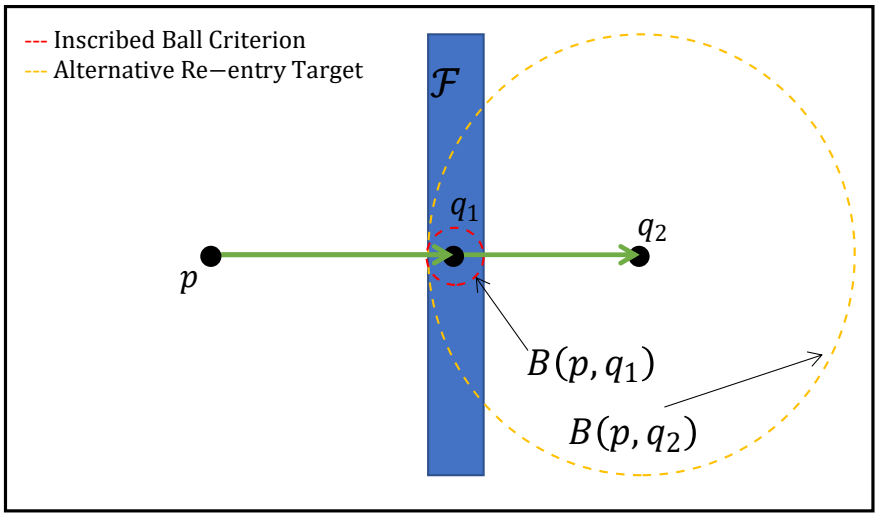

Figure 1-3. Given a feedback region $\mathcal{F}$, an initial starting point p, and a target point $q_1 \in \mathcal{F}$, the ball $B(p, q_1)$ about q_1 inscribed in $\mathcal{F}$ represents the maximum allowed region of uncertainty based on IBC. For this geometry, a much larger region of uncertainty may be allowed for a majority of starting points p, provided q_1 does not lie in $\mathcal{F}$, replacing q_1 with q_2, for example.

DNN. The weights for the outer layer of the DNN were updated according to a continuous update law, whereas the weights for the inner layers were updated at discrete times seeking to minimize a loss function.

1.3 Outline of the Dissertation

Similar to the framework in [22], Chapter 2 and [27] considers a single agent tasked with tracking a desired path that may lie outside a known feedback region. State feedback is available when the agent is inside this region, and unavailable otherwise. Since the desired path may lie partially outside of the feedback region, the agent dead-reckons when feedback is not available. To achieve the task, a path-planning algorithm is designed to generate an auxiliary trajectory for the agent to track. The instabilities inherent to dead-reckoning can impede the agent's ability to return to the feedback region. This instability forces the auxiliary trajectory to alternate between following the desired path and returning to the feedback region. This framework relies on a Lyapunov-based switched system analysis [48] to derive dwell-time conditions dictating the duration a system can remain in each operating mode while ensuring stability.

The predominant factor affecting dwell-time conditions for Relay-Explorer problems is the need to guarantee the reacquisition of state feedback. To furnish this guarantee, results in [22] and [25] require the agent to dead-reckon to a point where the region of state uncertainty is contained within the feedback region, the *Inscribed Ball Criterion* (IBC). Crucially, these results only consider feedback regions where the dwell-time conditions only depend on the distance of the agent to the feedback region (e.g., circular regions in the plane, or, more generally, in higher dimensional Euclidean space, balls and half-spaces will have this property). However, applying the same approach in real-life applications, and to more general geometries results in unnecessarily conservative bounds. For example, when an agent moves towards a long and narrow rectangular feedback region, Figure 1-3 shows that a better strategy is to aim at a point beyond the region, affording a larger error margin at the target point. Intuitively, small perturbations in the shape of this region should not result in a change of strategy, motivating a topological approach. Moreover, it is clear that the preceding considerations could not be easily replicated for an arbitrary geometry of the feedback region, because of complex interactions between local properties (e.g., curvature at nearby boundary points) and global properties (e.g., concavities, spirals, etc.).

Chapter 2 addresses the need for generating re-entry guarantees for arbitrary geometries of the feedback region. To this end, separation properties of embedded spheres in $\mathbb{R}^D$, $D \geq 2$ are used (Sections 2.3.1–2.3.2). The resulting *Topological Re-entry Criterion* is applied to increase the maximum dwell-time by raising the upper bound on the allowed error growth, in a state-dependent manner, while being cognizant of the geometry of the feedback region in the agent's vicinity (Sections 2.3.3–2.3.5). The proposed framework generalizes the results in [22] from circular geometries in $\mathbb{R}^2$ to nearly arbitrary contractible geometries in $\mathbb{R}^D$ of the feedback region, by casting the problem of constructing auxiliary trajectories as an optimization problem (Section 2.3.4): selecting an optimal auxiliary trajectory is tantamount to computing, at every

point of the desired path, the largest tracking error the agent can afford without losing the guarantee of return (the agent's *uncertainty budget* at that point). In particular, this framework guarantees uniformly ultimately bounded errors for repeated optimal choices of the auxiliary trajectories (Theorem 2.4). To assess the degree of improvement offered by the topological re-entry criterion over the IBC, an algorithm for computing uncertainty budgets is given in Section 2.4 and numerical studies in Section 2.5.

Chapter 3 merges the idea of cooperative localization of MASs with Chapter 2 by using relative distance measurements between agents to put constraints on the possible locations for each agent within their respective region of uncertainty, improving the overall state estimation in the MAS. The resulting improved region of uncertainty is similar to the idea of feasible regions in [29], but here the regions of uncertainty are determined by the growth of the state estimation errors of the individual agents, not the measurement uncertainty, which are then constrained by the distance measurements, resulting in corrected state estimates and reduced error bounds. The reduction in the state estimation error is then used to trigger an update in the auxiliary path plan to allow the agents to delay upcoming detours into the feedback region.

In Section 3.1, the results of Chapter 2 are revisited. Section 3.2 states the control problem and provides a complete description of the hybrid system. Then in Section 3.3.2, the cooperative state estimation algorithm is proposed and its continuity considered. In Section 3.4.3, auxiliary path planning procedures are introduced along with trigger functions for determining when relative distance measurements should be used to update auxiliary path plans. Section 3.6 discusses the stability properties of the system.

Chapter 4 extends the the topological methods from Chapter 2 to time varying feedback regions. Specifically, this work introduces a novel framework for image-based tracking systems, addressing scenarios where the tracking agent needs to discontinue tracking the target agent either due to the need to fulfill other tasks or the target agent

becoming obscured. The developed approach deploys a Lyapunov-based Deep Neural Network (Lb-DNN) to learn the dynamics of the target agent when visible, and to predict its future trajectory when not visible.

Additionally, a related, but rarely examined question of where the tracking agent should point its camera to best reacquire tracking of the target (i.e., the target re-enters the tracking agent's FoV) is addressed. The typical solution is to assume that the estimation error does not grow beyond the dimensions of the FoV while the center of the camera's FoV is pointed at the predicted state of the target until the target becomes visible again. However, this solution is restrictive. For example, it may be advantageous to position the camera ahead of the predicted state of the target, in a particular orientation, to catch the target within the FoV once it exits the occlusion region (Figure 1-4). This reasoning is motivated by the work in Chapter 2, where the approach there is analogous to this target tracking problem in the sense that a path planning scheme is developed for the tracking agent to position its camera, and the resulting feedback region, so that the target is guaranteed to pass through the boundary of the FoV, thus guaranteeing that the reacquisition of tracking occurs. To ensure that target tracking resumes, the topologically inspired method from Chapter 2 is extended, utilizing the predicted trajectory of the target agent in a role analogous to that of the return path plan there. This method informs the tracker agent about the duration it can suspend tracking the target agent and specifies a pose for the camera for guaranteeing that tracking resumes at some later time. Simulation results are provided to demonstrate the performance of the proposed framework.

This chapter is structured as follows. Section 4.2 formally states the problem. Section 4.3 introduces the design and development of the estimator and predictor. Section 4.3 gives the stability analysis for the estimator and develops growth bounds of the pose estimation error while feedback is unavailable. Section 4.5 develops the topologically inspired methodology for guaranteeing reacquisition of tracking and gives

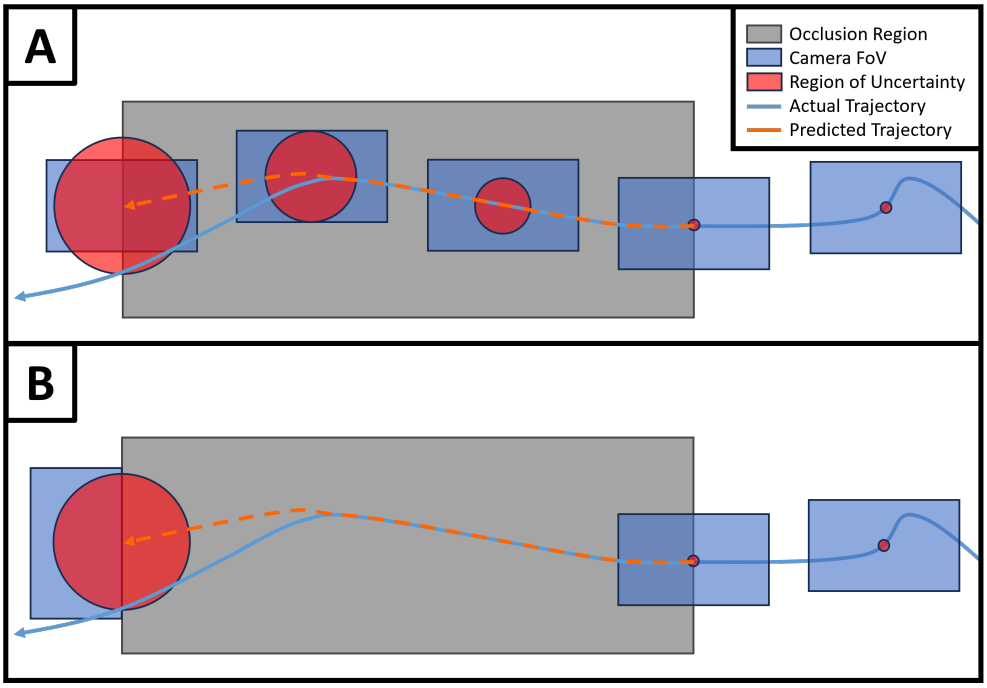

Figure 1-4. Image A depicts a strategy of having the camera following the predicted trajectory of the target; however, if the target is occluded for too long (breaking the dwell time condition), the target may leave the FoV, thus becoming lost to the tracking agent. Image B depicts the proposed idea of selecting a position to place the camera's FoV to catch the target as it leaves the occlusion region. This selection of a camera's pose may allow for an increase in the dwell time condition, since it allows for the region of uncertainty (the region where the target may be found within) to grow beyond the size of the FoV.

the final stability result for the switched system. Section 4.6 discusses a method for implementing the developed method for guaranteeing reacquisition of tracking. Section 4.7 discusses a series of simulations.

1.4 Notation

Let the space of quaternions be denoted by $\mathbb{H} \subseteq \mathbb{R}^4$. To accommodate space constraints, denote Cartesian products $A \times B \times C \times \cdots \times Z$ by $\langle\!\langle A, B, C, \ldots, Z \rangle\!\rangle$, suppressing braces for singletons. The p-norm of $v \in \mathbb{R}^D$ is denoted by $\|v\|_p$, where in the case that $p = 2$, $\|\cdot\|$, may be used. For any integer $D \geq 1$, the Euclidean distance between $p, q \in \mathbb{R}^D$ is denoted by $\texttt{dist}\,(p, q) \triangleq \|p - q\|_2$. The shortest distance from a point to a set is $\texttt{dist}(p, A) \triangleq \inf\{\texttt{dist}\,(p, q) : q \in A\}$. The diameter of $A \subset \mathbb{R}^D$ is $\texttt{diam}(A) \triangleq \sup\{\texttt{dist}\,(p, q) : p, q \in A\}$. Let the closed unit ball in $\mathbb{R}^D$ be defined as $\mathbb{B}^D \triangleq \{p \in \mathbb{R}^D : \|p\| \leq 1\}$, and let $\mathbb{S}^{D-1}$ denote the unit sphere in $\mathbb{R}^D$. The dimensions, $D, D-1$ respectively, will often be suppressed. Similarly, the open unit ball in $\mathbb{R}^D$ is defined as $\mathbb{B}^\circ \triangleq \{p \in \mathbb{R}^D : \|p\| < 1\}$. The closure of a set A is denoted by both $\texttt{cl}(A)$ and $\overline{A}$, when appropriate. The set of interior points of $A \subseteq \mathbb{R}^D$ is denoted by A°. The Minkowski sum and difference are denoted by $\oplus$ and $\ominus$, respectively. In Chapter 3, Minkowski sums will be denoted by $+$. Given $p \in \mathbb{R}^D$ and $r > 0$, the closed ball of radius r about p is defined as $B_r(p) \triangleq p \oplus r\mathbb{B}$. Similarly, the open ball is defined as $B_r^\circ(p) \triangleq p \oplus r\mathbb{B}^\circ$. A point is an interior point of a set if $B_r^\circ(p) \subseteq A$ for some $r > 0$. A different notion of interior is associated with embeddings of $\mathbb{S}^{D-1}$ in $\mathbb{R}^D$, see (2–11). The boundary of A is $\partial A \triangleq \texttt{cl}A \setminus A^\circ$. The convex hull of $A \subseteq \mathbb{R}^D$, denoted by $\text{conv}(A)$, is the minimal convex set containing A, whereas the convex closure of A, denoted by $\overline{\text{co}}(A)$, is the the closure of the convex hull of A, i.e., $\texttt{cl}(\text{conv}(A))$. Given a set S, its diagonal is defined as $\mathbf{\Delta}(S) \triangleq \{(s, s) : s \in S\} \subset S \times S$. The Clarke tangent cone to a set $S \subset \mathbb{R}^D$ at a point $x \in \mathbb{R}^D$ is denoted by $\mathbf{T}_S(x)$. A set $A \subset \mathbb{R}^D$ is said to be null, if it has Lebesgue measure zero. Let, $\texttt{ReLu}(x) \triangleq \max(0, x)$ be the Rectified Linear Unit function. The convolution operator is denoted by '$*$', and is defined as

$p(t) * q(t) = \int_{t_0}^{t} p(t-\tau)q(\tau)d\tau$, for any given $p, q : [t_0, \infty) \to \mathbb{R}$. A set-valued mapping $M : S \rightrightarrows T$ is a function from S to the power set of T. The regularized signum function $\text{SGN} : \mathbb{R} \rightrightarrows \mathbb{R}$ is denoted by $\text{SGN}(x)$ and has a value of -1 if $x < 0$, 1 if $x > 0$, and $[-1, 1]$ if $x = 0$. The vector of all ones is denoted by $\mathbf{1}$. The identity matrix of size n is denoted by $\mathbf{I}_n$. The matrix of size $n \times m$ with all elements being equal to zero is denoted by $\mathbf{0}_{n\times m}$. Column vectors constructed via vertical concatenation will be denoted by $[a; b; c; \dots] \triangleq [a^\top, b^\top, c^\top, \dots]^\top$. For vectors $v_i \in \mathbb{R}^{D_i \times 1}$, $i = 1, \dots, m$ the expression $(v_i)_{i=1}^m$ denotes the vector $[v_1; \dots; v_m]^\top \in \mathbb{R}^{(D_1+\dots+D_m)\times 1}$. For a vector $v = (v_i)_{i=1}^D \in \mathbb{R}^D$ define $|v| \triangleq (|v_i|)_{i=1}^D$, $\text{sgn}(v) \triangleq (\text{sgn}(v_i))_{i=1}^D$, $\texttt{ReLu}(v) \triangleq (\texttt{ReLu}(v_i))_{i=1}^D$, and $v^\lambda \triangleq (v_i^\lambda)_{i=1}^D$, for $\lambda \in \mathbb{R}$ when $v_i \geq 0$ for all i. For some matrix $A \in \mathbb{R}^{n\times m}$, the conjugate transpose of A is denoted by A^*. The maximum eigenvalue of A is denoted by $\lambda_{\text{max}}(A)$. The spectral norm of a matrix is defined as $\|A\|_S \triangleq \sqrt{\lambda_{\text{max}}(A^*A)}$. The Hadamard product of two matrices A,$B \in \mathbb{R}^{D\times E}$ is denoted by $A \odot B$. However, in Chapter 4 the Hamilton product, of two quaternions $q, p \in \mathbb{H}$, is defined as

$$q \odot p \triangleq \begin{bmatrix} q_s & -q_v^\top \\ q_v & q_s\mathbf{I}_3 + (q_v)^\times \end{bmatrix} p, \; w^\times \triangleq \begin{bmatrix} 0 & -w_3 & w_2 \\ w_3 & 0 & -w_1 \\ -w_2 & w_1 & 0 \end{bmatrix},$$

where $q_s \in \mathbb{R}$ and $q_v \in \mathbb{R}^3$ are the scalar and vector components of the quaternion q, respectively. The Moore-Penrose pseudo-inverse of a full row rank matrix $A \in \mathbb{R}^{n\times m}$ is denoted by A^+, where $A^+ \triangleq A^\top \left(AA^\top\right)^{-1}$. The right-to-left matrix product operator is represented by $\overset{\curvearrowleft}{\prod}$, i.e., $\overset{\curvearrowleft}{\prod_{p=1}^{m}} A_p = A_m \dots A_2 A_1$ and $\overset{\curvearrowleft}{\prod_{p=a}^{m}} A_p = I$ if $a > m$. The Kronecker product is denoted by $\otimes$. Given some matrix $A \triangleq [a_{i,j}] \in \mathbb{R}^{n\times m}$, where $a_{i,j}$ denotes the element in the i^{th} row and j^{th} column of A, the vectorization operator is defined as $\text{vec}(A) \triangleq [a_{1,1}, \dots, a_{1,m}, \dots, a_{n,1}, \dots, a_{n,m}]^T \in \mathbb{R}^{nm}$. Given any $A \in \mathbb{R}^{p\times a}$, $B \in \mathbb{R}^{a\times r}$, and $C \in \mathbb{R}^{r\times s}$, the vectorization operator satisfies the property [50, Proposition 7.1.9]

$$\text{vec}(ABC) \;=\; (C^\top \otimes A)\text{vec}\,(B)\,. \tag{1–1}$$

Differentiating (1–1) on both sides with respect to $\mathrm{vec}\,(B)$ yields the property

$$\frac{\partial}{\partial \mathrm{vec}\,(B)} \mathrm{vec}(ABC) \;=\; C^{\top} \otimes A. \tag{1–2}$$

CHAPTER 2
A TOPOLOGICALLY INSPIRED PATH-FOLLOWING METHOD WITH INTERMITTENT STATE FEEDBACK

This chapter and the result in [27] advances a topologically inspired method for guaranteeing re-acquisition of feedback for nearly arbitrary geometries in arbitrary dimensions, all while relaxing the dwell-time conditions and retaining the uniformly ultimately bounded stability result from preceding work. Numerical experiments in the plane demonstrate an increase of hundreds of percentage points, even for fairly generic geometries, in the tracking error the agent could afford, using the proposed method, without sacrificing stability.

2.1 Problem Statement

2.1.1 Agent Dynamics

Consider an agent with dynamics modeled by

$$\dot{x} = f(x,t) + \zeta(t) + d(t), \tag{2–1}$$

where $x : \mathbb{R}_{\geq 0} \to \mathbb{R}^D$, $D \geq 2$, denotes the state; $f : \mathbb{R}^D \times \mathbb{R}_{\geq 0} \to \mathbb{R}^D$ denotes locally Lipschitz drift dynamics; $d : \mathbb{R}_{\geq 0} \to \mathbb{R}^D$ denotes an exogenous disturbance; and $\zeta : \mathbb{R}_{\geq 0} \to \mathbb{R}^D$ denotes a control input. The following assumption is used in the subsequent development.

Assumption 2.1. The exogenous disturbance d satisfies $\|d(t)\| \leq \bar{d}$ for all $t \in \mathbb{R}_{\geq 0}$, where $\bar{d} \in \mathbb{R}_{>0}$ is known.

2.1.2 Control Objective

Let $\mathcal{F} \subset \mathbb{R}^D$ denote a known region where state feedback is available, i.e., state feedback is available to the agent if and only if $x \in \mathcal{F}$. The feedback region $\mathcal{F}$ is modeled as the closure of the interior region of a polyhedral sphere C. Equivalently, $\mathcal{F}$ is the image of an embedding of $\mathbb{B}^D$ in $\mathbb{R}^D$ (Section 2.3). The feedback-denied region, $\mathcal{F}^c \triangleq \mathbb{R}^D \setminus \mathcal{F}$, is the set of states where feedback is not available.

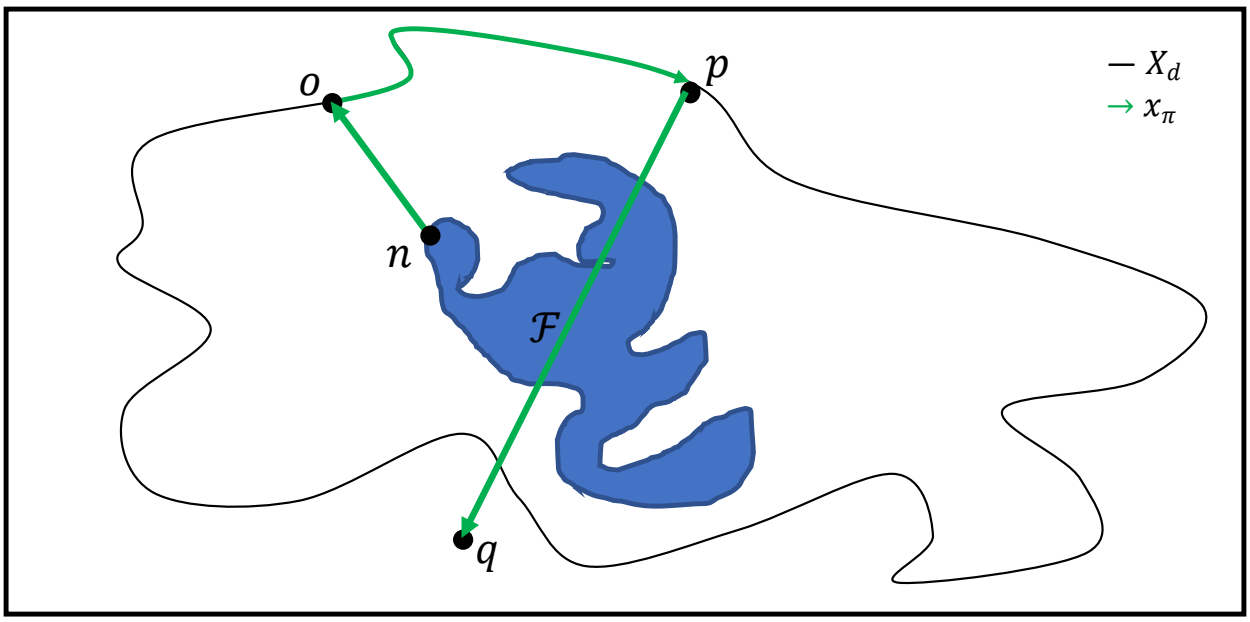

Figure 2-1. The auxiliary trajectory x_π, defined by a path plan $\pi =$ (n, o, p, q), is superimposed over the desired path X_d, for a generic feedback region $\mathcal{F}$ (Definition 1). Note that the point q need not lie in $\mathcal{F}$.

The agent is tasked with following a desired polygonal path X_d, which is provided as a sequence of way points $(\mathcal{P}_0, \ldots, \mathcal{P}_M)$ in $\mathbb{R}^D$, some of which may lie outside of $\mathcal{F}$. Repeated dead-reckoning along the sequence of way points is inherently unstable outside of $\mathcal{F}$. Instabilities during dead-reckoning motivates an approach where the agent follows a sequence of auxiliary trajectories, relaying between the desired path and the feedback region (Figure 2-1), to ensure the error system remains bounded.

Definition 2.1 (Auxiliary Trajectory)**.** There are two types of auxiliary trajectories. The auxiliary trajectory $x_\pi : \mathbb{R}_{\geq 0} \to \mathbb{R}^D$ with path plan $\pi = (n, o, p, q)$, is defined as the concatenation of three trajectories determined by four way points: n is the point of departure from the feedback region; o is the first point along a segment of X_d the agent selects to follow; p is the point of departure from X_d; and q is the target point for the return trajectory to the feedback region. From n to o, and from p to q, x_π is restricted to straight line trajectories with constant speed v_0. From o to p, x_π coincides with the desired path X_d, with a piecewise linear parametrization of constant speed v_0. For the

second type of auxiliary trajectory, with plan $\pi = (p, q)$, set x_π to coincide with a linearly parametrized line segment from p to q with constant speed v_0.

Remark 2.1. Plans $\pi = (p, q)$ are used for acquisition of feedback from points $p \notin \mathcal{F}$, while plans $\pi = (n, o, p, q)$ are used for tracking X_d and reacquiring feedback. A plan terminates the moment feedback is reacquired.

Assumption 2.2. It is assumed that feedback acquisition is instantaneous upon re-entry into the feedback region.

Remark 2.2. Between the executions of two plans, the agent travels through $\mathcal{F}$, taking advantage of the available feedback. Two cases may occur. If the next point $\mathcal{P}_m$ along X_d lies in $\mathcal{F}$, there is no need for auxiliary planning. Otherwise, the agent travels to the point $n \in \mathcal{F}$ closest to $\mathcal{P}_m$.

To quantify the tracking objectives, define

$$e \triangleq x - x_\pi, \quad \hat{e} \triangleq \hat{x} - x_\pi, \quad \tilde{e} \triangleq x - \hat{x}, \tag{2–2}$$

where $\hat{x} : \mathbb{R}_{\geq 0} \to \mathbb{R}^D$ is the agent's open-loop state estimate, and $e, \hat{e}, \tilde{e} : \mathbb{R}_{\geq 0} \to \mathbb{R}^D$ are the actual tracking error, estimated tracking error, and state estimation error, respectively. The challenge is to regulate the norm of the actual tracking error to remain, eventually, below a prescribed bound.

2.1.3 Switched Controller

Let $\mathcal{S} \triangleq \{a, u\}$ be the set of indices denoting the operating modes, where a and u correspond to the modes where feedback is available and unavailable, respectively. Mode a is active when $x \in \mathcal{F}^\circ$. Mode u is active otherwise. Let $\sigma(x) \in \mathcal{S}$ denote the switching signal indicating the active subsystem. The control input takes the form $\zeta \triangleq \zeta_a(x, t)$ when $\sigma(x) = a$, and $\zeta \triangleq \zeta_u(\hat{x}, t)$ when $\sigma(x) = u$, where $\zeta_a, \zeta_u : \mathbb{R}^D \times \mathbb{R}_{\geq 0} \to \mathbb{R}^D$ are the control inputs when feedback is available and unavailable, respectively. The closed loop error system for controllers of this kind were studied in [22], Section IV.

2.2 Error Bounds

To facilitate the analysis, the i^{th} instant when σ switches from u to a is denoted by $t_i^a \in \mathbb{R}_{\geq 0}$ for all $i \in \mathbb{Z}_{>0}$, i.e., the instant the agent enters the interior of the feedback region. The i^{th} instant when σ switches from a to u is denoted by $t_i^u \in \mathbb{R}_{\geq 0}$, i.e., the instant the agent exits $\mathcal{F}^\circ$. Based on the switching instants, dwell-times of the i^{th} activation of the subsystems a and u are defined as $\Delta t_i^a \triangleq t_i^u - t_i^a$ and $\Delta t_i^u \triangleq t_{i+1}^a - t_i^u$, respectively.

To analyze the switched system, candidate Lyapunov-like functions are defined as

$$V_e \triangleq \frac{1}{2}\|e\|^2, \quad V_{\hat{e}} \triangleq \frac{1}{2}\|\hat{e}\|^2, \quad V_{\tilde{e}} \triangleq \frac{1}{2}\|\tilde{e}\|^2, \tag{2–3}$$

where $V_e, V_{\hat{e}}, V_{\tilde{e}} : \mathbb{R}^D \to \mathbb{R}_{\geq 0}$. To ensure a bound on the error system, the following assumption is made.

Assumption 2.3. Based on the design of the control input in Section 2.1.3, it is assumed that the time derivatives of (2–3) yields

$$\dot{V}_e \leq -2\lambda_s V_e, \qquad \sigma = a, \tag{2–4}$$

$$\dot{V}_{\hat{e}} \leq -2\lambda_s V_{\hat{e}}, \qquad \sigma = u, \tag{2–5}$$

$$\dot{V}_{\tilde{e}} \leq \begin{cases} -2\lambda_{\tilde{e}} V_{\tilde{e}}, & \sigma = a, \\ 2\lambda_u V_{\tilde{e}} + \delta, & \sigma = u, \end{cases} \tag{2–6}$$

where $\lambda_s, \lambda_{\tilde{e}}, \lambda_u, \delta \in \mathbb{R}_{>0}$ are known constants.

Remark 2.3. An example of a controller satisfying the assumptions made thus far is given in Section VI of [22], where values for $\lambda_s, \lambda_{\tilde{e}}, \lambda_u$, and δ are shown to be functions of the agent dynamics and the disturbance bound $\bar{d}$.

While the agent is in the feedback-denied region (i.e., $\sigma = u$), solving the ordinary differential inequalities in (2–4)–(2–6) and substituting in (2–2) and (2–3) yields

$$\left\|\hat{e}(t)\right\| \leq \left\|\hat{e}\left(t_i^u\right)\right\| \mathrm{e}^{-\lambda_s \Delta t}, \tag{2–7}$$

$$\left\|\tilde{e}(t)\right\|^2 \leq \left\|\tilde{e}\left(t_i^u\right)\right\|^2 \mathrm{e}^{2\lambda_u \Delta t} + \frac{\delta}{\lambda_u}\left[\mathrm{e}^{2\lambda_u \Delta t} - 1\right], \tag{2–8}$$

for all $t \in [t_i^u, t_{i+1}^a)$, where $\Delta t \triangleq t - t_i^u$.

Upon each re-entry into $\mathcal{F}$, it is possible to reset the auxiliary path x_π to a new path and have $\hat{x}\left(t_{i+1}^a\right) = x\left(t_{i+1}^a\right)$ at t_{i+1}^a. In other words, the auxiliary path is updated based on the re-entry location of the agent instead of having to travel to the desired re-entry location before returning to the desired path to follow. Resetting the errors to zero results in the elimination of the minimum dwell-time condition and the vanishing of the initial conditions from the maximum dwell-time condition [22]. Since $e = \hat{e} + \tilde{e}$, and using the reset maps from [22], the bounds in (2–7) and (2–8) yield

$$\|e(t)\| \leq \rho(t - t_i^u), \quad t \in [t_i^u, t_{i+1}^a), \tag{2–9}$$

where

$$(\rho(\Delta t))^2 \triangleq \frac{\delta}{\lambda_u}\left[\mathrm{e}^{2\lambda_u \Delta t} - 1\right], \tag{2–10}$$

and $\rho(\Delta t)$ is referred to as the radius of uncertainty at time t. This bound holds for any trajectory under any controller satisfying Assumption 2.3, enabling the development of a dwell-time condition (Theorem 2.3).

2.3 Criteria for Guaranteed Re-entry

2.3.1 Preliminaries: Embedded Spheres in Euclidean Space

An embedded sphere in $\mathbb{R}^D$ is defined to be the image $C \triangleq \gamma\left(\mathbb{S}^{D-1}\right)$ of an injective continuous map $\gamma : \mathbb{S}^{D-1} \to \mathbb{R}^D$. For $D = 2$, the following classical result may be applied.

Theorem 2.1 (Jordan-Schöenflies, see [51], Thm. E1)**.** *An injective continuous map $\gamma : \mathbb{S}^1 \to \mathbb{R}^2$ extends to a homeomorphism $\Gamma : \mathbb{R}^2 \to \mathbb{R}^2$, a continuous map with continuous inverse satisfying $\Gamma(p) = \gamma(p)$ for all $p \in \mathbb{S}^1$. The mapping Γ is called a Schöenflies extension of γ.*

For higher dimensions $D > 2$, Schöenflies extensions exist under the additional condition that the embedding γ is *collared* [52], [53]. The embedding γ is collared if there is an injective continuous map $\widetilde{\gamma} : \mathbb{S}^{D-1} \times [-1, 1] \to \mathbb{R}^D$ such that $\widetilde{\gamma}(p, 0) = \gamma(p)$ for all $p \in \mathbb{S}^{D-1}$. It is well-known that polyhedral, and, more generally, piecewise-regular, maps γ (with finitely many faces) are collared ($\S 11$ in [54]).

The interior and exterior regions of a collared embedded sphere C are defined as

$$\text{int}\,(C) \triangleq \Gamma\left((\mathbb{B}^\circ)^D\right), \quad \text{ext}\,(C) \triangleq \Gamma\left(\mathbb{R}^D \backslash \mathbb{B}^D\right), \tag{2–11}$$

where Γ is any Schöenflies extension of γ. It is important to note $\text{int}(C)$ and $\text{ext}(C)$ do not depend on the choice of map γ—only on its image, C. They are also independent of the choice of the Schöenflies extension Γ. Moreover, the boundary sets $\partial\text{int}\,(C)$ and $\partial\text{ext}\,(C)$ coincide with C, and C separates every point $p \in \text{int}\,(C)$ from every point $q \in \text{ext}\,(C)$ in the sense that any continuous curve from p to q must intersect C. For the rest of this chapter the following assumption is made.

Assumption 2.4. The feedback region $\mathcal{F}$ is the closure of $\text{int}(C)$, where C is a collared embedded sphere in $\mathbb{R}^D$.

2.3.2 Construction of a Target Region

In the notation of Section 2.2, given t_i^u, consider a plan $\pi = (n, o, p, q)$. Alternatively, consider $\pi = (p, q)$, while setting $t_i^u = 0$. Let x_π be the associated auxiliary trajectory. Let $p = x_\pi(t_i^p)$ and $q = x_\pi(t_i^q)$, then the initial and final uncertainty radii for the plan π are defined as

$$\rho_{init}(\pi) \triangleq \rho(t_i^p - t_i^u), \quad \rho_{fin}(\pi) \triangleq \rho(t_i^q - t_i^u), \tag{2–12}$$

where ρ is defined in (2–10). The regions of uncertainty are

$$U_{init}(\pi) \triangleq B_{\rho_{init}(\pi)}(p), \quad U_{fin}(\pi) \triangleq B_{\rho_{fin}(\pi)}(q). \tag{2–13}$$

In [22] and [25], re-entry is guaranteed by selecting $q \in \mathcal{F}$ so that $U_{fin}(\pi) \subset \mathcal{F}$. This method is referred to as the Inscribed Ball Criterion (IBC). Treating this inclusion as a

constraint results in a bound on $\rho_{fin}(\pi)$, and hence also on $\rho_{init}(\pi)$, since the function ρ is known. The example in Figure 1-3 illustrates the need for a target region much larger than $\mathcal{F}$, in which to fit $U_{fin}(\pi)$, to obtain less conservative bounds. In this section, such target regions are introduced.

Recall that $\mathcal{F}^\circ = \text{int}\,(C)$. Given a point $p \in \text{ext}\,(C)$ and a closed, connected region $R \subset \mathbb{R}^D$ with $p \in R^\circ$, define $T_{C,R}\,(p)$ to be the collection of all points $q \in R^\circ$ for which any smooth curve $\gamma : [0,1] \to R^\circ$ from p to q must pass through a point of C. Let $E_{C,R}\,(p)$ denote the set of all $y \in C$ such that, for some $q \in T_{C,R}\,(p)$ there is a smooth curve $\gamma : [0,1] \to R^\circ$ from p to q that crosses C exactly once at y.

Remark 2.4. In the above, it is permissible to restrict attention to smooth curves γ which intersect C transversely, i.e., their tangent line at any point of intersection with C and the tangent to C at that point together span $\mathbb{R}^D$ ($\S 10$ of [54]).

Lemma 2.1. *If $q \in T_{C,R}\,(p)$, then any curve in R from p to q must pass through a point of $E_{C,R}\,(p)$.*

Proof. Suppose a curve $\gamma : [0,1] \to R^\circ$ starts at point $p = \gamma\,(0)$ and terminates at the point $q = \gamma\,(1)$. Let $t' \triangleq \inf\{t \in [0,1] : \gamma\,(t) \in C\}$ be the first time γ crosses C. By Remark 2.4, one may assume γ only crosses C transversely. Set $q' \triangleq \gamma\,(t')$, and let $\mathcal{U}$ be a neighborhood of q' not containing any other intersection point of γ and C such that $C \cap \mathcal{U}$ is a single interval. Find $\Delta t > 0$ such that $\gamma([t', t' + \Delta t]) \subset \mathcal{U}$ and now set $q'' \triangleq \gamma(t' + \frac{\Delta t}{2})$. Since the curve $\gamma' \triangleq \gamma\big|_{[0,t'+\Delta t/2]}$ crosses C exactly once, $q'' \in \text{int}(C)$ and $q' \in E_{C,R}(p)$, as required (Figure 2-2(left)). □

2.3.3 Guarantee of Re-entry into the Feedback Region

Assume once more the agent is executing a plan $\pi = (n, o, p, q)$ over the time period $t \in [t_i^u, t_{i+1}^a]$. At time t_i^p, the agent departs in the direction of $\mathcal{F}$ by dead-reckoning to a point $q \in \mathbb{R}^D$ (note that it is possible for q to not lie in $\mathcal{F}$). For all $t \in [t_i^p, t_i^q]$, $t_i^q - t_i^p = \frac{\|q-p\|}{v_0}$, $x_\pi(t) = p + (t - t_i^p)v$, where $v = v_0 \frac{q-p}{\|q-p\|}$. The true position $x(t)$ is guaranteed to lie in the ball $B_{\rho(\Delta t)}(x_\pi(t))$, where Δt and ρ are defined in (2–7) and (2–10), respectively.

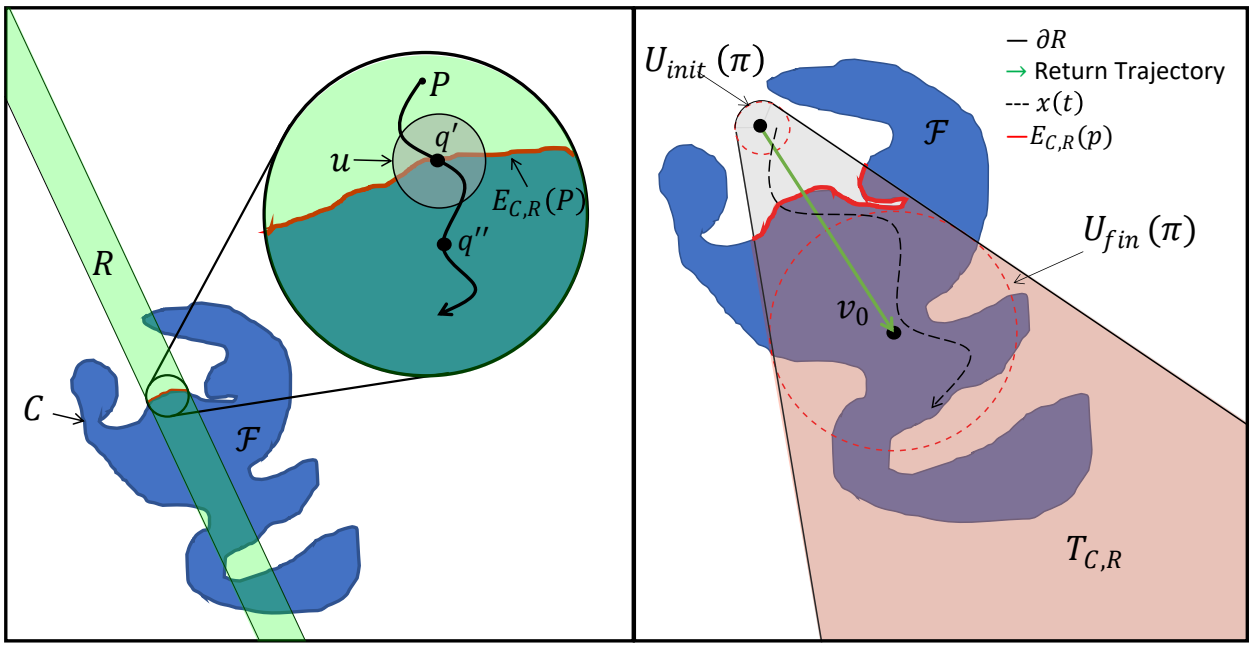

Figure 2-2. Illustration of the proofs of Lemma 2.1 (left) and Theorem 2.2 (right) in the plane.

Theorem 2.2. *Suppose* $U(\pi) \triangleq \bigcup_{t\in[t_i^p,t_i^q]} B_{\rho(t-t_i^u)}(x_\pi(t))$ *is contained in the interior of a region* R*. If* $U_{fin}(\pi) \subset T_{C,R}(p)$ *then there exists* $t \in [t_i^p, t_i^q]$ *with* $x(t) \in \mathcal{F}$*.*

Proof. If $U_{fin}(\pi) \subset T_{C,R}(p)$, then $q = x(t_i^q) \in T_{C,R}(p)$. Apply Lemma 2.1 to this point and the curve $\gamma : [t_i^p, t_i^q] \to R$, concluding that γ had to pass through a point of $E_{C,R}(p)$. Thus, $x(t)$ entered int(C) at some earlier time $t \in (t_i^p, t_i^q)$ (Figure 2-2 (right)). □

Remark 2.5. If R is selected as a convex region, then ensuring $U_{init}(\pi) \subset R$ and $U_{fin}(\pi) \subset T_{C,R}(p)$ suffices for meeting the requirements of Theorem 2.2.

2.3.4 Path-Planning with Infinite Cylinders

Theorem 2.2 states region R should be selected so the error growth in (2–9) of the agent is accounted for in R up until re-entry can be guaranteed. Since an upper bound on the error growth rate is given in (2–9), R may be designed to contain all possible trajectories of $x(t)$, given a plan $\pi = (n, o, p, q)$. In principle, given the reference point of departure $p = x_\pi(t_i^p)$ and a reference target velocity vector v with $\|v\| = v_0$, R could always be selected to be the (unbounded) cone of uncertainty $\bigcup_{t\in[t_i^p,\infty)} B_{\rho(t-t_i^u)}(p +$

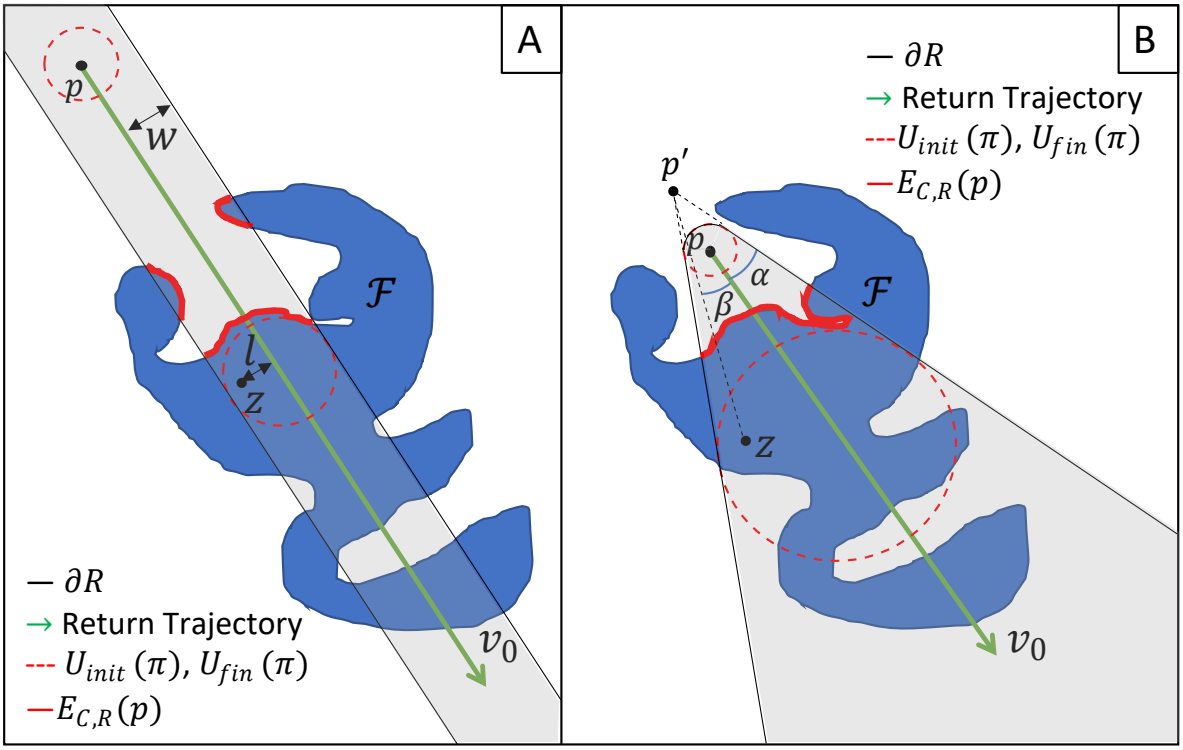

Figure 2-3. Illustrations of possible target regions R for use with the planner. The cylinder geometry implemented in this chapter is shown in A. More general geometries are possible (for example the conical region shown in B), but are not discussed here due to higher computational overhead.

$(t - t_i^p)v)$ in that direction. However, this choice is challenging from a computational perspective, because of the nonlinearity of ρ.

Given any point $p \in \mathcal{F}^c$, the planner needs to select q and a region R best suited for guaranteeing the agent's return to $\mathcal{F}$. In general, to apply Theorem 2.2 a rich collection $\mathcal{R}(p)$ of regions R satisfying $p \in R^\circ$ with sufficiently large $T_{C,R}(p)$ for some $R \in \mathcal{R}(p)$ must be designed.

Figure 2-3 presents two alternatives to the approach using cones of uncertainty: the cylindrical geometry in Figure 2-3(A) and a conical geometry in Figure 2-3(B). The subsequent development only considers the cylindrical geometry, in the interest of reducing computational cost. Specifically, consider

$$\mathcal{R}(p) \triangleq \left\{ R_{p,v,w} : v \in \mathbb{R}^D, \|v\| = v_0, w > 0 \right\}, \tag{2–14}$$

where $R_{p,v,w}$ is the solid cylinder of radius w whose axis passes through p and has direction v (Figure 2-3(A)),

$$R_{p,v,w} \triangleq \left\{ z \in \mathbb{R}^D : \left\| (z-p) - \frac{(z-p)\cdot v}{v_0^2} v \right\| \leq w \right\}. \tag{2–15}$$

A pair (v, w) will be referred to as return parameters. For $R = R_{p,v,w}$, the following observations are made.

- For excessively large values of w (e.g., w big enough for $C \subset R$) then $T_{C,R}(p) = \mathcal{F}$. Therefore, any ball contained in $T_{C,R}(p)$ provides little improvement upon IBC of guaranteeing return.
- More generally, $R \setminus C$ has no more than two unbounded components. When there is only one such component, the existence of a ball of radius w contained in $T_{C,R}(p)$ cannot be guaranteed.
- In all other cases, the collection of balls of radius w contained in $T_{C,R}(p)$ is non-empty: a point of the form $q = p + \alpha v$ always exists with $\alpha > 0$ and $B_w(q) \subset T_{C,R}(p)$ (Figure 2-3(A)).

The developed planner seeks to maximize the arc length from o to p along X_d subject to the constraint of re-entry being guaranteed by $\mathcal{R}(p)$. As a result, maximizing $t_i^p - t_i^u$ subject to the existence of a point $q = p + \alpha v$ with $B_w(q) \subset T_{C,R}(p)$ and $R = R_{p,v,w}$ provides a lower bound on the time the agent could spend tracking X_d, which the planner seeks to maximize. Therefore, the planner looks to solve the following optimization problem:

$$\begin{aligned} \Delta t^* \triangleq \max_{p,v,w,\alpha} & \left(\rho^{-1}(w) - \alpha\right) \\ s.t. & \begin{cases} B_w(p+\alpha v) \subset T_{C,R}(p), \\ R = R_{p,v,w} \in \mathcal{R}(p), \end{cases} \end{aligned} \tag{2–16}$$

given a ball $B_w(q) \subset T_{C,R}(p)$. To guarantee re-entry, it is required that $x(t_i^q) \in B_w(q)$ and $\rho(t_i^q - t_i^u) \leq w$. It then follows that $t_i^p - t_i^u \leq \rho^{-1}(w) - \alpha$ because $\alpha = t_i^q - t_i^p$.

For each $R = R_{p,v,w} \in \mathcal{R}(p)$, the Maximum Allowed Uncertainty Radius *(MAUR)* is defined as

$$\begin{aligned} \texttt{MAUR}(p,v,w) \triangleq \max_{\alpha>0} \rho(\rho^{-1}(w) - \alpha) \\ s.t.\, B_w(p+\alpha v) \subset T_{C,R}(p), \end{aligned} \tag{2–17}$$

representing the agent's budget of uncertainty at the point p for the return parameters v, w. In practice, assuming the distance between any two consecutive way points along X_d does not exceed some small $\epsilon > 0$, the optimization in (2–16) ranges over all $p = \mathcal{P}_{m'}$, $m' \geq m$, where m satisfies $o = \mathcal{P}_m$. Note that it is possible for the optimal p to satisfy $p = o$. Hence, an optimal path plan, $\pi^* = (n^*, o, p^*, q^*)$, will be given by

$$n^* \triangleq \arg\min_n \left\{ \texttt{dist}\,(n,o) : n \in \mathcal{F} \right\}, \tag{2–18}$$

$$(p^*, v^*, w^*, \alpha^*) \triangleq \arg\max_{p,v,w,\alpha} \left(\rho^{-1}(w) - \alpha \right), \tag{2–19}$$

$$q^* \triangleq p^* + \alpha^* v^*, \tag{2–20}$$

subject to the same constraints as (2–16), and noting that $p = x_{\pi^*}(\Delta t^*)$ is an implicit constraint on π^*.

2.3.5 Dwell-Time Analysis

Definition 2.2 (Feasible Region)**.** For every point $p \in \mathcal{F}^c$, let the feasible region $\mathcal{G}$ be defined by

$$\mathcal{G} \triangleq \mathcal{F} \cup \left\{ p \in \mathcal{F}^c : \frac{\texttt{dist}(p, \mathcal{F})}{v_0} < \tau(p) \right\}, \tag{2–21}$$

where $\tau(p) \triangleq \max_{v,w,\alpha} \{\rho^{-1}(w) - \alpha\}$, subject to $B_w(p+\alpha v) \subset T_{C,R}(p)$ and $R = R_{p,v,w}$. The feasible region for initialization is defined by

$$\mathcal{G}_0 \triangleq \mathcal{F} \cup \{ p \in \mathcal{F}^c \colon \tau(p) > 0 \}. \tag{2–22}$$

Theorem 2.3. *Suppose an agent is given whose motion is governed by* (2–1) *and the controller from Section 2.1.3. Moreover, suppose Assumptions 2.1–2.3 are satisfied. Let $\mathcal{F}$ be a region satisfying Assumption 2.4. Also suppose that, given $x(0) \in \mathcal{G}_0$ and $e(0) = \hat{e}(0) = \tilde{e}(0) = 0$, the agent executes a sequence of plans as follows: (a) if $x(0) \in \mathcal{F}$ then let $\pi_i = (n_i, o_i, p_i, q_i), i \geq 1$ each with an associated region $R_i \in \mathcal{R}(p_i)$ as defined in* (2–14)*; (b) otherwise, let $\pi_0 = (p_0, q_0)$ with $p_0 = x(0)$ and an associated region $R_0 \in \mathcal{R}(p_0)$, followed by a sequence of plans as in (a). If, between plan executions the agent is confined to $\mathcal{F}$, and all the plans satisfy the re-entry condition of Theorem 2.2—that is $U_{fin}(\pi_i) \subset T_{C,R_i}(p_i)$ for all i—then the actual tracking error is ultimately bounded, uniformly over $\mathcal{G}_0$ and the set of plans, provided the switching signal satisfies the maximum dwell-time condition $\rho(\Delta t_i^u) \leq \rho_{fin}(\pi_i)$, written explicitly as*

$$\Delta t_i^u \leq \frac{1}{2\lambda_u} ln \left(\frac{\lambda_u \left(\rho_{fin}(\pi_i)\right)^2}{\delta} + 1 \right), \tag{2–23}$$

where $\rho_{fin}(\pi_i)$ is defined in (2–12)*.*

Proof. For $x(0) \in \mathcal{G}_0 \setminus \mathcal{F}$ it takes at most $\rho^{-1}(\texttt{diam}(\mathcal{F}))$ time to acquire feedback. Therefore, without loss of generality assume $x(0) \in \mathcal{F}$. With Assumptions 2.1–2.3 satisfied, suppose that plan π_i also satisfies $U_{fin}(\pi_i) \subset T_{C,R_i}(p_i)$. By Theorem 2.2, x is guaranteed to re-enter into the feedback region $\mathcal{F}$, while $\rho_{fin}(\pi_i)$ bounds the error growth from above. By invoking Theorem 1 in [22] the tracking error is ultimately bounded uniformly over $\mathcal{G}_0$ and the set of plans, since it satisfies the dwell-time condition (2–23). □

Theorem 2.4. *Suppose X_d is a polygonal curve contained in the feasible region $\mathcal{G}$. Then X_d can be tracked with a guarantee of re-entry, for any initial condition $x(0) \in \mathcal{G}_0$, provided the error system is initialized with $e(0) = \hat{e}(0) = \tilde{e}(0) = 0$.*

Proof. Suppose X_d is a polygonal curve contained in the feasible region $\mathcal{G}$. For each m, let $\nu(m)$ denote the smallest $m' > m$ such that $\mathcal{P}_{m'} \notin \mathcal{F}$. The proof proceeds by

induction. For the base step, at time $t = 0$, if $x(0) \in \mathcal{F}$ then set $t_1^a = 0$; otherwise, the agent executes $\pi_0 = (p_0, q_0)$ with $p_0 = x(0)$ and $q_0 = x(0) + \alpha_0 v_0$, where (v_0, w_0, α_0) realizes the maximum in the definition of $\tau(x(0))$. By Theorem 2.2, entry into $\mathcal{F}$ is guaranteed, resulting in $t_1^a \in [0, \alpha_0]$. For the induction hypothesis, assume plans $\pi_i = (n_i, o_i, p_i, q_i = p_i + \alpha_i v_i)$, $i = 1, \ldots, k$ have been constructed so that (a) $o_1 = \mathcal{P}_0$; (b) $p_i = \mathcal{P}_{m_i}$ with $1 < m_1 < \ldots < m_k$; (c) $o_{i+1} = \mathcal{P}_{\nu(m_i)}$ for $i = 1, \ldots, k-1$; and (d) the conditions of Theorem 2.3 hold.

Let $x : [0, t_{k+1}^a] \to \mathbb{R}^D$ be an execution of these plans and note $x(t_{k+1}^a) \in \mathcal{F}$. For the induction step, compute a point $n_{k+1} \in \mathcal{F}$ at minimum distance to $o_{k+1} \triangleq \mathcal{P}_{\nu(m_k)}$. Select π_{k+1} to be the optimal plan $\pi^* = (n^*, o, p^*, q^* = p^* + \alpha^* v^*)$ from Section 2.3.4, for a choice of $n^* = n_{k+1}$ and $o = o_{k+1}$. Set $p_{k+1} = p^*$, $\alpha_{k+1} = \alpha^*$, $v_{k+1} = v^*$, and $q_{k+1} = q^*$.

Now extend x as follows: first, the agent proceeds from $x(t_{k+1}^a)$ to n_{k+1} through $\mathcal{F}$—while tracking X_d, if $\nu(m_k) > m_k + 1$—defining the behavior of x over the time interval $[t_{k+1}^a, t_{k+1}^u]$; next, the agent executes the plan π_{k+1}, which guarantees re-entry into $\mathcal{F}$ at some time $t_{k+2}^a \leq t_{k+2}^q$. Now it is required to show that the dwell-time condition $\rho\left(\Delta t_{k+1}^u\right) \leq \rho_{fin}(\pi_{k+1})$ of Theorem 2.3 is satisfied.

Since ρ is strictly increasing, this is equivalent to requiring $\Delta t_{k+1}^u \leq \rho^{-1}\left(\rho_{fin}(\pi_{k+1})\right) = t_{k+1}^q - t_{k+1}^u$. Recalling that $\Delta t_{k+1}^u = t_{k+2}^a - t_{k+1}^u$ finishes the argument. □

Remark 2.6. Note the path plan π_{k+1} in the proof covers the range of consecutive way points $o_{k+1} = \mathcal{P}_{\nu(m_k)}, \ldots, \mathcal{P}_{m_{k+1}} = p_{k+1}$ along X_d, $\nu(m_k) \geq m_k + 1$, while the preceding plan π_k covered the range $o_k = \mathcal{P}_{\nu(m_{k-1})}, \ldots, \mathcal{P}_{m_k} = p_k \subset X_d$. Hence, progress will be made along X_d by any execution of π_{k+1}. In particular, there are no Zeno executions.

2.4 Precomputation and Plan Generation

Since the geometry of the feedback region and the evolution of the region of uncertainty are known, a brute-force algorithm can be used to obtain all of the needed information for future path-planning, provided the way points $\mathcal{P}_m$, $m = 0, \ldots, M-1$,

Algorithm 2.1 Data-Set for R

Require: X_d as a list of points $\mathcal{P}_0, \ldots, \mathcal{P}_{M-1} \in \mathbb{R}^D$
Require: $\mathcal{F} = \mathtt{cl}(\mathrm{int}(C))$, C provided as a sequence of vertices
for $m := 0$ to $M - 1$ **do**
  $p \leftarrow \mathcal{P}_m$
  for $j := 0$ to $J - 1$ **do**
    $v \leftarrow v_0 \cdot \left[\cos \frac{2\pi j}{J}, \sin \frac{2\pi j}{J}\right]$
    for $k := 0$ to $K - 1$ **do**
      $w \leftarrow w_k$
      $R \leftarrow R_{p,v,w}$
      $T_{C,R}(p) \leftarrow$FINDTARGETREGION(p, R, v, w)
      $q_{m,j,k} \leftarrow$FINDTARGETPOINT($p, v, w, T_{C,R}(p)$)
      $\rho_{m,j,k} \leftarrow$Equation (2–26)
    end for
  end for
end for
return $(q_{m,j,k}, \rho_{m,j,k})_{m=0,j=0,k=0}^{M-1,J-1,K-1}$
function FINDTARGETREGION(p, R, v, w)
  $A \leftarrow R \setminus \mathcal{F}$
  for all $a \in$REGIONS(A) **do**
    if $p \in \mathring{a}$ **then**
      $B \leftarrow a$
      Exit
    end if
  end for
  return $R \setminus B$
end function
function FINDTARGETPOINT(p, v, w, T)
  $\alpha^* \leftarrow \min\{\alpha > 0 \colon B_w(p + \alpha v) \subseteq T\}$
  return $p + \alpha^* v$
end function
function REGIONS(A)
  return the list of connected components of A
end function

form a subdivision of X_d of sufficiently fine mesh[1] $\epsilon > 0$. For each m, an approximation to the solution of the optimization problem (2–16) for $\mathcal{P}_m$ is obtained by solving for $\texttt{MAUR}(\mathcal{P}_m, v, w)$—see (2–17)—over a sufficiently dense range of possible return parameters (v, w), and storing the solution in a data-set. The plans π_i constructed in the preceding section are then selected based on the information in the *data-set* to satisfy the mission objectives. To select a return trajectory, the agent solves the optimization problem in (2–19) by executing a search over the data-set.

To construct the data-set, for each point $\mathcal{P}_m$, $m = 0, \ldots, M-1$, return parameters (v_j, w_k) are considered, with $v_j \triangleq v_0 \cdot [\cos(\theta_j), \sin(\theta_j)]$, $\Theta \triangleq \left\{\theta_j \triangleq \frac{2\pi j}{J} : j = 0, \ldots, J-1\right\}$, and $W \triangleq \{w_0, \ldots, w_{K-1}\} \subset \mathbb{R}_{\geq 0}$. Given the feedback region $\mathcal{F}$, Algorithm 2.1 computes $T_{C,R}(\mathcal{P}_m)$ for each $R = R_{\mathcal{P}_m, v_j, w_k}$. Next, the nearest return target and associated MAUR are computed as

$$q_{m,j,k} \triangleq \mathcal{P}_m + \alpha_{m,j,k} v_j, \tag{2–24}$$

$$\alpha_{m,j,k} \triangleq \min\left\{\alpha > 0 : B_{w_k}(q_{m,j,k}) \subset T_{C,R}(\mathcal{P}_m)\right\}, \tag{2–25}$$

$$\rho_{m,j,k} \triangleq \rho\left(\rho^{-1}(w_k) - \alpha_{m,j,k}\right). \tag{2–26}$$

Note that $\rho^{-1}(w_k) - \alpha_{m,j,k} \leq 0$ means $\mathcal{P}_m \notin \mathcal{G}$, in which case X_d cannot be tracked with a guarantee of re-entry using this method. Also note that $v_0 \alpha_{m,j,k} = \texttt{dist}(\mathcal{P}_m, q_{m,j,k})$.

Upon termination, the result is a three dimensional array denoted by $\rho_{m,j,k} \in \mathbb{R}^{M \times J \times K}$, where each element of the array is the MAUR at point $\mathcal{P}_m \in X_d$, associated with a return trajectory $\theta_j \in \Theta$, and a width $w_k \in W$.

Remark 2.7. In some applications, it may be necessary to further restrict the MAUR to ensure a certain degree of accuracy while tracking X_d. If this is the case, the user may

[1] Recall that a subdivision S of X_d has mesh $\mu(S) \leq \epsilon$ if $\texttt{dist}(p, q) \leq \epsilon$ for every pair of consecutive points p, q in the subdivision.

use this predetermined desired upper bound as long as it is less than the MAUR at the point of departure.

The size of the data-set, $M \times J \times K$, can easily become prohibitive for optimization by brute force search. To reduce the search space, some of the iterations for the different $R \in \mathcal{R}(\mathcal{P}_m)$ may be bypassed by selecting a single return trajectory and/or single width. In the numerical experiments in Section 2.5, a single pair of return parameters, (v, w) is assigned to each $\mathcal{P}_m$. Specifically, v is set to equal the vector which bisects the smallest sector emanating from $\mathcal{P}_m$ and containing $\mathcal{F}$; next, w is selected as the largest $w_k \in W$ such that $R = R_{\mathcal{P}_m,v,w_k}$ satisfies $T_{C,R}(p) \neq \mathcal{F}$. This results in the data-set having size M. Algorithm 2 assigns the largest possible radius of uncertainty ρ_m to the points q_m, but it may fail to account for the effects of the distance traveled from $\mathcal{P}_m$ to q_m. In (2–26), maximizing w_k may come at the expense of α_m having to become large, as well. Ultimately, this simplification trades geometric information for computational efficiency.

2.5 Numerical Experiments

Experiments were conducted in MATLAB® to investigate different geometries for the feedback region. In each experiment the MAURs ρ_m generated by Algorithm 2 (Section 2.4) are compared with the corresponding MAURs—denoted by ρ'_m—generated by IBC.

Remark 2.8. In this chapter, the MATLAB® functions, `subtract`, `isinterior`, and `regions` are used to implement the operations on lines 16, 18, and 30 in Algorithm 2.1, respectively. All regions were implemented as members of the `polyshape` class in the "Elementary Polygon" library.

2.5.1 Experiment: A Generic Example

The task space is a rectangular region in the plane with unitless dimensions $2{,}048 \times 1{,}536$. Generic polygonal feedback region $\mathcal{F}$ and desired path X_d were hand-drawn (Figure 2-4). X_d was then subdivided to ensure a mesh size at most 1, resulting in $8{,}449$ way points. The parameters are $\lambda_u = 3$, δ=5, and $v_0 = 2{,}000$, to ensure $\rho'_m > 0$ exists for all m.

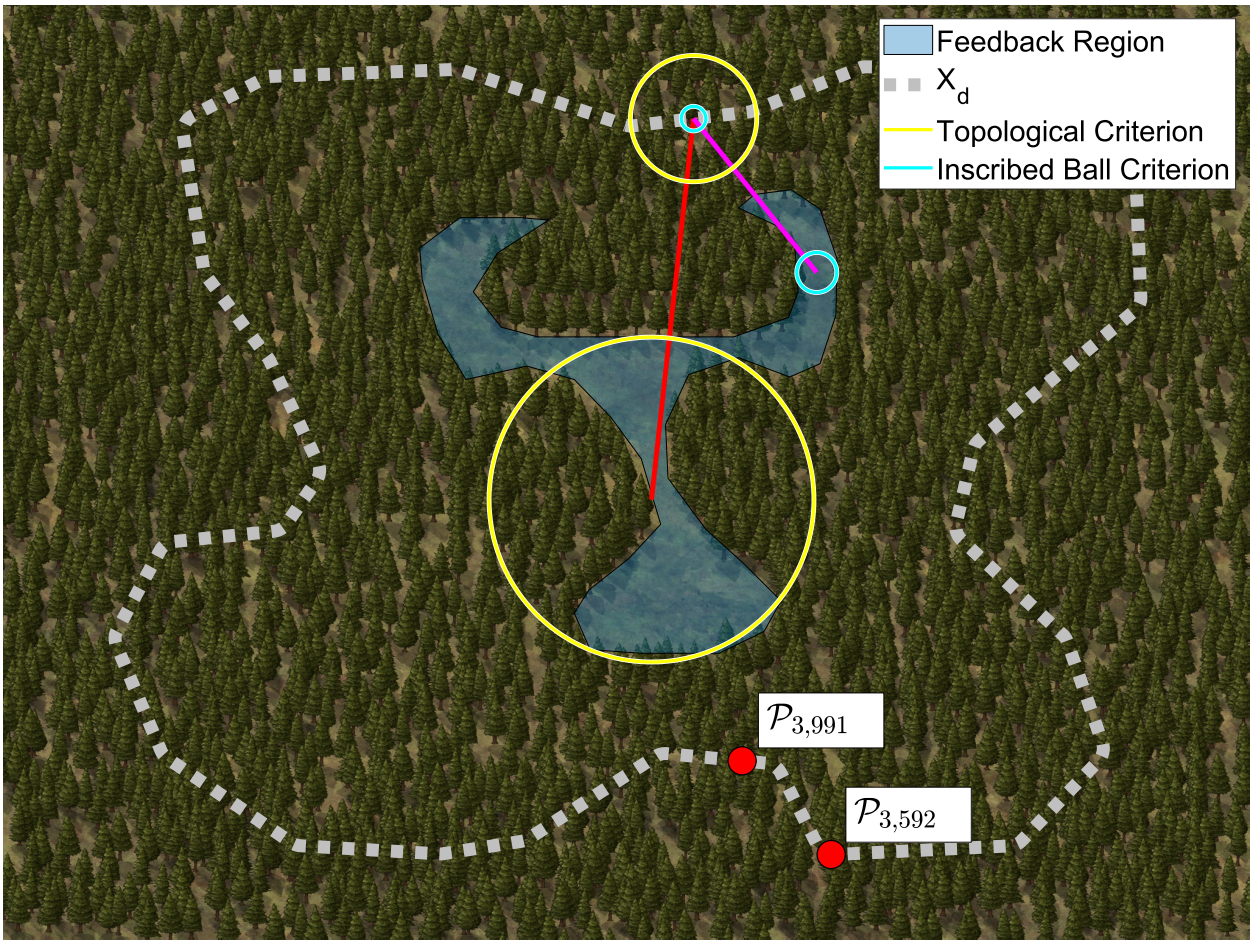

Figure 2-4. Comparison of criteria for guaranteed re-entry at a point. The MAUR for the topological criterion is larger than that of IBC. Hence, the agent can afford more uncertainty about its position while guaranteeing re-entry along a different path (red instead of magenta). Note the IBC return trajectory (magenta) is shorter, indicating a possible trade-off between maintaining tracking uncertainty budgets and minimizing deviation from the desired path.

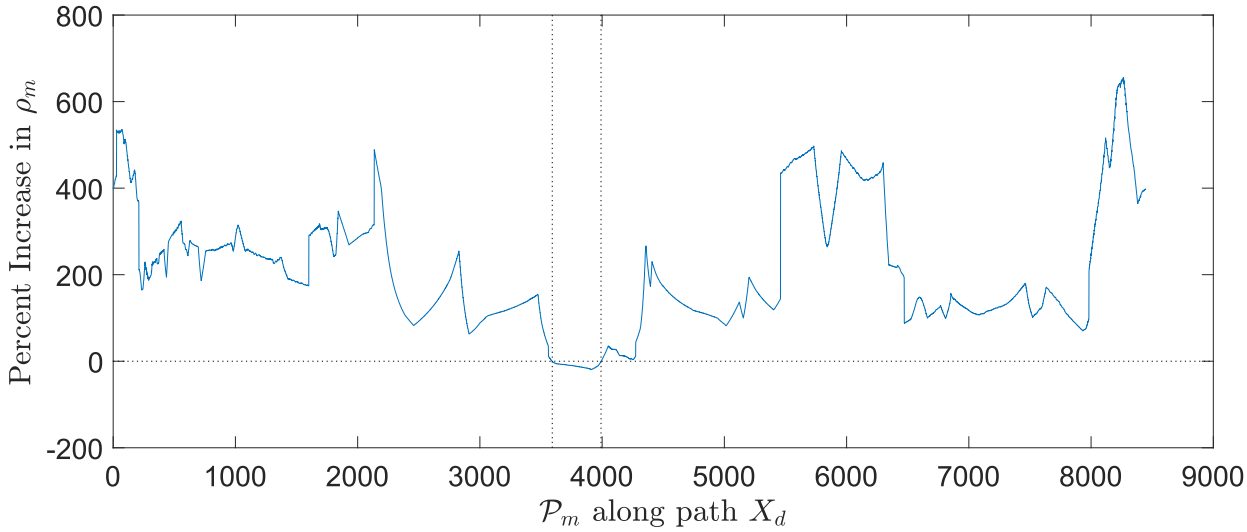

Figure 2-5. Percent increase, μ_m, in the MAUR at the point of departure $\mathcal{P}_m \in X_d$ using the proposed criterion for guaranteed re-entry. Note $\mu_m < 0$ between $\mathcal{P}_{3592}$ and $\mathcal{P}_{3991}$ (vertical dashed lines).

Figure 2-5 plots the percent increase $\mu_m \triangleq \frac{\rho_m - \rho'_m}{\rho'_m} * 100$ as a function of m. The plot indicates that Algorithm 2 provides a significant improvement over IBC for this specific geometry. However, IBC outperforms Algorithm 2 ($\mu_m < 0$) for points $\mathcal{P}_{3592}$ to $\mathcal{P}_{3991}$ (Figure 2-5; also see the points marked in Figure 2-4). This reduction in the performance of Algorithm 2 results from the MAUR being generated from only one pair of return parameters. Had Algorithm 2.1 been deployed instead of Algorithm 2, the list of possible return trajectories would have included the one suggested by IBC, guaranteeing $\mu_m \geq 0$ at every point. Despite its sub-optimal performance, for this geometry, Algorithm 2 provides an average improvement of 209% over IBC, with the largest value of μ_m being 656%.

Using a Windows 10 PC equipped with an Intel® Core™ i7-8086K CPU, the algorithms were developed and executed in MATLAB® with the assistance of the `parfor` function found in the Parallel Computing Toolbox™. Using the `tic` and `toc` functions to measure computation time, under similar computational conditions (i.e., CPU temperature, available memory, etc), the simplified algorithm required 5,332 seconds to execute while the inscribed circle method required 223 seconds to execute.

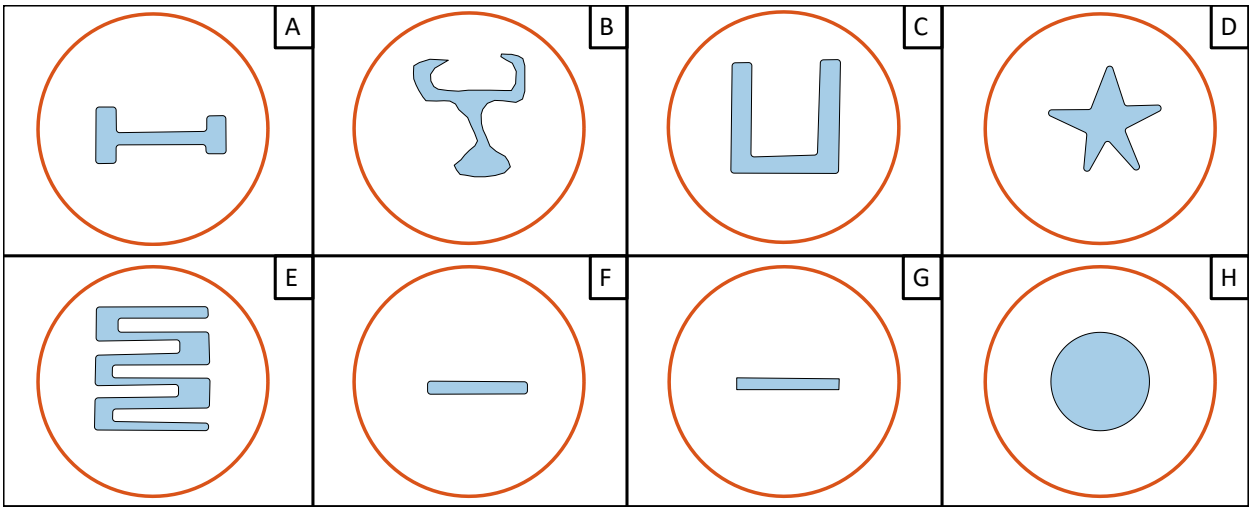

Figure 2-6. Geometries: (A) Dumbbell, (B) Generic, (C) Horseshoe, (D) Star, (E) Switchback, (F) Rounded Rectangle, (G) Standard Rectangle, (H) Circle.

2.5.2 Experiment: Sample Geometries

To gain more insight into the interaction between the uncertainty radii and the geometry of the feedback region, a select number of example feedback regions was considered (Figure 2-6). In geometries A–G, the polygons were hand drawn, and the circular region H was approximated by a regular polygon with 100 vertices.

The same parameters were used in these experiments that were used in Section 2.5.1. A polygonal approximation of a circle is used as the desired path X_d. To ensure the same mesh requirement, $6{,}401$ vertices was used. The initial point $\mathcal{P}_1$ along X_d is the rightmost point of the circle, with X_d oriented counter-clockwise.

2.5.3 Baseline Experiment: Concentric Circles

As a baseline for comparing the two methods, we replicate the settings of [22]. C and X_d were taken to be (approximate) concentric circles (Figure 2-6(H)). The two methods render near identical results: the value of μ_m fluctuates at high frequency between -0.21% and 2.74%. The fluctuations are caused by the discrete approximation of the circular boundary of the feedback region C by a regular polygon.

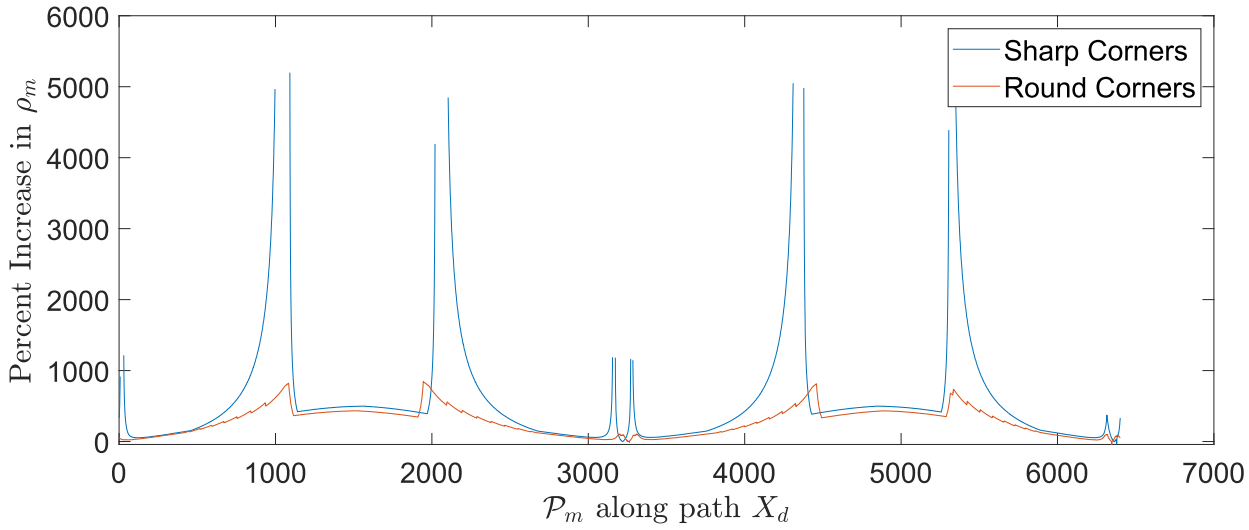

Figure 2-7. Percent increase, μ_m, in the MAUR for two types of rectangular feedback regions. One with sharp corners and one with rounded corners.

2.5.4 Baseline Experiment: Rectangles

Figure 2-7 plots the functions μ_m for the two rectangular geometries (Figure 2-6(F,G)) and confirms the intuitive argument, presented in the introduction (Figure 1-3), behind Algorithms 1 and 2. Also, note how the sharp corners of the standard rectangle cause ρ'_m to approach zero, resulting in the spikes in μ_m visible in the figure. This spiking is due to the fact that, for points $\mathcal{P}_m$ whose nearest point projection to $\mathcal{F}$ results in a return trajectory collinear with an edge of the rectangle, no inscribed ball can be constructed. Figure 2-7 demonstrates how rounding the corners mitigates this problem.

2.5.5 Comparing Multiple Geometries

Figure 2-8 presents a comparison of the functions μ_m for the geometries in Figure 2-6(A–F). The observation made in Section 2.5.4, motivated "rounding" the corners of all the feedback region shapes. Given these experiments (Figure 2-8), with a total of $46{,}855$ data points (including the generic example), the mean-average increase in the maximum allowed radius of uncertainty was found to be 233%. The largest mean-average for a single geometry was 354%, which was observed in the "star" geometry (Figure 2-6(D)), whereas the "switchback" geometry (Figure 2-6(E)) yielded the

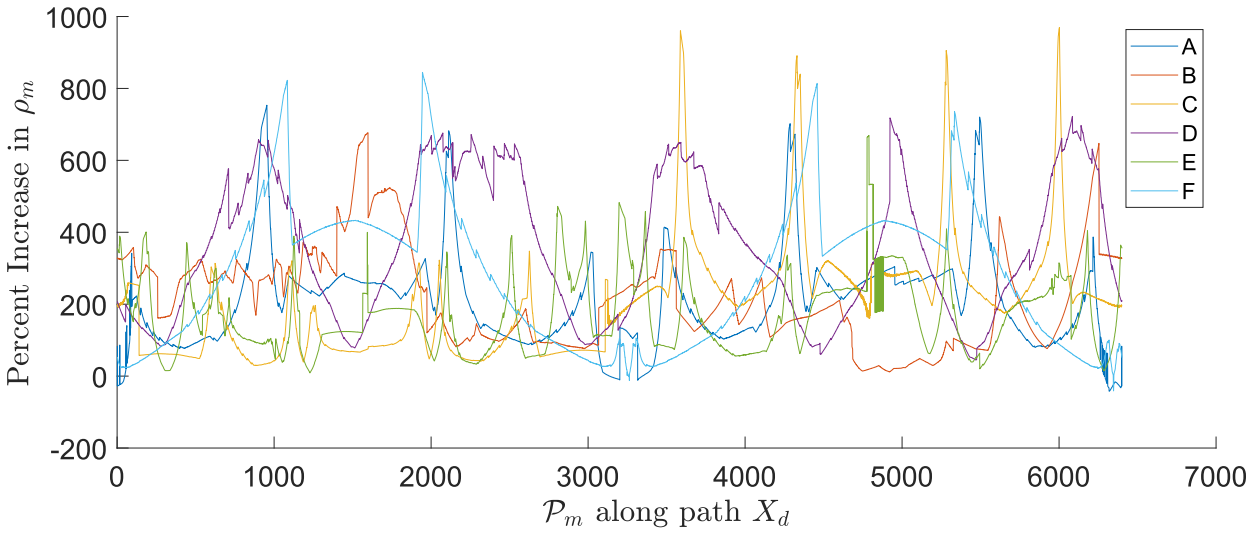

Figure 2-8. Percent increase, μ_m, in the MAUR at the point of departure from X_d for a variety of geometries.

smallest mean-average of 168%. The largest increase at a single point was found to be 969%, seen in the "horseshoe" geometry (Figure 2-6(C)). The smallest single point was found in the "dumbbell" geometry with a value of -42%.

Overall, even across a range of unique geometries, the topological criterion for guaranteed re-entry in Theorem 2.2 is superior to IBC, in terms of MAUR. The topological criterion was shown to render large improvements even though the sub-optimal Algorithm 2 was used instead of Algorithm 1. It is expected that Algorithm 1, with a much richer data-set, would generate larger values for the optimal MAUR. Moreover, Algorithm 1 is guaranteed to remove any instances where IBC outperforms the topological method. This guarantee is due to the fact the richer data-set would include the suggested return trajectories generated by IBC.

2.6 Conclusion

Given an autonomous agent in Euclidean space, a topologically motivated method for guaranteeing re-entry of the agent into a feedback region was developed, with the aim of extending the reach of existing methods to include arbitrary geometries of the feedback region. This method was integrated into an existing framework for developing

dwell-times for an autonomous system tasked with following a desired path in the presence of intermittent state feedback. A path-planning algorithm leveraging the new topological re-entry criterion is presented and evaluated against the same planner using IBC for synthetic and generic example geometries. The new topological method was shown to increase the time an agent is able to safely operate in a feedback-denied region, for a variety of geometries. A simplified and sub-optimal implementation of the new method yields improvements in the allowed error growth by hundreds of percentage points. This outcome, as well as computational inefficiencies in the current algorithm, motivate future investigation along several lines of inquiry. Among these, more efficient methods for computing MAURs and optimizing the choice of return trajectories, as well as a method for implementing the "cone of uncertainty"—rather than an infinite strip—as a target region (Section 2.3.4), are of great interest to the future development of an optimal implementation. Additionally, it could be beneficial to investigate methods for reducing the size of the region of uncertainty, as this would increase the dwell-time. Future research could also focus on applying the topological criterion for guaranteed re-entry to the task of optimizing traditional long-term tracking objectives such as total time to task completion, rather than merely maximizing each individual segment.

CHAPTER 3
MULTI-AGENT LOCALIZATION USING GEOMETRIC CONSTRAINTS WITH INTERMITTENT STATE FEEDBACK

Chapter 2 established a framework for developing dwell-time conditions and path planning techniques to guarantee stability, for systems where the objective required operation in locations where feedback is unavailable. This chapter extends the study of Relay-Explorer problems to multi-agent systems so cooperative localization can enhance the path tracking performance of each agent and extend the duration the ensemble of agents can spend operating without state feedback. To accomplish these goals, a new paradigm in cooperative localization methodology is developed that exploits the geometric qualities of the agents' dynamics and communication characteristics of a multi agent system. Hybrid system theory is used to model and analyze the proposed localization method and path planning strategy. In a comparative simulation study the cooperative behavior is shown to yield significant improvements in performance over a non-cooperative system.

3.1 Preliminaries

3.1.1 Hybrid Differential Inclusions

A hybrid differential inclusion (HDI) [49] is a tuple $\mathcal{H} = (C, D, F, G)$, denoted by:

$$\mathcal{H}: \begin{cases} \dot{z} \in F(z), & z \in C, \\ z^+ \in G(z), & z \in D, \end{cases} \tag{3–1}$$

where $F : C \rightrightarrows \mathbb{R}^n$, $G : D \rightrightarrows \mathbb{R}^n$ are called the flow and jump maps; $C, D \subset \mathbb{R}^n$ are the flow and jump sets, respectively; and z^+ indicates the value of the state after a jump. Solutions of $\mathcal{H}$ evolve continuously over the flow set according to the constraints on the dynamics imposed by the flow map. When the state is in the jump set D, it is allowed to jump to states specified by the jump map G.

A set $A \subset \mathbb{R}_{\geq 0} \times \mathbb{Z}_{\geq 0}$ is a hybrid time domain, if there is a non-decreasing sequence of non-negative reals $(t_j)_{j=0}^{m}$, $m \in \mathbb{Z}_{\geq 0} \cup \{\infty\}$, $t_0 = 0$, $t_m \in \mathbb{R}_{\geq 0} \cup \{\infty\}$, such that

$A = \bigcup_{j=1}^{\infty} I_j$, where $I_j = [t_{j-1}, t_j] \times \{j-1\}$. The sequence $(t_j)_{j=0}^m$ is called the jump sequence of the time domain A. A hybrid arc ϕ is a function $\phi : \text{dom}\phi \to \mathbb{R}^n$, where (a) $\text{dom}\phi \subset \mathbb{R}_{\geq 0} \times \mathbb{Z}_{\geq 0}$ is a hybrid time domain with jump sequence $(t_j)_{j=0}^m$; and (b) ϕ is a locally absolutely continuous function of I_j, for every j. A solution of $\mathcal{H}$ is a hybrid arc ϕ such that, for all $j > 0$, (1) $\phi(t, j-1) \in C$ for almost all $t \in [t_{j-1}, t_j]$, and $\dot{\phi}(t, j-1) \in F(\phi(t, j-1))$ for almost all $t \in I_j$; and (2) $\phi(t_{j-1}, j-1) \in D$ and $\phi(t_{j-1}, j) \in G(\phi(t_{j-1}, j-1))$. Multiple consecutive jumps during a time duration of zero in the t-coordinate of a solution $\phi(t, j)$) is said to have multiple jumps in null-time.

3.1.2 Graphs

Let $\mathcal{A} \triangleq \{1, \ldots, N\}$ be a finite non-empty set denoting a list of N agents. The configuration space over $\mathcal{A}$ is defined as $\text{Conf}(\mathcal{A}) \triangleq ((\mathbb{R})^2)^{\mathcal{A}}$. We will refer to $\mathbf{x} \triangleq (x^i)_{i \in \mathcal{A}} \in \text{Conf}(\mathcal{A})$ as a configuration of a multi agent system (MAS) of particle agents in $\mathbb{R}^2$. For any $s > 0$, the graph $\mathcal{G}_s(\mathbf{x})$ on a configuration $\mathbf{x}$ is the undirected graph with agent (or vertex) set $\mathcal{A}$ and edge set $\mathcal{E}_s(\mathbf{x})$ defined by setting $ij \in \mathcal{E}_s(\mathbf{x})$ if and only if $d_{ij} \triangleq \|x^i - x^j\| \leq s$, where we denote $ij \triangleq \{i, j\}$ for all $i, j \in \mathcal{A}$, $i \neq j$. Let $A(\mathcal{G}_s(\mathbf{x})) \triangleq [a_{ij}] \in \mathbb{R}^{N \times N}$ denote the adjacency matrix of $\mathcal{G}_s(\mathbf{x})$, where $a_{ij} = 1$ if and only if $ij \in \mathcal{E}_s(\mathbf{x})$ and $a_{ij} = 0$ otherwise. The neighborhood $\tilde{\mathcal{N}}^i(\mathbf{x})$ of an agent $i \in \mathcal{A}$ is the set of all agents $j \in \mathcal{A} \setminus \{i\}$ with $ij \in \mathcal{E}_s(\mathbf{x})$. Let $\mathcal{N}^i(\mathbf{x}) \triangleq [b_j(\mathbf{x})]_{j=1}^N \in \mathbb{R}^N$, where $b_j(\mathbf{x}) = 1$ if $d_{ij} \leq s$, or $b_j(\mathbf{x}) = 0$ if $d_{ij} > s$ or $i = j$, be the indicator vector of the set $\tilde{\mathcal{N}}^i(\mathbf{x})$. Note that $\tilde{\mathcal{N}}^i(\mathbf{x})$ coincides with the i^{th} column of the adjacency matrix of $\mathcal{G}_s(\mathbf{x})$.

3.1.3 Feedback Regions

Let $\mathcal{F} \subset \mathbb{R}^2$ denote a known region where state feedback is available. The feedback region $\mathcal{F}$ is modeled as the closure of the interior region of a polygonal Jordan Curve $\mathcal{J}$ [27]. The feedback-denied region, $\mathcal{F}^{\complement} \triangleq \mathbb{R}^2 \setminus \mathcal{F}$, is the set of states where feedback is not available, also let $\mathcal{F}^*$ denote the closure of $\mathcal{F}^{\complement}$, which is the closure of the exterior of $\mathcal{J}$.

The following notion was introduced in Chapter 2. Given a point $p \in \mathcal{F}^{\complement}$, and a closed, connected region $R \subset \mathbb{R}^2$ with $p \in R^\circ$, define $T_R(p)$ to be the collection of all points $q \in R^\circ$ for which any smooth curve $\gamma : [0,1] \to R^\circ$ from p to q must pass through a point of $\mathcal{J}$.

3.1.4 Guarantee of Re-entry and MAURs

Consider an agent at an unknown point $x_0 \in p + \rho_0 \mathbb{B}$, where $p \in \mathcal{F}^{\complement}$ and $\rho_0 > 0$ are known. The agent's motion is subject to unknown disturbances, but suppose that there is a $\bar{S} > 0$ and a known function $\rho : [0,\infty) \to [0,\infty)$ with $\rho(0) = \rho_0$ such that, for any choice of target point $q \in \mathbb{R}^2$, an available control input $u_q(\tau)$, $\tau \in [0,\infty)$ exists generating a trajectory $x_q(\tau)$ of the agent such that $x_q(0) = x_0$, $\|\dot{x}_q(\tau)\| \leq \bar{S}$ and $\|x_q(\tau) - x_\pi(\tau)\| \leq \rho(\tau)$ for all $\tau \geq 0$, where $x_\pi(\tau) \triangleq p + S\tau \frac{q-p}{\|q-p\|}$ is a constant speed reference trajectory from p to q, with $S \in \mathbb{R}_{>0}$ being the desired operating speed of the agent. Suppose also that ρ is strictly monotone increasing and unbounded, representing the fact that the uncertainty about its position grows over time. Thus, the agent's knowledge regarding its position at time τ amounts to $x_q \in U_q(\tau) \triangleq x_\pi(\tau) + \rho(\tau)\mathbb{B}$. Overall, this behavior gives rise to the uncertainty cone

$$U(p,q) \triangleq \bigcup_{\tau \in [0,\tau_q]} U_q(\tau),\ \tau_q \triangleq \tfrac{\|q-p\|}{S}. \tag{3–2}$$

The agent is tasked with reacquiring feedback, in the sense that it needs to select a point $q \in \mathbb{R}^2$ such that $x_q(\tau) \in \mathcal{F}$ is guaranteed for some $\tau > 0$. Let $R(p,q)$ denote the strip of width $2\rho(\tau_q)$ centered about the line through p and q. By Theorem 2 of [27], if the agent selects the target q, then it is guaranteed to re-enter the feedback region at some time $\tau \in (0,\tau_q]$, provided $U_q(\tau_q) \subset T_{R(p,q)}(p)$. Therefore, the set of return targets for the initial data (p,ρ_0) is defined as

$$\texttt{target}\,(p,\rho_0) \triangleq \arg\min_q \{\|q-p\| : q \in \mathbb{R}^2, U_q(\tau_q) \subset T_{R(p,q)}\,(p)\}. \tag{3–3}$$

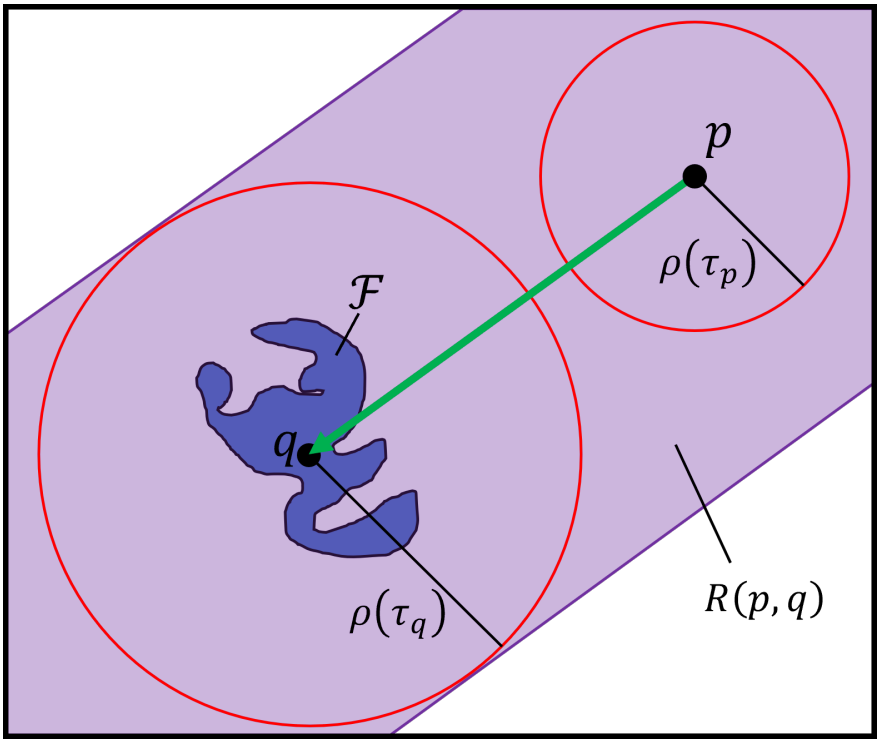

Figure 3-1. Given an uncertainty radius of $\rho(\tau_p) > \texttt{diam}(\mathcal{F})$, it is impossible to have a $U_q(\tau_q) \subseteq \mathcal{F}$ since $\texttt{diam}(U_q(\tau_q)) > 2\texttt{diam}(\mathcal{F})$.

For a point $p \in \mathcal{F}^{\complement}$ define $\texttt{ur}(p) \triangleq \{\rho \in \mathbb{R}_{\geq 0} : \texttt{target}(p, \rho) \neq \varnothing\}$. If $\rho \in \texttt{ur}(p)$ and $\rho > \rho' > 0$ then $\rho' \in \texttt{ur}(p)$. Therefore the maximum allowed uncertainty radius at p is defined as $\texttt{maur}(p) \triangleq \sup \texttt{ur}(p)$ and then $\texttt{ur}(p) = (0, \texttt{maur}(p)]$.

Remark 3.1. $\texttt{maur}(p) \leq \texttt{diam}(\mathcal{F})$, always. If not, then there is a point q with $\rho(\tau_q) > \texttt{diam}(\mathcal{F})$ and such that $R(p,q)$ contains a point of $\mathcal{F} \cap \overline{pq}$. But then $R(p,q)$ must contain the whole of $\mathcal{F}$, which implies $T_R(p) = \mathcal{F}$. But then $q \in \mathcal{F}$ and $U_q(\tau_q) \subseteq \mathcal{F}$, which is impossible because $\texttt{diam}(U_q(\tau_q)) > 2\texttt{diam}(\mathcal{F})$ (Figure 3-1).

Definition 3.1 (Feasible Region)**.** For every point $p \in \mathcal{F}^{\complement}$, let the feasible region for an agent be defined by

$$\mathcal{G} \triangleq \mathcal{F} \cup \left\{ p \in \mathcal{F}^{\complement} : \rho\left(\|p - \mathcal{F}\|/S\right) < \texttt{maur}\left(p\right) \right\}. \tag{3–4}$$

The feasible region for initialization for agent i is defined by

$$\mathcal{G}_0 \triangleq \mathcal{F} \cup \left\{ p \in \mathcal{F}^{\complement} : \texttt{maur}\left(p\right) > 0 \right\}. \tag{3–5}$$

In the presence of multiple agents $i \in \mathcal{A}$ with different dynamics these regions are denoted, respectively, by $\mathcal{G}^i, \mathcal{G}_0^i$.

Lemma 3.1. *$\mathcal{G}_0$ is bounded.*

Proof. Let $p \in \mathcal{G}_0$ and $q \in \texttt{target}(p, \rho)$, for $\rho \in \texttt{ur}(p)$. By Remark 3.1, $\rho \leq \texttt{diam}(\mathcal{F}) \triangleq \delta$, so $q \in \mathcal{F} + \delta\mathbb{B}$. Since $\mathcal{F} + \delta\mathbb{B}$ is compact, $\tau_q \leq T(p)$ where $T(p)$ is independent of the choice of q. Since $\|\dot{x}_q\| \leq \bar{S}$ and $x_q(\tau) \in \mathcal{F}$ for some $\tau \in [0, \tau_q]$, we conclude that $\|p - x_q(\tau)\| \leq \tau_q \bar{S}$, as desired. □

Corollary 3.1. *There is $\vartheta > 0$ with $\vartheta\mathbb{B} \supseteq \mathcal{G}_0 + \texttt{diam}(\mathcal{F})\mathbb{B}$.*

3.2 Problem Formulation

3.2.1 Individual Agent Characteristics

Consider a single agent i with state variables $Z^i = [x^i, \hat{x}^i, x_\pi^i, \tau^i]$, where $x^i : [0, \infty) \to \mathbb{R}^2$, $\hat{x}^i : [0, \infty) \to \mathbb{R}^2$, $x_\pi^i : [0, \infty) \to \mathbb{R}^2$, and $\tau^i : [0, \infty) \to [0, \infty)$ denote the true position state, the estimated position state, the desired position state, and the agent's personal clock, respectively. The agent has two modes of operation: state feedback is available (i.e., $x^i \in \mathcal{F}$) and state feedback is unavailable (i.e., $x^i \in \mathcal{F}^{\complement}$). When feedback is available the agent has dynamics described by the differential inclusion[1]

$$\dot{Z}^i \in F_a^i\left(Z^i\right) \triangleq \left\langle\!\left\langle \boldsymbol{\Delta}\left(\mathcal{D}^i + \bar{d}^i\mathbb{B}\right), v_\pi^i(\tau^i), 1\right\rangle\!\right\rangle, \tag{3–6}$$

where $\mathcal{D}^i = \mathcal{D}^i(Z^i) = f^i(x^i) + u^i(Z^i)$, $f^i : \mathbb{R}^2 \to \mathbb{R}^2$ is the locally Lipschitz drift dynamics; $\bar{d}^i > 0$ is a known bound on the norm of the unknown disturbance; $u^i : \mathbb{R}^6 \to \mathbb{R}^2$ is the controller; and $v_\pi^i(\tau^i) = \dot{x}_\pi^i(\tau^i)$ is the desired trajectory to be tracked. When feedback is unavailable the agent has dynamics described by the differential inclusion

$$\dot{Z}^i \in F_u^i\left(Z^i\right) \triangleq \left\langle\!\left\langle \mathcal{D}^i + \bar{d}^i\mathbb{B}, \hat{\mathcal{D}}^i, v_\pi^i(\tau^i), 1\right\rangle\!\right\rangle, \tag{3–7}$$

[1] When feedback is available $\hat{x}^i = x^i$, thus the $\boldsymbol{\Delta}$ operator is used to force this fact for all $\dot{Z}^i$.

where $\hat{\mathcal{D}}^i = \hat{\mathcal{D}}^i(Z^i) = f^i(\hat{x}^i) + u^i(Z^i)$. Note the difference between (3–6) and (3–7), where the former enforces equality between the first two coordinates and the second enforces separate constraints on the same coordinates. The dynamics in (3–6) and (3–7) imply that the state estimate $\hat{x}^i$ flows according to the predictor $\hat{\mathcal{D}}^i$ when feedback is unavailable, while coinciding with x^i when feedback is available. The controller u^i needs to be designed so that it does not depend on x^i when feedback is unavailable. This need motivates the definition of three error signals as

$$e^i \triangleq x^i - x^i_\pi, \quad \hat{e}^i \triangleq \hat{x}^i - x^i_\pi, \quad \tilde{e}^i \triangleq x^i - \hat{x}^i, \tag{3–8}$$

where $e^i, \hat{e}^i, \tilde{e}^i \in \mathbb{R}^2$ are the true tracking error (TTE), estimated tracking error (ETE) and state estimation error (SEE), respectively. Only $\hat{e}^i$ is measurable when feedback is unavailable.

3.2.2 Cooperative Control Objective

Each agent i with state $x^i : [0, \infty) \to \mathbb{R}^2$ is tasked with following a prescribed polygonal path X^i_d provided as a sequence of waypoints $\mathcal{P}^i_\kappa \in \mathbb{R}^2 \setminus \partial\mathcal{F}$, $\kappa = 1, \ldots, M^i$. Let the arc length of the sub-path of X^i_d from a point $p \in [\mathcal{P}_{k-1}, \mathcal{P}_k]$ to a point $q \in [\mathcal{P}_l, \mathcal{P}_{l+1}]$, $1 \leq k \leq l$, be defined as

$$\Lambda^i(p, q) \triangleq \|p - \mathcal{P}^i_k\| + \sum_{\kappa=k}^{l-1} \|\mathcal{P}^i_{\kappa+1} - \mathcal{P}_\kappa\| + \|q - \mathcal{P}^i_l\|. \tag{3–9}$$

Repeated dead-reckoning with a state estimator $\hat{x}^i : [0, \infty) \to \mathbb{R}^2$ along the sequence of way points is inherently unstable outside of $\mathcal{F}$, because the actual position and state estimator drift away from one another. This intermittency in state feedback motivates an approach where each agent i follows a sequence of auxiliary trajectories x^i_π relaying between the desired path and the feedback region (Figure 3-2). The challenge is to regulate the norms of the TTE $e^i = x^i - x^i_\pi$ for every agent. The tracking objective for agent i is defined as regulating the signal e^i to a ball, and communication between agents will be used to reduce the SEE component of the regulation objective.

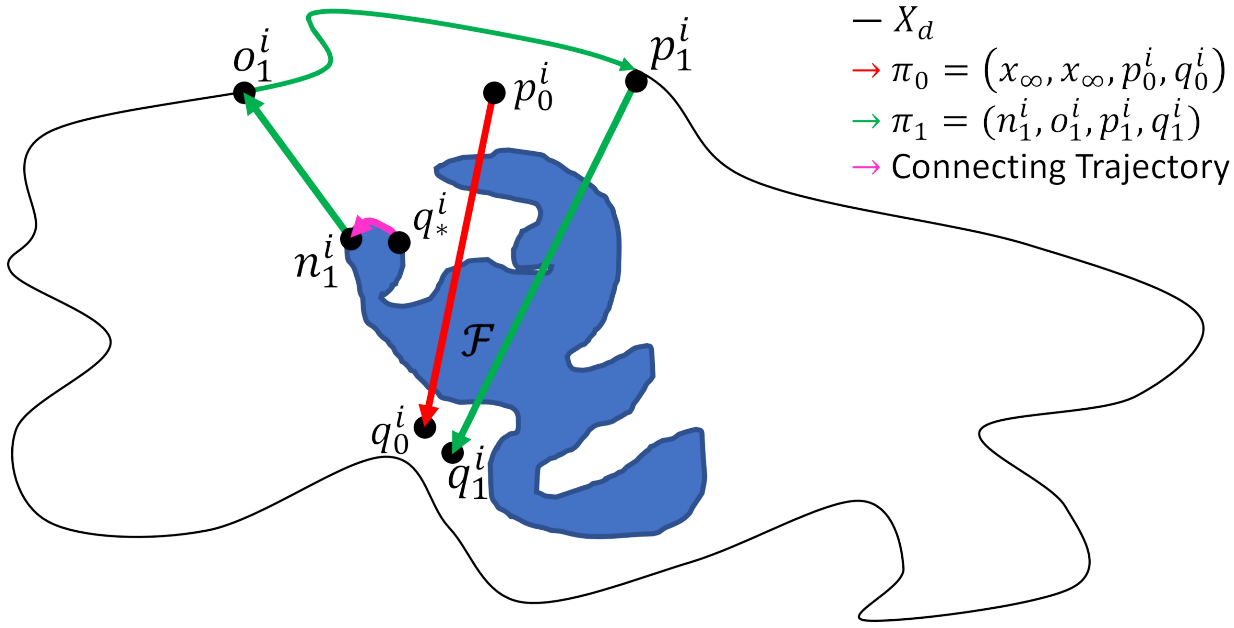

Figure 3-2. Depiction of two auxiliary path plans, and a connecting trajectory. In red, an auxiliary trajectory parameterized by $\pi^i = (x_\infty, x_\infty, p^i, q^i)$ is used for the purpose of initially gaining feedback. In green, an auxiliary trajectory x_π^i, defined by a path plan $\pi^i = (n^i, o^i, p_2^i, q_2^i)$, is superimposed over the desired path X_d^i, for a generic feedback region $\mathcal{F}$ (Definition 1). In pink, a connecting trajectory is used to join the path plan q_*^i to n_1^i. Note that the point q^i need not lie in $\mathcal{F}$.

Observe that the problem is only feasible if $X_d^i \subset \mathcal{G}^i$ and $x^i(0) \in \mathcal{G}_0^i$. By Corollary 3.1, there exists $\vartheta > 0$ such that $\vartheta\mathbb{B}$ contains $\mathcal{G}_0^i + \texttt{diam}(\mathcal{F})\mathbb{B}$ for all agents $i \in \mathcal{A}$. A point x_∞ is selected for future use such that

$$x_\infty \in \mathbb{R}^2 \setminus \vartheta\mathbb{B} \subseteq \mathbb{R}^2 \setminus \bigcup_{i\in\mathcal{A}} \left(\mathcal{G}_0^i + \texttt{diam}(\mathcal{F})\mathbb{B}\right). \tag{3–10}$$

Definition 3.2 (Auxiliary Trajectory)**.** There are two types of auxiliary trajectories. The auxiliary trajectory $x_\pi^i : [0, \infty) \to \mathbb{R}^2$ with path plan $\pi^i = (n^i, o^i, p^i, q^i) \in \mathbb{R}^8$ is a function $x_\pi^i = x_\pi^i(\tau^i)$, defined as the concatenation of four trajectories determined by five way points: $x_\pi^i(0)$ is the initial point at which the plan is computed; the n^i is the point of departure from the feedback region; $o^i = \mathcal{P}_\ell^i$ is the first point along a segment of X_d^i the agent selects to follow; $p^i = \mathcal{P}_{\ell'}^i$ for $\ell' \geq \ell$, is the point of departure from X_d^i; and q^i is the target point for the return trajectory to the feedback region. From the initial point $x_\pi^i(0)$ to

n^i a path is selected that is entirely contained within $\mathcal{F}$. From n^i to o^i, x^i_π coincides with a straight line trajectory with speed S^i; this path is referred to as leg $\overline{no}$ of the plan π. From o^i to p^i, x^i_π coincides with the desired path X^i_d, with a piecewise linear parametrization with speed S^i; this path is referred to as leg $\overline{op}$ of π. Then, from p^i to q^i, x^i_π coincides with the straight line trajectory from p^i through q^i with speed S^i; this path is referred to as leg $\overline{pq}$ of π. For the second type of auxiliary trajectory—with plan $\pi^i = (x_\infty, x_\infty, p^i, q^i)$, see (3–10)—set x^i_π to coincide with a linearly parameterized ray from p^i through q^i with speed S^i. The variable τ^i is a personal clock for agent i, which is reset to zero each time the agent departs from the feedback region. Let $\tau^i_o, \tau^i_p, \tau^i_q$ be the values of τ^i determined by $x^i_\pi(\tau^i_o) = o^i$, $x^i_\pi(\tau^i_p) = p^i$, and $x^i_\pi(\tau^i_q) = q^i$ (the scheduled arrival times for each way point). Additionally, let $v^i_\pi \triangleq \dot{x}^i_\pi$, which is defined for all $\tau^i \in [0, \infty)$, except possibly for $\tau^i = \tau^i_o, \tau^i_p, \tau^i_q$, and the times corresponding to the break points $\mathcal{P}^i_k$, $\ell < k < \ell'$. Note that, $v^i_\pi(\tau^i) \in \mathbb{R}^2$ is piecewise constant and eventually constant because x^i_π is piecewise linear, as depicted in Figure 3-2. The set of all plans for agent i is denoted by $\texttt{Plans}^i$.

Plans $\pi^i = (x_\infty, x_\infty, p^i, q^i)$ are used for acquisition of feedback from points $p^i \notin \mathcal{F}$, while plans $\pi^i = (n^i, o^i, p^i, q^i)$ are used for tracking X^i_d and reacquiring feedback. The execution of an auxiliary trajectory terminates the moment feedback is reacquired, at a point q^i_*, and a new plan of type $\pi^i = (n^i, o^i, p^i, q^i)$ is computed, together with a plan of the agent's motion through $\mathcal{F}$ from the point q^i_* to the departure point of the new plan.

Definition 3.3 (Connecting Trajectory)**.** Given points $q^i_*, n^i \in \mathcal{F}$, a connecting trajectory from q^i_* to n^i is an absolutely continuous trajectory $x^i_\pi : [0, \tau^i_n] \to \mathcal{F}$ with $x^i(0) = q^i_*$ and $x^i_\pi(\tau^i_n) = n^i$.

3.3 Controller Design

3.3.1 Agent Controller

Based on (3–8) and the subsequent stability analysis, the controller u^i is designed as

$$u^i \triangleq \begin{cases} \psi^i\left(x^i, e^i, k_1^i, \beta^i, \tau^i\right) - \bar{d}^i \text{sgn}(e^i), & x^i \in \mathcal{F}, \\ \psi^i\left(\hat{x}^i, \hat{e}^i, k_2^i, \alpha^i, \tau^i\right), & x^i \in \mathcal{F}^{\complement}, \end{cases} \tag{3–11}$$

where $k_1^i > 0$, $k_2^i > 0$, $\alpha^i \in (0,1)$, and $\beta^i \in (0,1)$ are control gains, and ψ^i is the continuous[2] function, for $\gamma > 0$,

$$\psi^i\left(\xi, \eta, \kappa, \gamma, \tau^i\right) \triangleq v_\pi^i\left(\tau^i\right) - f^i\left(\xi\right) - \kappa|\eta|^\gamma \odot \text{sgn}(\eta). \tag{3–12}$$

To bound the error signals as functions of time, the Lyapunov candidates

$$V_e^i \triangleq \frac{1}{2}\|e^i\|^2, \quad V_{\hat{e}}^i \triangleq \frac{1}{2}\|\hat{e}^i\|^2, \quad V_{\tilde{e}}^i \triangleq \frac{1}{2}\|\tilde{e}^i\|^2, \tag{3–13}$$

are considered, where $V_e^i, V_{\hat{e}}^i, V_{\tilde{e}}^i : \mathbb{R}^2 \to \mathbb{R}_{\geq 0}$. Since the controller defined in (3–11) has a discontinuous right side when $x^i \in \mathcal{F}$, generalized time derivatives from [56] are used to evaluate the evolution of the Lyapunov candidates.

Definition 3.4 (Generalized time derivative)**.** Let $F : \mathbb{R}^n \rightrightarrows \mathbb{R}^n$ have nonempty and compact values. The generalized time derivative of a locally Lipschitz-continuous function $V : \mathbb{R}^n \to \mathbb{R}$ with respect to F is the function $\dot{\overline{V}}_F : \mathbb{R}^n \to \mathbb{R}$ defined as

$$\dot{\overline{V}}_F(x) \triangleq \max_{p \in \eth V(x)} \max_{q \in F(x)} p^\top q, \tag{3–14}$$

where $\eth V$denotes the Clarke gradient of V [57].

Remark 3.2. Note that, $\dot{V}(x(t)) \leq \dot{\overline{V}}_F(x(t))$ for any solution $x(t)$ of the differential inclusion $\dot{x} \in F(x)$.

[2] See [55] for discussion.

Since V_e^i is continuous, its generalized time derivative with respect to F_a^i reduces to

$$\left(\dot{\overline{V}}_e^i\right)_{F_a^i} \triangleq \max_{q \in F_a^i} [e^i, 0, -e^i, 0] q. \tag{3–15}$$

Substituting (3–6) and (3–11) into (3–15) yields

$$\left(\dot{\overline{V}}_e^i\right)_{F_a^i} = -k_1 \|e^i\|_{\beta^i+1}^{\beta^i+1} - \bar{d}^i \|e^i\|_1 + \bar{d}^i \max_{Y \in \mathbb{B}} \left(e^i\right)^\top Y. \tag{3–16}$$

Using (3–13), and the facts $\|e^i\|_{\beta^i+1} \geq \|e^i\|_2$ and $\max_{Y \in \mathbb{B}} (e^i)^\top Y \leq \max_{Y \in \mathbb{B}} \|e^i\| \|Y\| \leq \|e^i\| \leq \|e^i\|_1$, (3–16) is bounded as

$$\left(\dot{\overline{V}}_e^i\right)_{F_a^i} \leq -2^{\frac{\beta^i+1}{2}} k_1^i \left(V_e^i\right)^{\frac{\beta^i+1}{2}}, \quad x^i \in \mathcal{F}. \tag{3–17}$$

Similar to the steps taken to obtain (3–15), the generalized time derivatives of $V_{\hat{e}}^i$ and $V_{\tilde{e}}^i$ with respect to F_u^i reduce to

$$\left(\dot{\overline{V}}_{\hat{e}}^i\right)_{F_u^i} = -2^{\frac{\alpha^i+1}{2}} k_2 \left(V_{\hat{e}}^i\right)^{\frac{\alpha^i+1}{2}}, \quad x^i \in \mathcal{F}^{\complement}, \tag{3–18}$$

and

$$\left(\dot{\overline{V}}_{\tilde{e}}^i\right)_{F_u^i} = f^i\left(x^i\right) - f^i\left(\hat{x}^i\right) + \bar{d}^i \max_{Y \in \mathbb{B}} \left(\tilde{e}^i\right)^\top Y, \quad x^i \in \mathcal{F}^{\complement}. \tag{3–19}$$

Then using the fact that $\max_{Y \in \mathbb{B}} (\tilde{e}^i)^\top Y \leq \|\tilde{e}^i\|_2$, the Lipschitz property of f^i, and Young's inequality, (3–19) is bounded as

$$\left(\dot{\overline{V}}_{\tilde{e}}^i\right)_{F_u^i} \leq 2\lambda^i V_{\tilde{e}}^i + \delta^i, \quad x^i \in \mathcal{F}^{\complement}, \tag{3–20}$$

where $\lambda^i = L^i + \frac{1}{2\epsilon^i}$, $\delta^i = \frac{\epsilon^i}{2}(\bar{d}^i)^2$, L^i is a Lipschitz constant for f^i, $\delta^i \triangleq \frac{1}{2}(\bar{d}^i)^2$, and $\epsilon^i > 0$. By Remark 3.2, integrating (3–20) over $[t_0, t]$ along a solution of the closed loop differential inclusion (3–7), substituting in $V_{\tilde{e}}^i$ from (3–13), and solving for $\|\tilde{e}^i(t)\|$ yields

$$\|\tilde{e}^i(t)\| \leq \sqrt{\|\tilde{e}^i(t_0)\|^2 \mathrm{e}^{2\lambda^i \Delta t} + \frac{\delta^i}{\lambda^i}\left(\mathrm{e}^{2\lambda^i \Delta t} - 1\right)}. \tag{3–21}$$

For the case where $\hat{e}^i \in \mathbb{R}$, integrating (3–18) over $[t_0, t]$, substituting $V_{\hat{e}}^i$ from (3–13), and then solving for $\hat{e}^i$ yields

$$\hat{e}^i = \begin{cases} \left(|\hat{e}^i(t_0)|^{A^i} - k_2^i A^i \Delta t\right)^{\frac{1}{A^i}} \operatorname{sgn}(\hat{e}^i(t_0)), & \Delta t < T_s^i\left(\hat{e}_0^i\right), \\ 0, & \Delta t \geq T_s^i\left(\hat{e}_0^i\right), \end{cases} \tag{3–22}$$

where $\Delta t \triangleq t - t_0$, $A^i \triangleq 1 - \alpha^i$, and $T_s^i(\hat{e}_0^i) \triangleq \frac{1}{k_2^i A^i}|\hat{e}^i(t_0)|$ is a settling time function [55]. Expanding (3–22) to non-scalar error systems, while considering the possible differences in settling times between coordinates, yields

$$\hat{e}^i(t) = \left[\texttt{ReLu}\left(|\hat{e}^i(t_0)|^{A^i} - k_2^i A^i \Delta t \cdot \mathbf{1}\right)\right]^{\frac{1}{A^i}} \odot \operatorname{sgn}\left(\hat{e}_0^i\right), \tag{3–23}$$

where $\texttt{ReLu}(\cdot)$ captures the nature of the piecewise expression in (3–22). Note that $\|\hat{e}^i(t)\| = 0$ for $\Delta t \geq T_s^i(\hat{e}^i(t_0)) \triangleq \frac{1}{k_2^i A^i}\|\hat{e}^i(t_0)\|_\infty^{A^i}$, where the infinity norm accounts for the possible differences in settling times between each coordinate of $\hat{e}$.

Provided the bounds on the initial conditions $\hat{\varrho}^i = \hat{e}^i(t_0)$, and $\tilde{\varrho}^i \geq \|\tilde{e}^i(t_0)\|$ are satisfied, an upper bound, representing the worse case estimate for the growth of the TTE (i.e., $e^i = \hat{e}^i + \tilde{e}^i$), for the interval $[t_0, t]$ is

$$\rho^i\left(\Delta t, \hat{\varrho}^i, \tilde{\varrho}^i\right) \triangleq \|\hat{\rho}^i\left(\Delta t, \hat{\varrho}^i\right)\| + \tilde{\rho}^i\left(\Delta t, \tilde{\varrho}^i\right), \tag{3–24}$$

where

$$\hat{\rho}^i\left(\Delta t, \hat{\varrho}^i\right) \triangleq \left[\texttt{ReLu}\left(|\hat{\varrho}^i|^{A^i} - k_2^i A^i \Delta t \cdot \mathbf{1}\right)\right]^{\frac{1}{A^i}} \odot \operatorname{sgn}\left(\hat{\varrho}^i\right), \tag{3–25}$$

and

$$\tilde{\rho}^i\left(\Delta t, \tilde{\varrho}^i\right) \triangleq \sqrt{\left(\tilde{\varrho}^i\right)^2 \mathrm{e}^{2\lambda^i \Delta t} + \frac{\delta^i}{\lambda^i}\left(\mathrm{e}^{2\lambda^i \Delta t} - 1\right)}. \tag{3–26}$$

Additionally, the rate at which $\tilde{\rho}$ grows, given the initial condition $\tilde{\varrho}^i$, is found by computing the time derivative of (3–26), yielding

$$\dot{\tilde{\rho}}^i \triangleq \left[\lambda^i \left(\tilde{\varrho}^i\right)^2 + \delta^i\right] \mathsf{e}^{2\lambda^i \Delta t} \left(\tilde{\rho}^i\right)^{-1}. \tag{3–27}$$

Remark 3.3. The use of the sliding mode controller (3–11) implicitly assumes agent i is capable of sampling e^i at infinite frequency. This allows the TTE to be null through each traversal of the feedback region. In practice, however, small fluctuations of the TTE will occur, which may cause unexpected departures from the feedback region. This issue is addressed in Section 3.5 by insetting the feedback region..

3.3.2 State Estimation

3.3.2.1 Communication and Extended State Structures

For the purpose of reducing the SEE $\tilde{e}^i$ for agent $i \in \mathcal{A}$, agent i will intermittently request information from any agent at a distance no more than R_{comm} away, where R_{comm} is the communication radius. For each agent i, a sample-and-hold state variable $\mathcal{N}^i \in \{0,1\}^N \subset \mathbb{R}^N$ is introduced to keep track of the set of agents $j \neq i$ with which i communicated last, to aid in computations reducing $\tilde{e}^i$. The hybrid dynamics of $\mathcal{N}^i$ is given by $\dot{\mathcal{N}}^i = 0$ between sampling events and $(\mathcal{N}^i)^+ = \mathcal{N}^i(\mathbf{x})$ during sampling events (see notation in Section 3.1.2, where s is selected as $s = R_{\text{comm}}$).

Each agent has the extended state

$$X^i \triangleq \left(\mathcal{N}^i, \pi^i, \mathtt{mode}^i, x^i, \hat{x}^i, x^i_\pi, \tau^i, \tau^i_{\text{trig}}, \tilde{\rho}^i, \mathtt{b}^i\right) \tag{3–28}$$

and state space

$$\mathcal{X}^i \triangleq \langle\langle \{0,1\}^N, \mathtt{Plans}^i, \{0,1,2,3\}, \mathbb{R}^6, [0,\infty)^3, \{0,1\}\rangle\rangle, \tag{3–29}$$

where $\mathtt{mode}^i \in \{0,1,2,3\}$ is the operating mode of agent i, as defined in Figure 3-3, $\tau^i_{\text{trig}} \in [0,\infty)$ is a timing variable, and $\mathtt{b}^i \in \{0,1\}$ is a binary variable used for enforcing the order of jumps (Section 3.5).

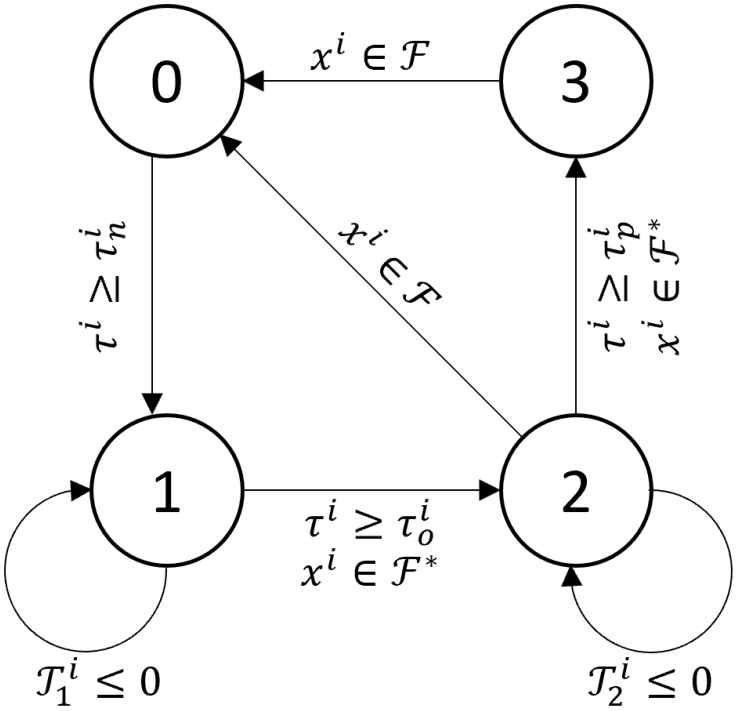

Figure 3-3. Illustration of the operational modes for agent i. $\texttt{mode}^i = 0$ when $x^i \in \mathcal{F}$. Otherwise, $\texttt{mode}^i = 1$ when $\tau^i \geq \tau_n^i$, $\texttt{mode}^i = 2$ when $\tau^i \geq \tau_o^i$, and $\texttt{mode}^i = 3$ when $\tau^i \geq \tau_p^i$. Arrows $(n \to m)$ represent jump transitions between modes. Arrow labels represent an idealized set of conditions for transitioning between modes. $\mathcal{T}_m$, $m = 1, 2$ are trigger functions, which will be discussed in detail in Section 3.4. Note that some conditions for mode transitions are suppressed, and will be discussed in further detail in Section 3.5.

The ensemble state space is defined as $\mathcal{X} \triangleq \prod_{i\in\mathcal{A}} \mathcal{X}^i$, where $X \triangleq (X^i)_{i\in\mathcal{A}}$. Observe that $\mathcal{X}$ is the finite disjoint union of the closed sets $\mathcal{X}^A$ where $A \in \{0,1\}^{N\times N}$ and $X \in \mathcal{X}^A$ if and only if $\mathcal{N}^i$ coincides with the i^{th} column of A for all $i \in \mathcal{A}$. The subspace $\mathcal{X}^A$ may be regarded as the state space for a system of agents gathering information from neighbors assigned by the matrix A, regardless of distances.

3.3.2.2 Cooperative State Estimation

For each agent $i \in \mathcal{A}$ the region of uncertainty about the position x^i is defined as $U^i \triangleq \hat{x}^i + \tilde{\rho}^i\mathbb{B}$, where $\tilde{\rho}^i$ is the agent's current bound on $\|\tilde{e}^i\|$. However, the agent may attempt to communicate with its neighbors $\mathcal{N}^i$ to improve the error bound $\tilde{\rho}^i$, as follows. Let $\tilde{\mathcal{N}}^i$ denote the set of $j \in \mathcal{A}$ such that $\mathcal{N}^i_j = 1$. For any $j \in \tilde{\mathcal{N}}^i$, it follows that $x^i \in U^j_i \triangleq d_{ij}\mathbb{S} + U^j = (\hat{x}^j + d_{ij}\mathbb{S}) + \tilde{\rho}^j\mathbb{B}$. Note that U^j_i is either a ball (when $d_{ij} < \tilde{\rho}^j$) or an annulus about $\hat{x}^j$, with internal radius $d_{ij} - \tilde{\rho}^j$ and external radius $d_{ij} + \tilde{\rho}^j$ (Figure 3-5). Taking into account all $j \in \tilde{\mathcal{N}}^i$ yields

$$x^i \in \hat{U}^i(X) \triangleq U^i \cap \bigcap_{j\in\tilde{\mathcal{N}}^i} U^i_j(X). \tag{3–30}$$

Instead of modeling the exact shape of $\hat{U}^i$ as a function of τ^i, the circumscribed ball about $\hat{U}^i$ is used to bound the SEE as

$$(P^i, H^i) \triangleq \arg\min_{r,h} \left\{ r \geq 0, h \in \mathbb{R}^2 : \hat{U}^i \subseteq h + r\mathbb{B} \right\}, \tag{3–31}$$

where P^i, H^i are the circumradius and circumcenter of this ball, respectively, and are uniquely defined by X^i and X^j, $j \in \tilde{\mathcal{N}}^i$ (Figure 3-4). By construction, $P^i \leq \tilde{\rho}^i$, making it potentially advantageous to apply jumps with an update of the form $(\tilde{\rho}^i)^+ = P^i$, $(\hat{x}^i)^+ = H^i$ when $P^i < \tilde{\rho}^i$, though additional conditions must be considered, which are reflected in a collection of event triggers discussed in Section 3.4.

During implementation, computing $\hat{U}^i(X)$, but more importantly P^i and H^i, may be done using Boolean set operations found in standard computational geometry libraries. For example, the Computational Geometry Algorithms Library (CGAL) [58] will output

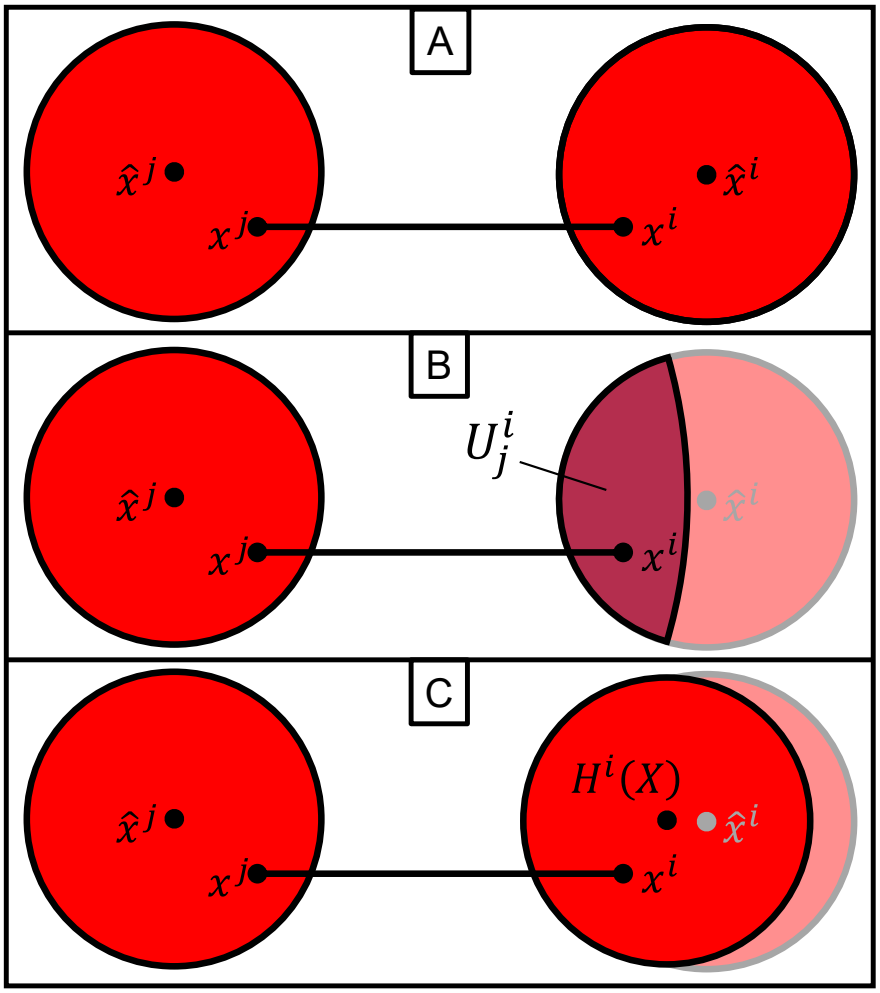

Figure 3-4. Illustration of the process for calculating updated radius of uncertainty $P^i(X)$ and the updated state estimate $H^i(X)$. First, in sub-figure A, the relative distance measurement between agents i and j is illustrated. Second, in sub-figure B, U_j^i is illustrated. Finally, the updated radius of uncertainty $P^i(X)$ and the updated state estimate $H^i(X)$ is illustrated, which was determined by a minimum bounding circle algorithm.

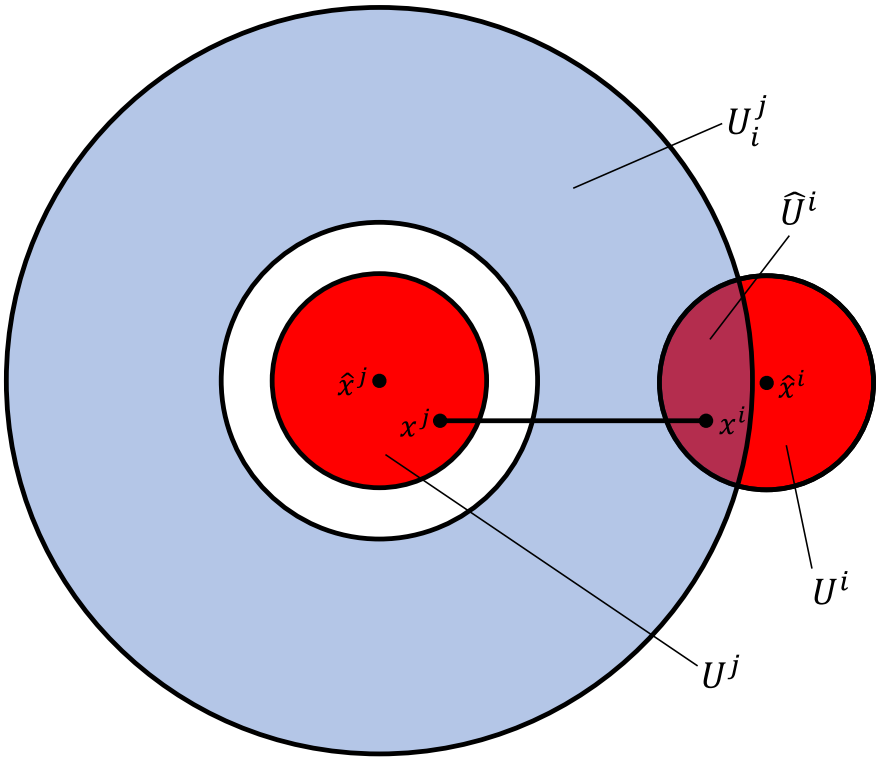

Figure 3-5. Illustration of relative distance measurements between agents i and j being used to compute $U_i^j(X)$ and $\hat{U}^i(X)$.

an arrangement of circular arcs exactly representing the boundary of $\hat{U}^i$; following this, an algorithm for enclosing these arrangements of continuous arcs produces P^i and H^i (e.g., the algorithms in [59] and [60]). Other minimum enclosing ball algorithms such as [61] can be used for simpler implementations of the state estimation update algorithm, where $\hat{U}^i$ is upper bounded by a polygon.

In general, H^i and P^i are not continuous as functions of $\mathbf{x}$ (that is, with $\mathcal{N}^i(\mathbf{x})$ substituted for $\mathcal{N}^i$) because of the discontinuous changes in the collection of neighbor sets $\mathcal{N}^i(\mathbf{x})$. For each $i \in \mathcal{A}$, trajectories of the sample-and-hold dynamics of $\mathcal{N}^i$ may not coincide with $\mathcal{N}^i(\mathbf{x})$, see Figure 3-6. In fact, the matrix $\mathcal{N}$ with columns $\mathcal{N}^i$ will often differ from the adjacency matrix of the actual communication graph because of the possible asynchrony of updates as designed in Section 3.5. Thus, $\mathcal{N}^i$ represents not the actual network structure, but agent i's current estimate of its neighbor set, according to which it executes the plan until an update occurs. The hybrid state space structure of

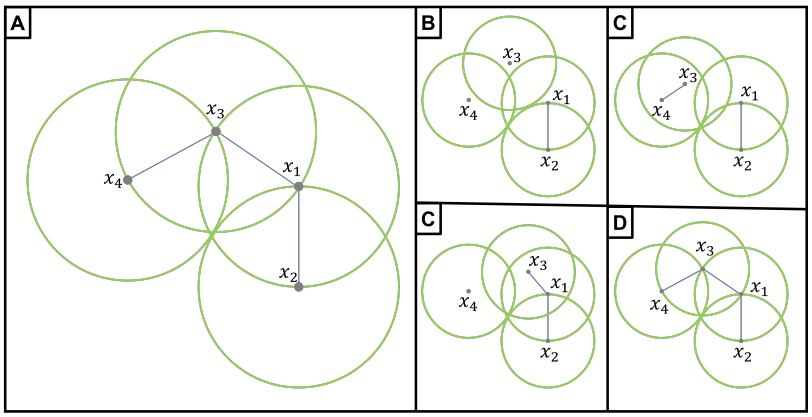

Figure 3-6. A configuration (A) of four agents, with R_{comm} indicated in green gives rise to a communication graph with edges indicated in blue. Several arbitrarily small motions of agent 3 alter the graph discontinuously into one of four graphs (B)-(E). An update by agent 3 executed shortly after the motion will alter $\mathcal{N}^3$ accordingly, but not $\mathcal{N}^1, \mathcal{N}^2$ or $\mathcal{N}^4$.

$\mathcal{X}$, where each of the closed, mutually disjoint subspaces $\mathcal{X}^A$, $A \in \{0,1\}^{N\times N}$ accounts for the possible states of the system under one specific network-wide estimate, A, of the network structure was motivated by this observation. Note that A may not be the adjacency matrix of any graph due to the asynchrony of the local network state updates. Nevertheless, each estimated structure influences the behavior of the ensemble. The following lemma establishes the continuity of the collaborative state estimate update (the functions H^i and P^i) as a function of the extended ensemble state space $\mathcal{X}$, keeping in mind these functions depend on the estimated local network state $\mathcal{N}^i$ rather than on $\mathcal{N}^i(\mathbf{x})$.

Lemma 3.2. *H^i and P^i are continuous functions of $X \in \mathcal{X}$.*

Proof. Fix $i \in \mathcal{A}$. Since the $\mathcal{X}^A$, $A \in \{0,1\}^{N\times N}$, are pairwise disjoint closed sets, it suffices to prove that H^i, P^i are continuous on each $\mathcal{X}^A$. Fix A. Thus $\mathcal{N}^i$ is fixed, and denote $B \triangleq \tilde{\mathcal{N}}^i$. By definition, as functions of $\mathcal{X}^A$, both H^i and P^i depend only on $\hat{x}^i, \tilde{\rho}^i, \hat{x}^j, \tilde{\rho}^j, d_{ij}, j \in B$. Let $\mathcal{K}$ be the space of non-empty compact subsets of $\mathcal{G}_0 + \texttt{diam}(\mathcal{F})\mathbb{B}$, with the Hausdorff metric. $\mathcal{K}$ is compact because $\mathcal{G}_0 + \texttt{diam}(\mathcal{F})\mathbb{B}$ is compact (Lemma 3.1). Then $(U_i^j)_{j\in B}$ is a uniformly continuous map of $X \in \mathcal{X}^A$ into $\mathcal{K}^B$.

Let $\tilde{\mathcal{K}} \triangleq \{(F_j)_{j\in B} \in \mathcal{K}^B : \bigcap_{j\in B} F_j \neq \varnothing\}$. Then $\tilde{\mathcal{K}}$ is a closed subspace of $\mathcal{K}^B$ and is therefore compact. The intersection map $\tilde{\mathcal{K}} \to \mathcal{K}$ is continuous and hence uniformly continuous. Since the map $X \mapsto \hat{U}^i$ is the composition of uniformly continuous maps, it is uniformly continuous on $\mathcal{X}^A$. Finally, $\mathcal{K} \to (\mathcal{G}_0 + \mathtt{diam}(\mathcal{F})\mathbb{B}) \times [0,\infty)$ maps every $F \in \mathcal{K}$ to the center and radius of its circumscribed ball is continuous. Therefore, (H^i, P^i) is a continuous function of $\mathcal{X}^A$ as a composition of continuous maps. □

3.4 Path Planning

For the purpose of the computations in this section it is more convenient to keep track of the timeline according to a prescribed or hypothetical piecewise-linear trajectory. The following durations will be useful to consider:

$$T^i(n,o,p) \triangleq \tfrac{\|n-o\|+\Lambda^i(o,p)}{S^i}, \quad T^i(o,p) \triangleq \tfrac{\Lambda^i(o,p)}{S^i},$$

where o, p are points along X^i_d and $n \in \mathcal{G}^i$ is any point.

3.4.1 Initial Plans

An agent i with initial actual state $x^i(0) \in \mathcal{G}^i_0$ selects an initial path plan of the form (n^i, o^i, p^i, q^i) if $x^i(0) \in \mathcal{F}$. Otherwise, the agent selects a path plan of the form $(x_\infty, x_\infty, p^i, q^i)$ since the agent's only objective at this point is to acquire state feedback. In the first case, select

$$\begin{aligned} n^i &\in \left\{n \in \mathcal{F}_{\mathsf{in}} : \|\mathcal{P}^i_1 - n\| \leq \|\mathcal{P}^i_1 - \mathcal{F}_{\mathsf{in}}\|\right\}, \\ o^i &\triangleq \mathcal{P}^i_1, \\ p^i &\triangleq \mathcal{P}^i_{\max\kappa(X)}, \\ q^i &\in \mathtt{target}\left(p^i, \rho^i\left(T^i(n^i,o^i,p^i),0,0\right)\right), \end{aligned} \tag{3–32}$$

where $\kappa(X) \triangleq \{k \geq 1 : \rho^i\left(T^i(n^i,o^i,\mathcal{P}^i_k),0,0\right) \leq \mathtt{maur}(\mathcal{P}^i_k)\}$. In the second case, $x^i(0) \in \mathcal{F}^{\complement}$, the path plan is selected as

$$p^i \triangleq x^i, \quad q^i \in \mathtt{target}\left(p^i, 0\right). \tag{3–33}$$

3.4.2 Generating a New Plan

Once a path plan $\pi^i(X) = (n^i, o^i, p^i, q^i)$ is terminated at time $\tau^i(X)$ by agent i re-entering the feedback region, a new path plan $\pi^i(X)^+ = \texttt{rpl}^i(X) \triangleq \langle\!\langle n^i_{\texttt{r}}, o^i_{\texttt{r}}, p^i_{\texttt{r}}, q^i_{\texttt{r}} \rangle\!\rangle$ is generated, whose components are defined as follows. Let ℓ be the largest integer such that $T^i(n^i, o^i, \mathcal{P}^i_{\ell-1}) < \tau^i(X)$, meaning that $\mathcal{P}^i_{\ell-1}$ is the last waypoint on X^i_d visited by the agent. Let $\kappa(X) \triangleq \{k \geq \ell : \rho^i\left(T^i(n^i_{\texttt{r}}, o^i_{\texttt{r}}, \mathcal{P}^i_k), 0, 0\right) \leq \texttt{maur}(\mathcal{P}^i_k)\}$, which is the collection of indices of waypoints farther along X^i_d from which a return to $\mathcal{F}$ is guaranteed. Then,

$$
\begin{aligned}
n^i_{\texttt{r}} &\triangleq \left\{n \in \mathcal{F}_{\mathsf{in}} : \|\mathcal{P}^i_\ell - n\| \leq \|\mathcal{P}^i_\ell - \mathcal{F}_{\mathsf{in}}\|\right\}, \\
o^i_{\texttt{r}} &\triangleq \mathcal{P}^i_\ell, \\
p^i_{\texttt{r}} &\triangleq \mathcal{P}^i_{\max \kappa(X)}, \\
q^i_{\texttt{r}} &\triangleq \texttt{target}\left(p^i, \rho^i\left(T^i(n^i_{\texttt{r}}, o^i_{\texttt{r}}, p^i_{\texttt{r}}), 0, 0\right)\right),
\end{aligned}
$$

Note that the point $o^i_{\texttt{r}}$ is selected to ensure progress along X^i_d, and that all $n \in n^i_{\texttt{r}}$ are at equal distances to $o^i_{\texttt{r}}$, which makes $q^i_{\texttt{r}}$ independent of the choice of such n.

3.4.3 Updated Path Plans and Trigger Functions

Any update of the state estimate $\hat{x}^i$, $\tilde{\rho}^i$ provides an opportunity to update the plan $\pi = \pi^i$. Things to consider include tracking performance, distance traveled along X^i_d, and completion time. The path plan is updated differently depending on the current mode (Figure 3-7). Denoting $\pi^+ = \texttt{upd}^i(X) \triangleq \left\langle\!\!\left\langle n^i_+, o^i_+, p^i_+, q^i_+ \right\rangle\!\!\right\rangle$, always select $o^i_+ = o^i$ to ensure that o^i is visited. On the first leg of the plan, a state estimate update would be compatible with n^i_+ being set to $H^i(X)$; on the second leg, $n^i_+ = n^i$. On both legs, the reduction in the initial SEE may allow for pushing p^i_+ farther along X^i_d than the original p^i was. Similarly to the preceding sections, the following definitions are given, with small variations.

Set ℓ so that $o^i = \mathcal{P}^i_\ell$ and, for every $k \geq \ell$ let $\rho^i_*(X, k)$ be the projected bound on the TTE upon arrival at $\mathcal{P}^i_k$, depending on the required type of update. Then

$$
\kappa\left(X\right) \triangleq \{k \geq \ell : \rho^i_*\left(X, k\right) \leq \texttt{maur}(\mathcal{P}^i_k)\}
$$

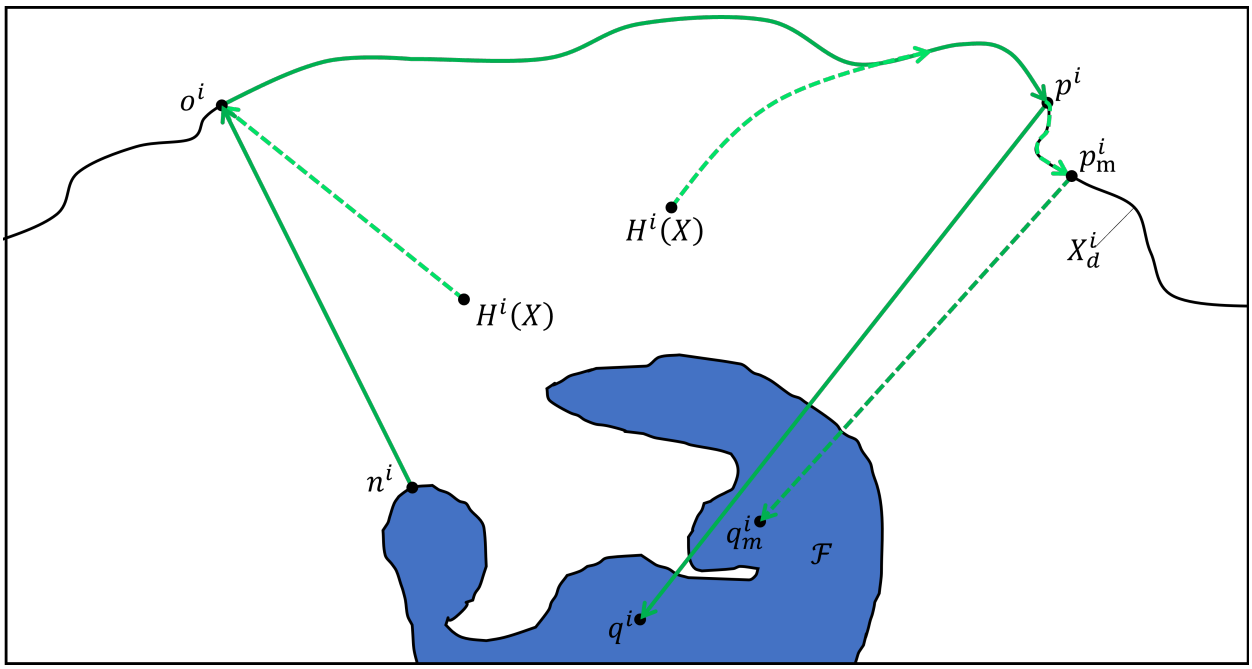

Figure 3-7. Possible changes in the auxiliary trajectory of agent i due to accepted state-estimate updates. An example is given for each leg of a path plan π.

is the set of indices $k \geq \ell$ corresponding to the points $\mathcal{P}^i_k$ eligible to be counted as return targets for the new plan. The quantity

$$\rho^i_* (X) \triangleq \rho^i_* (X, \max \kappa (X))$$

is a bound on the TTE at the farthest admissible return point, resulting in $p^i_+ \triangleq \mathcal{P}^i_{\max \kappa(X)}$. Any choice of return target from the set $q^i_+ \triangleq \texttt{target}(p^i_+, \rho^i_*(X))$ is an acceptable choice for a guaranteed return trajectory. It remains to set the values of $\rho^i_*(X, k)$ separately for each mode, while making any additional considerations.

3.4.3.1 $\texttt{mode}^i = 1$

In this mode, $\texttt{mode}^i = 1$, select $n^i_+ = H^i(X)$ and set

$$\rho^i_* (X, k) \triangleq \rho^i \left(T^i(H^i (X), o^i, \mathcal{P}^i_k), 0, P^i (X) \right).$$

The resulting update is only beneficial when uncertainty reduction resulting from updating the state estimate yields a sufficient improvement in the estimation error bound

upon arrival at o^i. This condition corresponds to the trigger condition $\mathcal{T}_1^i(X) \leq 0$, where

$$\begin{aligned} \mathcal{T}_1^i(X) &\triangleq \Psi_1^i + \rho_1^i - \rho_{\mathtt{n}}^i, \\ \rho_1^i &\triangleq \rho^i\left(\|H^i(X) - o^i\|/S^i, 0, P^i(X)\right), \\ \rho_{\mathtt{n}}^i &\triangleq \rho^i\left(\|x_\pi^i - o^i\|/S^i, 0, \tilde{\rho}^i\right), \end{aligned} \tag{3–34}$$

and $\Psi_1^i \geq 0$ is a user-defined threshold.

3.4.3.2 $\mathtt{mode}^i = 2$

In this mode, $\mathtt{mode}^i = 2$, select $n_+^i = n^i$ and

$$\rho_*^i(X, k) \triangleq \rho^i\left(T^i\left(x_\pi^i, \mathcal{P}_k^i\right), H^i(X) - x_\pi^i, P^i(X)\right).$$

This update is only beneficial when uncertainty reduction resulting from updating the state estimate yields a sufficient improvement in the error bound upon arrival at p^i. This condition corresponds to the trigger condition $\mathcal{T}_2^i(X) = 0$, where

$$\begin{aligned} \mathcal{T}_2^i(X) &\triangleq \mathtt{ReLu}\left(\Psi_2^i + \rho_2^i - \rho_{\mathtt{n}}^i\right), \\ \rho_2^i &\triangleq \rho^i\left(T^i\left(x_\pi^i, p^i\right), H^i(X) - x_\pi^i, P^i(X)\right), \\ \rho_{\mathtt{n}}^i &\triangleq \rho^i\left(T^i\left(x_\pi^i, p^i\right), \hat{e}^i, \tilde{\rho}^i\right), \end{aligned} \tag{3–35}$$

and $\Psi_2^i > 0$ is a user-defined threshold.

3.4.3.3 $\mathtt{mode}^i = 3$

Even though it may be beneficial to do state estimate updates while in mode 3 to possibly reduce the maximum time it may take for an agent to return to the feedback region, implementation would require knowledge of $\mathtt{maur}(H^i(X))$ and $\mathtt{target}(H^i(X), P^i(X))$, which is not part of the precomputed data used in modes 1 and 2. Additionally, there are currently no efficient methods for computing this data in real-time.

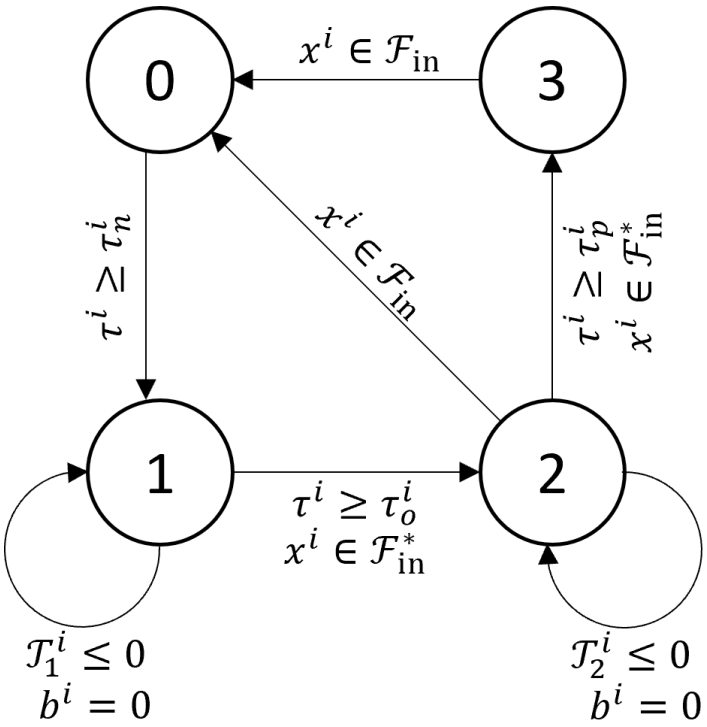

Figure 3-8. To achieve desirable solution properties, modifications to the ideal mode transition conditions, as seen in Figure 3-3, were necessary, giving rise to the realized conditions seen here and in (3–44). For example, it is now required that $x^i \in \mathcal{F}_{\text{in}}^*$ rather than $x^i \in \mathcal{F}^*$.

3.5 The Assembled Hybrid System

To avoid chattering effects along $\partial\mathcal{F}$ (Remark 3.3), the idealized mode transitions provided in Figure 3-3 are replaced with the mode transitions defined in Figure 3-8, using an inset $\mathcal{F}_{\text{in}}$ of $\mathcal{F}$ by a small distance for which $\mathcal{F}_{in} \cap \partial\mathcal{F} = \emptyset$. Consequently, the flow set of the ensemble hybrid system is constructed as follows, as dictated by the constraints characteristic of each operational mode, for each agent. Let $\varpi^i : \mathcal{X} \to \mathcal{X}^i$ be the standard projection such that ${C^i}_m = (\varpi^i)^{-1}(\tilde{C}_m^i)$, where

$$\tilde{C}_0^i \triangleq \left\{ X^i \in \mathcal{X}^i \;\middle|\; \begin{array}{l} \texttt{mode}^i = 0,\ \texttt{b}^i = 0, \\ \tau^i \leq \tau_n^i \end{array} \right\}, \tag{3–36}$$

$$\tilde{C}_1^i \triangleq \left\{ X^i \in \mathcal{X}^i \;\middle|\; \begin{array}{l} \texttt{mode}^i = 1,\ \texttt{b}^i = 0, \\ \tau^i_{\mathsf{trig}} \leq T^i_{\mathsf{max}} \end{array} \right\}, \tag{3–37}$$

$$\tilde{C}_2^i \triangleq \left\{ X^i \in \mathcal{X}^i \;\middle|\; \begin{array}{l} \texttt{mode}^i = 2,\ \texttt{b}^i = 0, \\ \tau^i_{\mathsf{trig}} \leq T^i_{\mathsf{max}}, x^i \in \mathcal{F}^*_{\mathsf{in}} \end{array} \right\}, \tag{3–38}$$

$$\tilde{C}_3^i \triangleq \left\{ X^i \in \mathcal{X}^i \;\middle|\; \begin{array}{l} \texttt{mode}^i = 3,\ \texttt{b}^i = 0, \\ x^i \in \mathcal{F}^*_{\mathsf{in}} \end{array} \right\}, \tag{3–39}$$

where $T^i_{\mathsf{max}} \in \mathbb{R}_{>0}$ is the duration of time that must elapse before a trigger update may occur. Define the ensemble flow set as

$$C \triangleq \bigcap_{i \in \mathcal{A}} C^i, \quad C^i \triangleq \bigcup_{m=0}^{3} C^i_m. \tag{3–40}$$

$$C = \bigcup_{\mathbf{m} \in \mathbf{M}} C_{\mathbf{m}}, \quad C_{\mathbf{m}} \triangleq \bigcap_{i \in \mathcal{A}} C^i_{\mathbf{m}(i)}, \tag{3–41}$$

where $\mathbf{m} \colon \mathcal{A} \to \{0,1,2,3\}$ is a function that assigns modes, and $\mathbf{M}$ denotes the set of all mode assignments. Observe that C is closed. The ensemble flow map is

$$F(X) \triangleq \prod_{i \in \mathcal{A}} F^i\left(X^i\right), \; F^i\left(X^i\right) \triangleq F^i_{\texttt{mode}^i}\left(X^i\right), \tag{3–42}$$

where, recalling (3–28), the maps $F^i_{\mathtt{m}} : C \cap [\texttt{mode}^i = \mathtt{m}] \rightrightarrows \mathbb{R}^{N+19}$ are defined as

$$\begin{aligned} F^i_0(X^i) &\triangleq \langle\langle 0,0,0, \boldsymbol{\Delta}\left(\mathcal{D}^i + \bar{d}^i\mathbb{B}\right), v^i_\pi(\tau^i), 1,0,0,0\rangle\rangle, \\ F^i_m(X^i) &\triangleq \langle\langle 0,0,0, \mathcal{D}^i + \ \bar{d}^i\mathbb{B}, \hat{\mathcal{D}}^i\ , v^i_\pi(\tau^i), 1,1,\theta,0\rangle\rangle, \end{aligned} \tag{3–43}$$

for $m = 1,2,3$, where $\theta \triangleq [\lambda^i(\tilde{\varrho}^i)^2 + \delta^i]\mathrm{e}^{2\lambda^i\Delta t}(\tilde{\rho}^i)^{-1}$, based on (3–27).

Transitions between operational modes, state estimate updates, and communication structure changes happen in the sets

$$
\begin{aligned}
D_{*}^{i} &\triangleq \left\{X \in \mathcal{X} : \tau_{\mathsf{trig}}^{i} \geq T_{\mathsf{max}}^{i}, \mathtt{mode}^{i} \in \{1,2\}, \mathtt{b}^{i} = 0\right\}, \\
D_{\#1}^{i} &\triangleq \left\{X \in \mathcal{X} : \mathcal{T}_{1}^{i}\left(X\right) > 0, \mathtt{mode}^{i} = 1, \mathtt{b}^{i} = 1\right\}, \\
D_{\#2}^{i} &\triangleq \left\{X \in \mathcal{X} : \mathcal{T}_{2}^{i}\left(X\right) > 0, \mathtt{mode}^{i} = 2, \mathtt{b}^{i} = 1\right\}, \\
D_{11}^{i} &\triangleq \left\{X \in \mathcal{X} : \mathcal{T}_{1}^{i}\left(X\right) \leq 0, \mathtt{mode}^{i} = 1, \mathtt{b}^{i} = 1\right\}, \\
D_{22}^{i} &\triangleq \left\{X \in \mathcal{X} : \mathcal{T}_{2}^{i}\left(X\right) \leq 0, \mathtt{mode}^{i} = 2, \mathtt{b}^{i} = 1\right\}, \\
D_{20}^{i} &\triangleq \left\{X \in \mathcal{X} : x^{i} \in \mathcal{F}_{\mathsf{in}}, \mathtt{mode}^{i} = 2, \mathtt{b}^{i} = 0\right\}, \\
D_{30}^{i} &\triangleq \left\{X \in \mathcal{X} : x^{i} \in \mathcal{F}_{\mathsf{in}}, \mathtt{mode}^{i} = 3, \mathtt{b}^{i} = 0\right\}, \\
D_{01}^{i} &\triangleq \left\{X \in \mathcal{X} : \tau^{i} \geq \tau_{n}^{i}, \mathtt{mode}^{i} = 0, \mathtt{b}^{i} = 0\right\}, \\
D_{12}^{i} &\triangleq \left\{X \in \mathcal{X} : \tau^{i} \geq \tau_{o}^{i}, x^{i} \in \mathcal{F}_{\mathsf{in}}^{*}, \mathtt{mode}^{i} = 1, \mathtt{b}^{i} = 0\right\}, \\
D_{23}^{i} &\triangleq \left\{X \in \mathcal{X} : \tau^{i} \geq \tau_{p}^{i}, x^{i} \in \mathcal{F}_{\mathsf{in}}^{*}, \mathtt{mode}^{i} = 2, \mathtt{b}^{i} = 0\right\}.
\end{aligned}
\tag{3–44}
$$

Note that D_{mm}^{i}, $m = 1, 2$ depends on the ensemble state of the MAS rather than just the individual state X^{i}. The ensemble jump set is defined as $D \triangleq \bigcup_{i \in \mathcal{A}} D^{i}$, where D^{i} is the union of the sets defined in (3–44). The jump map for agent i is defined as

$(G^i(X))^j = X^j$ for all $j \in \mathcal{A} \setminus \{i\}$ and

$$
\begin{aligned}
&(G^i((\mathcal{N}^i,\ \pi^i\ ,\mathtt{mode}^i, x^i,\ \hat{x}^i\ , x^i_\pi, \tau^i, \tau^i_{\mathsf{trig}}, \tilde{\rho}^i, \mathtt{b}^i)_{i\in\mathcal{A}}))^i \triangleq \\
&\begin{cases}
\langle\langle \mathcal{N}^i(\mathbf{x}),\ \pi^i\ ,\mathtt{mode}^i, x^i,\ \hat{x}^i\ , x^i_\pi, \tau^i,\ \ 0\ \ , \tilde{\rho}^i,\ 1\ \rangle\rangle,\ X\in D^i_*, \\
\langle\langle\ \ \mathcal{N}^i\ \ ,\ \pi^i\ ,\ \ 1\ \ ,x^i,\ \hat{x}^i\ , x^i_\pi, \tau^i,\ \ 0\ \ , \tilde{\rho}^i,\ 0\ \rangle\rangle,\ X\in D^i_{\#1}, \\
\langle\langle\ \ \mathcal{N}^i\ \ ,\ \pi^i\ ,\ \ 2\ \ ,x^i,\ \hat{x}^i\ , x^i_\pi, \tau^i,\ \ 0\ \ , \tilde{\rho}^i,\ 0\ \rangle\rangle,\ X\in D^i_{\#2}, \\
\langle\langle\ \ \mathcal{N}^i\ \ ,\mathtt{upd}^i,\ \ 1\ \ ,x^i, H^i, H^i, \tau^i,\ \ 0\ \ , P^i,\ 0\ \rangle\rangle,\ X\in D^i_{11}, \\
\langle\langle\ \ \mathcal{N}^i\ \ ,\mathtt{upd}^i,\ \ 2\ \ ,x^i, H^i, x^i_\pi, \tau^i,\ \ 0\ \ , P^i,\ 0\ \rangle\rangle,\ X\in D^i_{22}, \\
\langle\langle\ \ \mathcal{N}^i\ \ ,\mathtt{rpl}^i,\ \ 0\ \ ,x^i,\ x^i\ ,\ x^i\ ,\ 0\ ,\ \ 0\ \ ,\ 0\ ,\mathtt{b}^i\rangle\rangle, X\in D^i_{20}, \\
\langle\langle\ \ \mathcal{N}^i\ \ ,\mathtt{rpl}^i,\ \ 0\ \ ,x^i,\ x^i\ ,\ x^i\ ,\ 0\ ,\ \ 0\ \ ,\ 0\ ,\mathtt{b}^i\rangle\rangle, X\in D^i_{30}, \\
\langle\langle\ \ \mathcal{N}^i\ \ ,\ \pi^i\ ,\ \ 1\ \ ,x^i,\ \hat{x}^i\ , x^i_\pi,\ 0\ , \tau^i_{\mathsf{trig}}, \tilde{\rho}^i\ , \mathtt{b}^i\rangle\rangle,\ X\in D^i_{01}, \\
\langle\langle\ \ \mathcal{N}^i\ \ ,\ \pi^i\ ,\ \ 2\ \ ,x^i,\ \hat{x}^i\ , x^i_\pi, \tau^i, \tau^i_{\mathsf{trig}}, \tilde{\rho}^i\ , \mathtt{b}^i\rangle\rangle,\ X\in D^i_{12}, \\
\langle\langle\ \ \mathcal{N}^i\ \ ,\ \pi^i\ ,\ \ 3\ \ ,x^i,\ \hat{x}^i\ , x^i_\pi, \tau^i, \tau^i_{\mathsf{trig}}, \tilde{\rho}^i\ , \mathtt{b}^i\rangle\rangle,\ X\in D^i_{23},
\end{cases}
\end{aligned}
\tag{3–45}
$$

where $\mathtt{rpl}^i(X)$ depends on the operating mode and is defined in Section 3.4.2, whereas $H^i(X), P^i(X)$, and $\mathtt{upd}^i(X)$ depend on the communication structure, and are defined in Sections 3.3.2 and 3.4.3. Further, for values of X where (3–45) is ambiguous, $G^i(X)$ is to be understood as a set, containing all the listed outcomes. The ensemble jump map is $G(X) \triangleq \bigcup_{i\in\mathcal{A}} G^i(X)$.

Remark 3.4. The purpose of the binary variable $\mathtt{b}^i$ is to enforce a particular order of the state update: given an initial condition where $\mathtt{b}^i = 0$, it is impossible for agent i to have a state $X^i \in D^i_{11} \cup D^i_{22}$ unless the prior state of agent i was contained in D^i_*, thus forcing agent i to update the communication status with the other agents before computing the triggering function for a state estimate update, assuring accurate information is used, as well as the continuity of the $\hat{x}^i, \tilde{\rho}^i$ components of the jump map, by Lemma 3.2.

3.6 Properties of Solutions

3.6.1 Hybrid Basic Conditions

Having a HDI that is nominally well-posed leads to favorable robustness and temporal properties [49, Chapter 6]. To have a HDI that is nominally well-posed, it suffices for the HDI to satisfy the hybrid basic conditions (HBC): (a) C and D are closed; (b) F is outer semicontinuous and locally bounded on C, with (closed) convex values; and (c) G is outer semicontinuous and locally bounded on D [49, Theorem 6.30]. In the case where (a–c) hold with the possible exception that F and/or G are not outer semicontinuous, the Krasovskii regularization $\hat{\mathcal{H}}$ of the HDI is still known to satisfy the HBC [49, Lemma 5.16]. Recall that the regularized HDI is defined as $\hat{\mathcal{H}} \triangleq (\overline{C}, \hat{F}, \overline{D}, \hat{G})$, where,

$$\begin{aligned} \hat{F}(X) &\triangleq \bigcap_{\delta>0} \overline{\text{co}} F\left((X+\delta\mathbb{B}) \cap \overline{C}\right), \\ \hat{G}(X) &\triangleq \bigcap_{\delta>0} \overline{G\left((X+\delta\mathbb{B}) \cap \overline{D}\right)}. \end{aligned} \tag{3–46}$$

Solutions of $\hat{\mathcal{H}}$ are called Krasovskii solutions of $\mathcal{H}$.

Lemma 3.3. *The sets C and D are closed.*

Proof. The set C is closed, by construction. Note that, in (3–44), $D^i_{mm} \cup D^i_{\#m}$ is closed for all $i \in \mathcal{A}$, showing that D is closed as well. □

Remark 3.5. Observe also that the sets D^i_{11} and D^i_{22} defined in (3–44) are closed for all $i \in \mathcal{A}$. By Lemma 3.2, (3–34), and (3–35), the trigger functions $\mathcal{T}^i_1$ and $\mathcal{T}^i_2$ are continuous over $\mathcal{X}$ for all $i \in \mathcal{A}$. Since $\mathcal{X}$ is closed, so are all the D^i_{11} and D^i_{22}.

Lemma 3.4. *Let $\hat{F}$, $\hat{G}$ be the Krasovskii regularizations of F,G respectively. Then $\hat{F}(X) = \prod_{i\in\mathcal{A}} \hat{F}^i(X^i)$, where for each i, $\hat{F}^i(X^i) = F^i(X^i)$ for $X^i \in C^i \setminus C^i_0$, and*

$$\begin{aligned} \hat{F}^i &= \left\langle\!\!\left\langle 0,0,0,\boldsymbol{\Delta}(\hat{f}^i), v^i_\pi(\tau^i),1,0,0,0 \right\rangle\!\!\right\rangle, \\ \hat{f}^i &\triangleq f^i + \psi^i\left(x^i,e^i,k^i_1,\beta^i,\tau^i\right) + \bar{d}^i\left(\textit{SGN}(e^i)+\mathbb{B}\right), \end{aligned} \tag{3–47}$$

otherwise. Further, $\hat{G} = \bigcup_{i \in \mathcal{A}} \hat{G}^i(X)$*, where for each* i*,* $\hat{G}^i(X)$ *is defined in the same way as (3–45) where the plans* $\mathtt{upd}^i(X) = \left\langle\!\left\langle n_+^i, o^i, p_+^i, q_+^i \right\rangle\!\right\rangle$ *are replaced with* $\widehat{\mathtt{upd}^i}(X)$ *and* $\mathcal{N}^i(\mathbf{x})$ *is replaced with*

$$\left(\hat{\mathcal{N}}^i(\mathbf{x})\right)_j \triangleq \begin{cases} 0, & d_{ij} > R_{comm} \ \vee \ j = i, \\ \{0,1\}, & d_{ij} = R_{comm}, \\ 1, & d_{ij} < R_{comm}. \end{cases}$$

Moreover,

$$\widehat{\mathtt{upd}^i}\left(X\right) \subseteq \bigcup_{p \in \{\mathcal{P}_k^i : k \in \kappa(X)\}} \left\langle\!\left\langle n_+^i, o^i, p, \mathtt{target}\left(p, \rho_*^i\left(X\right)\right) \right\rangle\!\right\rangle, \tag{3–48}$$

where $\kappa\left(X\right)$ *and* $\rho_*^i\left(X\right)$ *are defined in Section 3.4.3, implying that every plan in* $\hat{G}^i(X)$ *has a guarantee of re-entry. There also exists a discontinuity in* $(G^i(X))^i$ *when* $\mathcal{T}_1^i(X) = 0$ *and* $X \in D_{\#1}^i \cup D_{11}^i$*, thus the regularization at this point is*

$$\begin{aligned} (\hat{G}^i(X))^i = &\left\langle\!\left\langle \mathcal{N}^i, \pi^i, 1, x^i, \hat{x}^i, x_\pi^i, \tau^i, 0, \tilde{\rho}^i, 0 \right\rangle\!\right\rangle \\ &\cup \left\langle\!\left\langle \mathcal{N}^i, \widehat{\mathtt{upd}^i}\left(X\right), 1, x^i, H^i, H^i, \tau^i, 0, P^i, 0 \right\rangle\!\right\rangle. \end{aligned}$$

Similarly, when $\mathcal{T}_2^i(X) = 0$ *and* $X \in D_{\#2}^i \cup D_{12}^i$*, the regularized jump map is*

$$\begin{aligned} (\hat{G}^i(X))^i = &\left\langle\!\left\langle \mathcal{N}^i, \pi^i, 2, x^i, \hat{x}^i, x_\pi^i, \tau^i, 0, \tilde{\rho}^i, 0 \right\rangle\!\right\rangle \\ &\cup \left\langle\!\left\langle \mathcal{N}^i, \widehat{\mathtt{upd}^i}\left(X\right), 2, x^i, H^i, x_\pi^i, \tau^i, 0, P^i, 0 \right\rangle\!\right\rangle. \end{aligned}$$

Proof. The regularization of the flow map $\hat{F}$ is determined by direct computation using the fact that the only discontinuities in $\hat{F}$ are due to the additive signum function term in (3–11), when feedback is available. Similarly, the regularization of the jump map $\hat{G}$ is determined through observing that the only discontinuities of $\hat{G}^i$ are due to discontinuities in the update of the communication neighborhood $\mathcal{N}^i$ and of the plan update map $\mathtt{upd}^i$. The regularization of $\mathcal{N}^i(\mathbf{x})$ is determined by direct computation.

To address $\widehat{\mathtt{upd}^i}(X)$, the notation of Section 3.4.3 is used for the rest of the proof. Since n^i_+ and o^i are continuous maps, and q^i_+ is an outer semicontinuous function of p^i_+, we only need to compute the regularization of p^i_+ as a function of $X \in \mathcal{X}$. Since $p^i_+(X) = \mathcal{P}^i_{\max \kappa(X)}$ by definition, to prove (3–48), it suffices to verify that there is a $\delta > 0$ such that $\kappa(X') \subseteq \kappa(X)$ for all $X' \in X + \delta\mathbb{B}$.

For $\mathtt{mode}^i = 1$, let $\epsilon > 0$ be such that[3] $\rho^i_*(X, k) > \mathtt{maur}(\mathcal{P}^i_k) + \epsilon$ for all $k \notin \kappa(X)$. Let δ be small enough that $|\rho^i_*(X, k) - \rho^i_*(X', k)| < \epsilon$ for every $X' \in X + \delta\mathbb{B}$ and every $k \geq \ell$. Then for $k \notin \kappa(X)$, $\rho^i_*(X', k) > \rho^i_*(X, k) - \epsilon > \mathtt{maur}(\mathcal{P}^i_k)$, which implies $k \notin \kappa(X')$. The proof for leg $\overline{op}$ is nearly identical. Under these conditions, for small enough δ, the only possible difference between X^i and X'^i is in the components $x^i, \hat{x}^i$ and the continuity of ρ^i carries the argument.

For the discontinuity when $\mathcal{T}^i_m = 0$, for $m \in \{1, 2\}$, $(\hat{G}^i(X))^i$ is determined by direct computation. □

3.6.2 Stability of Krasovskii Solutions

Define the set $\mathcal{I}^i_0$ of admissible initial conditions for agent i as the set of all $X \in C$ such that $x^i \in \mathcal{G}^i_0$, $\hat{x}^i = x^i_\pi = x^i$, $\tilde{\rho}^i = 0$, $\mathtt{b}^i = 0$ and either (a) $x^i \in \mathcal{F}$, $\mathtt{mode}^i = 0$ and $\pi^i = (n^i_0, o^i_0, p^i_0, q^i_0)$ has a guarantee of re-entry; or (b) $\mathtt{mode}^i = 3$ and $\pi^i = (x_\infty, x_\infty, p^i_0, q^i_0)$, where $p^i_0 = x^i$ and q^i_0 is selected in the same way as Section 3.4.1. Define the set of admissible initial conditions for the MAS as $\mathcal{I}_0 \triangleq \bigcap_{i \in \mathcal{A}} \mathcal{I}^i_0$.

Theorem 3.1. *Krasovskii solutions of $\mathcal{H}$ with initial conditions in $\mathcal{I}_0$ have uniformly ultimately bounded true tracking error (i.e., TTE).*

Proof. By Lemma 3.4, Krasovskii solutions of $\mathcal{H}$ have a guarantee of re-entry for all path plan updates, for each agent $i \in \mathcal{A}$. Then [27, Theorem 3] applied separately to

[3] Note that the projected bound on the TTE is monotone-increasing as a function of k.

each agent $i \in \mathcal{A}$, implies that the TTE for agent i is ultimately bounded, uniformly over $\mathcal{G}_0^i$. □

Claim 3.1. For any agent i with a state X^i such that $\texttt{mode}^i = 0$, x^i remains in $\mathcal{F}$ until $\tau^i \geq \tau_n^i$. That is to say, there are no accidental departures from $\mathcal{F}$.

Proof. Given the initial conditions defined by $\mathcal{I}_0^i$ and by the resetting of the TTE dictated by the jump maps D_{20}^i and D_{30}^i, agent i is always initialized in the feedback region $\mathcal{F}$ ($\texttt{mode}^i = 0$) with a zero TTE (i.e., $e^i = 0$). Then by the exponential convergence to 0 of $\|e^i\|$ observed in (3–17), it is concluded that $\|e^i\| = 0$ for the duration of time that $x^i \in \mathcal{F}$. Further, since a path plan π is constructed such that $x_\pi^i \in \mathcal{F}$ for the duration of $\tau^i \in [0, \tau_n^i)$, it is concluded that $x^i \in \mathcal{F}$ until $\tau^i \geq \tau_n^i$. □

3.6.3 Properties of Solutions

The following lemma addresses properties of the flow map.

Lemma 3.5 (Viability Condition)**.** *For an arbitrary $X_0 \in C \setminus D$ there exists a neighborhood U of X_0 such that for every $X \in U \cap C$, $\hat{F}(X) \cap \mathbf{T}_C(X) \neq \emptyset$.*

Proof. Let $\mathbf{m} \in \mathbf{M}$ be the unique mode assignment satisfying $X_0 \in C_{\mathbf{m}}$. Since the $C_{\mathbf{m}}$ are pairwise disjoint compact sets, there is a neighborhood W of X_0 such that $W \cap C = W \cap C_{\mathbf{m}}$. From the fact that the constraints defining the $C_{\mathbf{m}(i)}^i$ for different i are separated it follows that $T_C(X) = \bigcap_{i \in \mathcal{A}} T_{C_{\mathbf{m}(i)}^i}(X)$ for every $X \in W$. Thus, verifying that $\hat{F}(X) \cap \mathbf{T}_C(X) \neq \emptyset$ for $X \in W \cap C$ is tantamount to verifying that, for each $i \in \mathcal{A}$, $\hat{F}^i(X^i)$ contains a point satisfying the defining inequalities for $\mathbf{T}_{C_{\mathbf{m}(i)}^i}(X)$. Let $\varpi^i : \mathcal{X} \to \mathcal{X}^i$ be the standard projection. Then, ${C^i}_{\mathbf{m}(i)} = (\varpi^i)^{-1}(\tilde{C}_{\mathbf{m}(i)}^i)$, and $\mathbf{T}_{{C^i}_{\mathbf{m}(i)}}(X) = (d_X \varpi^i)^{-1}(\mathbf{T}_{\tilde{C}^i{}_{\mathbf{m}(i)}}(X))$, where $d_X \varpi^i$ is the differential (at X) of ϖ^i, which happens to coincide with the projection to the i^{th} coordinate. Then by the corollary to [57, Theorem 2.4.5], $\mathbf{T}_{\tilde{C}_{\mathbf{m}(i)}^i}(X)$ can be computed as

$$\mathbf{T}_{\tilde{C}_{\mathbf{m}(i)}^i}(X^i) \supseteq \langle\langle \mathbf{T}_{\{0,1\}^N}(\mathcal{N}^i), \mathbf{T}_{\texttt{Plans}^i}(\pi^i), \mathbf{T}_{\{\mathbf{m}(i)\}}(\texttt{mode}^i),$$

$$\mathbf{T}_{\mathcal{F}_{\mathsf{in}}^{\mathtt{C}}}(x^i), \mathbf{T}_{\mathbb{R}^2}(\hat{x}^i), \mathbf{T}_{\mathbb{R}^2}(x_\pi^i), \mathbf{T}_{[0,\tau_n^i)}(\tau^i),$$
$$\mathbf{T}_{[0,T_{\mathsf{max}}^i)}(\tau_{\mathsf{trig}}^i), \mathbf{T}_{[0,\infty)}(\tilde{\rho}^i), \mathbf{T}_{\{0\}}(\mathsf{b}^i)\rangle\rangle,$$

where it is observed that $\mathbf{T}_{\mathcal{F}_{\mathsf{in}}^{\mathtt{C}}}(x^i) = \mathbf{T}_{\mathbb{R}}(x^i)$, $\mathbf{T}_{[0,\tau_n^i)}(\tau^i) = \mathbf{T}_{[0,\infty)}(\tau^i)$, and $\mathbf{T}_{[0,T_{\mathsf{max}}^i)}(\tau_{\mathsf{trig}}^i) = \mathbf{T}_{[0,\infty)}(\tau_{\mathsf{trig}}^i)$, for all $X \in C \setminus D$. Therefore,

$$\mathbf{T}_{\tilde{C}_{\mathbf{m}(i)}^i}(X^i) \supseteq \langle\langle \{0\}^N, \{0\}, \{0\}, \mathbb{R}^2, \mathbb{R}^2, \mathbb{R}^2, [0,\infty), [0,\infty),$$
$$[0,\infty), \{0\}\rangle\rangle \supseteq \left(F_0^i(X^i) \cup F_m^i(X^i)\right).$$

Recall that $F^i \subset \hat{F}_i$. □

To address properties of jumps, it is necessary to decompose the jump set D to examine possible jump sequences. Any $X \in D$ belongs in one of the subsets of D listed in the collection $\mathfrak{D}$,

$$\mathfrak{D} \triangleq \{D_{01}^i, D_*^i \cap \{\mathtt{mode}^i = 1\} \setminus D_{12}^i, D_{\#1}^i, D_{11}^i, D_{12}^i \setminus D_*^i, D_*^i \cap D_{12}^i,$$
$$D_*^i \cap \{\mathtt{mode}^i = 2\} \setminus (D_{20}^i \cup D_{23}^i), D_{\#2}^i, D_{22}^i, D_{20}^i \setminus (D_*^i \cup D_{23}), D_{23}^i \setminus (D_*^i \cup D_{20}), D_*^i \cap D_{23}^i \setminus D_{20}^i, \tag{3–49}$$
$$D_{20}^i \cap D_{23}^i \setminus D_*^i, D_*^i \cap D_{20}^i \setminus D_{23}^i, D_*^i \cap D_{20}^i \cap D_{23}^i, D_{30}^i\}.$$

Details for the construction of $\mathfrak{D}$ can be found in Appendix A.1. For any $D' \in \mathfrak{D}$, with the exception of $D_*^i \cap \{\mathtt{mode}^i = 1\}$ and $D_*^i \cap \{\mathtt{mode}^i = 2\}$, any $X \in D'$ has the possibility of being mapped by G to the flow set C. Further, any $X \in D'$, for any $D' \in \mathfrak{D}$ has the possibility of being mapped by G into some other element of $\mathfrak{D}$. A complete map of the possible transitions is provided in Figure 3-9. Now that a viability condition has been established it can now be shown that every maximal solution of $\hat{\mathcal{H}}$ is complete.

Lemma 3.6. *Every maximal solution of $\hat{\mathcal{H}}$ is complete.*

Proof. By Lemma 3.5, the viability condition of [49, Proposition 6.10] is satisfied. It suffices to show that alternatives (b) and (c) of [49, Proposition 6.10] do not occur,

therefore concluding that every maximal solution of $\hat{\mathcal{H}}$ is complete, as it is the only remaining option. Alternative (b) does not occur by Theorem 3.1. Alternative (c) does not occur since $\hat{G}(D) \subset \overline{C} \cup D$, by direct inspection of Figure 3-9. □

Remark 3.6. In practice there is an assumption that there are no accidental departures from the feedback region as this will result in the termination of a solution according to $\mathcal{H}$ (i.e., there would be maximal solutions that are not complete). It was shown in Claim 3.1 that no accidental departures occur for the modeled hybrid system; however, it was also acknowledged in Remark 3.3 that this is not a good assumption due to the use of a sliding mode controller. Thus there is a need to use $\mathcal{F}_{\text{in}}$ instead of $\mathcal{F}$ to achieve robustness to this modeling deficiency, allowing for practical implementation.

Lemma 3.7. *No complete solution of $\hat{\mathcal{H}}$ is discrete.*

Proof. By direct inspection of Figure 3-9, for any agent i, the extended state ϕ^i may not experience more than 4 consecutive null-time jumps at any time along any solution ϕ of the system $\hat{\mathcal{H}}$. The critical observation is that the graph of jump transitions in Figure 3-9 is a directed acyclic graph [62], implying a bound on the length of a directed path; in this particular case, 6 happens to be the best bound. See Appendix A.1 for the full construction of the DAG. Since there are N agents, it follows that no solution may experience more than $6N$ consecutive jumps before flow resumes. Therefore, no complete solution of $\hat{\mathcal{H}}$ is discrete. □

Theorem 3.2. *No solution of $\hat{\mathcal{H}}$ has vanishing times between jumps.*

Proof. By Theorem 3.1, all solutions of $\hat{\mathcal{H}}$ are bounded. Then according to [63, Theorem 1], the nominally well-posed system $\hat{\mathcal{H}}$ only has solutions with vanishing times between jumps if it has a complete discrete solution, which is not the case according to Lemma 3.7. □

Remark 3.7. The conclusion that no solution of $\hat{\mathcal{H}}$ has vanishing times between jumps is a stronger claim than simply showing that no solution to $\hat{\mathcal{H}}$ is Zeno [63].

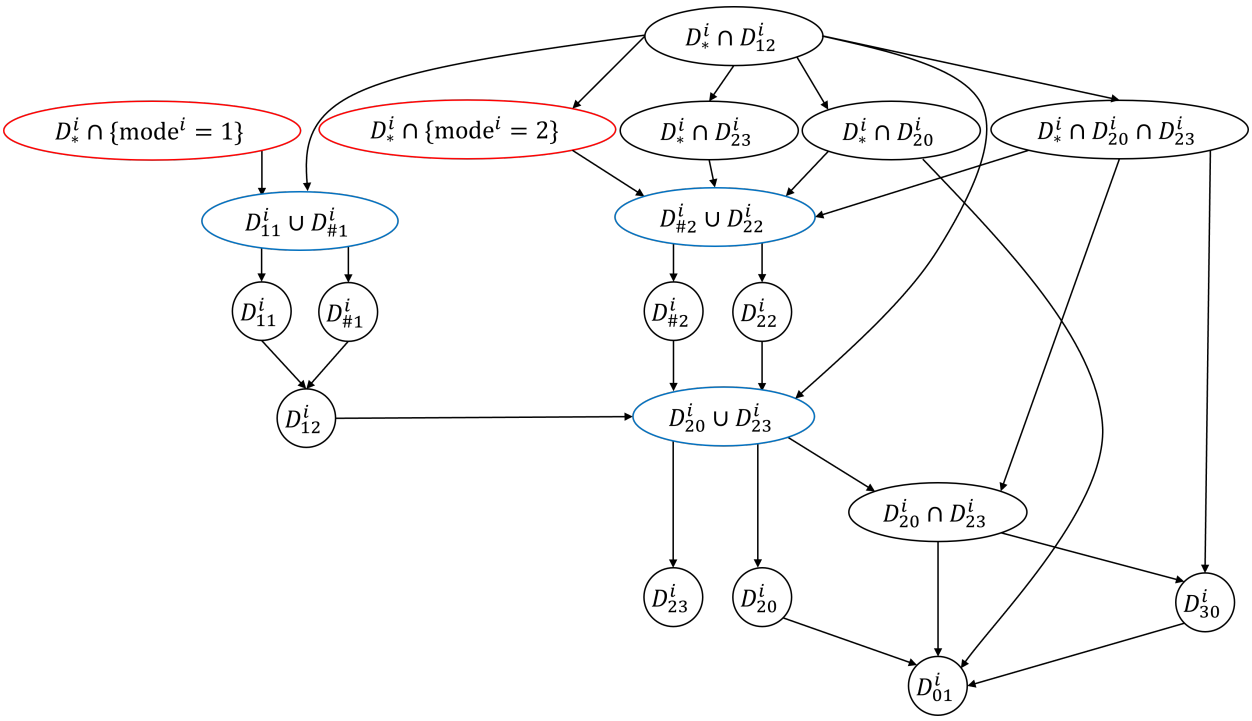

Figure 3-9. Depiction of the directed graph representing all possible sequences of null-time jumps. Arrows pointing to black nodes represent a possible subset of D that a solution can jump to in null-time. Each blue node represents the union of its child nodes. These nodes do not represent a particular state in D with a defined jump mapping, but rather are used for reducing the number of arrows in the graph to increase legibility. An arrow entering a blue node indicates a possible jump into any of its child nodes. Red nodes must jump into a subset of D, whereas black nodes may jump into the flow set C. By inspection this graph contains no directed cycles (Lemma 3.6).

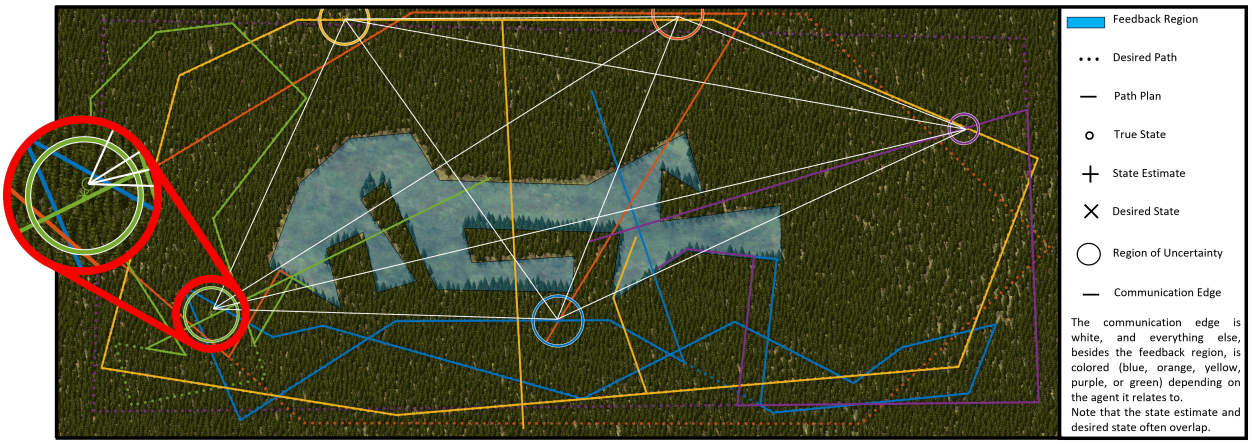

Figure 3-10. Snapshot of a simulation where the agents were always communicating and an estimate update rate of 0.1 Hz was used. The values for $\tilde{\rho}$ can be seen in Figure 3-11.

3.7 Simulation Results

3.7.1 Simulation Setup

A comparative investigation through simulation was conducted in MATLAB® to show the effectiveness of the cooperative behavior proposed in this paper. The simulated world has dimensions of 1024m $\times$ 438.75m, with a polygonal non-convex feedback region (Figures 3-10 and 3-11). Each simulation is composed of five agents ($N = 5$) initialized randomly within the inset feedback region $\mathcal{F}_{\text{in}}$ (inset distance of 2.5m). Each agent is assigned a different desired path, but with a random starting point along that path. Each agent had the following dynamical components in common: $\bar{d}^i = 0.01$m/s, $\epsilon^i = 100$ $k_1^i = 16$, $k_2^i = 16$, $\alpha^i = 0.5$, $\beta^i = 0.5$, $f^i(x^i) = 0.01x^i$ m/s, $L^i = 0.01$m/s, $S^i = 3.8$ m/s, and $\Psi_1^i = \Psi_2^i = 1 \times 10^{-6}$. A unique and randomly generated smooth disturbance function was assigned to each agent, for each simulation. Three hundred comparative simulations were performed, each for $3,600$s. For each comparison, three communication profiles were compared: no communication, 200m communication radius for each agent, and always communicating. For each communication profile, all initial conditions of the problem, and disturbance function were kept the same. Additionally, the first one hundred simulations were done with an cooperative state estimate update

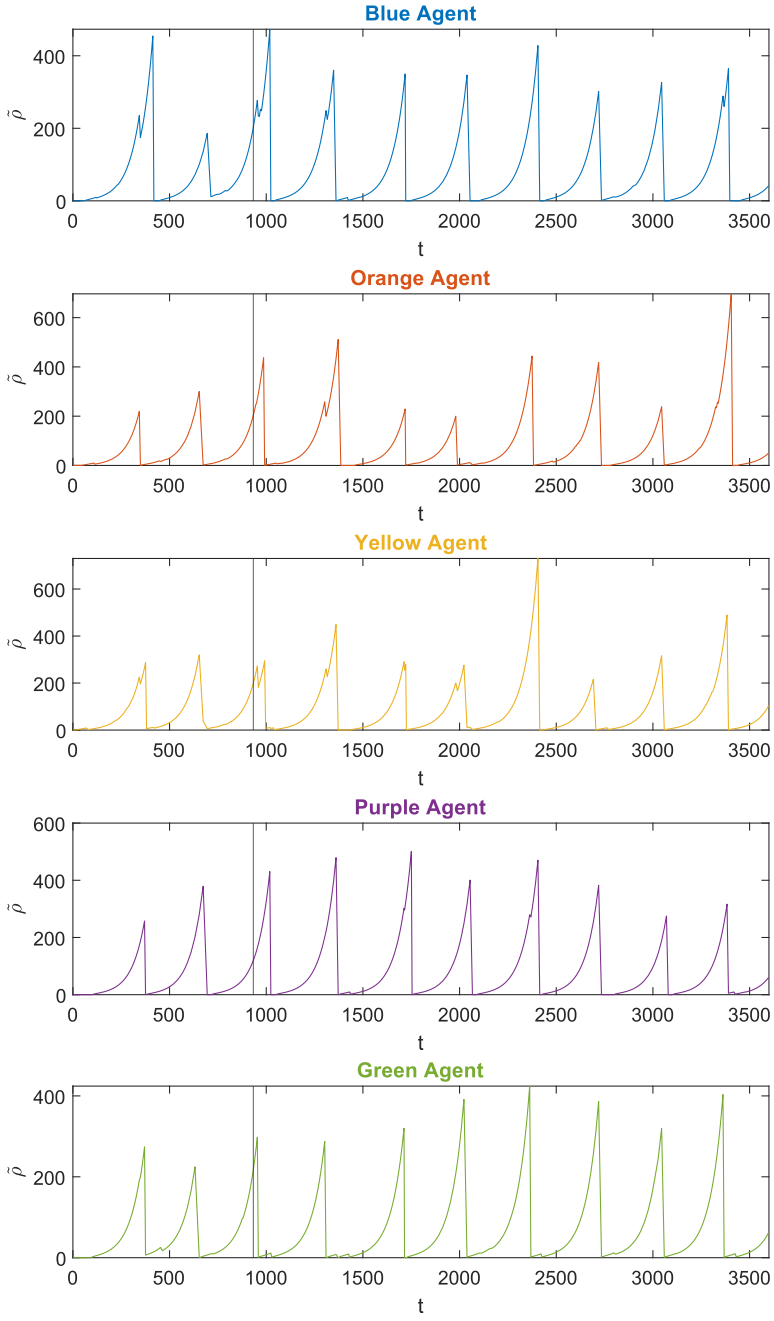

Figure 3-11. Plot of the radius of uncertainty $\tilde{\rho}^i$ as a function of time for the simulation in Figure 3-10. The vertical line on each plot represents the time where the snapshot in Figure 3-10 was taken. This simulation resulted in the largest value for $\mathfrak{R}_2$ (Table 3-1), which was specifically realized by the state estimates affecting the Yellow agent, where a series of three substantial state estimate updates nearly resulted in the radius of uncertainty being zero, allowing the Yellow agent to do more than one full loop about its desired path.

rate of 0.1 Hz (i.e., $T^i_{\text{max}} = 10$s for all agents), the second set of one hundred simulations had an update rate of 1 Hz, and the final one hundred simulations had an update rate of 10 Hz.

To facilitate a comparative performance of the cooperative behavior, the state vector X^i is augmented by the causally inert vector $\mathfrak{T}^i_{\text{sim}} \triangleq (\tau^i_0, \tau^i_1, \tau^i_2, \tau^i_3, \mathfrak{T}^i_1, \mathfrak{T}^i_2)$ to include the timing variables which measure the time agent i spends in each operating mode 0, 1, 2, and 3, the maximum total dwell-time of agent i in operating modes 1, 2 and 3 given a path plan π^i, and the maximum total dwell-time in mode 2 given a path plan π^i, respectively.

Each simulation was performed using MATLAB®'s ODE45 solver. A relative tolerance and an absolute tolerance of 1×10^{-4} were selected. The state estimation update algorithm was implemented with the use of the Boolean set operation functions found in MATALB®'s Computational Geometry library, and Welzl's algorithm [61] was used for computing the minimum bounding ball. The values of τ^i_0, τ^i_1, τ^i_2, τ^i_3, $\mathfrak{T}^i_1$, and $\mathfrak{T}^i_2$ are specially recorded just prior to the execution of the jump map when $\tilde{X} \in \tilde{D}^i_{20} \cup \tilde{D}^i_{30}$. At each recording instance ℓ the functions

$$\left(\mathfrak{R}^i_1\right)_\ell \triangleq \frac{\tau^i_1 + \tau^i_2 + \tau^i_3 - \mathfrak{T}^i_1}{\mathfrak{T}^i_1} * 100,$$
$$\left(\mathfrak{R}^i_2\right)_\ell \triangleq \frac{\tau^i_2 - \mathfrak{T}^i_2}{\mathfrak{T}^i_2} * 100,$$

are computed, and also recorded. $\mathfrak{R}^i_1$ measures the percent increase in the total time that agent i spends in the operating modes 1, 2, and 3 (i.e., the feedback denied region) compared to the worst-case dwell-time for the path plan π^i used to determine $\mathfrak{T}^i_1$. The worst-case dwell-time is only realized if the agent must utilize the full length of the return trajectory to reacquire feedback, but typically the agent will reacquire feedback much sooner. The next metric, $\mathfrak{R}^i_2$ measures a similar quantity, but instead of modes 1, 2, and 3, this metric measures the percent increase in time spent in mode 2 (i.e., time spent tracking the desired path X^i_d).

3.7.2 Results

A statistical analysis of the recorded results (i.e.,$\mathfrak{R}_1$ and $\mathfrak{R}_2$) was conducted. The minimum, maximum, mean, and median for each simulation type was calculated and tabulated in Table 3-1.

3.8 Discussion

Simulation results confirm an improvement in performance when cooperative state estimation is used (Table 3-1). Depending on the estimation update rate and communication structure, the agents were able to spend more time tracking the desired path ($\mathfrak{R}_2$), and in some instances, they were able to increase the total time in the feedback denied region $(\mathfrak{R}_1)$, despite the conservative nature of the developed dwell-times (a consequence of guaranteeing re-entry into the feedback region with unknown disturbances). The largest increase in time spent tracking the desired path was observed in a simulation where there was always communication among all of the agents and where the estimate update rate was 0.1 Hz (Figure 3-10 for a snap shot of this particular simulation). Here an improvement of 478% was observed. As expected, simulations where the agents were always communicating yielded the best performance, but what was unexpected was that a faster estimate update rate does not necessarily yield better performance, on average. Based on the recorded results, it was seen that an update rate of 1Hz yielded the best results, on average. This phenomenon can be explained by first observing two facts.

Fact 3.1. *Let $\hat{d}_{ij} \triangleq \|\hat{x}_i - \hat{x}_j\|$ be the distance between the state estimates of agent i and j. The region of uncertainty reduces as $|\hat{d}_{ij} - d_{ij}|$ increases (Figure 3-13).*

Fact 3.2. *The use of the minimum enclosing ball in* (3–31) *adds uncertainty to the ideal uncertainty region $\hat{U}^i$ (Figure 3-4).*

Figure 3-12 shows how a slower estimate update rate can yield better results. Scenarios like the one illustrated are more likely to be realized if there is a tendency for the agents to continue drifting away from their respective state estimates (Fact 3.1),

which is the case for the simulations done in this study due to the presence of the persistent drift dynamics $f^i(x^i) = 0.01x^i$ (Figure 3-14). Even though the tendency to drift in the same direction is present, the addition of state uncertainty from the minimum enclosing ball diminishes the results of the following state estimate update (Fact 3.2), which is observed in the illustrated scenario (Figure 3-12). This observation may motivate the use of dynamic state estimate update rates if there is more knowledge of the nature of the drift dynamics.

In regions where there is a tendency to continue drifting a slower update rate could be beneficial, whereas in other areas it may be beneficial to have a faster estimate update rate to increase the chances of capturing a beneficial update. However, future work should aim to develop a dynamic model for uncertainty regions that are not modeled as a ball since the hindrance of the minimum enclosing ball would no longer be present; therefore, a faster update rate would always be preferable. Future work should also aim at developing algorithms for computing return trajectories in real-time, allowing for state estimate updates while an agent is operating in mode 3. Something else to consider may be the computational complexity when a large number of agents are communicating with each other. In [64], the authors considered a similar problem and developed an algorithm for selecting a smaller number of agents to be used in an update. Finally, other information, such as knowledge of communication radii of the agent, could also yield better updates.

3.9 Conclusion

Chapter 2 considered the problem of tracking a desired trajectory with state feedback limited to a known region of general shape and advanced a method for planning detours to reacquire state feedback, with guaranteed success. This chapter generalizes our previous work to a multi-agent setting, where independent agents with independent tracking tasks cooperate to improve each other's state estimators. Improved state estimation is achieved through opportunistic sharing of relative distance

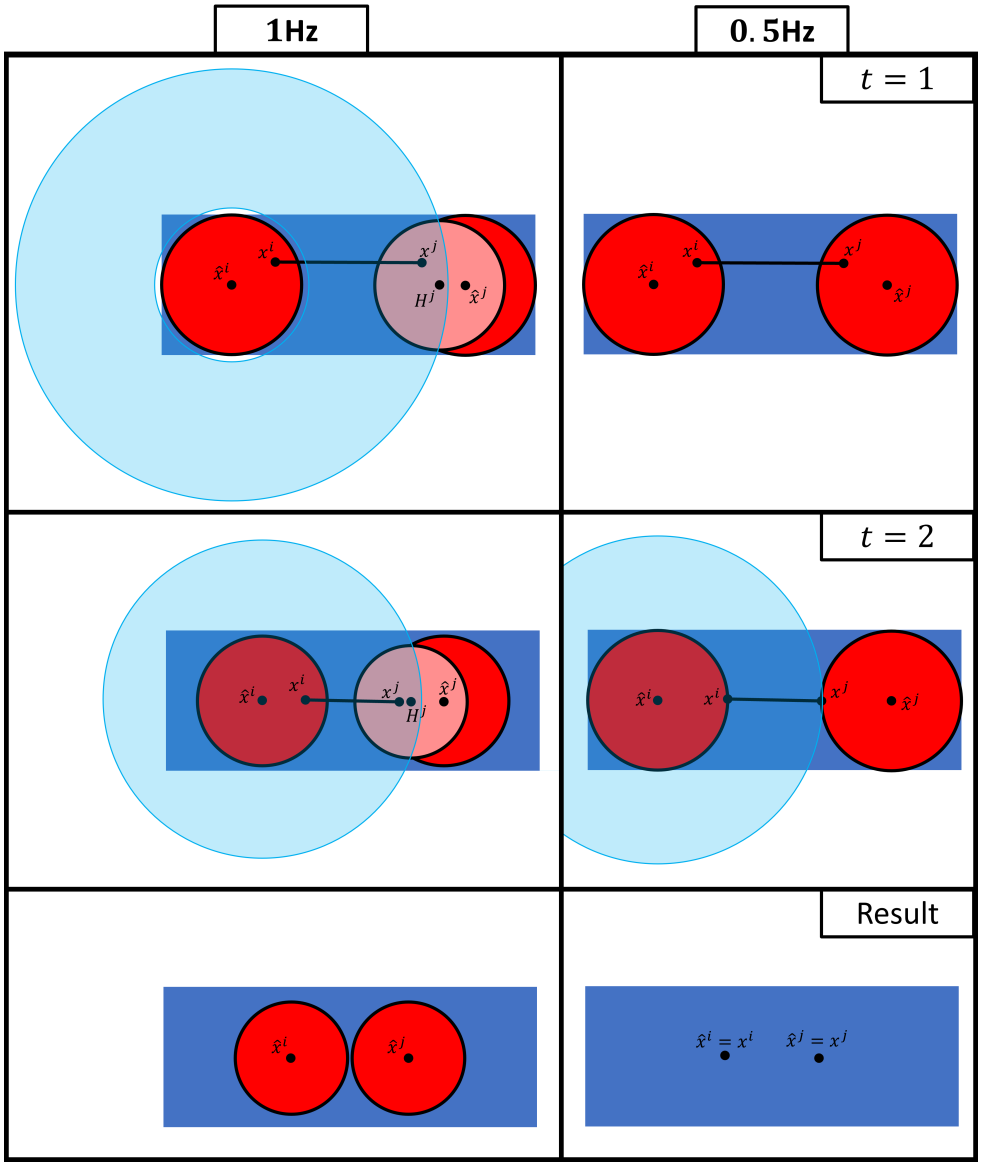

Figure 3-12. Illustration of an example scenario where it is beneficial to have a slower state estimate update rate. Agents i and j have the same initial conditions for both scenarios; however, the left scenario has an update rate of 1Hz and the right has a 0.5Hz update rate. Updates in the state estimate and the region of uncertainty are shown in pink and then propagated to the next time step in the next frame. To increase legibility, only the update for agent j is shown in pink, but the update is realized for both agents in the next frame. The bottom pane of the image shows the results after the updates at $t = 2$. Here, it is beneficial to delay an update only if there is a tendency for d_{ij} to continue to diverge from $\hat{d}_{ij}$, otherwise the scenario depicted here would not necessarily happen, because bounding the updated uncertainty region by the minimum enclosing ball adds uncertainty (Fact 3.2).

		$\mathfrak{R}_1$			$\mathfrak{R}_2$		
		Median	Mean	Max	Median	Mean	Max
0.1 Hz	Never Communicating	-15.57	-14.52	-4.50	-0.00	-0.00	0.03
	200m Communication Radius	-14.64	-10.14	90.88	0.01	6.49	192.40
	Always Communicating	-8.65	5.00	325.18	5.29	29.55	478.28
1 Hz	Never Communicating	-15.58	-14.46	-5.07	-0.00	-0.00	0.03
	200m Communication Radius	-14.49	-9.44	76.21	0.01	7.53	133.45
	Always Communicating	-7.45	9.48	281.15	6.50	36.05	466.71
10Hz	Never Communicating	-15.57	-14.42	-4.59	-0.00	-0.00	0.03
	200m Communication Radius	-14.38	-9.55	66.80	0.01	7.27	123.21
	Always Communicating	-7.12	7.17	291.90	7.03	31.76	469.58

Table 3-1. Tabulated simulation results showing the median, mean, and max values for the metrics $\mathfrak{R}_1$ and $\mathfrak{R}_2$, for each combination of update frequency (i.e, 0.1Hz, 1Hz, and 10Hz) and communication structure (i.e., never communicating, 200m communication radius, and always communicating).

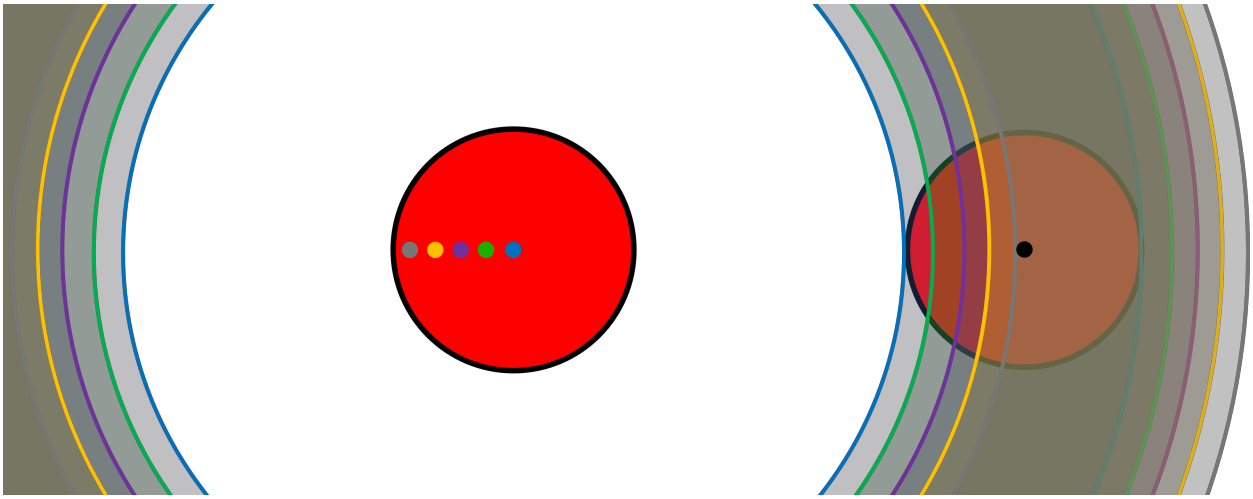

Figure 3-13. Illustration of the different annuli for different values of d_{ij}. For the left region of uncertainty (red circle), the actual state (agent i) was varied (different colored dots), and the actual state for agent j in the region of uncertainty on the right is kept equal to the state estimate at the center of the region of uncertainty. It is observed that when d_{ij} diverges from $\hat{d}_{ij}$, the resulting annuli (i.e, U_i^j, color correlated with respect to the varied actual state) causes a greater reduction in the region of uncertainty (3–30). Even though this figure only illustrates the scenario where U_i^j is an annulus, the same conclusions can be made when it is a circle.

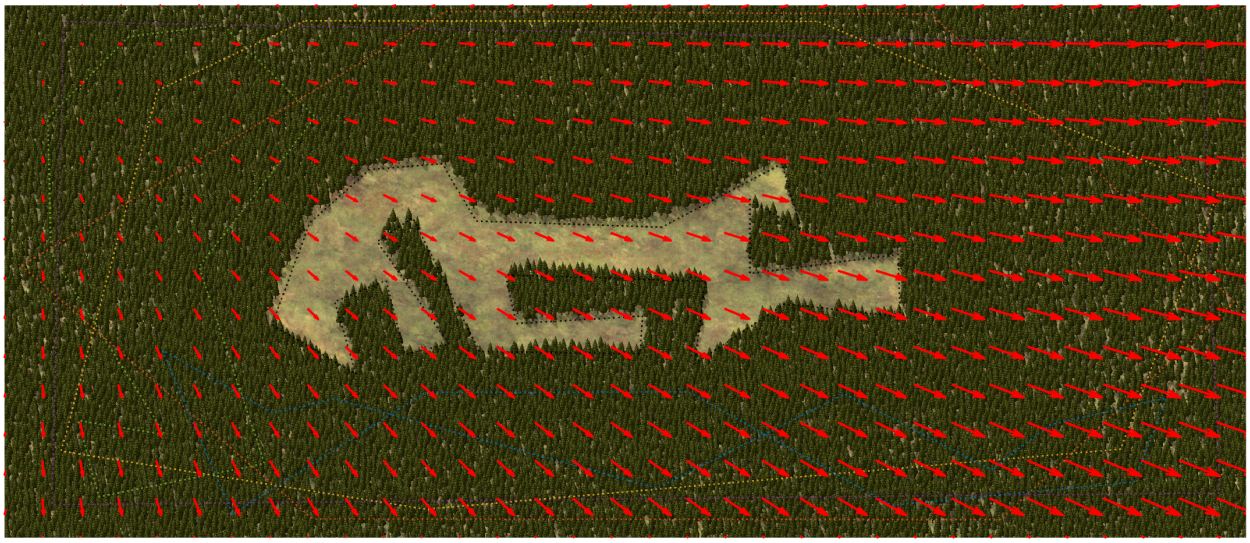

Figure 3-14. A vector field of the drift dynamics $f^i(x^i) = 0.01x^i$, which was common to all agents for all simulation runs. This drift dynamics function resulted in a tendency for d_{ij} to diverge from $\hat{d}_{ij}$.

measurements and state estimation data as the agents enter a communication distance of one another. The discontinuous character of this interaction, in addition to the presence of unmodeled disturbances, motivates the use of hybrid differential inclusions and their Krasovskii regularizations.

The developed cooperative localization method accounts for individual agent dynamics and uses the relative distance measurements to yield provably improved updates for the state estimator of each agent. Improved state estimation is critical for enhancing tracking performance. These updates trigger the re-planing auxiliary trajectories, ultimately allowing agents to travel further along the desired paths without destabilizing the system or exceeding the user-prescribed tracking error limits.

Although the developed controller results in closed-loop dynamics not satisfying the hybrid basic conditions, it is shown that Krasovskii solutions retain the re-entry guarantees necessary for stability; however, their optimality in terms of maximizing time spent tracking the desired trajectories remains an open question. Also, temporal properties of maximal solutions are studied and it was concluded that there are no vanishing times between jumps (e.g., Zeno behavior).

A comparative simulation study was conducted which showed that the cooperative behavior enables the agents to spend more time tracking the desired paths. Simulations also confirmed that when more agents are communicating with one another performance is increased, as expected. However, it was also shown that special considerations need to be made about the state estimation update frequency. The update frequency must be considered as a consequence of not having a dynamical model for uncertainty regions that are not circular, thus requiring the need to bound the reduced uncertainty regions by a minimum enclosing ball. Future work could focus on removing the need to bound the reduced uncertainty regions by a ball by developing a dynamical model for regions of uncertainty that are not necessarily a ball

CHAPTER 4
IMAGE-BASED TARGET TRACKING IN THE PRESENCE OF INTERMITTENT POSE MEASUREMENTS VIA LYAPUNOV-BASED DEEP NEURAL NETWORKS

This chapter introduces a novel framework for image-based tracking systems, addressing scenarios where the tracking agent needs to discontinue tracking a target either due to the need to fulfill other tasks or the target becoming obscured. The proposed approach deploys a Lyapunov-based Deep Neural Network (Lb-DNN) to learn the dynamics of the target when visible, and to predict its future trajectory when not visible. To ensure that target tracking resumes, the topologically inspired method from Chapter 2 is further generalized, using the predicted trajectory of the target. This method informs the tracker agent about the duration it can suspend tracking the target and specifies a pose for the camera for guaranteeing that tracking resumes at some later time. Simulation results are provided to demonstrate the efficacy of the developed methodology for the task of tracking a target intermittently, where the topologically-inspired camera placement algorithm is successfully deployed to reacquire tracking of the target

4.1 Preliminaries

4.1.1 Lyapunov Based Deep Neural Networks

DNNs are known to approximate any given continuous function on a compact set, based on the universal function approximation theorem [65]. Following the work in [66], let $\sigma \in \mathbb{R}^{L_{\text{in}}}$ denote the DNN input with size $L_{\text{in}} \in \mathbb{Z}_{>0}$, and $\Theta \in \mathbb{R}^{p}$ denote the vector of DNN parameters (i.e., weights and bias terms) with size $\mathcal{K} \in \mathbb{Z}_{>0}$. Then, a fully-connected feedforward DNN $\Phi(\sigma, \Theta)$ with output size $L_{\text{out}} \in \mathbb{Z}_{>0}$ is defined using a recursive relation $\Phi_j \in \mathbb{R}^{L_{j+1}}$ modeled as

$$\Phi_j \triangleq \begin{cases} W_j^{\top} \phi_j \left(\Phi_{j-1} \right), & j \in \{1, \ldots, k\}, \\ W_j^{\top} \sigma_a, & j = 0, \end{cases} \tag{4–1}$$

where $\Phi(\sigma, \Theta) = \Phi_k$, and $\sigma_a \triangleq \begin{bmatrix} \sigma^\top & 1 \end{bmatrix}^\top$ denotes the augmented input that accounts for the bias terms, $k_h \in \mathbb{Z}_{>0}$ denotes the total number of hidden layers, $W_j \in \mathbb{R}^{L_j \times L_{j+1}}$ denotes the matrix of weights and biases, $L_j \in \mathbb{Z}_{>0}$ denotes the number of nodes in the j^{th} layer for all $j \in \{0, \ldots, k_h\}$ with $L_0 \triangleq L_{\text{in}} + 1$ and $L_{k_h+1} = L_{\text{out}}$. The vector of smooth activation functions is denoted by $\phi_j : \mathbb{R}^{L_j} \to \mathbb{R}^{L_j}$ for all $j \in \{1, \ldots, k_h\}$. If the DNN involves multiple types of activation functions at each layer, then ϕ_j may be represented as $\phi_j \triangleq [\varsigma_{j,1}; \ldots; \varsigma_{j,L_j-1}; 1]$, where $\varsigma_{j,i} : \mathbb{R} \to \mathbb{R}$ denotes the activation function at the i^{th} node of the j^{th} layer. For the DNN architecture in (4–1), the vector of DNN weights is defined as $\Theta \triangleq \begin{bmatrix} \text{vec}(W_0)^\top & \ldots & \text{vec}(W_{k_h})^\top \end{bmatrix}^\top \in \mathbb{R}^{\mathcal{K}}$, where $\mathcal{K} = \Sigma_{j=0}^{k_h} L_j L_{j+1}$. The Jacobian of the activation function vector at the j^{th} layer is denoted by $\phi_j' : \mathbb{R}^{L_j} \to \mathbb{R}^{L_j \times L_j}$, and $\phi_j'(y) \triangleq \frac{\partial}{\partial z} \phi_j(z)\big|_{z=y}$, for all $y \in \mathbb{R}^{L_j}$. Let the Jacobian of the DNN with respect to the weights be denoted by $\Phi'(\sigma, \Theta) \triangleq \frac{\partial}{\partial \theta} \Phi(\sigma, \Theta)$, which can be represented using $\Phi'(\sigma, \Theta) = \begin{bmatrix} \Phi_0', & \Phi_1', & \ldots, & \Phi_k' \end{bmatrix}$, where $\Phi_j' \triangleq \frac{\partial}{\partial \text{vec}(W_j)} \Phi(\sigma, \Theta)$ for all $j \in \{0, \ldots, k_h\}$. Additionally, let the Hessian of the the DNN with respect to the weights be denoted by $\Phi''(\sigma, \Theta) \triangleq \frac{\partial^2}{\partial \Theta^2} \Phi(\sigma, \Theta)$. Then, using (4–1) and the property of the vectorization operator in 1–2 yields

$$\Phi_0' = \left(\prod_{l=1}^{\overset{\curvearrowleft}{k_h}} W_l^\top \phi_l'(\Phi_{l-1}) \right) (I_{L_1} \otimes \sigma_a^\top), \tag{4–2}$$

and

$$\Phi_j' = \left(\prod_{l=j+1}^{\overset{\curvearrowleft}{k_h}} W_l^\top \phi_l'(\Phi_{l-1}) \right) \left(I_{L_{j+1}} \otimes \phi_j^\top(\Phi_{j-1}) \right), \tag{4–3}$$

for all $j \in \{1, \ldots, k_h\}$. A fully-connected DNN is described here for simplicity of exposition. The following observer/predictor and adaptation law development can be generalized for any network architecture Φ with a corresponding Jacobian Φ'. The reader is referred to [67]– [70] for extending the subsequent development to ResNets, LSTMs, PINNs, and dropout architectures, respectively.

4.1.2 Filippov Regularization

Given the differential equation $\dot{y} = h(y,t)$ with a discontinuous right-hand-side (RHS) $h : \mathbb{R}^n \times [0,\infty) \to \mathbb{R}^n$, Filippov's theory of differential inclusions (e.g., [71] and [72]) can be used to establish that solutions exist almost everywhere (a.e.), i.e., for almost all $t \in [0,\infty)$, for $\dot{y} \overset{a.e.}{\in} K[h](y)$, where $K[h]$ denotes the regularization of the function h, defined as

$$K[h] \triangleq \bigcap_{\delta>0} \bigcap_{M \text{ null}} \overline{\text{co}}\left(h\left(B_\delta^\circ(y) \setminus M\right)\right),$$

where M runs over all null subsets of $\mathbb{R}^n \times [0,\infty)$. For example, the Filippov regularization of the sign function is computed as $K[\text{sgn}](x) = \text{SGN}(x)$, where $\text{SGN}(x) = 1$, when $x > 0$, $\text{SGN}(x) = -1$, when $x < 0$, and $\text{SGN}(x) = [-1,1]$ when $x = 0$, or as another example, the Filippov regularization for the normalization function $h(x) = x/\|x\|$ of a vector $x \in \mathbb{R}^n$ is $K[h](x) = h(x)$ when $x \neq 0$ and $K[h](x) = B_1(0)$ when $x = \mathbf{0}$.

4.2 Problem Formulation

4.2.1 Tracker and Target Kinematic Relationships

The objective of this paper is to develop a dynamic observer/predictor to estimate the pose, linear and angular velocity, and linear and angular acceleration of the target using the tracker agent's camera, despite the target intermittently leaving the FoV of the tracker agent. Let the tracker agent's camera reference frame be denoted by $\mathcal{C}$ which has an origin at the principal point of the camera, denoted by C, with basis $\{\mathbf{c}_1, \mathbf{c}_2, \mathbf{c}_3\}$, where the $\mathbf{c}_1$-axis is parallel with the image plane's vertical; the $\mathbf{c}_2$-axis is parallel with the image plane's horizontal; and the $\mathbf{c}_3$-axis is directed along the camera's line of sight and collinear with the optical axis (Figure 4-1). The inertial reference frame is denoted by $\mathcal{I}$ with an origin at the arbitrary point I with basis $\{\mathbf{i}_1, \mathbf{i}_2, \mathbf{i}_3\}$. The target's reference frame is denoted by $\mathcal{T}$, which has an origin at an arbitrarily selected feature point, denoted by T, with basis $\{\mathbf{t}_1, \mathbf{t}_2, \mathbf{t}_3\}$.

The pose of the tracker agent (i.e., the pose of $\mathcal{C}$ with respect to $\mathcal{I}$) is defined as ${}^{\mathcal{I}}X_{\mathcal{C}} \triangleq [{}^{\mathcal{I}}x_{\mathcal{C}}; {}^{I}\delta_{\mathcal{C}}]$, where ${}^{\mathcal{I}}x_{\mathcal{C}} \in \mathbb{R}^3$ is the position of $\mathcal{C}$ with respect to $\mathcal{I}$, expressed in

$\mathcal{I}$, and ${}^{\mathcal{I}}\delta_{\mathcal{C}} \in \mathbb{S}^3$ is the quaternion parameterization of the rotation matrix ${}^{\mathcal{I}}_{\mathcal{C}}R \in \mathbb{R}^{3\times3}$, representing the orientation of $\mathcal{C}$ with respect to $\mathcal{I}$, where $\mathbb{S}^3$ denotes the space of all versors (i.e., a quaternion of norm 1).

Assumption 4.1. ${}^{\mathcal{I}}X_{\mathcal{C}}$ is always measurable.

The pose of the target (i.e., the pose of $\mathcal{T}$ with respect to $\mathcal{I}$) is defined as ${}^{\mathcal{I}}X_{\mathcal{T}} \triangleq [{}^{\mathcal{I}}x_{\mathcal{T}}; {}^{\mathcal{I}}\delta_{\mathcal{T}}]$, where ${}^{\mathcal{I}}x_{\mathcal{T}} \in \mathbb{R}^3$ is the position of $\mathcal{T}$ with respect to $\mathcal{I}$, expressed in $\mathcal{I}$, and ${}^{\mathcal{I}}\delta_{\mathcal{T}} \in \mathbb{S}^3$ is the quaternion parameterization of the rotation matrix ${}^{\mathcal{I}}_{\mathcal{T}}R \in \mathbb{R}^{3\times3}$, representing the orientation of $\mathcal{T}$ with respect to $\mathcal{I}$. However, since the pose of the target cannot be directly measured with respect to the inertial frame, the tracker agent's camera reference frame is used, thus the relative pose of the target with respect to the camera (i.e., $\mathcal{T}$ with respect to $\mathcal{C}$, expressed in $\mathcal{C}$) is defined as ${}^{\mathcal{C}}X_{\mathcal{T}/\mathcal{C}} \triangleq [{}^{\mathcal{C}}x_{\mathcal{T}/\mathcal{C}}; {}^{\mathcal{C}}\delta_{\mathcal{T}}]$, where ${}^{\mathcal{C}}x_{\mathcal{T}/\mathcal{C}} \in \mathbb{R}^3$ is the position of $\mathcal{T}$ with respect to $\mathcal{C}$, expressed in $\mathcal{C}$, and ${}^{\mathcal{C}}\delta_{\mathcal{T}} \in \mathbb{S}^3$ is the quaternion parameterization of the rotation matrix ${}^{\mathcal{C}}_{\mathcal{T}}R \in \mathbb{R}^{3\times3}$, representing the orientation of $\mathcal{T}$ with respect to $\mathcal{C}$. The kinematic relationship is given by

$$
\begin{aligned}
{}^{\mathcal{I}}x_{\mathcal{T}} &= {}^{\mathcal{I}}x_{\mathcal{C}} + {}^{\mathcal{I}}_{\mathcal{C}}R\,{}^{\mathcal{C}}x_{\mathcal{T}/\mathcal{C}}, \\
{}^{\mathcal{I}}\delta_{\mathcal{T}} &= {}^{\mathcal{I}}\delta_{\mathcal{C}} \odot {}^{\mathcal{C}}\delta_{\mathcal{T}},
\end{aligned}
$$

which is illustrated in Figure 4-1. The time-derivative of ${}^{\mathcal{I}}X_{\mathcal{T}}$ is expressed as

$$
{}^{\mathcal{I}}\dot{X}_{\mathcal{T}} = Q({}^{\mathcal{I}}\delta_{\mathcal{T}})\,{}^{\mathcal{I}}\xi_{\mathcal{T}}, \tag{4–4}
$$

where

$$
Q \triangleq \begin{bmatrix} {}^{\mathcal{I}}_{\mathcal{T}}R & \mathbf{0}_{3\times3} \\ \mathbf{0}_{4\times3} & \frac{1}{2}B({}^{\mathcal{I}}\delta_{\mathcal{T}}) \end{bmatrix},\ B({}^{\mathcal{I}}\delta_{\mathcal{T}}) \triangleq \begin{bmatrix} -({}^{\mathcal{I}}\delta_{\mathcal{T}})_v^{\top} \\ ({}^{\mathcal{I}}\delta_{\mathcal{T}})_s\mathbf{I}_3 + ({}^{\mathcal{I}}\delta_{\mathcal{T}})_v^{\times} \end{bmatrix},
$$

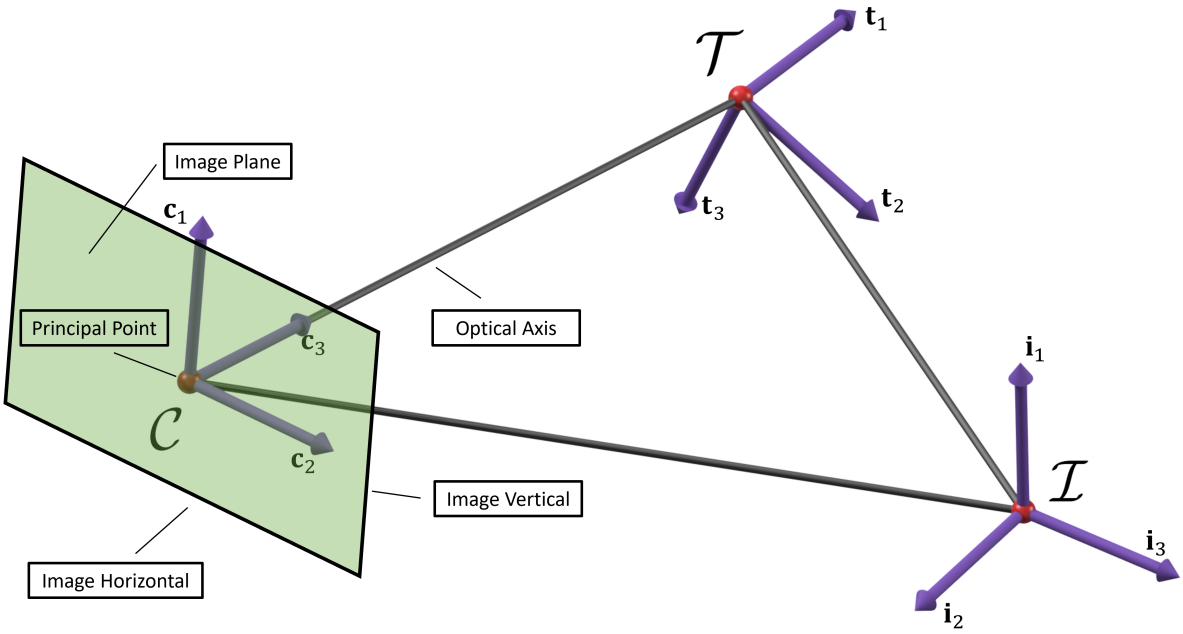

Figure 4-1. Kinematic diagram between the three reference frames: Inertial ($\mathcal{I}$), Target ($\mathcal{T}$), and Camera ($\mathcal{C}$).

${}^{\mathcal{I}}\xi_{\mathcal{T}} \triangleq [{}^{\mathcal{I}}v_{\mathcal{T}}; {}^{\mathcal{I}}\omega_{\mathcal{T}}]$, and ${}^{\mathcal{I}}v_{\mathcal{T}} \in \mathbb{R}^3$, ${}^{\mathcal{I}}\omega_{\mathcal{T}} \in \mathbb{R}^3$ are the translational velocity and angular velocity, respectively [73, Chapter 3.4]. Notice that from (4–4), ${}^{\mathcal{I}}\xi_{\mathcal{T}}$ may be expressed as

$$ {}^{\mathcal{I}}\xi_{\mathcal{T}} = Q^{+}({}^{\mathcal{I}}\delta_{\mathcal{T}})\, {}^{\mathcal{I}}\dot{X}_{\mathcal{T}}, \tag{4–5} $$

since $Q^{+}Q = \mathbf{I}_{6\times 6}$.

4.2.2 Tracking with Occlusions

As a consequence of environmental effects and task-definition (e.g., obstacles, battery life, terrain, etc), the tracking agent is confined to the operating region $\mathcal{O} \subset \mathcal{E}$, where $\mathcal{E} \subset \mathbb{R}^3$ is convex and compact. The physical space occupied by the target is denoted by $\mathscr{T}({}^{\mathcal{I}}X_{\mathcal{T}}) \subset \mathcal{O}$ (i.e., all the 3D feature points on the target for the given state ${}^{\mathcal{I}}X_{\mathcal{T}}$). When appropriate, the argument for $\mathscr{T}(\cdot)$ will be suppressed for brevity (i.e., $\mathscr{T} = \mathscr{T}({}^{\mathcal{I}}X_{\mathcal{T}})$). Pose measurements from the tracking agent's camera may only be available when the target is within the tracker agent's FoV (i.e., $\mathscr{T} \subset F({}^{\mathcal{I}}X_{\mathcal{C}})$) where $F({}^{\mathcal{I}}X_{\mathcal{C}}) \subset \mathcal{O}$ is the space contained in the FoV for a given camera pose ${}^{\mathcal{I}}X_{\mathcal{C}}$. However,

there may be occlusion zones $\mathscr{O} \subset \mathbb{R}^3$ which obscure the target, despite it being in the FoV of the tracking agent. Specifically, if ${}^{\mathcal{I}}X_{\mathcal{T}} \in \mathscr{O}$, feedback is unavailable. The resulting requirement for pose measurements to be available is for $\mathscr{T} \subset \mathcal{F}({}^{\mathcal{I}}X_{\mathcal{C}})$, where $\mathcal{F}({}^{\mathcal{I}}X_{\mathcal{C}}) \triangleq F({}^{\mathcal{I}}X_{\mathcal{C}}) \setminus \mathscr{O}$ denotes the feedback region, i.e., the sub-region of the FoV that is not obscured by the occlusion zones. When appropriate, the argument of the feedback region will be suppressed for brevity (i.e., $\mathcal{F} = \mathcal{F}({}^{\mathcal{I}}X_{\mathcal{C}})$).

Remark 4.1. In practice, occlusion zones depend on the tracker agent camera's pose with respect to objects that may obscure the target. Generation of these zones would be based on camera properties and environmental characteristics, but to simplify the problem, this discussion is omitted.

4.3 Estimation and Prediction

To achieve target tracking, a deep neural network (DNN)-based state estimator and predictor are developed using the pose measurements from the tracker's camera as feedback. These pose measurements are used to tune the weights of the DNN to improve the approximation of the dynamics of the target. Pose measurements are available except when the target exits the FoV or enters an occlusion zone. When pose measurements are unavailable a predictor can be used to predict where the target is based on the learned DNN model of the target's dynamics and propagating that model forward in time. This approach gives two modes of operation for the tracker, which motivates the use of a switching signal $\sigma(t) \in \{a, u\}$, where $\sigma(t) = a$ when feedback is available (i.e., $\mathscr{T} \subset \mathcal{F}$) and $\sigma(t) = u$ when feedback is unavailable (i.e., $\mathscr{T} \not\subset \mathcal{F}$). Let $t_j^a \in \mathbb{R}_{\geq 0}$ denote the j^{th} instance in time when $\sigma(t)$ turns from u to a (i.e., the j^{th} time that target enters into the tracker's FoV allowing for pose measurements), and similarly let $t_j^u \in \mathbb{R}_{>0}$ represent the j^{th} instance in time when $\sigma(t)$ turns from a to u. (i.e., the j^{th} time that the target leaves the tracker's FoV or enters an occluded region), where $j \in \{1, 2, 3, \dots\}$. Additionally, define $\Delta t_j^a \triangleq t - t_j^a$ to be the time that has elapsed since

the j^{th} instance in time when $\sigma(t) = a$, and $\Delta t_j^u \triangleq t - t_j^u$ to be the time that has elapsed since the j^{th} instance in time when $\sigma(t) = u$.

4.3.1 Modeling Assumptions

Assumption 4.2. The target is initially visible (i.e., $\mathscr{T} \subset \mathcal{F}$) to the tracker agent.

Assumption 4.3. The target's pose ${}^{\mathcal{I}}X_{\mathcal{T}}$ is confined to a known convex compact domain $\Omega \subset \mathbb{R}^7$ (i.e., ${}^{\mathcal{I}}X_{\mathcal{T}} \in \Omega$). Let $\overline{X}$ denote a known bound satisfying $\sup_{\omega \in \Omega} \|\omega\| \leq \overline{X}$, which is assumed to be known.

Assumption 4.4. The target velocity is a time-independent Lipschitz continuous function of the target pose. Recalling (4–4), the target's velocities ${}^{\mathcal{I}}\dot{X}_{\mathcal{T}}$ are bounded such that $\sup_{{}^{\mathcal{I}}X_{\mathcal{T}} \in \Omega} \|{}^{\mathcal{I}}v_{\mathcal{T}}\| \leq \bar{v}$ and $\sup_{{}^{\mathcal{I}}X_{\mathcal{T}} \in \Omega} \|{}^{\mathcal{I}}\omega_{\mathcal{T}}\| \leq \bar{\omega}$, where $\bar{v}$ and $\bar{\omega}$ are known constants. Additionally, let $\sup_{{}^{\mathcal{I}}X_{\mathcal{T}} \in \Omega} \|{}^{\mathcal{I}}\dot{X}_{\mathcal{T}}\| \leq \overline{\mathcal{V}}$, where $\overline{\mathcal{V}}$ is a known constant.

Assumption 4.5. There is a known bound $A \in \mathbb{R}_{\geq 0}$ on the linear acceleration of the target, which satisfies $\sup_{{}^{\mathcal{I}}X_{\mathcal{T}} \in \Omega} \|{}^{\mathcal{I}}\ddot{x}_{\mathcal{T}}\| \leq A$.

The target is modeled by the multi-input and multi-output (MIMO) second order nonlinear system

$$\begin{aligned} {}^{\mathcal{I}}\dot{X}_{\mathcal{T}} &= {}^{\mathcal{I}}_{2}X_{\mathcal{T}}, \\ {}^{\mathcal{I}}_{2}\dot{X}_{\mathcal{T}} &= f\left({}^{\mathcal{I}}X_{\mathcal{T}}, {}^{\mathcal{I}}_{2}X_{\mathcal{T}}\right), \end{aligned} \tag{4–6}$$

where ${}^{\mathcal{I}}_{2}X_{\mathcal{T}} \in \mathbb{R}^7$ denotes the velocity state, and $f : \mathbb{R}^7 \times \mathbb{R}^7 \to \mathbb{R}^7$ is an unknown continuous function. ${}^{I}_{2}\dot{X}_{T}$ can be approximated using a DNN as

$$f\left({}^{\mathcal{I}}X_{\mathcal{T}}, {}^{\mathcal{I}}_{2}X_{\mathcal{T}}\right) = \Phi\left({}^{\mathcal{I}}X_{\mathcal{T}}, {}^{\mathcal{I}}_{2}X_{\mathcal{T}}, \Theta\right) + \varepsilon\left({}^{\mathcal{I}}X_{\mathcal{T}}, {}^{\mathcal{I}}_{2}X_{\mathcal{T}}\right),$$

where Φ is a $\mathcal{C}^2$ function[1] , $\varepsilon : \mathbb{R}^7 \to \mathbb{R}^7$ is the unknown reconstruction error. According to the universal function approximation theorem [65], for any $Y > 0$ this approximation can

[1] Smooth activation functions are considered in this chapter, but the work in [66] uses a switched systems analysis accounts for nonsmooth activation functions, which can be applied here so that one can use nonsmooth activation functions, such as rectified linear units (ReLUs).

be made arbitrarily accurate over the compact set

$$\mathcal{Z} \triangleq \left(\overline{X} + \overline{\mathcal{V}} + Y\right) \mathbb{B}, \tag{4–7}$$

thus dependence on ${}^{\mathcal{I}}X_{\mathcal{T}}$ and ${}^{\mathcal{I}}_{2}X_{\mathcal{T}}$ is allowed by Assumptions 4.3 and 4.4.

Assumption 4.6. The bounds on the function reconstruction error ε over $\mathcal{Z}$ and its time-derivative $\dot{\varepsilon}$ are known, specifically, $\|\varepsilon\| \leq \bar{\varepsilon}$ and $\|\dot{\varepsilon}\| \leq \bar{\varepsilon}^{*}$, where $\bar{\varepsilon}, \bar{\varepsilon}^{*} \in \mathbb{R}_{>0}$ are known constants [74].

The objective is to prove that the pose and velocity estimates of the target converge to the actual pose and velocity states of the target. To observe the states ${}^{\mathcal{I}}X_{\mathcal{T}}$ and ${}^{\mathcal{I}}_{2}X_{\mathcal{T}}$ in (4–6), the DNN-based observer/predictor

$$\begin{aligned} {}^{\mathcal{I}}\dot{\hat{X}}_{\mathcal{T}} &= {}^{\mathcal{I}}_{2}\hat{X}_{\mathcal{T}}, \\ {}^{\mathcal{I}}_{2}\dot{\hat{X}}_{\mathcal{T}} &= \begin{cases} \Phi\left({}^{\mathcal{I}}X_{\mathcal{T}}, {}^{\mathcal{I}}_{2}\hat{X}_{\mathcal{T}}, \hat{\Theta}\right) + \nu, & \sigma(t) = a, \\ \Phi\left({}^{\mathcal{I}}\hat{X}_{\mathcal{T}}, {}^{\mathcal{I}}_{2}\hat{X}_{\mathcal{T}}, \hat{\Theta}\right), & \sigma(t) = u, \end{cases} \end{aligned} \tag{4–8}$$

is developed, where ${}^{\mathcal{I}}\hat{X}_{\mathcal{T}} \triangleq [{}^{\mathcal{I}}\hat{x}_{\mathcal{T}}; {}^{\mathcal{I}}\hat{\delta}_{\mathcal{T}}]$ and ${}^{\mathcal{I}}_{2}\hat{X}_{\mathcal{T}} \in \mathbb{R}^{7}$ denote the state estimates of ${}^{\mathcal{I}}X_{\mathcal{T}}$ and ${}^{\mathcal{I}}_{2}X_{\mathcal{T}}$, respectively, $\hat{\Theta} \in \mathbb{R}^{\mathcal{K}}$ is the estimate of the ideal weights, and $\nu \in \mathbb{R}^{7}$ is a subsequently designed function that involves closed-loop pose estimation error feedback to ensure convergence of the pose and velocity estimates.

Proof. The ideal DNN weight vector is bounded such that $\|\Theta\| \leq \overline{\Theta}$, where $\overline{\Theta} \in \mathbb{R}_{\geq 0}$ is a known constant. □

4.3.2 Observer and Predictor Development

The estimation error $e \in \mathbb{R}^{7}$ is defined as

$$e \triangleq {}^{\mathcal{I}}X_{\mathcal{T}} - {}^{\mathcal{I}}\hat{X}_{\mathcal{T}}. \tag{4–9}$$

To facilitate the stability analysis, the filtered error signal $r \in \mathbb{R}^{7}$ is defined as

$$r \triangleq \dot{e} + \alpha e + \eta, \tag{4–10}$$

where $\alpha \in \mathbb{R}_{>0}$ and $\eta \in \mathbb{R}^7$ is the output of the dynamic filter (cf., [68], [75], and [76]) defined as

$$\eta \triangleq p - (k+\alpha)e, \tag{4–11}$$

where $p \in \mathbb{R}^7$, defined as

$$\dot{p} \triangleq \begin{cases} -(k+2\alpha)p - e_f + \left((k+\alpha)^2 + 1\right)e, & \sigma(t) = a, \\ 0, & \sigma(t) = u, \end{cases} \tag{4–12}$$

$$p(t_j^a) = (k+\alpha)e(t_j^a),$$

is used as an internal filter variable, and $e_f \in \mathbb{R}^7$ is an auxiliary output of the filter

$$\dot{e}_f \triangleq \begin{cases} p - \alpha e_f - (k+\alpha)e, & \sigma(t) = a, \\ 0, & \sigma(t) = u, \end{cases} \tag{4–13}$$

$$e_f(t_j^a) = 0,$$

where $k \in \mathbb{R}_{>0}$ is a gain. Using (4–10) and (4–11), the time-derivative of η is

$$\dot{\eta} = -(k+\alpha)r - \alpha\eta + e - e_f. \tag{4–14}$$

When $\sigma(t) = a$, the closed-loop dynamics of the filtered estimation error

$$\begin{aligned} \dot{r} = {} & \Phi\left({}^{\mathcal{I}}X_{\mathcal{T}}, {}^{\mathcal{I}}_{2}X_{\mathcal{T}}, \Theta\right) - \Phi\left({}^{\mathcal{I}}X_{\mathcal{T}}, {}^{\mathcal{I}}_{2}\hat{X}_{\mathcal{T}}, \Theta\right) \\ & + \varepsilon\left({}^{\mathcal{I}}X_{\mathcal{T}}, {}^{\mathcal{I}}_{2}X_{\mathcal{T}}\right) + O\left(\|\tilde{\Theta}\|^2\right) + e - e_f - \nu \\ & + \alpha\dot{e} - (k+\alpha)r - \alpha\eta + \Phi'\left({}^{\mathcal{I}}X_{\mathcal{T}}, {}^{\mathcal{I}}_{2}\hat{X}_{\mathcal{T}}, \hat{\Theta}\right)\tilde{\Theta} \end{aligned} \tag{4–15}$$

is determined using (4–6), (4–8), and (4–14). Based on the stability analysis the robustness term of the state estimator is designed as

$$\nu \triangleq -\left(\gamma(k+\alpha)+2\alpha\right)\eta+\left(\gamma-\alpha^2\right)e+\beta\text{sgn}((e+e_f)), \tag{4–16}$$

where $\gamma,\beta\in\mathbb{R}_{>0}$ are control gains. Substituting (4–16) and the Taylor series expansion,

$$\Phi\left({}^{I}X_T,{}^{I}_{2}\hat{X}_T,\Theta\right)=\Phi\left({}^{\mathcal{I}}X_{\mathcal{T}},{}^{\mathcal{I}}_{2}\hat{X}_{\mathcal{T}},\hat{\Theta}\right)+\Phi'\left({}^{\mathcal{I}}X_{\mathcal{T}},{}^{\mathcal{I}}_{2}\hat{X}_{\mathcal{T}},\hat{\Theta}\right)\tilde{\Theta}+O\left(\|\tilde{\Theta}\|^2\right),$$

into (4–15), the expression can be rewritten as

$$\dot{r}=\tilde{N}+N-kr-\beta\text{sgn}((e+e_f))+\gamma(k+\alpha)\eta-\gamma e \tag{4–17}$$

where $\tilde{\Theta}\triangleq\Theta-\hat{\Theta}$ is the ideal weight mismatch error, $O\left(\|\tilde{\Theta}\|^2\right)$ are the higher order terms of the Taylor series expansion of $\Phi\left({}^{I}X_T,\Theta\right)$, the auxiliary function $\tilde{N}$ is defined as

$$\tilde{N}\triangleq e-e_f+\Phi\left({}^{\mathcal{I}}X_{\mathcal{T}},{}^{\mathcal{I}}_{2}X_{\mathcal{T}},\Theta\right)-\Phi\left({}^{\mathcal{I}}X_{\mathcal{T}},{}^{\mathcal{I}}_{2}\hat{X}_{\mathcal{T}},\Theta\right), \tag{4–18}$$

and $N\triangleq N_1+N_2$ is broken up into two parts defined as

$$N_1\triangleq O\left(\|\tilde{\Theta}\|^2\right)+\varepsilon\left({}^{\mathcal{I}}X_{\mathcal{T}},{}^{\mathcal{I}}_{2}X_{\mathcal{T}}\right), \tag{4–19}$$

$$N_2\triangleq\Phi'\left({}^{\mathcal{I}}X_{\mathcal{T}},{}^{\mathcal{I}}_{2}\hat{X}_{\mathcal{T}},\hat{\Theta}\right)\tilde{\Theta}. \tag{4–20}$$

Fact 4.1. *The higher order terms of the Taylor series expansion of* $\Phi\left({}^{\mathcal{I}}X_{\mathcal{T}},{}^{\mathcal{I}}_{2}X_{\mathcal{T}},\Theta\right)$ *are bounded such that* $\|O\left(\|\tilde{\Theta}\|^2\right)\|\leq\overline{O}$*, where* $\overline{O}\in\mathbb{R}_{>0}$ *is a known constant. This bound is due to the fact that* Φ *is smooth.*

The weight update law for the Lb-DNN in (4–8) is designed based on the Lyapunov-based analysis as

$$\dot{\hat{\Theta}}\triangleq\begin{cases}\text{proj}(\Gamma((e+e_f)^\top\Phi'({}^{\mathcal{I}}X_{\mathcal{T}},{}^{\mathcal{I}}_{2}\hat{X}_{\mathcal{T}},\hat{\Theta}))^\top), & \sigma(t)=a,\\ 0, & \sigma(t)=u,\end{cases} \tag{4–21}$$

where proj$(\cdot)$ is the projection operator defined in [77, Appendix E, eq. (E.4)], and $\Gamma \in \mathbb{R}^{\mathcal{K}\times\mathcal{K}}$ is a positive definite constant adaptation gain matrix.

Let $\mathcal{P} \triangleq \{\upsilon \in \mathbb{R}^{28} : \|\upsilon\| < b\}$, where $b \in \mathbb{R}_{>0}$ is a constant, then by Assumptions 4.6–4.3.1, Fact 4.1, the triangle inequality, and the use of the projection operator, the auxiliary functions (4–18)–(4–20) can be upper-bounded as

$$\|\tilde{N}\| \leq \zeta_1 \|z\|, \tag{4–22}$$

$$\|N_1\| \leq \zeta_2, \tag{4–23}$$

$$\|N_2\| \leq \zeta_3, \tag{4–24}$$

$$\|\dot{N}_1\| + \|\dot{N}_2\| \leq \zeta_4 + \zeta_5 \|z\|, \tag{4–25}$$

for all $z \in \mathcal{P}$, where $\zeta_1, \zeta_2, \zeta_3, \zeta_4, \zeta_5 \in \mathbb{R}_{>0}$ are known constants, and $z \triangleq [e; e_f; \eta; r]$ is the stacked error signal.

To facilitate the forthcoming stability analysis, let $y \triangleq [z; \sqrt{2Q}; \sqrt{2P}]$, where the auxiliary term $Q \in \mathbb{R}$ is defined as

$$Q \triangleq \frac{\alpha}{2} \tilde{\Theta}^\top \Gamma^{-1} \tilde{\Theta}, \tag{4–26}$$

which is positive definite (i.e., $Q \geq 0$) since Γ is a positive-definite matrix. According to Assumption 4.3.1 and the projection operator, Q can be bounded as

$$Q \leq \overline{\Gamma} \triangleq 2\alpha \overline{\Theta}^2 \|\Gamma^{-1}\|_S. \tag{4–27}$$

Similar to the auxiliary term defined in [78], the auxiliary term $P \in \mathbb{R}$ is defined as

$$\begin{aligned} P = {} & \beta \|e + e_f\|_1 - (e + e_f)^\top N + \mathsf{e}^{-\lambda_p t} * \zeta_5 \|z\|^2 \\ & + \mathsf{e}^{-\lambda_p t} * \left((\alpha - \lambda_p) \left(\beta \|e + e_f\|_1 - (e + e_f)^\top N \right) \right) \\ & + \mathsf{e}^{-\lambda_p t} * (e + e_f)^\top \dot{N} + \alpha \mathsf{e}^{-\lambda_p t} * (e + e_f)^\top N_2, \end{aligned} \tag{4–28}$$

where $\lambda_p \in \mathbb{R}_{>0}$ is a user selected constant. Using Leibniz's integral rule, the time-derivative of (4–28) is

$$\dot{P} \triangleq -\lambda_p P - r^\top \left(N_1 - \beta \text{sgn}((e + e_f))\right) - \left(\dot{e} + \dot{e}_f\right)^\top N_2 + \zeta_5 \|z\|^2. \tag{4–29}$$

For the forthcoming Lyapunov analysis, it will be necessary to show that $P \geq 0$, which is established in the following lemma.

Lemma 4.1. *Given any collection of Filippov solutions e, e_f, η, and r, to (4–10) and (4–13)–(4–15), respectively; if the gain conditions*

$$\alpha > \lambda_p, \tag{4–30}$$

$$\beta > \zeta_2 + \zeta_3 + \frac{\alpha\zeta_3 + \zeta_4}{\alpha - \lambda_p}, \tag{4–31}$$

are satisfied, then $P(t) \geq 0$.

Proof. This inequality can be verified by applying Hölder's inequality, and the gain conditions (4–30) and (4–31) to (4–28) (cf., [78, Appendix: Proof of Lemma 4]). □

4.4 Estimator Analysis

For the open and connected set $\mathcal{D} \triangleq \{\upsilon \in \mathbb{R}^{30} : \|\upsilon\| < b\}$, where $b \in \mathbb{R}_{>0}$ is a constant, the Lyapunov candidate $V : \mathcal{D} \to \mathbb{R}$, which is a Lipschitz continuous and positive definite function, is defined as

$$V(y) \triangleq \frac{\gamma}{2} e^\top e + \frac{\gamma}{2} e_f^\top e_f + \frac{\gamma}{2} \eta^\top \eta + \frac{1}{2} r^\top r + Q + P, \tag{4–32}$$

which satisfies

$$\Lambda_1 \|y\|^2 \quad \leq V(y) \quad \leq \Lambda_2 \|y\|^2, \tag{4–33}$$

where $\Lambda_1 \triangleq \min\left\{\frac{\gamma}{2}, \frac{1}{2}\right\}$ and $\Lambda_2 \triangleq \max\left\{\frac{\gamma}{2}, 1\right\}$. Additionally, let $\mathcal{S} \subset \mathcal{D}$ be the set of permissible initial conditions (i.e., $y(t_0) \in \mathcal{S}$)

$$\mathcal{S} \triangleq \left\{\upsilon \in \mathbb{R}^{30} : \|\upsilon\|^2 < \tfrac{\Lambda_1}{\Lambda_2} b^2 - \tfrac{2\overline{\Gamma}}{\Lambda_2}\right\}. \tag{4–34}$$

Since the universal function approximation property only holds on the compact domain $\mathcal{Z}$, it is necessary to show that the inputs to the DNN remain in the compact domain for all $t \in [0, \infty)$, which is accomplished by showing that y is constrained to a compact domain, specifically, $y(t) \in \mathcal{D}$ for all $t \in [0, \infty)$, when $y(0) \in \mathcal{S}$.

Theorem 4.1. *The DNN-based observer in* (4–8) *along with its update laws in* (4–16) *and* (4–21)*, ensures asymptotic estimation when* $\sigma = a$ *in the sense that*

$$\|e\| \to 0 \text{ and } \|\dot{e}\| \to 0 \text{ as } t \to \infty,$$

provided that $y(0) \in \mathcal{S}$*,* $Y > (3+\alpha)b$ *from* (4–7)*, the control gain* k *is selected sufficiently large based on the gain conditions in* (4–30) *and* (4–31)*, and the sufficient condition*

$$\lambda > \zeta_5 + \frac{\epsilon \zeta_1^2}{2},$$

is satisfied, where $\lambda \triangleq \min\left\{\alpha\gamma, k - \frac{1}{2\epsilon}, \lambda_p\right\}$*,* $\epsilon, \gamma, \lambda_p \in \mathbb{R}_{>0}$*, and* $k > \frac{1}{2\epsilon}$*.*

Proof. Let $\dot{y} = h$ represent the closed-loop differential equations in (4–10), (4–13), (4–14), (4–17), (4–21), and (4–29), where $h \in \mathbb{R}^{30}$ denotes the right-hand side of the closed-loop error signals. The generalized time-derivative of (4–32) exists a.e., and $\dot{V} \overset{a.e.}{\in} \dot{\tilde{V}}$, where $\dot{\tilde{V}} \triangleq \cap_{\xi \in \partial V(y)} \xi^\top K[\Psi]^\top$, ∂V is the generalized gradient of V (see [79]), and $\Psi \triangleq [\dot{e}; \dot{e}_f; \dot{\eta}; \dot{r}; \frac{1}{2}Q^{-1/2}\dot{Q}; \frac{1}{2}P^{-1/2}\dot{P}]$. Since V is continuously differentiable, $\dot{\tilde{V}}$ reduces to $\dot{\tilde{V}} = \nabla V^\top K[\Psi] = [e^\top, e_f^\top, \eta^\top, r^\top, \sqrt{2Q}, \sqrt{2P}]K[\Psi]$. Using the calculus for $K[\cdot]$ from ([80, Theorem 1; Properties 2, 5, and 7]), and the projection property in [77, Appendix E, Lemma E.1.iv], and substituting in (4–10), (4–13), (4–14), (4–17), (4–20), (4–21), (4–26), and (4–29), $\dot{\tilde{V}}$ can be rewritten as

$$\begin{aligned}
\dot{\tilde{V}} \subset\ & \gamma e^\top (r - \alpha e - \eta) + \gamma e_f^\top (\eta - \alpha e_f) + \gamma \eta^\top (-(k+\alpha) r - \alpha \eta + e - e_f) \\
& + r^\top \left(\tilde{N} + N + \gamma(k+\alpha)\eta\right) - r^\top (kr + \beta K[\text{sgn}](e + e_f) + \gamma e) \\
& - \alpha \left((e+e_f)^\top N_2 - r^\top (N_1 - \beta K[\text{sgn}](e+e_f))\right. \\
& - (\dot{e} + \dot{e}_f)^\top N_2 + \zeta_5 \|z\|^2 - \lambda_p P.
\end{aligned} \tag{4–35}$$

Using the fact that $K[\text{sgn}((e+e_f))] = \text{SGN}(e+e_f)$, the set in (4–35) reduces to a scalar inequality, since the RHS of (4–35) is continuous a.e., i.e., the RHS is continuous except for the Lebesgue measure zero set of times when $r^\top \text{SGN}(e+e_f) - r^\top \text{SGN}(e+e_f) = \{0\}$ [78, Lemma 1]. Canceling common terms yields

$$\dot{\tilde{V}} \overset{a.e.}{\leq} -\alpha\gamma e^\top e - \alpha\gamma e_f^\top e_f - \alpha\gamma\eta^\top\eta - kr^\top r - \lambda_p P + r^\top \tilde{N} - \zeta_5\|z\|^2. \tag{4–36}$$

Using Young's inequality and the bound in (4–22) yields

$$\dot{\tilde{V}} \overset{a.e.}{\leq} -\alpha\gamma\|e\|^2 - \alpha\gamma\|e_f\|^2 - \alpha\gamma\|\eta\|^2 - (k-\tfrac{1}{2\epsilon})\|r\|^2 - \lambda_p P + \left(\zeta_5 + \tfrac{\epsilon\zeta_1^2}{2}\right)\|z\|^2, \tag{4–37}$$

where $\epsilon \in \mathbb{R}_{>0}$ is a user-defined constant that comes as a result of using Young's inequality. Provided that the sufficient conditions $\lambda > \zeta_5 + \frac{\epsilon\zeta_1^2}{2}$ and $k > \frac{1}{2\epsilon}$ are satisfied

$$\dot{\tilde{V}} \overset{a.e.}{\leq} -c\left(\|z\|^2 + P\right), \tag{4–38}$$

for $c > \lambda - \zeta_5 - \frac{\epsilon\zeta_1^2}{2}$.

Then solving the differential inequality in (4–38), and using the bounds in (4–33) and (4–27), $\|y(t)\| \leq \sqrt{\frac{1}{\Lambda_1}\left(\Lambda_2\|y(t_0)\|^2 + 2\overline{\Gamma}\right)}$ when $y \in \mathcal{D}$. Thus, if $\|y(t_0)\| \leq \sqrt{\frac{\Lambda_1}{\Lambda_2}b^2 - \frac{2\overline{\Gamma}}{\Lambda_2}}$, then $\|y\| < b$, as required by the definition of $\mathcal{D}$. Therefore, if $y(0) \in \mathcal{S}$, then $y \in \mathcal{D}$ for all $t \in [0,\infty)$, thus the bounds in (4–22)–(4–25) hold. To show that the universal function approximation property holds, let $\Upsilon \subset \mathcal{Z}$ be defined as $\Upsilon \triangleq \{v \in \mathcal{Z} : \|v\| \leq \overline{X} + (3+\alpha)b + \overline{\mathcal{V}}\}$. Using the fact that $\|y(t)\| \leq b$ implies that $\|e\| \leq b$ and $\|r\| \leq b$, Assumptions 4.3 and 4.4, (4–9), and (4–10) it is shown that $\|[{}^{\mathcal{I}}X_{\mathcal{T}}; {}^{\mathcal{I}}_{2}\hat{X}_{\mathcal{T}}]\| \leq \overline{X} + (3+\alpha)b + \overline{\mathcal{V}}$. Therefore, if $y(0) \in \mathcal{S}$, then $[{}^{\mathcal{I}}X_{\mathcal{T}}; {}^{\mathcal{I}}_{2}X_{\mathcal{T}}] \in \Upsilon \subset \mathcal{Z}$ for all $t \in [0,\infty)$.

The inequalities in (4–33) and (4–38) show that $V \in \mathcal{L}_\infty$; thus $e, e_f, \eta, r, Q, P \in \mathcal{L}_\infty$. Since $\eta = \dot{e}_f + \alpha e_f$ by (4–11) and (4–13), and by (4–10) and (4–14), then $\dot{e}, \dot{e}_f, \dot{\eta} \in \mathcal{L}_\infty$ since $e, e_f, \eta, r \in \mathcal{L}_\infty$. Since ${}^{I}X_T \in \mathcal{L}_\infty$ by Assumption 4.3, then ${}^{I}\hat{X}_T \in \mathcal{L}_\infty$ according to (4–9). Since $e, e_f, \eta \in \mathcal{L}_\infty$, then $v \in \mathcal{L}_\infty$. By the projection operator, $\dot{r} \in \mathcal{L}_\infty$ since $e, e_f, \eta, r \in \mathcal{L}_\infty$, $\|\varepsilon\|$ and $\|\mathcal{O}\left(\|\tilde{\Theta}\|^2\right)\|$ are bounded, according to Assumption 4.6 and

Fact 4.1. Since $\dot{e}, \dot{e}_f, \dot{\eta}, \dot{r} \in \mathcal{L}_\infty$, it is concluded that $z \in \mathcal{L}_\infty$. From [81, Corollary 1], $c\|z\|^2 \to 0$ as $t \to \infty$, for all $y(t_0) \in \mathcal{S}$. From the definition of z, $\|e\|, \|\eta\|, \|r\| \to 0$ as $t \to \infty$. Then by (4–10) it is also concluded that $\|\dot{e}\| \to 0$ as $t \to \infty$. Note that the set of permissible initial conditions can be made arbitrarily large to include any initial condition by increasing b. □

For the forthcoming dwell time analysis, it is necessary to derive bounds on the growth rate of the target's position error when feedback is unavailable. To this end, define

$$e_p \triangleq {}^{\mathcal{I}}x_{\mathcal{T}} - {}^{\mathcal{I}}\hat{x}_{\mathcal{T}}, \tag{4–39}$$

to be the position error of the target.

Lemma 4.2. *If the conditions of Theorem 4.1 are satisfied, then while $\sigma(t) = a$, the velocity estimation error $\|\dot{e}\|$ is bounded by the measurable function*

$$\begin{aligned}
\|\dot{e}_p\| &\overset{a.e.}{\leq} \min\{\bar{v}, \rho_a\}, \\
\rho_a &\triangleq \sqrt{\frac{\epsilon_2\left(4\mu - 2\gamma\left(\|e\|^2 + \|e_f\|^2 + \|\eta\|^2\right)\right)}{2\epsilon_2 - 1} - \frac{(2-\epsilon_2)\|\alpha e + \eta\|^2}{2\epsilon_2 - 1}}, \\
\mu &\triangleq \overline{V}_0 e^{-c\Delta t_j^a/\Lambda_2} + 4\alpha\Lambda_2\overline{\Gamma}, \\
\overline{V}_0 &= \frac{\gamma}{2}\|e(t_j^a)\|^2 + \frac{\gamma}{2}\|e_f(t_j^a)\|^2 + \frac{\gamma}{2}\|\eta(t_j^a)\|^2 \\
&\quad + \frac{1}{2}\|e(t_j^a) + \eta(t_j^a)\|^2 + (\zeta_2 + \zeta_3)\|e(t_j^a) + e_f(t_j^a)\| \\
&\quad + \beta\|e(t_j^a) + e_f(t_j^a)\|_1 + \frac{\alpha^2}{2}\overline{\mathcal{V}}^2 + 2\overline{\Gamma},
\end{aligned} \tag{4–40}$$

for all $t \in [t_j^a, t_{j+1}^u)$, where $\epsilon_2 \in (\frac{1}{2}, \infty)$ is a user selected constant.

Proof. Using the bounds from (4–33) and the fact that $\|y\|^2 = \|z\|^2 + 2Q + 2P$, the inequality

$$-\|z\|^2 - 2P \leq 2Q - \frac{1}{\Lambda_2}V,$$

is realized, which can be used to bound (4–38), yielding

$$\dot{V} \overset{a.e.}{\leq} -\frac{c}{\Lambda_2} V + 2cQ. \tag{4–41}$$

Using the bound in (4–27), (4–41) can be bounded as

$$\dot{V} \overset{a.e.}{\leq} -\frac{c}{\Lambda_2} V + 2c\overline{\Gamma}. \tag{4–42}$$

Solving the differential inequality in (4–42), yields

$$V \overset{a.e.}{\leq} \mu, \tag{4–43}$$

where $\overline{V}_0 \geq V(t_j^a)$ is determined by the use of (4–10)–(4–25), (4–28), (4–27), Assumption 4.4, and the triangle inequality, yielding

$$V(t_j^a) \leq \overline{V}_0.$$

Then, using (4–10), (4–32), (4–43) and Young's inequality, a bound on $\|\dot{e}_p\|$ is

$$\|\dot{e}_p\| \overset{a.e.}{\leq} \min\left\{\bar{v}, \rho_a\right\}, \tag{4–44}$$

where $\epsilon_2 \in (\frac{1}{2}, \infty)$ is a user defined constant that comes as a consequence of Young's inequality. □

Lemma 4.3. *Suppose* $\kappa \geq 1$, $\lambda_u \triangleq \max\left\{\frac{1}{\epsilon_3}, \epsilon_3 + \epsilon_4\right\}$, $\delta_u \triangleq \frac{1}{\epsilon_4}(A^2 + \|\Phi\left({}^{\mathcal{I}}\hat{X}_{\mathcal{T}}, {}^{\mathcal{I}}_{2}\hat{X}_{\mathcal{T}}, \hat{\Theta}\right)\|^2)$, *and* $\epsilon_3, \epsilon_4 \in \mathbb{R}_{>0}$ *are user-selected constants, then while* $\sigma(t) = u$, *the error in the predicted position of the target* $\|e_p\|$, *is bounded by*

$$\begin{aligned} &\|e_p(t)\| \leq \rho_u\left(t, t_j^u\right), \\ &\rho_u\left(t_j^u, t\right) \triangleq \sqrt{\|e((t_j^u))\|^2 e^{\kappa\lambda_u \Delta t_j^u} - \frac{\delta_u}{\lambda_u} + \left(\min\{\bar{v}, \rho_a(t_j^u)\}^2 + \frac{2\delta_u}{\lambda_u}\right) e^{\kappa\lambda_u \Delta t_j^u}}. \end{aligned} \tag{4–45}$$

Proof. Consider the Lyapunov candidate V_u, which is a Lipschitz continuous positive definite function defined as

$$V_u \triangleq \frac{1}{2} e^\top e + \frac{1}{2} \dot{e}^\top \dot{e}. \tag{4–46}$$

Taking the time-derivative of (4–46) and substituting in (4–8), yields

$$\dot{V}_u = e^\top \dot{e} + \dot{e}^\top \left({}^{\mathcal{I}}\ddot{X}_{\mathcal{T}} - \Phi \left({}^{\mathcal{I}}\hat{X}_{\mathcal{T}}, {}^{\mathcal{I}}_{2}\hat{X}_{\mathcal{T}}, \hat{\Theta} \right) \right). \tag{4–47}$$

Then, using Young's inequality, the triangle inequality, Assumption 4.5, and substituting in (4–46), (4–47) is bounded such that

$$\dot{V}_u \leq \lambda_u V_u + \delta_u. \tag{4–48}$$

Solving the ordinary differential inequality in (4–48) yields

$$V_u(t) \leq \left(V_u(t_0) + \frac{\delta_u}{\lambda_u} \right) \mathsf{e}^{\lambda_u \Delta t} - \frac{\delta_u}{\lambda_u}. \tag{4–49}$$

Solving for $\|e_p\|$ by substituting in (4–46) into (4–49) and using the fact that $\|e_p\| \leq \|e\|$ yields

$$\|e_p\|^2 \leq 2 \left(V_u(t_j^u) + \frac{\delta_u}{\lambda_u} \right) \mathsf{e}^{\lambda_u \Delta t_j^u} - \frac{2\delta_u}{\lambda_u}. \tag{4–50}$$

Using (4–44), (4–50) is further bounded as

$$\|e_p\|^2 \leq \left(\|e((t_j^u))\|^2 + \min\{\bar{v}, \rho_a(t_j^u)\}^2 + \frac{2\delta_u}{\lambda_u} \right) \mathsf{e}^{\lambda_u \Delta t_j^u} - \frac{2\delta_u}{\lambda_u}. \tag{4–51}$$

The growth rate in the exponential term of (4–51) can then be scaled by $\kappa \in \mathbb{R}_{>0}$, where $\mathsf{e}^{\lambda_u \Delta t_j^u} \leq \mathsf{e}^{\kappa \lambda_u \Delta t_j^u}$, if $\kappa \geq 1$, yielding the desired result in (4–45). □

4.5 Guarantee of Reacquisition

Whenever the target leaves the FoV or becomes occluded, the tracker is required to determine a new placement for the camera that would guarantee target reacquistion within a certain interval of time using the estimator and predictor.

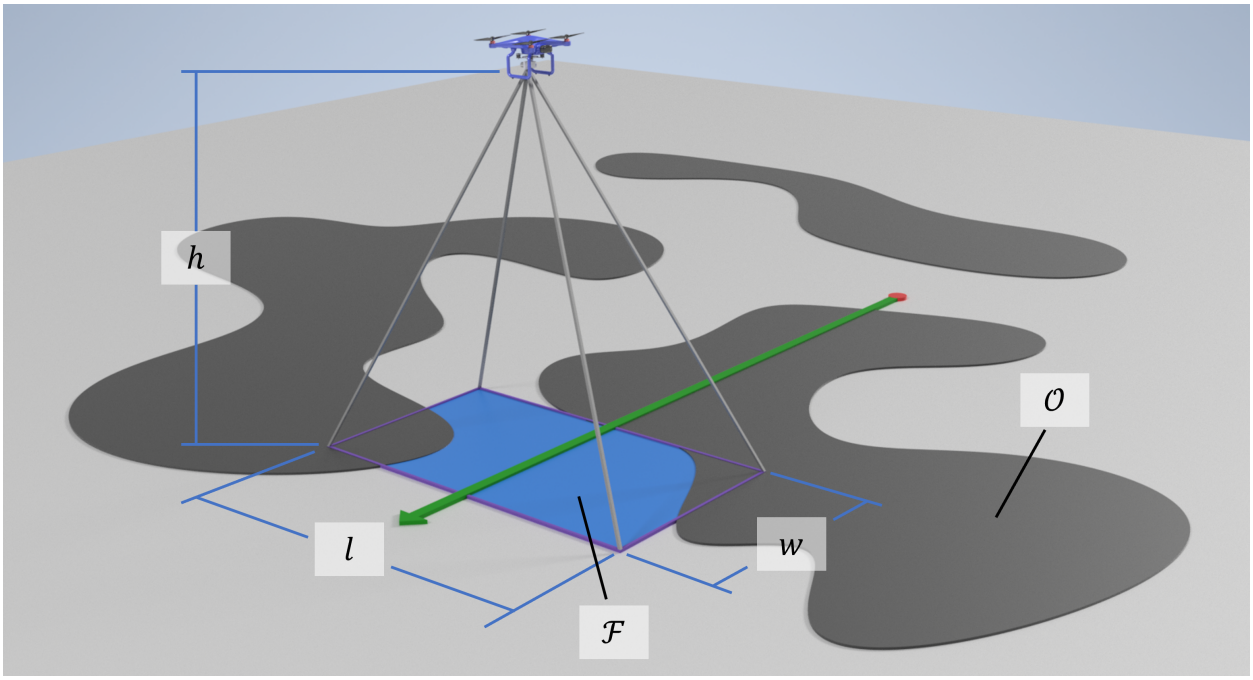

Figure 4-2. Illustration of the feedback region $\mathcal{F}$ (blue region) as a result of the camera's location and properties, with respect to the occlusion zone $\mathcal{O}$ (black region).

For the remainder of this paper, it is assumed for computation simplicity that the target is restricted to the xy-plane and the tracker agent's motion is restricted to the plane parallel to the xy-plane, at height h, with the camera pointed in the direction of the negative z-axis. Let $\pi_{xy} : \mathbb{R}^3 \to \mathbb{R}^2$ denote the projection to the xy-plane. The camera properties determine the dimensions $w(h) \times l(h)$ of the camera's FoV (Figure 4-2). Since $h > 0$ is fixed, w and l are also fixed.

Assumption 4.7. The boundary of the occlusion zone $\partial\mathcal{O}$ is the union of a finite collection of pairwise-disjoint regular Jordan curves (cf., [27, Assumption 4 and Theorem 1]).

The feedback region at any given moment is the set difference of the FoV and the occlusion zones, which may be written as a set-valued function of the camera frame (in relation to the fixed inertial frame) as

$$\mathcal{F}\left({}^{\mathcal{I}}X_{\mathcal{C}}\right) \triangleq \left\{\pi_{xy}({}^{\mathcal{I}}x_{\mathcal{C}} + {}^{\mathcal{I}}_{\mathcal{C}}RP) : P \in \mathcal{H} \setminus \mathcal{O}\right\}, \tag{4–52}$$

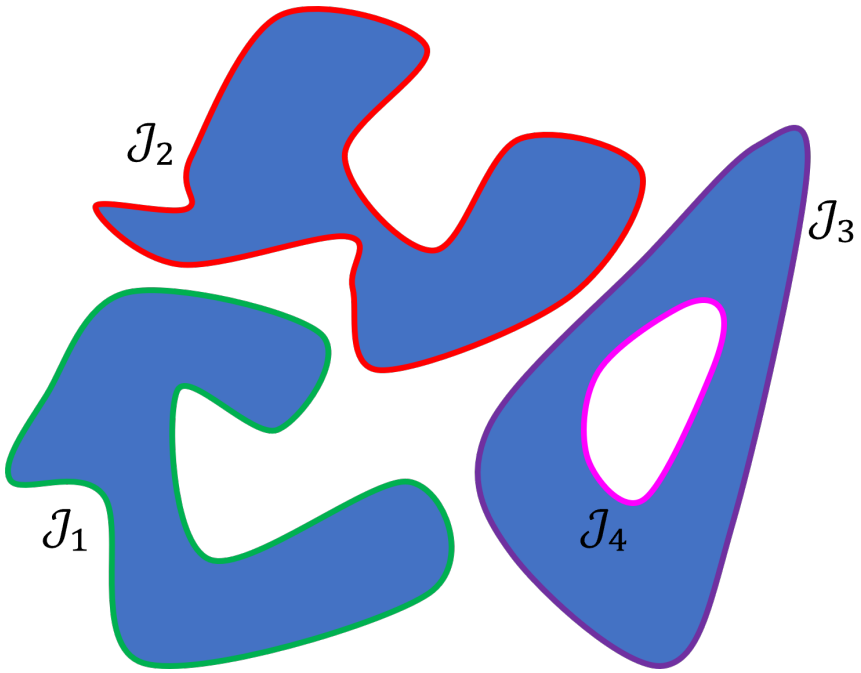

Figure 4-3. The boundary of the feedback region $\mathcal{F}$ (blue region) is decomposed into four disjoint Jordan Curves: $\mathcal{J}_1$, $\mathcal{J}_2$, $\mathcal{J}_3$, and $\mathcal{J}_4$.

where, $\mathcal{H} \triangleq \left[-\frac{l}{2}, \frac{l}{2}\right] \times \left[-\frac{w}{2}, \frac{w}{2}\right] \times \{0\}$. As a result of Assumption 4.7, the boundary of the feedback region $\partial\mathcal{F}\left({}^{\mathcal{I}}X_{\mathcal{C}}\right)$ is also the union of a finite collection of pairwise-disjoint regular Jordan curves (Figure 4-3).

As the target disappears from view, the tracker may still generate a predicted trajectory ${}^{\mathcal{I}}\hat{x}_{\mathcal{T}}$ with error bounds according to (4–45). Define the region of uncertainty at time t as

$$U(t_j^u, t) \triangleq B^{\circ}_{\rho_u(t_j^u,t)}({}^{\mathcal{I}}\hat{x}_{\mathcal{T}}(t)). \tag{4–53}$$

Then the target position is located in the cone of uncertainty, defined at time t as

$$U_{\text{cone}}(t_j^u, t) \triangleq \bigcup_{\tau\in[t_j^u,t]} U(t_j^u, \tau). \tag{4–54}$$

4.5.1 Target Regions

Based on [27] the notion of a target region is introduced as follows.

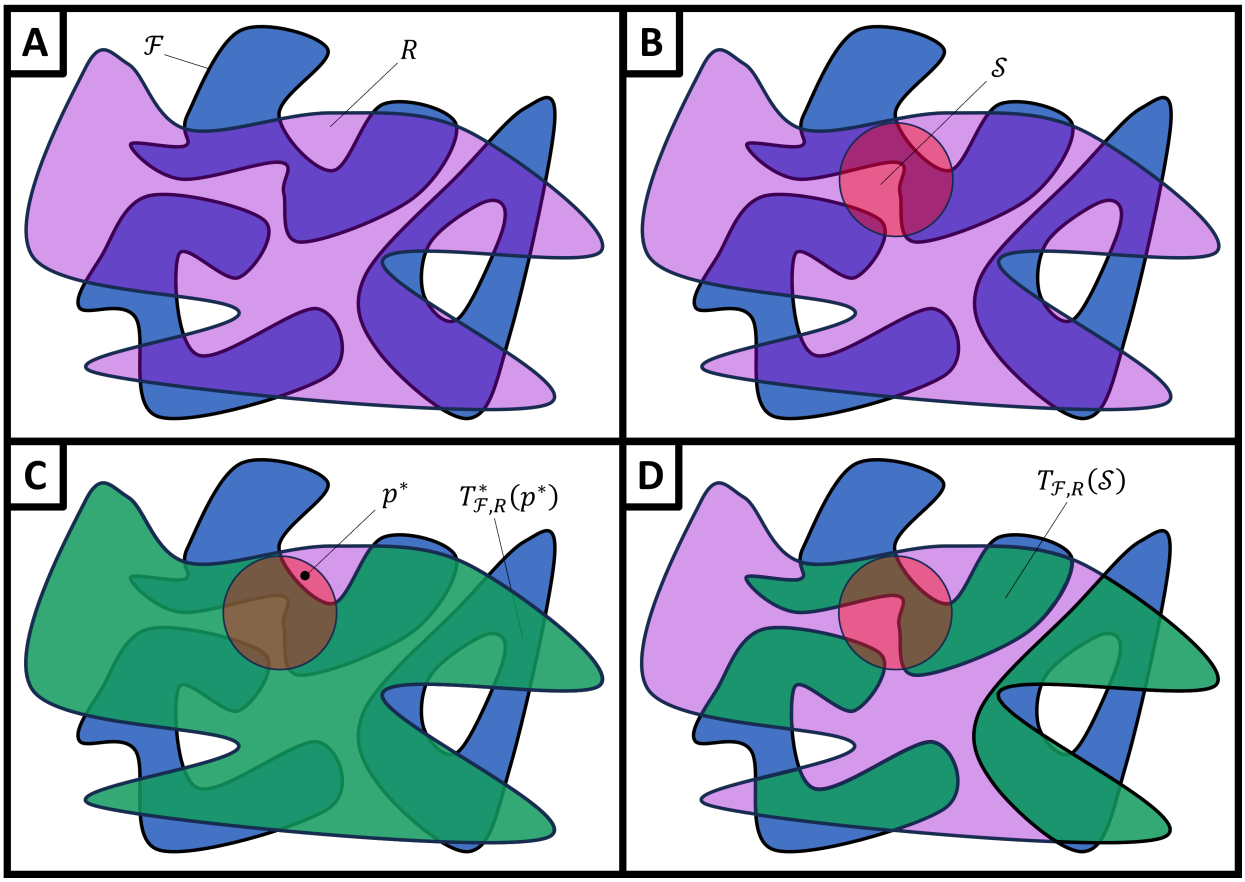

Figure 4-4. For a given feedback region and bounding region (blue and purple region, A), and an initialization (red region, B), the target region for a point p^* (green, C) is the region where all curves originating from p^* must eventually enter the feedback region before entering the target region. The target region (green, D) is the region where all curves originating from the region of uncertainty is either already in the feedback region or must eventually enter the feedback region before entering the target region.

Definition 4.1 (Target Region)**.** Given a region $\mathcal{F} \subset \mathbb{R}^2$, a set $\mathcal{S} \subset \mathbb{R}^2$, and a closed connected region $R \subset \mathbb{R}^2$ such that $\texttt{cl}(\mathcal{S}) \subset R^\circ$, let the target region be defined as

$$T_{\mathcal{F},R}(\mathcal{S}) \triangleq \bigcap_{p^* \in \mathcal{S} \setminus \mathcal{F}} T^*_{\mathcal{F},R}(p^*),$$

where $T^*_{\mathcal{F},R}(p^*)$ is the collection of all points $q \in R^\circ$ for which any smooth curve $\gamma : [0,1] \to R^\circ$ from p^* to q must pass through a point of $\partial\mathcal{F}$. An example of the target region's construction is depicted in Figure 4-4.

Definition 4.2 (Boundary for Reacquisition)**.** Given regions $\mathcal{F} \subset \mathbb{R}^2$, $\mathcal{S} \subset \mathbb{R}^2$, and a closed connected region $R \subset \mathbb{R}^2$ such that $\texttt{cl}(\mathcal{S}) \subset R^\circ$, let $E_{\mathcal{F},R}(S)$ to be the set of all $y \in \partial\mathcal{F}$ such that for some $q \in T_{\mathcal{F},R}(S)$ there is a smooth curve $\gamma : [0,1] \to R^\circ$ from a point $p \in S \setminus \mathcal{F}$ to q that crosses $\partial\mathcal{F}$ exactly once at y.

4.5.2 Guaranteeing Reacquisition

The following lemma and theorem establish criteria for guaranteeing reacquisition, given a feedback region $\mathcal{F}$.

Lemma 4.4. *If $p \in U(t^u_j, t) \setminus \mathcal{F}$ and $q \in T_{\mathcal{F},R}(U(t^u_j, t))$, then any curve in R from p to q must pass through a point of $E_{\mathcal{F},R}(U(t^u_j, t))$.*

Proof. Similarly to [27, Proof of Lemma 1], suppose a curve $\gamma : [0,1] \to R^\circ$ starts at a point $p = \gamma(0) \in U(t^u_j, t) \setminus \mathcal{F}$ and terminates at a point $q = \gamma(1) \in T_{\mathcal{F},R}(U(t^u_j, t))$. Let $\tau' \triangleq \inf\{\tau \in [0,1] : \gamma(\tau) \in \partial\mathcal{F}\}$ be the first time γ crosses $\partial\mathcal{F}$. By Remark 3 of [27], one may assume γ only crosses $\partial\mathcal{F}$ transversely. Set $q' \triangleq \gamma(\tau')$, and let $\mathcal{U}$ be a neighborhood of q' not containing any other intersection point of γ and $\partial\mathcal{F}$ such that $\partial\mathcal{F} \cap \mathcal{U}$ is a single interval. Find $\Delta\tau > 0$ such that $\gamma([\tau', \tau' + \Delta\tau]) \subset \mathcal{U}$ and now set $q'' \triangleq \gamma(\tau' + \frac{\Delta t}{2})$. Since the curve $\gamma' \triangleq \gamma|_{[0,\tau'+\Delta t/2]}$ crosses $\partial\mathcal{F}$ exactly once, one finds that $q'' \in \mathcal{F}^\circ$ and $q' \in E_{\mathcal{F},R}(U(t^u_j, t))$, as required. □

Theorem 4.2. *Suppose that $U_{cone}(t^u_j, t^B)$ is contained in the interior of a region R, where $t^u_j \le t^A \le t^B$, and $U(t^u_j, t^B) \subset T_{\mathcal{F},R}(U(t^u_j, t^A))$ then there exists $t \in [t^A, t^B]$ with ${}^{\mathcal{I}}x_{\mathcal{T}}(t) \in \mathcal{F}$.*

Proof. Notice that the point ${}^{\mathcal{I}}x_{\mathcal{T}}(t^A) \in U(t_j^u, t^A)$ could be located in $\mathcal{F}$. Hence, ${}^{\mathcal{I}}x_{\mathcal{T}}(t)$ entered $\mathcal{F}$ at $t = t^A$. Otherwise, apply Lemma 4.4 to this point and the curve $\gamma : [t^A, t^B] \to R$, concluding that γ had to pass through a point of $E_{\mathcal{F},R}(U(t_j^u, t^A))$. Thus, ${}^{\mathcal{I}}x_{\mathcal{T}}(t)$ entered $\mathcal{F}^\circ$ at some time $t \in (t^A, t^B]$. □

Remark 4.2. Theorem 4.2 only shows that the tracked featured point ${}^{\mathcal{I}}x_{\mathcal{T}}(t) \in \mathcal{F}$, but this may not be sufficient for guaranteeing reacquisition of the target. In the case that it is required that $\mathscr{T} \subset \mathcal{F}$, it is sufficient to show that ${}^{\mathcal{I}}x_{\mathcal{T}}(t) \in \mathcal{F}_{\mathscr{T}}$, where $\mathcal{F}_{\mathscr{T}} \triangleq \mathcal{F} \ominus B_{\texttt{diam}(\mathscr{T})}(0)$ is the inset of $\mathcal{F}$ by a distance of $\texttt{diam}(\mathscr{T})$.

Following Theorem 4.2, the goal could be to maximize the amount of time available for the tracker agent to spend on tasks other than tracking the target (i.e, make t^A as large as possible, and call this optimal value τ_A^*) while guaranteeing that reacquisition of the target will occur at some $t \in [\tau_A^*, \tau_B^*]$, where τ_B^* is the maximum length of time the tracker may need to wait before reacquisition of the target occurs. If the goal is to maximize t^A, then the tracker agent's planner seeks to find a camera pose $P^* \triangleq [p^*; o^*]$, where $p^* \in \mathbb{R}^3$ is the optimal position of the camera and $o^* \in \mathbb{R}^4$ is the optimal orientation, that jointly maximizes

$$(P^*, \tau_A^*, \tau_B^*) \triangleq \underset{P, \tau_A, \tau_B}{\text{argmax}} \tau_A$$
$$\text{s.t.} \begin{cases} U(t_j^u, \tau_B) \subset T_{\mathcal{F},R}(U(t_j^u, \tau_A)), \\ \mathcal{F} = \mathcal{F}(P), \\ t_j^u \leq \tau_A \leq \tau_B, \end{cases} \tag{4–55}$$

for a given bounding region $R \supset U_{\text{cone}}(t_j^u, \tau^B)$, where the tracker agent needs to satisfy ${}^{\mathcal{I}}X_{\mathcal{C}} = P^*$ for all $t \in [\tau_A^*, \tau_B^*]$ to guarantee reacquisition. Alternatively, if the goal is to minimize the time without tracking, then the tracker agent's planner seeks to find a

camera pose that solves the optimization problem

$$(P^*, \tau_A^*, \tau_B^*) \triangleq \underset{P,\tau_A,\tau_B}{\text{argmin}} \tau_B$$
$$\text{s.t.} \begin{cases} U(t_j^u, \tau_B) \subset T_{\mathcal{F},R}(U(t_j^u, \tau_B)), \\ \mathcal{F} = \mathcal{F}(P), \\ t_j^u \leq \tau_A \leq \tau_B. \end{cases} \tag{4–56}$$

Theorem 4.3. *Suppose that the conditions of Theorem 4.1 are satisfied and b is sufficiently large, if there exists a solution to either of the optimization problems in (4–55) or (4–56), for all $j \in \mathbb{Z}$, then the error signal y is ultimately bounded, uniformly over $\mathcal{D}$, provided that the switching signal $\sigma(t)$ satisfies the maximum dwell-time condition $\rho_u(t_j^u, t) \leq \rho_u(t_j^u, \tau_B^*)$, written explicitly as*

$$\Delta t_j^u \leq \frac{1}{\lambda_u} \ln \left(\frac{\rho_u(t_j^u, \tau_B^*) + \frac{\delta_u}{\lambda_u}}{V_u(t_j^u) + \frac{\delta_u}{\lambda_u}} \right), \tag{4–57}$$

where τ_B^* is as defined in (4–55) or (4–56).

Proof. While $\sigma(t) = a$, y remains bounded according to (4–43), in the sense that $\|y\| \overset{a.e.}{\leq} \sqrt{\mu/\Lambda_1}$. Then suppose that $U(t_j^u, \tau_B^*) \subset T_{\mathcal{F},R}(U(t_j^u, \tau_A^*))$ and ${}^{\mathcal{I}}X_{\mathcal{C}} = P^*$ for all $t \in [\tau_A^*, t_{j+1}^a)$, then by Theorem 4.2 and Remark 4.2, reacquistion of the target is guaranteed to have occurred at some $t \in [\tau_A^*, \tau_B^*]$. While $\sigma(t) = u$, (4–49) is used to show that e and $\dot{e}$ are bounded in the sense that

$$\|[e; \dot{e}]\| \leq E_1 \triangleq \sqrt{2 \left(V_u(t_j^u) + \frac{\delta_u}{\lambda_u} \right) \mathrm{e}^{\lambda_u \Delta T} - \frac{\delta_u}{\lambda_u}}, \tag{4–58}$$

where $\Delta T \triangleq \tau_B^* - t_j^u$. Since $\dot{e}_f = 0$ while $\sigma(t) = u$, $e_f(t) = e_f(t_j^u)$ and is therefore bounded. Since $\dot{p} = 0$, from (4–12), while $\sigma(t) = u$, $p(t) = p(t_j^u)$, thus η is bounded in the sense that

$$\|\eta\| \leq E_2 \triangleq \|p(t_j^u)\| + (k + \alpha) E_1, \tag{4–59}$$

according to (4–58). Using (4–58) and (4–59), and the fact that $e_f(t) = e_f(t_j^u)$, r is bounded in the sense that

$$\|r\| \leq E_3 \triangleq \|p(t_j^u)\| + (1 + k + 2\alpha)E_1. \tag{4–60}$$

Using (4–23)–(4–25) and (4–58)–(4–60), P is bounded in the sense that

$$\begin{aligned} &P \leq E_4, \\ &E_4 \triangleq \beta\left(E_1 + \|e_f(t_j^u)\|\right) + \frac{\left(E_1 + \|e_f(t_j^u)\|\right)^2}{2} + \frac{(\zeta_2 + \zeta_3)^2}{2} \\ &\quad + \frac{\zeta_5 \overline{Z}^2 + (\alpha - \lambda_p)\beta\sqrt{7}\left(E + \|e_f(t_j^u)\|\right)}{\sqrt{\lambda_p}} + (\alpha - \lambda_p)\frac{\left(E_1 + \|e_f(t_j^u)\|\right)^2 + (\zeta_2 + \zeta_3)^2}{2\sqrt{\lambda_p}} \\ &\quad + \frac{\left(E_1 + \|e_f(t_j^u)\|\right)^2 + (\zeta_4 + \zeta_5\overline{Z})^2}{2\sqrt{\lambda_p}} + \alpha\frac{\left(E_1 + \|e_f(t_j^u)\|\right)^2 + \zeta_3^2}{2\sqrt{\lambda_p}}, \end{aligned} \tag{4–61}$$

where $\overline{Z} \triangleq \sqrt{E_1^2 + \|e_f(t_j^u)\|^2 + E_2^2 + E_3^2}$. Additionally, Q is bounded according to (4–27). Since e, e_f, η, r, Q, and P are bounded it is then concluded that y is bounded while $\sigma(t) = u$, in the sense that

$$\|y\| \leq E \triangleq \max\left\{E_1, \|e_f(t_j^u)\|, E_2, E_3, \sqrt{2E_4}, \sqrt{2\overline{\Gamma}}\right\}. \tag{4–62}$$

If $b > \sqrt{\frac{\Lambda_2 E^2 + 2\overline{\Gamma}}{\Lambda_1}}$, then $y(t_{j+1}^a) \in \mathcal{S}$ and the requirements to resume tracking the target are satisfied according to Theorem 4.1, therefore, y is ultimately bounded, uniformly over $\mathcal{D}$. □

4.6 Implementation

When solving the optimization problems in (4–55) and (4–56), it would be ideal to select $R = U_{\text{cone}}(t_j^u, \tau_B)$; however, U_{cone} is difficult to implement since it would require the computation of the union of an infinite number of balls. Instead, U_{cone} can be approximated by computing the union of a finite number of stadiums (i.e., a rectangle with semicircles at a pair of opposite sides). To construct this region, the predicted trajectory of the target ${}^{\mathcal{I}}\hat{x}_{\mathcal{T}}(t)$ for $t \in [t_j^u, t^B]$ is first discretized at a regular interval

of $\Delta t \in \mathbb{R}_{>0}$ from t_j^u to $t^B = L\Delta t$, for $L \in \mathbb{Z} \setminus \{0\}$, resulting in the approximation ${}^{\mathcal{I}}\tilde{x}_{\mathcal{T}}(t) \approx {}^{\mathcal{I}}\hat{x}_{\mathcal{T}}(t)$, defined as

$$
{}^{\mathcal{I}}\tilde{x}_{\mathcal{T}}(t) \triangleq \begin{cases} a(1,t), & t_j^u \le t < \Delta t, \\ a(2,t), & \Delta t \le t < 2\Delta t, \\ \vdots & \vdots \\ a(L,t), & (L-1)\Delta t \le t \le L\Delta t, \end{cases} \tag{4–63}
$$

$$
\begin{aligned}
a(k,t) \triangleq {}^{\mathcal{I}}\hat{x}_{\mathcal{T}}(t_j^u + (L-1)\Delta t) + \frac{{}^{\mathcal{I}}\hat{x}_{\mathcal{T}}(t_j^u + L\Delta t)}{\Delta t}(t - (L-1)\Delta t) \\
- \frac{{}^{\mathcal{I}}\hat{x}_{\mathcal{T}}(t_j^u + (L-1)\Delta t)}{\Delta t}(t - (L-1)\Delta t).
\end{aligned}
$$

Remark 4.3. This discretization results in a discretization error $e_{\Delta t} \triangleq {}^{\mathcal{I}}\hat{x}_{\mathcal{T}}(t) - {}^{\mathcal{I}}\tilde{x}_{\mathcal{T}}(t)$ which has the known bound $\bar{e}_{\Delta t} \in \mathbb{R}_{>0}$ satisfying $\sup_{{}^{\mathcal{I}}\hat{X}_{\mathcal{T}} \in \Omega} \|e_{\Delta t}\| \le \bar{e}_{\Delta t}$ (Figure 4-5).

Over each time interval Δt, ${}^{\mathcal{I}}\hat{x}_{\mathcal{T}}(t)$ is approximated by a line segment, which is then used to construct a stadium about each resulting line segment. Specifically, given the time interval $[t_j^u + (\ell-1)\Delta t, t_j^u + \ell\Delta t]$, for $\ell \in \{1, \dots L\}$, the circular components of the stadium for this line segment, denoted by $S(t_j^u, L, \Delta t)$, is defined as

$$
S(t_j^u, L, \Delta t) \triangleq B^{\circ}_{\rho_u\left(t_j^u + \ell\Delta t\right) + \bar{e}_{\Delta t}}\left({}^{\mathcal{I}}\hat{x}_{\mathcal{T}}\left(t_j^u + (\ell-1)\Delta t\right)\right) \cup B^{\circ}_{\rho_u\left(t_j^u + \ell\Delta t\right) + \bar{e}_{\Delta t}}\left({}^{\mathcal{I}}\hat{x}_{\mathcal{T}}\left(t_j^u + \ell\Delta t\right)\right). \tag{4–64}
$$

Finally, the bounding region $R(t_j^u, L, \Delta t)$ is then defined as

$$
R(t_j^u, L, \Delta t) \triangleq \bigcup_{\ell=1}^{L} \text{conv}\left(S(t_j^u, L, \Delta t)\right), \tag{4–65}
$$

where the convex hull takes the circular components in $S_{\Delta t}(\ell)$ and constructs the stadium for that segment (Figure 4-5). Using this bounding region, an algorithm for computing the state of the tracker agent's camera that guarantees reacqusition of

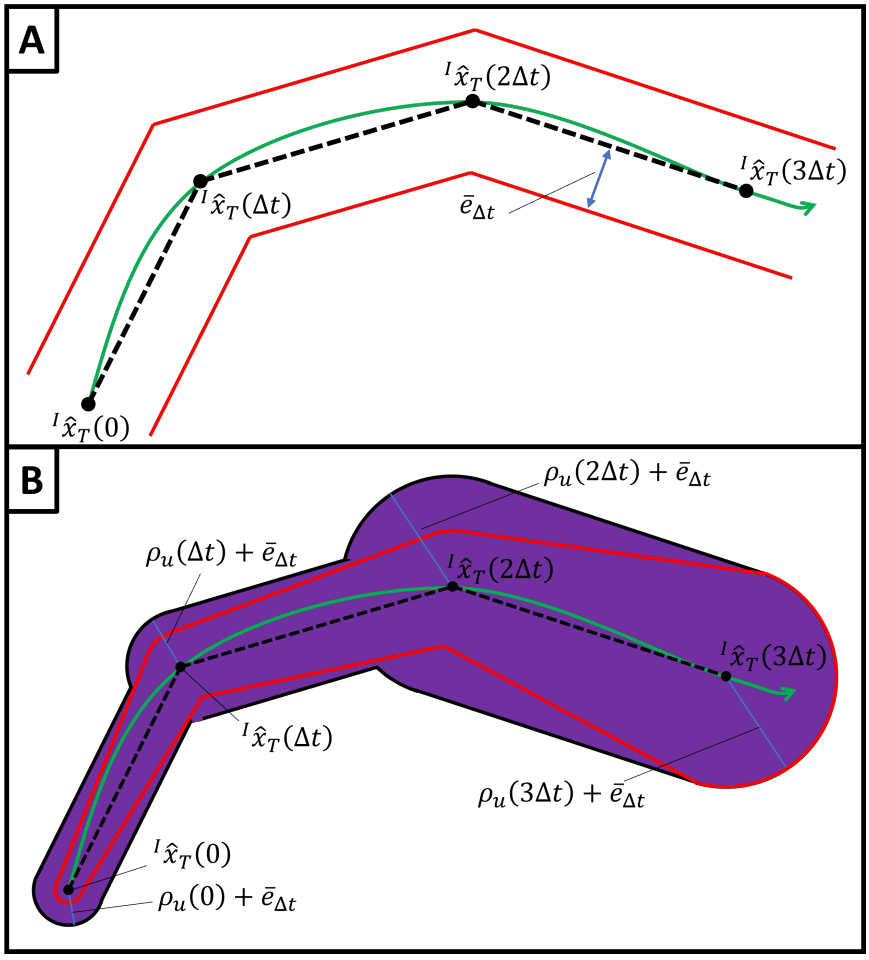

Figure 4-5. Subfigure **A** illustrates the discretization error of the path $^{\mathcal{I}}\hat{x}_{\mathcal{T}}(t)$ for $t \in [0, 3\Delta t]$, where subfigure **B** illustrates the bounding region about the discretized curve of $^{I}\hat{x}_T(t)$.

tracking the target is provided in Algorithm 4.1, which is an approximation of a solution to the optimization problem in (4–55)[2] .

Algorithm 4.1

Require: $\mathscr{O} \supset \mathbb{R}^2$, given as a sequence of verticies

Require: $\mathcal{P}$ as a list of points $p_0, \ldots, p_L \in \mathbb{R}^2$

Require: $\Delta_\theta \in \mathbb{R}_{>0}$

Require: $J = \frac{\pi}{2\Delta_\theta}$

Require: $\Delta t \in \mathbb{R}_{>0}$

Require: $t_j^u \in \mathbb{R}_{>0}$

$R \leftarrow$MAKEBOUNDINGREGION$((t_j^u, L, \Delta t, \mathcal{P}))$

for $i := 0$ to L **do**

  for $j := 0$ to J **do**

    $\mathcal{F} \leftarrow$MAKEFEEDBACKREGION(i, j)

    $\ell \leftarrow 0$

    $\ell^* \leftarrow L + 1$

    while $\texttt{check} = 0 \wedge \ell \neq L + 1$ **do**

      $T \leftarrow$MAKETARGETREGION$(R, \mathcal{F}, L - \ell)$

      $\texttt{check} \leftarrow$RETURNCHECK$(T, L - \ell)$

      if $\texttt{check} = 1$ **then**

        $\ell^* \leftarrow \ell$

      end if

      $\ell \leftarrow \ell + 1$

    end while

    $\ell_{i,j} \leftarrow \ell^*$

  end for

[2] Algorithm 4.1 can easily be modified to find a solution to the optimization problem in (4–56).

17: **end for**

18: $(i^*, j^*) \leftarrow \text{argmin}_{i,j}(\ell_{i,j})$

19: **return** $[p_{i^*}; j^*\Delta_\theta]$

20: **function** MAKEBOUNDINGREGION($(t_j^u, L, \Delta t, \mathcal{P})$)

21: **return** $R \leftarrow$Equation (4–65)

22: **end function**

23: **function** MAKEFEEDBACKREGION(i, j)

24: $F \leftarrow$MAKEFOV(i, j)

25: **return** $F \setminus \mathscr{O}$

26: **end function**

27: **function** MAKEFOV(i, j)

28: **return** the rectangle centered at p_i, with orientation

29: $j\Delta_\theta$, given as a sequence of four verticies

30: **end function**

31: **function** MAKETARGETREGION($R, \mathcal{F}, L - \ell$)

32: $U \leftarrow U(t_j^u + (L - \ell)\Delta t)$

33: $A \leftarrow U \setminus \mathcal{F}$

34: $B \leftarrow R \setminus \mathcal{F}$

35: **for all** $a \in$REGIONS(A) **do**

36: $p \leftarrow$FINDPOINT(a)

37: **for all** $b \in$REGIONS(B) **do**

38: **if** $p \in b^\circ$ **then**

39: $C_a \leftarrow b$

40: **Exit**

41: **end if**

42: **end for**

43: **end for**

44: $T \leftarrow R$

45: **for all** $a \in$REGIONS(A) **do**

46: $T \leftarrow T \setminus C_a$

47: **end for**

48: **return** T

49: **end function**

50: **function** FINDPOINT(a)

51: **return** any point $p \in a^{\circ}$

52: **end function**

53: **function** RETURNCHECK($T, L - \ell$)

54: `Check` $\leftarrow 0$

55: **for** $m := L - \ell$ to L **do**

56: $U \leftarrow U(t_j^u + m\Delta t)$

57: **if** $U \subset T$ **then**

58: `Check` $\leftarrow 1$

59: **Exit**

60: **end if**

61: **end for**

62: **return** `check`

63: **end function**

64: **function** REGIONS(A)

65: **return** the list of connected components of A

66: **end function**

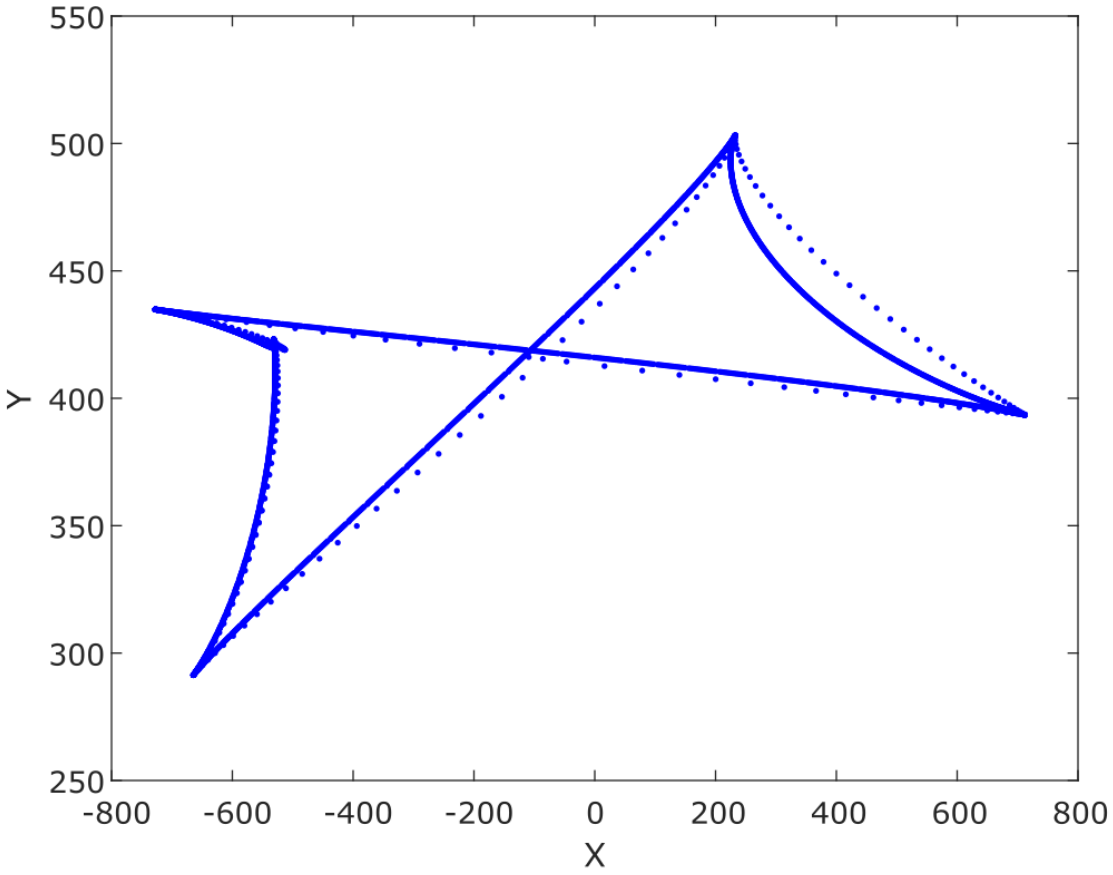

Figure 4-6. The target's trajectory generated by the use of MATLAB®'s `minjerkpolytraj` function.

4.7 Simulations

In this section, three simulations are performed. The first one focuses solely on the DNN-based estimator and the DNN's ability to learn the dynamics of a randomly generated trajectory. The next simulation focuses on the performance of the `MakeTargetRegion` function, as it is the critical component of Algorithm 4.1. This section is then concluded with a simulation of the performance of the DNN estimator/predictor in the presence of intermittent state feedback as a consequence of the target entering into the occlusion zone. Algorithm 4.1 is deployed to guarantee reacquisition of tracking.

4.7.1 DNN Estimation and Prediction Performance Simulation

To examine the performance of the DNN estimator/predictor developed in (4–8), a random trajectory for the target was first generated by using MATLAB®'s `minjerkpolytraj` function, which generates a minimum jerk polynomial trajectory for a sequence of waypoints, which in this case, were six randomly generated points contained within a rectangular region with dimensions of 2400x1200. The target then looped through these way points for a duration of $t = 5,000$. The generated path can be seen in Figure 4-6.While the target followed this trajectory, the estimator/predictor in (4–8) was deployed, where a fully-connected feedforward DNN composed of three hidden layers (i.e., $k_h = 3$), with three neurons per layer (i.e., $L_j = 3$). Further, the hyperbolic tangent activation function (tanh) was used on the output layer, and the rectified linear unit (ReLu) activation function was used on all other layers. Additionally, the following gains were selected: $\gamma = 0.1$, $k = 20$, $\alpha = 60$, $\beta = 0.0001$, $\Gamma = \begin{bmatrix} 10\mathbf{I}_{39} & \mathbf{0}_{39\times 8} \\ \mathbf{0}_{8\times 39} & 15\mathbf{I}_8 \end{bmatrix}$. The results of this simulation are seen in Figure 4-7.

4.7.2 Target Region Generation Simulation

In Algorithm 4.1, the core function, which would be fundamental to any algorithm that aims to compute optimal camera poses that guarantee reacquisition of tracking, is `MakeTargetRegion`. Thus it is of interest to demonstrate the efficacy of this algorithm when presented with a variety of complex geometries. To this end, a variety of combinations of occlusion zones, bounding regions, FoVs, and initialization regions were given as inputs to the `MakeTargetRegion` function, four of which are depicted in Figure 4-8. Using MATLAB®'s Computational Geometry library, specifically, the operations for `PolyShape` objects (i.e., `isinterior`, `convhull`, `intersect`, `subtract`, `union`, and `regions`), the algorithm was implemented, which was able to compute the target region for each test in less than 0.05 seconds on a computer with an Intel® Core™ i7-4790 CPU. The MATLAB® implementation of `MakeTargetRegion` is found in Appendix **??**.

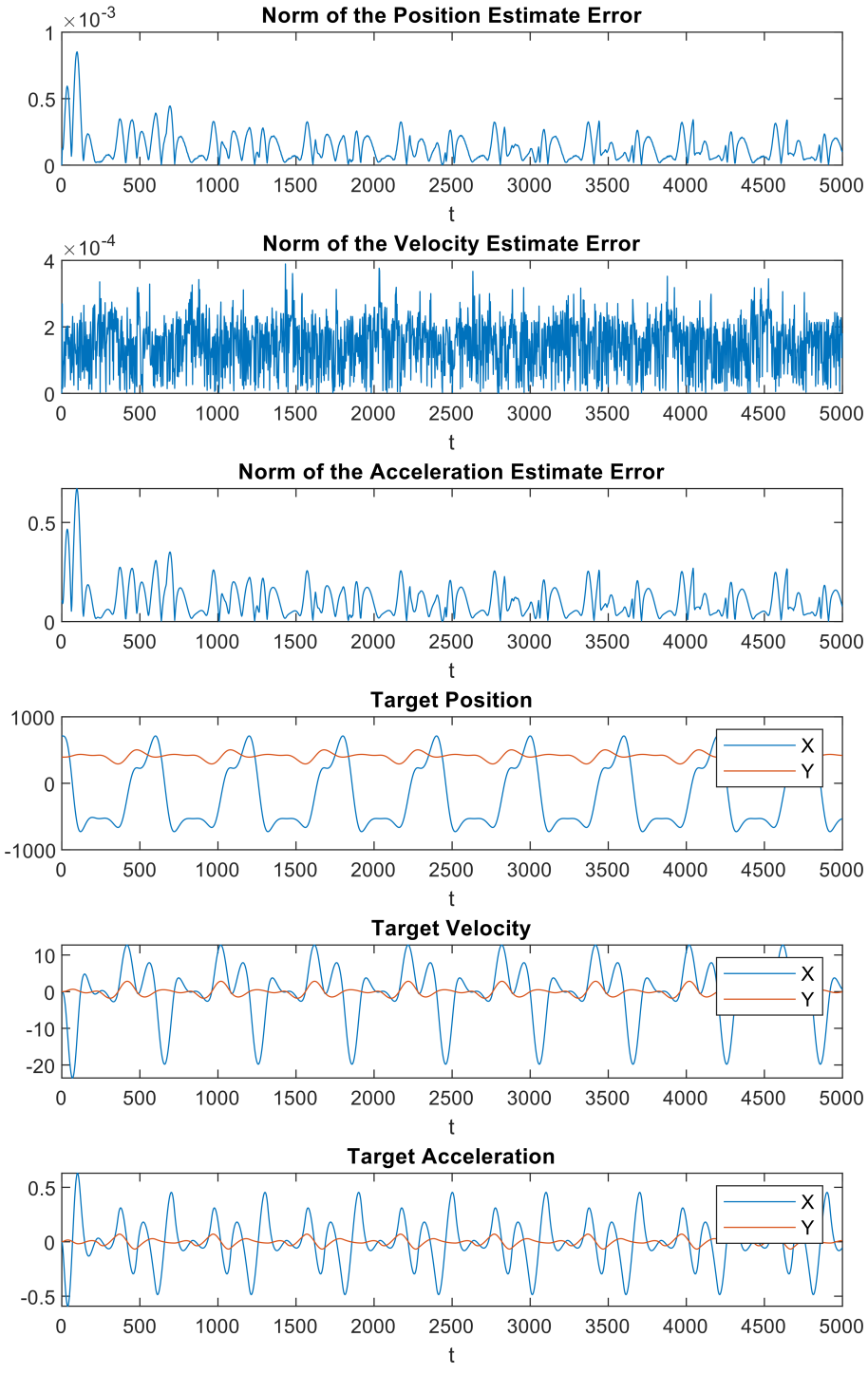

Figure 4-7. Plots of the norm of the position estimate error (i.e, $\|e\|$), norm of the velocity error (i.e, $\|\dot{e}\|$), norm of the acceleration estimate error (i.e, $\|\ddot{e}\|$), actual target position (i.e., ${}^{\mathcal{I}}x_{\mathcal{T}}$), actual target velocity (i.e., ${}^{\mathcal{I}}\dot{x}_{\mathcal{T}}$), and actual target acceleration (i.e., ${}^{\mathcal{I}}\ddot{x}_{\mathcal{T}}$). The dashed vertical line indicates the instance where the gains were reduced.

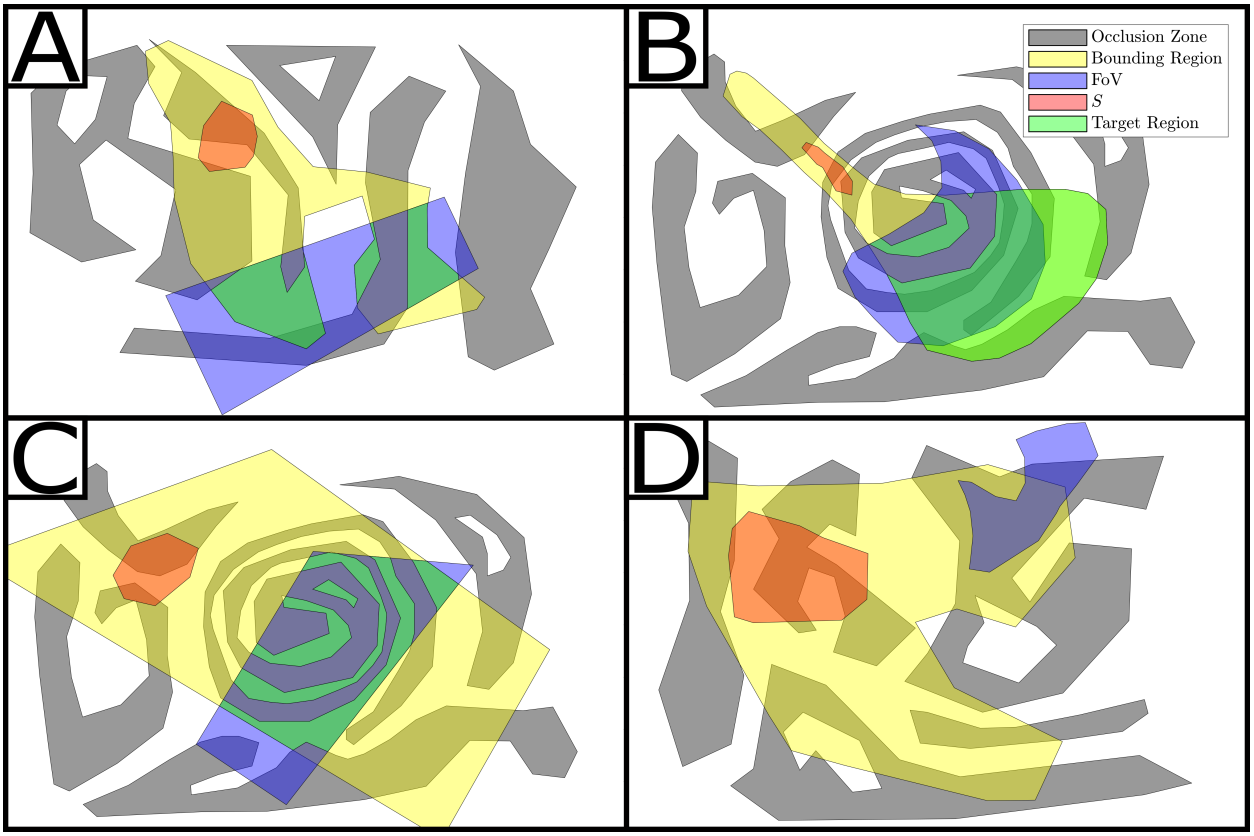

Figure 4-8. A sample of four computed target regions for a variety of occlusion regions, bounding regions, FoVs and initialization regions. Note that in sample D, the target region is the empty set. The computation times for the target regions are as follows: A) 0.0352 seconds; B) 0.0318 seconds; C) 0.0161 seconds; and D) 0.0443 seconds.

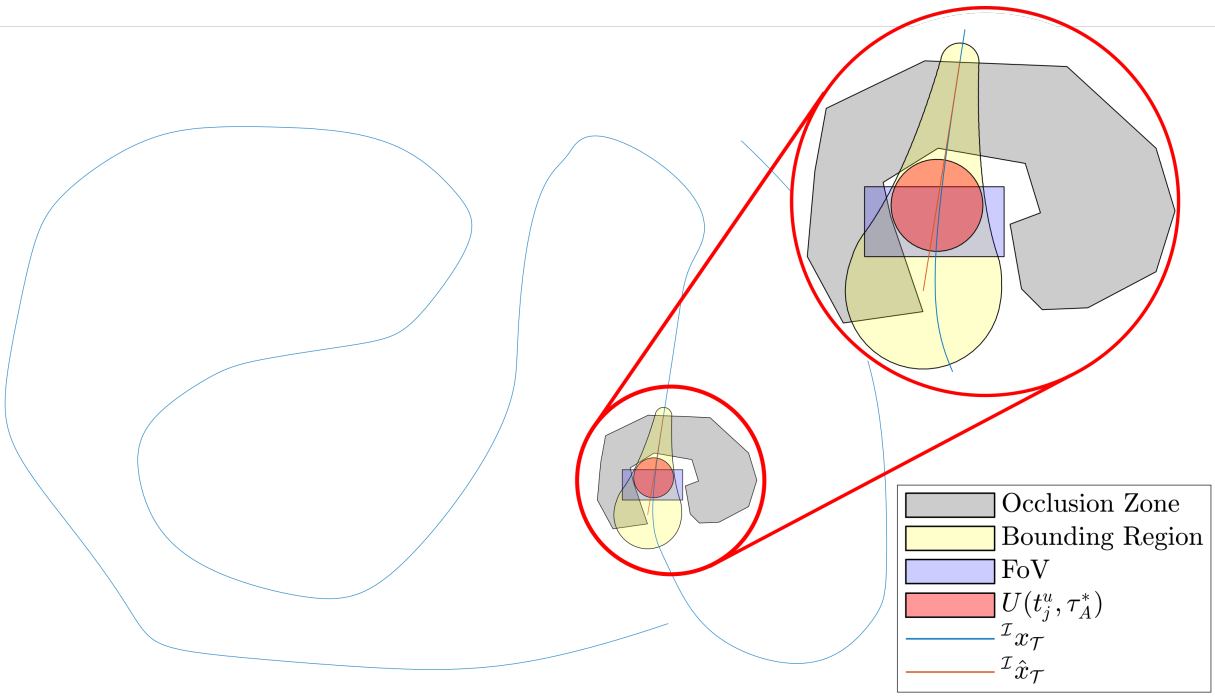

Figure 4-9. Illustration of the simulation scenario where the target passes through an occlusion region. The zoomed in region depicts the predicted trajectory, the bounding region, the optimal camera pose, and the region of uncertainty of the target when the camera is at the desired location. Here, $\tau_A^* = t_1^u + 10$.

4.7.3 Occlusion Simulation

To examine the performance of the DNN observer/predictor proposed in (4–8) and the effectiveness of the proposed camera placement scheme from Section 4.5, a trajectory for the target and an occlusion region was manually generated, as seen in Figure 4-9. For this study, the same DNN architecture from Section 4.7.1 was used, with the following gains: $\gamma = 0.1$, $k = 20$, $\alpha = 60$, $\beta = 0.01$, and $\Gamma = \begin{bmatrix} 15\mathbf{I}_{39} & \mathbf{0}_{39\times 8} \\ \mathbf{0}_{8\times 39} & 10\mathbf{I}_8 \end{bmatrix}$. For the construction of the bounding region R, the following constants for (4–45) were selected as: $\kappa = 0.1$, $\epsilon_3 = \epsilon_4 = 1$, where the acceleration bound was determined to be $A = 0.4081$. When the target was reacquired, reset maps were deployed to reinitialize the tracking error and filtering errors (i.e., ${}^{\mathcal{I}}\hat{x}_{\mathcal{T}}(t_2^a) = {}^{\mathcal{I}}x_{\mathcal{T}}(t_2^a)$, $e_f(t_2^a) = 0$, and $p(t_2^a) = 0$). The results of this simulation are in Figure 4-10.

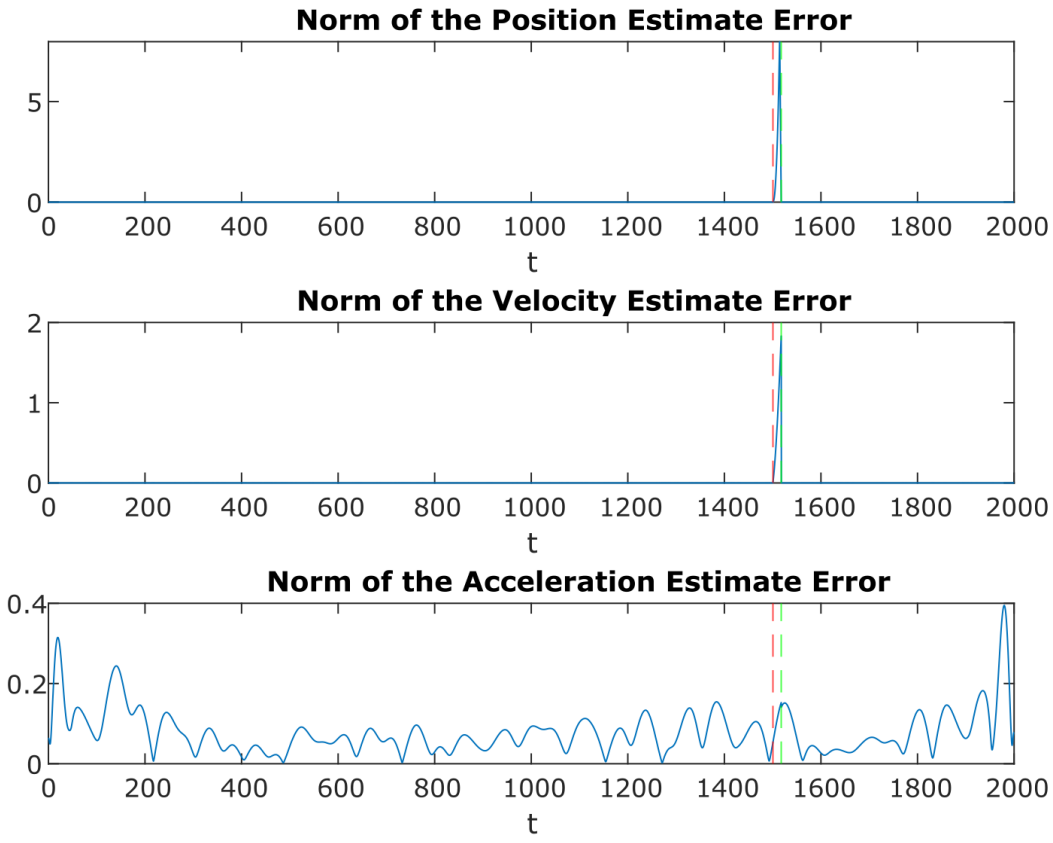

Figure 4-10. Plots of the norm of the position estimate error (i.e, $\|e\|$), norm of the velocity error (i.e, $\|\dot{e}\|$), and norm of the acceleration estimate error (i.e, $\|\ddot{e}\|$). The red vertical line indicates the instance when tracking was lost, whereas the green vertical line indicates when tracking was reacquired.

Despite the relatively quick computation times of the target region seen in Section 4.7.2, the computation time of the optimal camera pose according to Algorithm 4.1 is slow. In this simulation, it took 47.9267 seconds to find the optimal camera pose over the provided search space. In this case, the search space consisted of thirty test locations (i.e., $L = 30$) and seven orientation (i.e., $\Delta_\theta = \pi/12$). As a consequence of Algorithm 4.1's brute force approach, the `MakeTargetRegion` function was called $5,743$ times.

4.8 Conclusions

A Lb-DNN estimator and predictor was developed for image-based target tracking, in the presence of occlusions. A Lyapunov-based stability analysis indicates that the position and velocity estimates converge asymptotically to the actual position and velocities, while the target is within the tracking agent's field of view. To position the tracking agent's camera to reacquire a target, a method was developed for computing an optimal placement of the camera, guaranteeing reacquisition using separation properties of the boundaries of occluded regions that yielded an algorithm for computing locations to position the camera to guarantee target reacquisition. The performance of the estimator, predictor, and camera placement methodology was examined via a series of simulations. Future work could focus on developing more efficient algorithms for finding the best camera placement based on the theoretical methods proposed here. It may also be of interest to investigate ways of extending this camera placement methodology to a multi-agent system of cooperative agents for expanding the size of the feedback region by overlaying their cameras' FoVs, or dispersing the cameras for better coverage of the target's cone of uncertainty.

CHAPTER 5
CONCLUSIONS AND FUTURE WORK

5.1 Conclusions

This dissertation has presented contributions related to the advancement of path planning and estimation methods in the presence of intermittent state feedback, with a focus on the geometric aspects of the problem. Chapter 2 developed a topologically motivated method for guaranteeing the re-entry of an agent into a feedback region, constructing the foundation for subsequent work presented in this dissertation, as well as future work. Chapter 3 extended the study of relay-explorer problems to multi-agent systems so that the idea of cooperative localization can be used to enhance the path tracking performance of each agent and to extend the duration the ensemble of agents can spend operating without state feedback. In Chapter 4, the topological method for path planning from Chapter 2 was further generalized to address a higher-dimensional setting, with feedback regions of varying topology, geometry and orientation, including ones that have holes or multiple connected components. Additionally, more complex bounding regions that more closely approximate the cone of uncertainty were investigated. These improvements on the topological methodology, in conjunction with the Lb-DNN estimator and predictor scheme allowed for the development of a methodology for determining where the tracking agent ought to position its camera to guarantee reacquisition of tracking the target agent.

5.2 Future Work

5.2.1 Geometric Arrangements

Geometric arrangements are subdivisions of some space induced by geometric objects (e.g., spheres, simplicies, polytopes, polynomials, or Bézeir curves/surfaces) [58]. For example, Figure 5-1 shows an arrangement of eight parametric curves: C_1, C_2, C_3, C_4, C_5, C_6, C_7, and C_8. These curves result in two faces, one bounded (i.e., F_1), and the other unbounded (i.e., F_2).

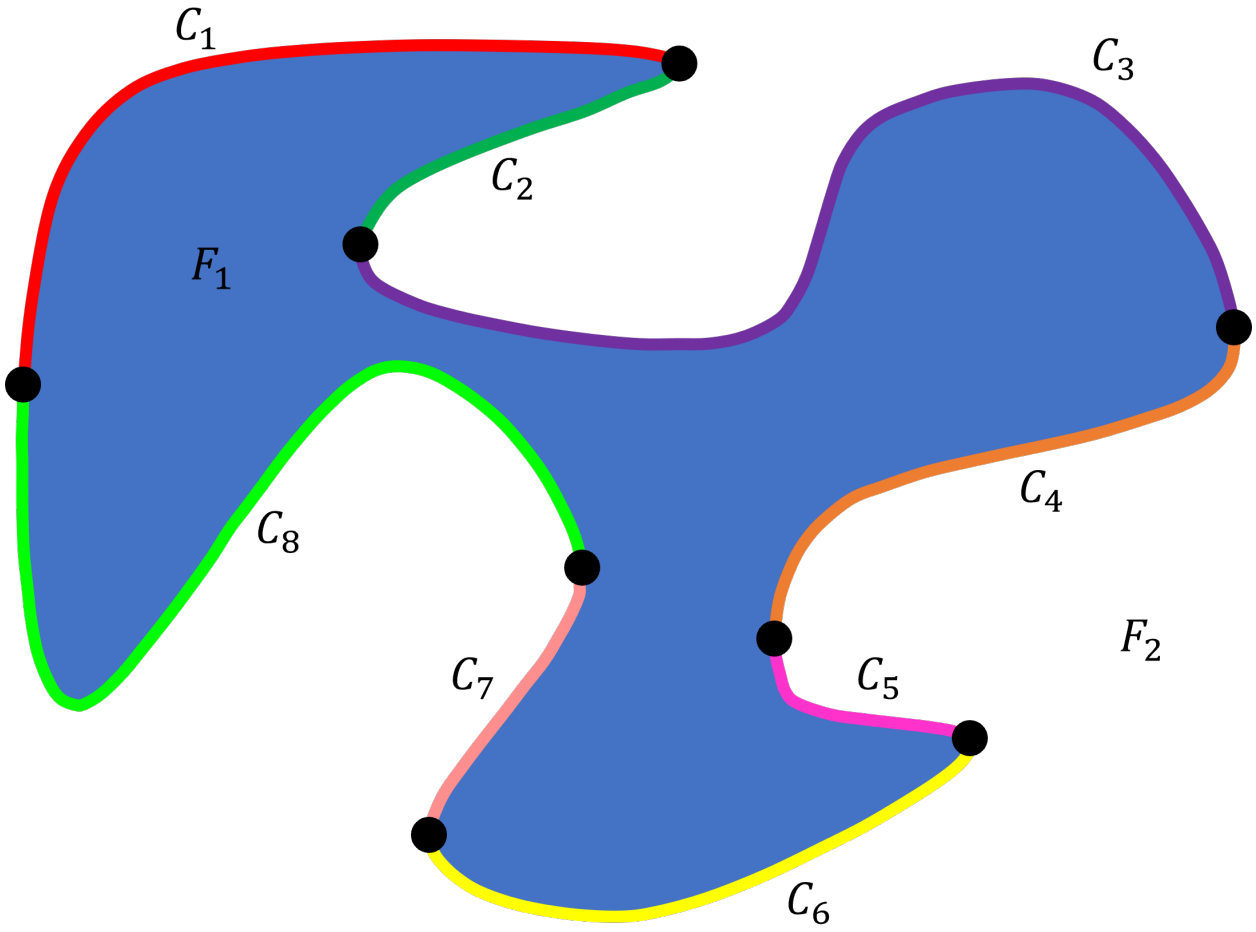

Figure 5-1. An example of an arrangement composed of eight parametric curves: C_1, C_2, C_3, C_4, C_5, C_6, C_7, and C_8. Arrangements of this type could be used to model feedback regions and regions of uncertainty.

The use of arrangements in the field of computational geometry has not only allowed for more computationally efficient algorithms, but it has also allowed for algorithms to move away from fixed-precision approximation methods to exact computing. In fixed-precision approximation, geometric operations such as Boolean operations (e.g., union, intersection, delete, etc) are approximated by constructing new geometric objects, whereas in exact computing operations are done on the geometric objects to modify them. Additionally, the use of arrangements, allows for more exact modeling. For example, feedback regions can be modeled by an arrangement of parametric curves, rather than being bounded by a polygon (Figure 5-1).

Given the long computation times of the MAURs (Chapter 2) and camera placement (Chapter 4)—as a result of the brute-force approaches in both of the proposed algorithms—more efficient algorithms are required so that further studies on this topic can be conducted. It is not practical to study, for example, the feasibility regions (Definition 2.2) or expand the research into more complex systems such as systems where reactive planning may be necessary. Current work is under development that leverages tools and ideas found in the field of computational geometry.

Additionally, arrangements can be extended to model the regions of uncertainty in Chapter 3 as an arrangement of parametric curves, specifically polynomials. The use of arrangements could be advantageous as it could allow for the development and implementation of operations that modify the region of uncertainty without the need to use a minimum bounding circle algorithm.

5.2.2 Bent Return Trajectories

Once an improved algorithm for computing MAURs is realized, a study into more complex return trajectories can be conducted to further increase the time an agent can spend in the feedback denied region. A simple example to show the significance of this study is seen in Figure 5-2 where a simple bent path return trajectory could be used rather than the traditional straight return trajectory.

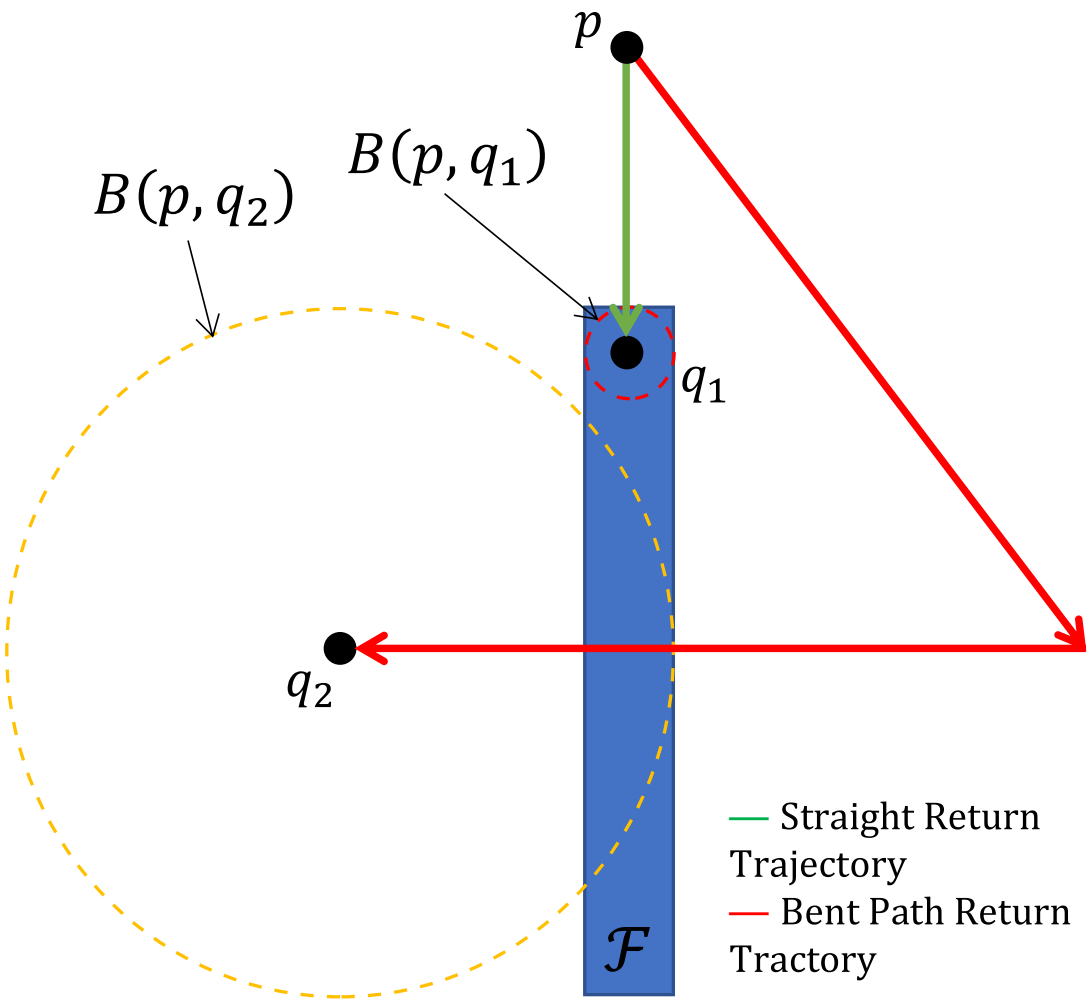

Figure 5-2. A bent path trajectory (red) may have advantages over the standard straight return trajectory (green) as this would increase the MAUR at point p.

5.2.3 MAURs as Control Barrier Functions

Control barrier functions (CBFs) are tools used for synthesizing controllers that provide mathematical guarantees of safety, which can be done by encoding state constraints as a safe set [82]. CBFs certify the existence of a control law that renders the safe set forward invariant, or in some cases, asymptotically stable, as seen in [83]. The motivation for using CBFs over other methods is due to their ability to be implemented in real-time with limited computational resources as in many spacecraft, while also providing robustness to model uncertainties and exogenous disturbances. CBF-based controllers have been implemented in [82] on computationally resource-constrained systems. A brief technical background on CBFs is now provided.

Consider a differential inclusion F with state $x \in \mathbb{R}^n$ and input $u \in \mathbb{R}^m$ modeled by $\dot{x} \in F(x,u)$, where $F : \mathbb{R}^n \times \mathbb{R}^m \rightrightarrows \mathbb{R}^n$ is the set-valued flow map. CBFs are vector valued functions $B : \mathbb{R}^n \to \mathbb{R}^d$ that guarantee the existence of control inputs that ensure the forward invariance (i.e. safety) of the safe set $S = \{x : B(x) \leq 0\}$, see [83].

Definition 5.1. A vector-valued function $B : \mathbb{R}^n \to \mathbb{R}^d$ with components $B(x) = [B_1(x); B_2(x); \ldots; B_d(x)]$, is called a CBF candidate defining the safe set S if $S = \{x \in \mathbb{R}^n : B \leq 0\}$. Also let $S_i \triangleq \{x \in \mathbb{R}^n : B_i \leq 0\}$ and $M_i \triangleq \{x \in \partial S : B_i(x) = 0\}$ for each $i \in \{1, \ldots, d\}$.

Definition 5.2. A continuously differentiable CBF candidate $B : \mathbb{R}^n \to \mathbb{R}^d$ defining the set $S \subset \mathbb{R}^n$ is a CBF for F and S on a set $\mathcal{O} \subset \mathbb{R}^n$ with respect to a function $\gamma : \mathbb{R}^n \to \mathbb{R}^d$ if **1)** there exists an ϵ-neighborhood of the boundary of S such that $\mathcal{N}_\epsilon(\partial S) \subset \mathcal{O}$, **2)** for each $i \in \{1, \ldots, d\}$, $\gamma_i(x) \geq 0$ for all $x \in \mathcal{N}_\epsilon(M_i) \setminus S_i$, and **3)** the regulation map

$$K_c(x) \triangleq \{u \in \mathbb{R}^m : \Gamma_i(x,u) \leq -\gamma_i(x), \forall i \in \{1, \ldots, d\}\}$$

is nonempty for all $x \in \mathcal{O}$,where for each $i \in \{1, \ldots, d\}$,

$$\Gamma_i(x,u) \triangleq \sup_{f \in F(x,u)} \langle \nabla B_i(x), f \rangle . \tag{5–1}$$

The set $K_c(x)$ represents a set of control inputs that ensure safety. One way to select inputs from $K_c(x)$ is to solve an optimization problem featuring the constraints defining K_c.

Assuming that there is a region $\Omega \subset \mathbb{R}^n$ where $\texttt{maur}(x)$ is continuously differentiable, a CBF candidate could be defined as

$$B_{\mathsf{m}} \triangleq \rho - \texttt{maur}(x), \tag{5–2}$$

where ρ is a state of a system, representing the radius of uncertainty (Chapter 3). The safe set could then be defined as $S_{\mathsf{m}} \triangleq \{[x;\rho] \in \mathbb{R}^n \times \mathbb{R}_{\geq 0} : B_{\mathsf{m}} \leq 0\}$. The goal would be to develop a control algorithm that makes the safe set forward invariant. However, the challenge in all of this would be to develop the conditions for where `maur` is continuously differentiable, and then computing its gradient, to satisfy (5–1). It would also be worth exploring recent developments for discontinuous CBFs (cf., [84] and [85]) to relax the continuity requirements.

5.2.4 Probabilistic Guarantee of Re-entry and Covariance Steering

In [1]– [88], path planning methods are presented that utilize the mean and covariance of the exogenous disturbance (modeled as zero-mean white Gaussian noise) on the system to generate optimal path plans that avoid collisions with elements located in the environment, under predefined chance constraints. A multidimensional Gaussian distribution if fully defined by the mean vector and covariance matrix. The centroid of this multidimensional distribution is described by the vector mean, while the ellipsoid shape comes from the covariance matrix (Figure 5-3). The multidimensional Gaussian distribution can be used to model the state of uncertainty of an agent in any arbitrary dimension. In [1], a system is provided, which is modeled as a stochastic linear system, where the state covariance (i.e. region of uncertainty) is steered in such a way that its shape is manipulated to accomplish obstacle avoidance.

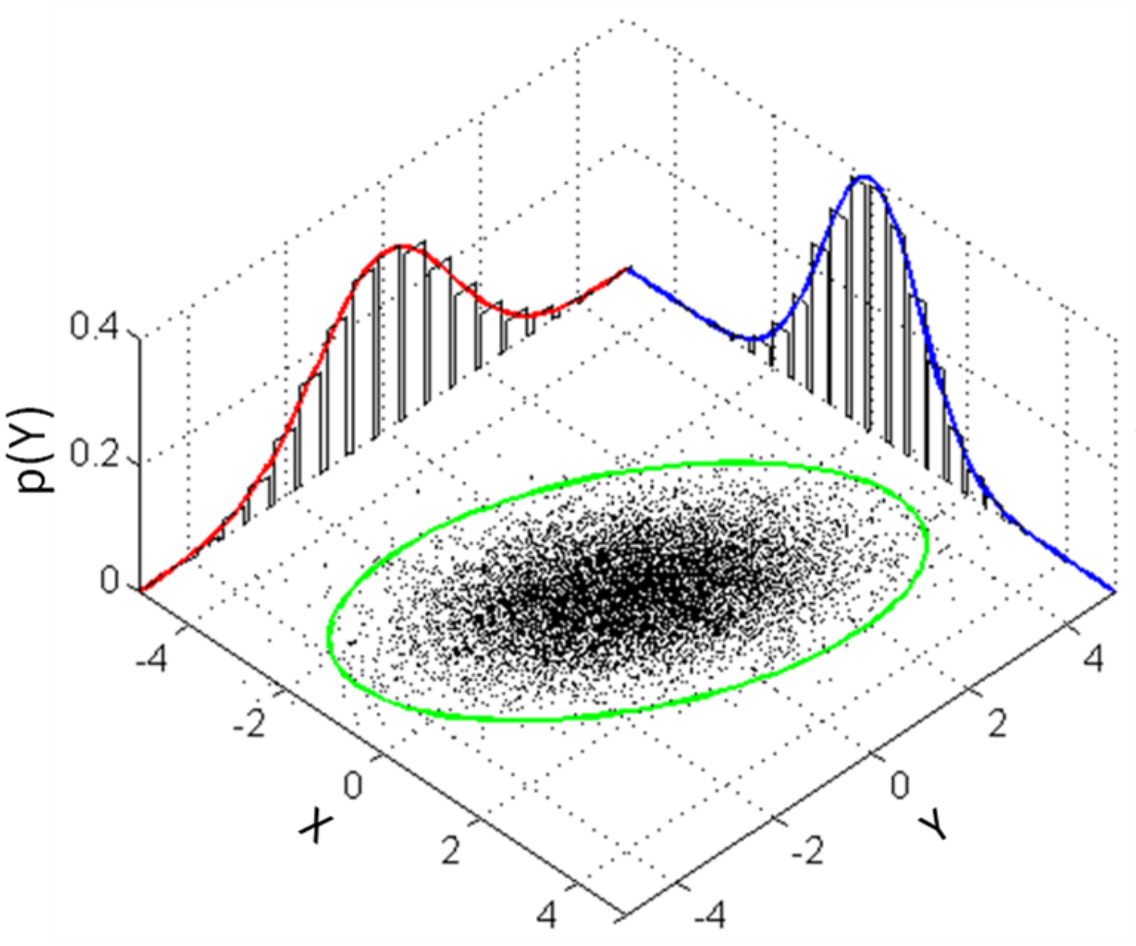

Figure 5-3. Geometric representation of the two dimensional Gaussian distribution in the plane, where the centroid is described by the vector mean and its shape is described by the covariance matrix. The green ellipse is referred to as the 3-sigma [89].

Consider the discrete-time linear time-varying system with additive noise

$$x_{k+1} = A_k x_k + B_k u_k + D_k w_k,$$

where $k = 0, \dots N-1$ is the time index, $x_k \in \mathbb{R}^{n_x}$ is the state, $u_k \in \mathbb{R}^{n_u}$ is the control input, and $w_k \in \mathbb{R}^{n_w}$ is Gaussian noise with zero mean and unit covariance. The initial state x_0 is drawn from the Gaussian distribution $x_0 \sim \mathcal{N}(\mu_0, \sigma_0)$, where $\mu_0 \in \mathbb{R}^{n_x}$ is the mean and $\sigma_0 \in \mathbb{R}^{n_x \times n_x}$ is the covariance. The goal is to steer the initial state to a finale state $x_N \sim \mathcal{N}(\mu_N, \sigma_N)$, where N is the terminal time index. To this end, a solver is developed to minimize the quadratic cost function $J(x_{0:N-1}, u_{0:N-1})$, defined as

$$J(x_{0:N-1}, u_{0:N-1}) \triangleq \mathbb{E}\left(\sum_{k=0}^{N-1} x_k^\top Q_k x_k + u_k^\top R_k u_k\right), \tag{5–3}$$

where $x_{0:N-1}$ is the state sequence, $u_{0:N-1}$ is the control sequence, $Q_k, R_k \succeq \mathbf{0}$ are constants. In addition, chance constraints are developed to prevent the agent from running into obstacles. To this end, the feasible set is defined as

$$\mathcal{X} \triangleq \mathcal{X}_\Omega \setminus \left(\bigcup_{j=1}^{N_{\text{obs}}} \mathcal{X}_j\right),$$

where $\mathcal{X}_\Omega \subset \mathbb{R}^{n_x}$ denotes the permissible operating region of the agent, and $\mathcal{X}_j \subset \mathbb{R}^{n_x}$ are the obstacles, for $j \in \{1, \dots N_{\text{obs}}\}$. Given $\mathcal{X}$, a chance constraint is applied to the states to enforce the probability of a constraint violation being smaller than a certain threshold, rather than using hard constraints since the noise, and therefore the state, is unbounded. The chance constraint is

$$P(x_k \in \mathcal{X}) \leq P_{\text{fail}}, \tag{5–4}$$

where $P(\cdot)$ is the probability of the event, and P_{fail} is the prescribed maximum probability threshold for failure. The control problem is to develop a control policy that minimizes the cost function in (5–3) subject to the initial state x_0, the terminal state x_N, and the state chance constraints in 5–4. An example of an optimal path plan is depicted in Figure 5-4,

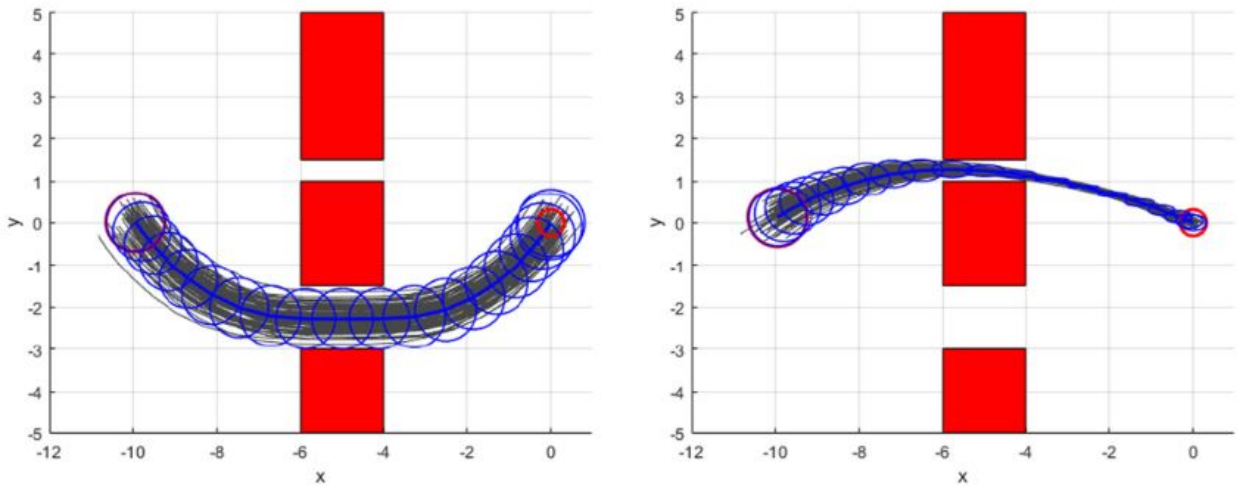

Figure 5-4. Example path plan solutions that steer only the mean (left) and both the mean and covariance (right) from an initial state to a final state. [1].

where the state covariance is steered in a way that stretches the state distribution so that it can fit through a narrow region of $\mathcal{X}$ while satisfying the chance constraint in 5–4.

Even though this work is primarily focused on obstacle avoidance, the same principles could be applied to generating path plans where the regions of uncertainty, modeled as a multidimensional Gaussian distribution, could be steered in a way that it can be squeezed into the feedback region. This ability would give path planning algorithms increased flexibility by increasing the dwell time as new methods for probabilistic guarantees of re-entry are developed.

5.2.5 Obfuscation of Feedback Regions and Objectives

In some applications it may be necessary to obfuscate the feedback region $\mathcal{F}$ or the agent's goals. For example, the agent may be operating in a military setting where the feedback region is a base of operations that provides feedback to an agent. Assume that there is an adversarial agent that wants to learn where this base of operations (i.e, feedback region $\mathcal{F}$) is so that the mechanism that provides state feedback could be neutralized (i.e., strategic placement of a jammer), or the adversary may be interested in learning what the mission objectives are (i.e., the desired path X_d). Regardless of the adversaries objectives, it is desirable to construct deceptive [90], private path plans [91].

From Chapter 3, recall equation (3–3)

$$\texttt{target}\,(p,\rho) \triangleq \arg\min_{q}\{\|q-p\| : q \in \mathbb{R}^2, U_q(\tau_q) \subset T_{R(p,q)}\,(p)\},$$

which is a set-valued function. Observe that the cardinality of `target`, computed at a point p, could be increased if the radius of uncertainty ρ at point p is made much less than $\texttt{maur}(p)$ (Figure 5-5). With a larger set of target points $q \in \texttt{target}\,(p,\rho)$, a path planner has more choices when it comes to selecting a path plan that guarantees re-entry, which could perhaps be considered deceptive and may obfuscate the agent's feedback region or objectives from the perspective of the adversary. Requiring ρ at p to be much less than $\texttt{maur}(p)$ may come at a cost. Increasing the number of available return trajectories would require a premature departure from X_d as it may become increasingly necessary to spend less time tracking X_d in favor of executing deceptive maneuvers. However, it is not clear if an early departure will result in the adversary learning more about the feedback region as this will increase the frequency of re-entries into the feedback region, thus increasing the information.

5.2.6 Time Varying DNN Estimator Gains

In Chapter 4, a Lb-DNN estimator was developed as

$$\begin{aligned}
{}^{\mathcal{I}}\dot{\hat{X}}_{\mathcal{T}} &= {}^{\mathcal{I}}_{2}\hat{X}_{\mathcal{T}}, \\
{}^{\mathcal{I}}_{2}\dot{\hat{X}}_{\mathcal{T}} &= \Phi\left({}^{\mathcal{I}}X_{\mathcal{T}}, {}^{\mathcal{I}}_{2}\hat{X}_{\mathcal{T}}, \hat{\Theta}\right) + \nu,
\end{aligned}$$

where

$$\nu \triangleq -\left(\gamma(k+\alpha)+2\alpha\right)\eta + \left(\gamma-\alpha^2\right)e + \beta\,\text{sgn}((e+e_f)),$$

is a robust term, designed to compensate for the errors induced by the DNN Φ. From the Lyapunov-based stability analysis in Section 4.4, it is seen that ν is designed to be robust against the worst-case error induced by the DNN. Accounting for this worst-case error can be understood as having no trust in the DNN's modeling accuracy, and thus

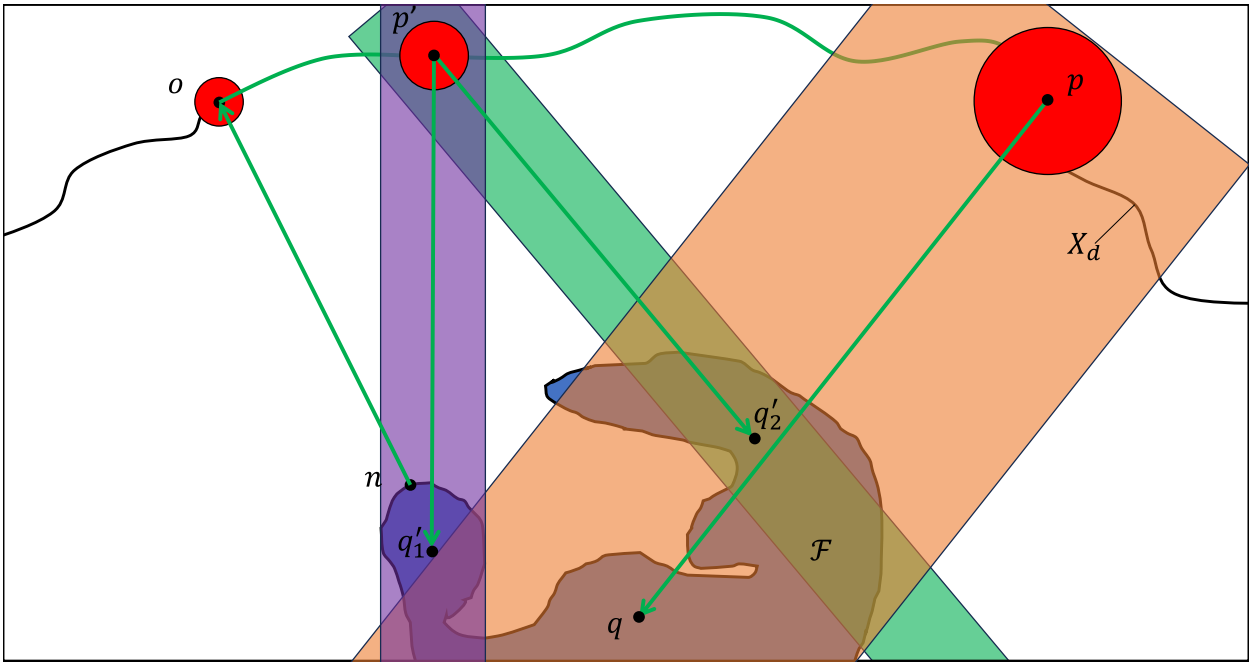

Figure 5-5. Illustration of three path plans. The first path plan $\pi = (n, o, p, q)$ is a path that maximizes the time spent tracking X_d (the bounding region in orange), whereas the second and third path plan $\pi_1' = (n, o, p', q_1')$ and $\pi_2' = (n, o, p', q_2')$ departs from X_d at an earlier time to allow for a larger set of possible return trajectories. Notice that a smaller bounding region (purple and green regions) can be used for a departure from point p' since the region of uncertainty (red) is much smaller than the one at point p. This smaller bounding region allows for a larger set of possible return trajectories.

there is a need for a compensator to be present to ensure stable tracking. However, this compensator hinders the learning of the DNN. The weight update law

$$\dot{\hat{\Theta}} \triangleq \text{proj}(\Gamma((e+e_f)^\top \Phi'({}^{\mathcal{I}}X_{\mathcal{T}}, {}^{\mathcal{I}}_{2}\hat{X}_{\mathcal{T}}, \hat{\Theta}))^\top),$$

updates the weights based on the error signals e and e_f, but if the tracking error and filtered error are primarily compensated for by ν rather than an accurate DNN model, then the effects of the weight update are minimal, and thus the learning is minimal as there is little error being induced by the DNN.

Initially, it makes sense to have heavy reliance on ν as the DNN initially begins to train, but as time evolves, it is reasonable to reduce the efficacy of ν by reducing the values of the robust gains (e.g., β, k, and γ) in favor of relying more on the DNN. This motivates the need to investigate time-varying gains, and a trust-metric (i.e., a metric for the modeling accuracy of the system being estiamted) that informs the dynamics of these gains. The benefits of reducing the efficacy of ν, can be seen in the following modifications to the simulation in Section 4.7.1.

To examine the performance of the DNN estimator developed in (4–8) with time-varying gains, the same random trajectory for the target was used (Figure 4-6). While the target followed this trajectory, the estimator in (4–8) was deployed, where a fully-connected feedforward DNN composed of three hidden layers (i.e., $k_h = 3$), with three neurons per layer (i.e., $L_j = 3$). Further, the hyperbolic tangent activation function (tanh) was used on the output layer, and the rectified linear unit (ReLu) activation function was used on all other layers. Additionally, the following gains were selected: $\gamma = 0.1$, $k = 20$, $\alpha = 60$, $\beta = 0.0001$, $\Gamma = \begin{bmatrix} 10\mathbf{I}_{39} & \mathbf{0}_{39\times 8} \\ \mathbf{0}_{8\times 39} & 15\mathbf{I}_8 \end{bmatrix}$. However, after 5000 seconds, the gains were reduced to the following: $k = 5$, $\alpha = 15$, $\Gamma = \begin{bmatrix} 2.5\mathbf{I}_{39} & \mathbf{0}_{39\times 8} \\ \mathbf{0}_{8\times 39} & 3.75\mathbf{I}_8 \end{bmatrix}$. The reduction in these gains is motivated by the expectation that the weight estimates are converging to the

ideal weights, in which case, the influence of the robust term in the estimator ν ought to be reduced in favor of relying on the performance of the trained DNN model of the target's dynamics. The results of this simulation are seen in Figure 5-6.

In the error plots in Figure 5-6, it is seen that the norm of the acceleration estimate error is greatly reduced (on average) after the change in gain values. However, it is also seen that there are larger spikes in the errors that occur. These spikes come as a consequence of the reduced efficacy of ν. Given the ad-hoc nature of the gain change, it isn't a surprise to see some aspects of the estimator's performance degrade, which is why there is a need to investigate a trust-metric for informing the dynamics of the gains.

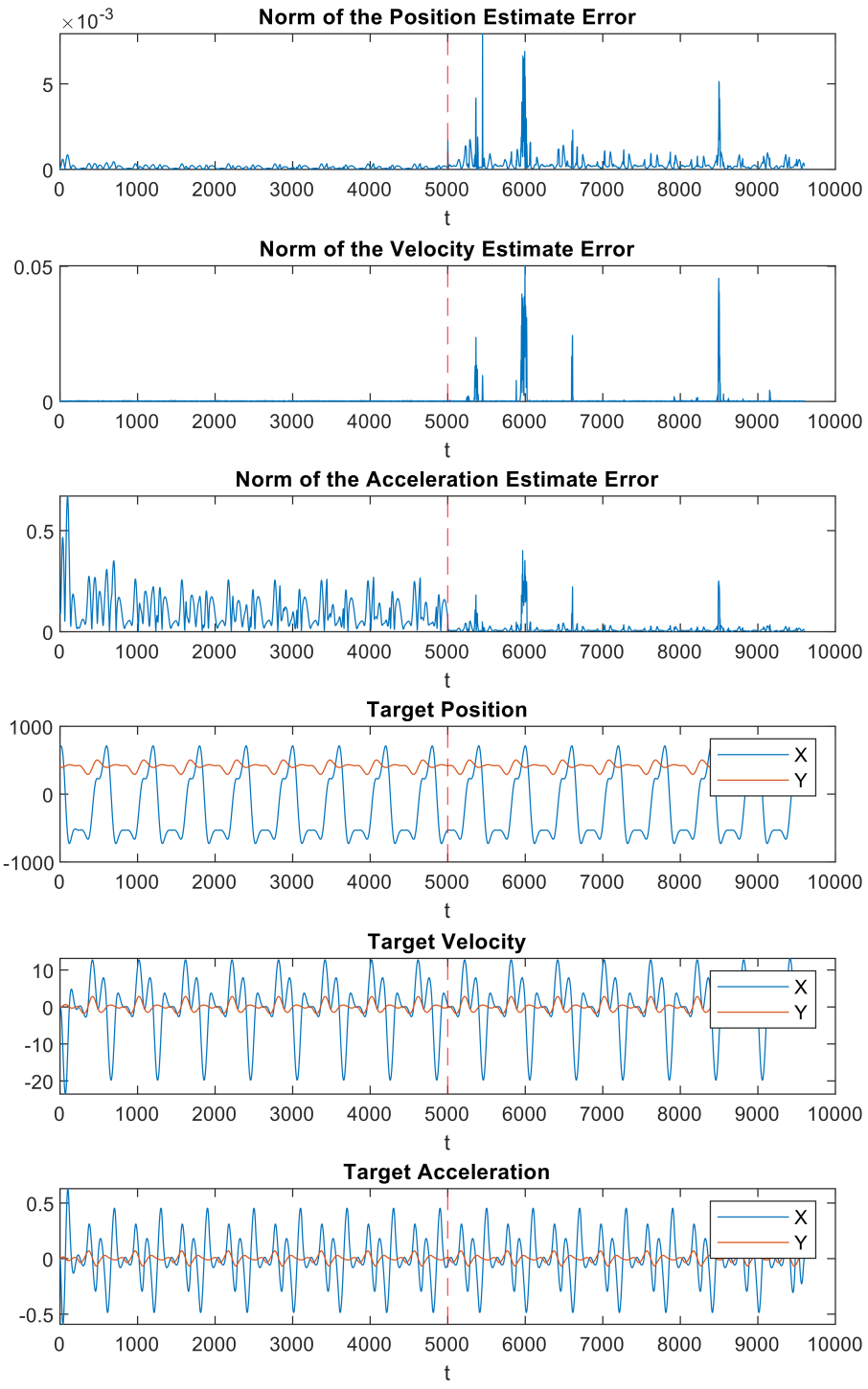

Figure 5-6. Plots of the norm of the position estimate error (i.e, $\|e\|$), norm of the velocity error (i.e, $\|\dot{e}\|$), norm of the acceleration estimate error (i.e, $\|\ddot{e}\|$), actual target position (i.e., ${}^{\mathcal{I}}x_{\mathcal{T}}$), actual target velocity (i.e., ${}^{\mathcal{I}}\dot{x}_{\mathcal{T}}$), and actual target acceleration (i.e., ${}^{\mathcal{I}}\ddot{x}_{\mathcal{T}}$). The dashed vertical line indicates the instance where the gains were reduced.

APPENDIX A
MULTI-AGENT LOCALIZATION USING GEOMETRIC CONSTRAINTS WITH INTERMITTENT STATE FEEDBACK OF POSSIBLE JUMPS

A.1 Construction of the Directed Acyclic Graph

Suppose that there is a state X such that agent $i \in \mathcal{A}$ has a state $X^i \in D^i$ such that $\texttt{mode}^i = 0$, then according to (3–44), X^i must be contained in D^i_{01}. Next, suppose that there is a state X such that agent $i \in \mathcal{A}$ has a state $X^i \in D^i$ such that $\texttt{mode}^i = 1$, then according to (3–44) X^i can potentially be contained in the intersection of any subset of the collection $(D^i_* \cap \{\texttt{mode}^i = 1\}, D^i_{\#1}, D^i_{11}, D^i_{12})$, creating $2^4 - 1$ possibilities, which are tabulated in Table A-1. However, not all of these combinations are admissible. For example, X^i can not be contained in $D^i_{\#1} \cap D^i_{12}$ since $D^i_{\#1} \cap D^i_{12} = \emptyset$, because $\texttt{b}^i$ cannot be equal to both 1 and 0. The admissible and inadmissible combinations for an agent with $\texttt{mode}^i = 1$ are tabulated in Table A-1.

Similarly, suppose that there is a state X such that agent $i \in \mathcal{A}$ has a state $X^i \in D^i$ such that $\texttt{mode}^i = 2$, then according to (3–44) X^i can potentially be contained in the intersection of any subset of the collection $(D^i_* \cap \{\texttt{mode}^i = 2\}, D^i_{\#2}, D^i_{22}, D^i_{23}, D^i_{20})$, creating $2^5 - 1$ possibilities. The admissible and inadmissible combinations for an agent with $\texttt{mode}^i = 2$ are tabulated in Table A-2.

Finally, suppose that there is a state X such that agent $i \in \mathcal{A}$ has a state $X^i \in D^i$ such that $\texttt{mode}^i = 3$, then according to (3–44), X^i must be contained in D^i_{30}.

Now that all of the admissible combinations of D^i have been identified, all possible jump sequences in null-time can be determined. To this end, let X^i be the state at jump time j, $(X^i)^+$ is the state at jump time $j+1$, $(X^i)^{++}$ is the state at jump time $j+2$, $(X^i)^{+++}$ is the state at jump time $j+3$, and so on, with each additional "$+$" representing the number of sequential jumps in null-time. Each possible jump sequence is now identified:

Combinations	Admissibility	Reason
$D^i_* \cap \{\texttt{mode}^i = 1\} \setminus D^i_{12}$	Admissible	No contradiction
$D^i_{\#1}$	Admissible	No contradiction
D^i_{11}	Admissible	No contradiction
$D^i_{12} \setminus D^i_*$	Admissible	No contradiction
$D^i_* \cap D^i_{12}$	Admissible	No contradiction
$D^i_{\#1} \cap D^i_{11}$	Inadmissible	$\mathcal{T}^i_1$ can't be both > 0 and ≤ 0
$D^i_* \cap \{\texttt{mode}^i = 1\} \cap D^i_{\#1}$	Inadmissible	$\mathfrak{b}^i$ can't be equal to both 1 and 0
$D^i_* \cap \{\texttt{mode}^i = 1\} \cap D^i_{11}$	Inadmissible	$\mathfrak{b}^i$ can't be equal to both 1 and 0
$D^i_{\#1} \cap D^i_{12}$	Inadmissible	$\mathfrak{b}^i$ can't be equal to both 1 and 0
$D^i_{11} \cap D^i_{12}$	Inadmissible	$\mathfrak{b}^i$ can't be equal to both 1 and 0
$D^i_* \cap \{\texttt{mode}^i = 1\} \cap D^i_{\#1} \cap D^i_{11}$	Inadmissible	$\mathfrak{b}^i$ can't be equal to both 1 and 0
$D^i_* \cap \{\texttt{mode}^i = 1\} \cap D^i_{\#1} \cap D^i_{12}$	Inadmissible	$\mathfrak{b}^i$ can't be equal to both 1 and 0
$D^i_* \cap \{\texttt{mode}^i = 1\} \cap D^i_{11} \cap D^i_{12}$	Inadmissible	$\mathfrak{b}^i$ can't be equal to both 1 and 0
$D^i_{\#1} \cap D^i_{11} \cap D^i_{12}$	Inadmissible	$\mathfrak{b}^i$ can't be equal to both 1 and 0
$D^i_* \cap \{\texttt{mode}^i = 1\} \cap D^i_{\#1} \cap D^i_{11} \cap D^i_{12}$	Inadmissible	$\mathfrak{b}^i$ can't be equal to both 1 and 0

Table A-1. $\texttt{mode}^i = 1$ combinations

A.1.1 $X^i \in D^i_{01}$

Suppose that there is a state X such that agent $i \in \mathcal{A}$ has the state $X^i \in D^i_{01}$, then according to the partial jump sets in (3–44) and the partial flow sets (3–36)–(3–39), $X^i \in \langle\!\langle \{0,1\}^N, \texttt{Plans}^i, \{0\}, \{n\}, \{n\}, \{n\}, \{\tau^i_n\}, \{0\}, \{0\}, \{0\} \rangle\!\rangle$. If $X^i \in D_{01}$, then the jump map in (3–45) yields $(X^i)^+ \in \langle\!\langle \{0,1\}^N, \texttt{Plans}^i, \{1\}, \{n\}, \{n\}, \{n\}, \{\tau^i_n\}, \{0\}, \{0\}, \{0\} \rangle\!\rangle$. Then according to the partial jump sets in (3–44) and the partial flow sets (3–36)–(3–39), $(X^i)^+$ must be contained in C^i_1. Therefore, there was one jump in null-time. The possible null-time jump sequences can be visualized in the DAG in Figure A-1.

A.1.2 $X^i \in D^i_* \cap \{\texttt{mode}^i = 1\} \setminus D^i_{12}$

Suppose that there is a state X such that agent $i \in \mathcal{A}$ has the state $X^i \in D^i_* \cap \{\texttt{mode}^i = 1\} \setminus D^i_{12}$, then according to the partial jump sets in (3–44) and the partial flow sets (3–36)–(3–39), $X^i \in \langle\!\langle \{0,1\}^N, \texttt{Plans}^i, \{1\}, \mathbb{R}^2, \mathbb{R}^2, \mathbb{R}^2, [\tau^i_n, \tau^i_o), [T^i_{\max}, \infty), [0, \infty), \{0\} \rangle\!\rangle$. If $X^i \in D^i_* \cap \{\texttt{mode}^i = 1\} \setminus D^i_{12}$ then the jump map in (3–45) yields $(X^i)^+ \in \langle\!\langle \{0,1\}^N, \texttt{Plans}^i, \{1\}, \mathbb{R}^2, \mathbb{R}^2, \mathbb{R}^2, [\tau^i_n, \tau^i_o), \{0\}, [0, \infty), \{1\} \rangle\!\rangle$. If $(X^i)^+ \in$

Combinations	Admissibility	Reason
$D^i_* \cap \{\texttt{mode}^i = 2\} \setminus (D^i_{20} \cup D^i_{23})$	Admissible	No contradiction
$D^i_{\#2}$	Admissible	No contradiction
D^i_{22}	Admissible	No contradiction
$D^i_{20} \setminus (D^i_* \cup D^i_{23})$	Admissible	No contradiction
$D^i_{23} \setminus (D^i_* \cup D^i_{20})$	Admissible	No contradiction
$(D^i_* \cap D^i_{20}) \setminus D^i_{23}$	Admissible	No contradiction
$(D^i_* \cap D^i_{23}) \setminus D^i_{20}$	Admissible	No contradiction
$D^i_{20} \cap D^i_{23} \setminus D^i_*$	Admissible	No contradiction
$D^i_* \cap D^i_{20} \cap D^i_{23}$	Admissible	No contradiction
$D^i_{\#2} \cap D^i_{22}$	Inadmissible	$\mathcal{T}^i_2$ can't be both > 0 and ≤ 0
$D^i_* \cap \{\texttt{mode}^i = 2\} \cap D^i_{\#2}$	Inadmissible	$\texttt{b}^i$ can't be equal to both 1 and 0
$D^i_* \cap \{\texttt{mode}^i = 2\} \cap D^i_{22}$	Inadmissible	$\texttt{b}^i$ can't be equal to both 1 and 0
$D^i_{\#2} \cap D^i_{20}$	Inadmissible	$\texttt{b}^i$ can't be equal to both 1 and 0
$D^i_{\#2} \cap D^i_{23}$	Inadmissible	$\texttt{b}^i$ can't be equal to both 1 and 0
$D^i_{22} \cap D^i_{20}$	Inadmissible	$\texttt{b}^i$ can't be equal to both 1 and 0
$D^i_{22} \cap D^i_{23}$	Inadmissible	$\texttt{b}^i$ can't be equal to both 1 and 0
$D^i_* \cap \{\texttt{mode}^i = 2\} \cap D^i_{\#2} \cap D^i_{22}$	Inadmissible	$\texttt{b}^i$ can't be equal to both 1 and 0
$D^i_* \cap \{\texttt{mode}^i = 2\} \cap D^i_{\#2} \cap D^i_{20}$	Inadmissible	$\texttt{b}^i$ can't be equal to both 1 and 0
$D^i_* \cap \{\texttt{mode}^i = 2\} \cap D^i_{\#2} \cap D^i_{23}$	Inadmissible	$\texttt{b}^i$ can't be equal to both 1 and 0
$D^i_* \cap \{\texttt{mode}^i = 2\} \cap D^i_{22} \cap D^i_{20}$	Inadmissible	$\texttt{b}^i$ can't be equal to both 1 and 0
$D^i_* \cap \{\texttt{mode}^i = 2\} \cap D^i_{22} \cap D^i_{23}$	Inadmissible	$\texttt{b}^i$ can't be equal to both 1 and 0
$D^i_{\#2} \cap D^i_{22} \cap D^i_{20}$	Inadmissible	$\texttt{b}^i$ can't be equal to both 1 and 0
$D^i_{\#2} \cap D^i_{22} \cap D^i_{23}$	Inadmissible	$\texttt{b}^i$ can't be equal to both 1 and 0
$D^i_{\#2} \cap D^i_{20} \cap D^i_{23}$	Inadmissible	$\texttt{b}^i$ can't be equal to both 1 and 0
$D^i_{22} \cap D^i_{20} \cap D^i_{23}$	Inadmissible	$\texttt{b}^i$ can't be equal to both 1 and 0
$D^i_* \cap \{\texttt{mode}^i = 2\} \cap D^i_{\#2} \cap D^i_{22} \cap D^i_{20}$	Inadmissible	$\texttt{b}^i$ can't be equal to both 1 and 0
$D^i_* \cap \{\texttt{mode}^i = 2\} \cap D^i_{\#2} \cap D^i_{22} \cap D^i_{23}$	Inadmissible	$\texttt{b}^i$ can't be equal to both 1 and 0
$D^i_* \cap \{\texttt{mode}^i = 2\} \cap D^i_{22} \cap D^i_{20} \cap D^i_{23}$	Inadmissible	$\texttt{b}^i$ can't be equal to both 1 and 0
$D^i_* \cap \{\texttt{mode}^i = 2\} \cap D^i_{\#2} \cap D^i_{20} \cap D^i_{23}$	Inadmissible	$\texttt{b}^i$ can't be equal to both 1 and 0
$D^i_{\#2} \cap D^i_{22} \cap D^i_{20} \cap D^i_{23}$	Inadmissible	$\texttt{b}^i$ can't be equal to both 1 and 0
$D^i_* \cap \{\texttt{mode}^i = 2\} \cap D^i_{\#2} \cap D^i_{22} \cap D^i_{20} \cap D^i_{23}$	Inadmissible	$\texttt{b}^i$ can't be equal to both 1 and 0

Table A-2. $\texttt{mode}^i = 2$ combinations

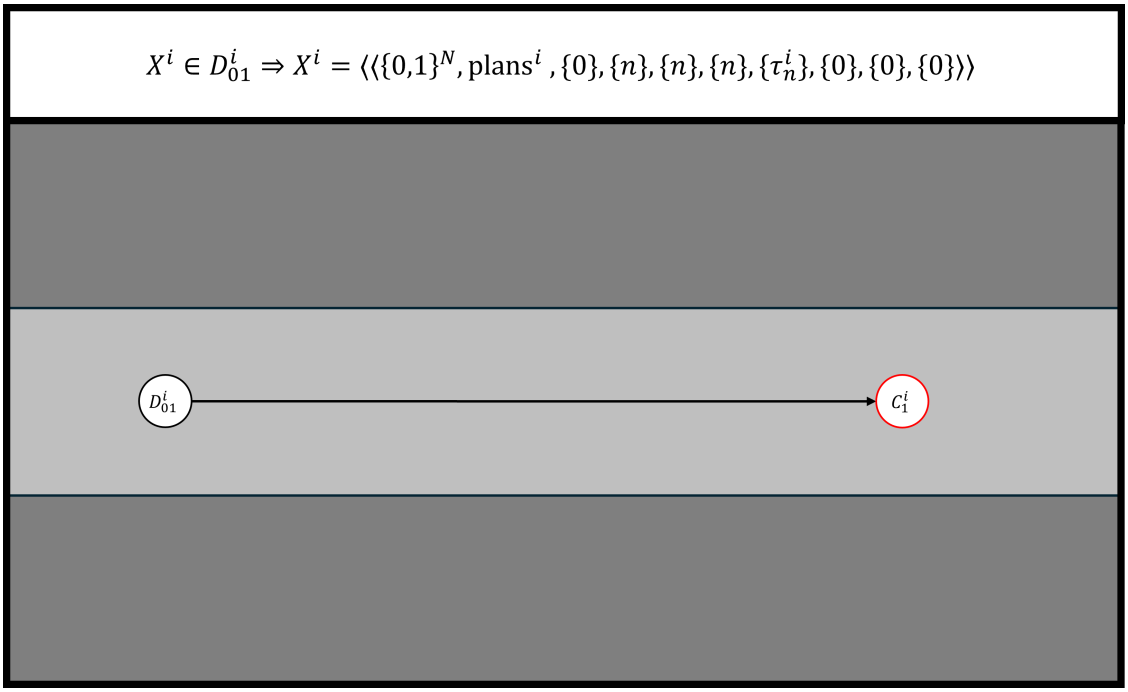

Figure A-1. Directed acyclic graph for $X^i \in D^i_{01}$.

$\langle\!\langle \{0,1\}^N, \texttt{Plans}^i, \{1\}, \mathbb{R}^2, \mathbb{R}^2, \mathbb{R}^2, [\tau^i_n, \tau^i_o), \{0\}, [0,\infty), \{1\} \rangle\!\rangle$, then according to the partial jump sets in (3–44) and the partial flow sets (3–36)–(3–39) implies that either $(X)^+ \in D^i_{\#1}$ or $(X)^+ \in D^i_{11}$.

- If $(X)^+ \in D^i_{\#1}$ then the jump map in (3–45) yields $(X^i)^{++} \in \langle\!\langle \{0,1\}^N, \texttt{Plans}^i, \{1\}, \mathbb{R}^2, \mathbb{R}^2, \mathbb{R}^2, [\tau^i_n, \tau^i_o), \{0\}, [0,\infty), \{0\} \rangle\!\rangle$. After this mapping, the operating mode remains the same (i.e., $\texttt{mode}^i = 1$). Then according to Table A-1, the partial jump sets in (3–44), and the partial flow sets (3–36)–(3–39), it is only possible for $(X^i)^{++}$ to be contained in C^i_1, since: $(X^i)^{++} \notin D^i_* \cap \{\texttt{mode}^i = 1\}$ because $\tau^i_{\text{trig}} = 0 < T^i_{\text{max}}$; $(X^i)^{++} \notin D^i_{\#1}$ because $\texttt{b}^i = 0 \neq 1$; $(X^i)^{++} \notin D^i_{11}$ because $\texttt{b}^i = 0 \neq 1$; $(X^i)^{++} \notin D^i_* \cap \{\texttt{mode}^i = 1\} \cap D^i_{12}$ because $\tau^i_{\text{trig}} = 0 < T^i_{\text{max}}$; and since $(X^i)^{++} \notin D^i_{12}$. Since $(X^i)^{++} \in C^i_1$, there were two jumps in null-time.
- If $(X)^+ \in D^i_{11}$ then the regularization of the jump map in (3–45) yields $(X^i)^{++} \in \langle\!\langle \{0,1\}^N, \texttt{Plans}^i, \{1\}, \mathbb{R}^2, \mathbb{R}^2, \mathbb{R}^2, [\tau^i_n, \tau^i_o), \{0\}, [0,\infty), \{0\} \rangle\!\rangle$. After this mapping, the operating mode remains the same (i.e., $\texttt{mode}^i = 1$). Then according to Table A-1, the partial jump sets in (3–44), and the partial flow sets (3–36)–(3–39), it is only possible for $(X^i)^{++}$ to be contained in C^i_1, since: $(X^i)^{++} \notin D^i_* \cap \{\texttt{mode}^i = 1\}$ because $\tau^i_{\text{trig}} = 0 < T^i_{\text{max}}$; $(X^i)^{++} \notin D^i_{\#1}$ because $\texttt{b}^i = 0 \neq 1$; $(X^i)^{++} \notin D^i_{11}$ because $\texttt{b}^i = 0 \neq 1$; $(X^i)^{++} \notin D^i_* \cap \{\texttt{mode}^i = 1\} \cap D^i_{12}$ because $\tau^i_{\text{trig}} = 0 < T^i_{\text{max}}$; and since $(X^i)^{++} \notin D^i_{12}$. Since $(X^i)^{++} \in C^i_1$, there were two jumps in null-time.

The possible null-time jump sequences can be visualized in the DAG in Figure A-2.

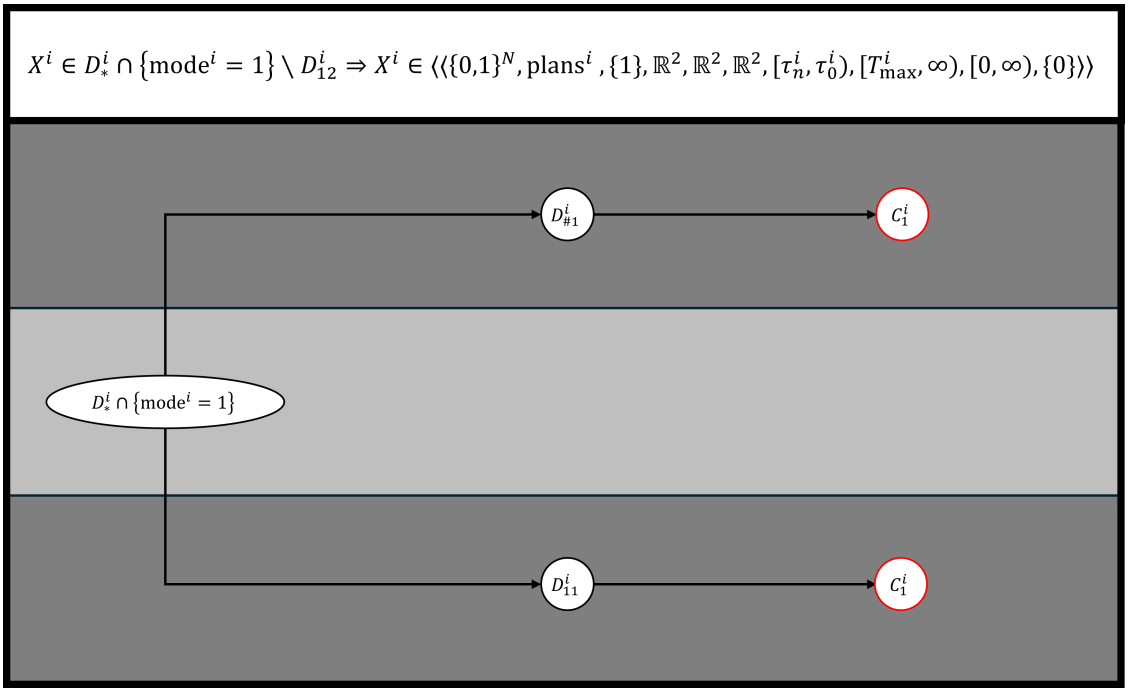

Figure A-2. Directed acyclic graph for $X^i \in D_*^i \cap \{\texttt{mode}^i = 1\} \setminus D_{12}^i$.

A.1.3 $X^i \in D_{\#1}^i$

Suppose that there is a state X such that agent $i \in \mathcal{A}$ has the state $X^i \in D_{\#1}^i$, then according to the partial jump sets in (3–44) and the partial flow sets (3–36)–(3–39), $X^i \in \langle\!\langle \{0,1\}^N, \texttt{Plans}^i, \{1\}, \mathbb{R}^2, \mathbb{R}^2, \mathbb{R}^2, [\tau_n^i, \infty), [0,\infty), [0,\infty), \{1\} \rangle\!\rangle$. If $X^i \in D_{\#1}^i$ then the jump map in (3–45) yields $(X^i)^+ \in \langle\!\langle \{0,1\}^N, \texttt{Plans}^i, \{1\}, \mathbb{R}^2, \mathbb{R}^2, \mathbb{R}^2, [\tau_n^i, \infty), \{0\}, [0,\infty), \{1\} \rangle\!\rangle$. Then according to Table A-1, the partial jump sets in (3–44), and the partial flow sets (3–36)–(3–39), it is only possible for $(X^i)^+$ to be contained in either $C_1^i \setminus D_{12}^i$ or D_{12}^i since: $(X^i)^+ \notin D_*^i \cap \{\texttt{mode}^i = 1\}$ because $\tau_{\text{trig}}^i = 0 < T_{\max}^i$; $(X^i)^+ \notin D_{\#1}^i$ because $\texttt{b}^i = 0 \neq 1$; $(X^i)^+ \notin D_{11}^i$ because $\texttt{b}^i = 0 \neq 1$; and $(X^i)^+ \notin D_*^i \cap \{\texttt{mode}^i = 1\} \cap D_{12}^i$ because $\tau_{\text{trig}}^i = 0 < T_{\max}^i$.

- If $(X^i)^+ \in C_1^i \setminus D_{12}^i$, then there was one jump in null-time.
- If $(X^i)^+ \in D_{12}^i$, then the jump map in (3–45) yields $(X^i)^{++} \in \langle\!\langle \{0,1\}^N, \texttt{Plans}^i, \{2\}, \mathbb{R}^2, \mathbb{R}^2, \mathbb{R}^2, [\tau_o^i, \infty), \{0\}, [0,\infty), \{1\} \rangle\!\rangle$. Then according to Table A-2, the partial jump sets in (3–44), and the partial flow sets (3–36)–(3–39), it is only possible for $(X^i)^{++}$ to be in: $C_2^i \setminus (D_{20}^i \cup D_{23}^i)$, $D_{20}^i \setminus D_{23}^i$, $D_{23}^i \setminus D_{20}^i$, or $D_{20}^i \cap D_{23}^i$ since: $(X^i)^{++} \notin D_*^i \cap \{\texttt{mode}^i = 2\}$ because $\tau_{\text{trig}}^i = 0 < T_{\max}^i$; $(X^i)^{++} \notin D_{\#2}^i$ because

$\mathtt{b}^i = 0 \neq 1$; $(X^i)^{++} \notin D^i_{22}$ because $\mathtt{b}^i = 0 \neq 1$; $(X^i)^{++} \notin D^i_* \cap \{\mathtt{mode}^i = 2\} \cap D^i_{20}$ because $\tau^i_{\mathsf{trig}} = 0 < T^i_{\mathsf{max}}$; $(X^i)^{++} \notin D^i_* \cap \{\mathtt{mode}^i = 2\} \cap D^i_{23}$ because $\mathtt{b}^i = 0 \neq 1$; and $(X^i)^{++} \notin D^i_* \cap \{\mathtt{mode}^i = 2\} \cap D^i_{20} \cap D^i_{23}$ because $\tau^i_{\mathsf{trig}} = 0 < T^i_{\mathsf{max}}$.

- If $(X^i)^{++} \in C^i_2 \setminus (D^i_{20} \cup D^i_{23})$, then there were two jumps in null-time.
- If $(X^i)^{++} \in D^i_{20} \setminus D^i_{23}$, then according to the partial jump sets in (3–44) and the partial flow sets (3–36)–(3–39) $(X^i)^{++} \in \langle\!\langle \{0,1\}^N, \mathtt{Plans}^i, \{2\}, \mathcal{F}^*_{\mathsf{in}}, \mathbb{R}^2, \mathbb{R}^2, [\tau^i_o, \infty), \{0\}, [0,\infty), \{1\} \rangle\!\rangle$. If $(X^i)^{++} \in D^i_{20} \setminus D^i_{23}$, then the jump map in (3–45) yields $(X^i)^{+++} \in \langle\!\langle \{0,1\}^N, \{\mathtt{rpl}^i\}, \{0\}, \mathcal{F}^*_{\mathsf{in}}, \mathbb{R}^2, \mathbb{R}^2, \{0\}, \{0\}, \{0\}, \{1\} \rangle\!\rangle$. For an agent i with $\mathtt{mode}^i = 0$, $(X^i)^{+++}$ can either be in $C^i_0 \setminus D^i_{01}$ or D^i_{01}.
  - If $(X^i)^{+++} \in C^i_0 \setminus D^i_{01}$, then there were three jumps in null-time.
  - If $(X^i)^{+++} \in D^i_{01}$, then according to the partial jump sets in (3–44) and the partial flow sets (3–36)–(3–39) $(X^i)^{+++} \langle\!\langle \{0,1\}^N, \{\mathtt{rpl}^i\}, \{0\}, \{n\}, \{n\}, \{n\}, \{0\}, \{0\}, \{0\}, \{1\} \rangle\!\rangle$. If $(X^i)^{+++} \in D^i_{01}$, then the jump map in (3–45) yields $(X^i)^{++++} \in \langle\!\langle \{0,1\}^N, \{\mathtt{rpl}^i\}, \{1\}, \{n\}, \{n\}, \{n\}, \{0\}, \{0\}, \{0\}, \{1\} \rangle\!\rangle$. Then according to the partial jump sets in (3–44) and the partial flow sets (3–36)–(3–39), $(X^i)^{++++}$ must be contained in C^i_1. Therefore, there were four jumps in null-time.
- If $(X^i)^{++} \in D^i_{23} \setminus D^i_{20}$, then according to the partial jump sets in (3–44) and the partial flow sets (3–36)–(3–39) $(X^i)^{++} \in \langle\!\langle \{0,1\}^N, \mathtt{Plans}^i, \{2\}, \mathbb{R}^2, \mathbb{R}^2, \mathbb{R}^2, [\tau^i_p, \infty), \{0\}, [0,\infty), \{1\} \rangle\!\rangle$. If $(X^i)^{++} \in D^i_{23} \setminus D^i_{20}$, then the jump map in (3–45) yields $(X^i)^{+++} = \langle\!\langle \{0,1\}^N, \mathtt{Plans}^i, \{3\}, \mathcal{F}^{\complement}, \mathbb{R}^2, \mathbb{R}^2, [\tau^i_p, \infty), \{0\}, [0,\infty), \{1\} \rangle\!\rangle$. Since $\mathtt{mode}^i = 3$ and $(X^i)^{+++} \notin D^i_{30}$, $(X^i)^{+++}$ must be contained in C^i_3. Since $(X^i)^{+++}$ must be in C^i_3, there were three jumps in null-time.
- If $(X^i)^{++} \in D^i_{20} \cap D^i_{23}$, then according to the partial jump sets in (3–44) and the partial flow sets (3–36)–(3–39) $(X^i)^{++} \in \langle\!\langle \{0,1\}^N, \mathtt{Plans}^i, \{2\}, \mathcal{F}^*_{\mathsf{in}}, \mathbb{R}^2, \mathbb{R}^2, [\tau^i_p, \infty), \{0\}, [0,\infty), \{1\} \rangle\!\rangle$. If $(X^i)^{++} \in D^i_{23} \cap D^i_{20}$, then the jump map in (3–45) yields $(X^i)^{+++} \in \langle\!\langle \{0,1\}^N, \mathtt{Plans}^i, \{3\}, \mathcal{F}^*_{\mathsf{in}}, \mathbb{R}^2, \mathbb{R}^2, [\tau^i_p, \infty), \{0\}, [0,\infty), \{1\} \rangle\!\rangle \cup \langle\!\langle \{0,1\}^N, \{\mathtt{rpl}^i\}, \{0\}, \mathcal{F}^*_{\mathsf{in}}, \mathcal{F}^*_{\mathsf{in}}, \mathcal{F}^*_{\mathsf{in}}, \{0\}, \{0\}, \{0\}, \{1\} \rangle\!\rangle$.
  - If $(X^i)^{+++} \in \langle\!\langle \{0,1\}^N, \mathtt{Plans}^i, \{3\}, \mathcal{F}^*_{\mathsf{in}}, \mathbb{R}^2, \mathbb{R}^2, [\tau^i_p, \infty), \{0\}, [0,\infty), \{1\} \rangle\!\rangle$, then according to the partial jump sets in (3–44) and the partial flow sets (3–36)–(3–39), $(X^i)^{+++}$ must be contained in D^i_{30}. Since $(X^i)^{+++} \in D^i_{30}$ then the jump map in (3–45) yields $(X^i)^{++++} \in \langle\!\langle \{0,1\}^N, \{\mathtt{rpl}^i\}, \{0\}, \mathcal{F}^*_{\mathsf{in}}, \mathcal{F}^*_{\mathsf{in}}, \mathcal{F}^*_{\mathsf{in}}, \{0\}, \{0\}, \{0\}, \{1\} \rangle\!\rangle$. For an agent i with $\mathtt{mode}^i = 0$, $(X^i)^{++++}$ can either be in $C^i_0 \setminus D^i_{01}$ or D^i_{01}.

- If $(X^i)^{++++} \in C_0^i \setminus D_{01}^i$, then there were four jumps in null-time.
- If $(X^i)^{++++} \in D_{01}^i$, then according to the partial jump sets in (3–44) and the partial flow sets (3–36)–(3–39) $(X^i)^{++++} \langle\!\langle \{0,1\}^N, \{\texttt{rpl}^i\}, \{0\}, \{n\}, \{n\}, \{n\}, \{0\}, \{0\}, \{0\}, \{1\} \rangle\!\rangle$. If $(X^i)^{++++} \in D_{01}^i$, then the jump map in (3–45) yields $(X^i)^{+++++} \in \langle\!\langle \{0,1\}^N, \{\texttt{rpl}^i\}, \{1\}, \{n\}, \{n\}, \{n\}, \{0\}, \{0\}, \{0\}, \{1\} \rangle\!\rangle$. Then according to the partial jump sets in (3–44) and the partial flow sets (3–36)–(3–39), $(X^i)^{+++++}$ must be contained in C_1^i. Therefore, there were five jumps in null-time.

* If $(X^i)^{+++} \in \langle\!\langle \{0,1\}^N, \{\texttt{rpl}^i\}, \{0\}, \mathcal{F}_{\text{in}}^*, \mathcal{F}_{\text{in}}^*, \mathcal{F}_{\text{in}}^*, \{0\}, \{0\}, \{0\}, \{1\} \rangle\!\rangle$, then for an agent i with $\texttt{mode}^i = 0$, $(X^i)^{+++}$ can either be in $C_0^i \setminus D_{01}^i$ or D_{01}^i.
  - If $(X^i)^{+++} \in C_0^i \setminus D_{01}^i$, then there were three jumps in null-time.
  - If $(X^i)^{+++} \in D_{01}^i$, then according to the partial jump sets in (3–44) and the partial flow sets (3–36)–(3–39) $(X^i)^{+++} \langle\!\langle \{0,1\}^N, \{\texttt{rpl}^i\}, \{0\}, \{n\}, \{n\}, \{n\}, \{0\}, \{0\}, \{0\}, \{1\} \rangle\!\rangle$. If $(X^i)^{+++} \in D_{01}^i$, then the jump map in (3–45) yields $(X^i)^{++++} \in \langle\!\langle \{0,1\}^N, \{\texttt{rpl}^i\}, \{1\}, \{n\}, \{n\}, \{n\}, \{0\}, \{0\}, \{0\}, \{1\} \rangle\!\rangle$. Then according to the partial jump sets in (3–44) and the partial flow sets (3–36)–(3–39), $(X^i)^{++++}$ must be contained in C_1^i. Therefore, there were four jumps in null-time.

The possible jump sequences can be visualized in the DAG in Figure A-3.

A.1.4 $X^i \in D_{11}^i$

Suppose that there is a state X such that agent $i \in \mathcal{A}$ has the state $X^i \in D_{11}^i$, then according to the partial jump sets in (3–44) and the partial flow sets (3–36)–(3–39), $X^i \in \langle\!\langle \{0,1\}^N, \texttt{Plans}^i, \{1\}, \mathbb{R}^2, \mathbb{R}^2, \mathbb{R}^2, [\tau_n^i, \infty), [0,\infty), [0,\infty), \{1\} \rangle\!\rangle$. If $X^i \in D_{11}^i$ then the jump map in (3–45) yields $(X^i)^+ \in \langle\!\langle \{0,1\}^N, \texttt{Plans}^i, \{1\}, \mathbb{R}^2, \mathbb{R}^2, \mathbb{R}^2, [\tau_n^i, \infty), \{0\}, [0,\infty), \{1\} \rangle\!\rangle$. Then according to Table A-1, the partial jump sets in (3–44), and the partial flow sets (3–36)–(3–39), it is only possible for $(X^i)^+$ to be contained in either $C_1^i \setminus D_{12}^i$ or D_{12}^i since: $(X^i)^+ \notin D_*^i \cap \{\texttt{mode}^i = 1\}$ because $\tau_{\text{trig}}^i = 0 < T_{\text{max}}^i$; $(X^i)^+ \notin D_{\#1}^i$ because $\texttt{b}^i = 0 \neq 1$; $(X^i)^+ \notin D_{11}^i$ because $\texttt{b}^i = 0 \neq 1$; and $(X^i)^+ \notin D_*^i \cap \{\texttt{mode}^i = 1\} \cap D_{12}^i$ because $\tau_{\text{trig}}^i = 0 < T_{\text{max}}^i$.

- If $(X^i)^+ \in C_1^i \setminus D_{12}^i$, then there was one jump in null-time.

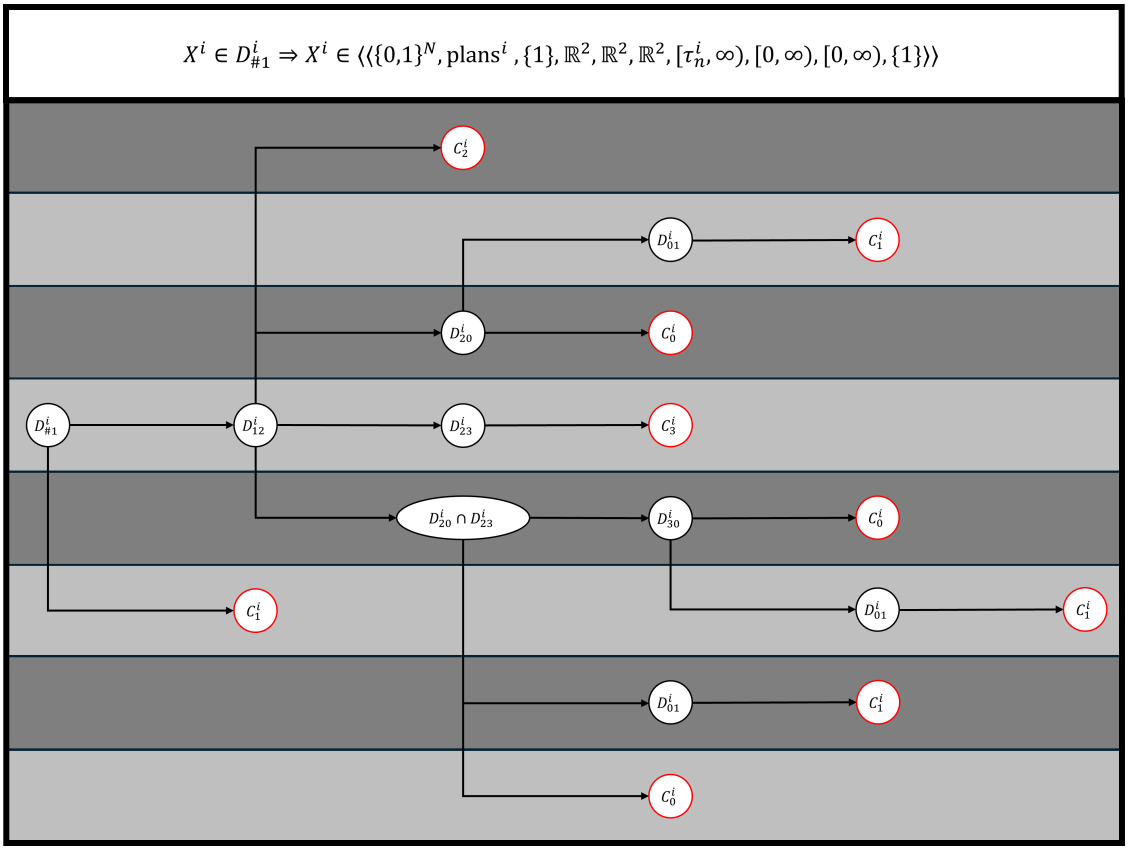

Figure A-3. Directed acyclic graph for $X^i \in D^i_{\#1}$.

- If $(X^i)^+ \in D^i_{12}$, then the jump map in (3–45) yields $(X^i)^{++} \in \langle\!\langle \{0,1\}^N, \texttt{Plans}^i, \{2\}, \mathbb{R}^2, \mathbb{R}^2, \mathbb{R}^2, [\tau^i_o, \infty), \{0\}, [0,\infty), \{1\} \rangle\!\rangle$. Then according to Table A-2, the partial jump sets in (3–44), and the partial flow sets (3–36)–(3–39), it is only possible for $(X^i)^{++}$ to be in: $C^i_2 \setminus (D^i_{20} \cup D^i_{23})$, $D^i_{20} \setminus D^i_{23}$, $D^i_{23} \setminus D^i_{20}$, or $D^i_{20} \cap D^i_{23}$ since: $(X^i)^{++} \notin D^i_* \cap \{\texttt{mode}^i = 2\}$ because $\tau^i_{\text{trig}} = 0 < T^i_{\text{max}}$; $(X^i)^{++} \notin D^i_{\#2}$ because $\texttt{b}^i = 0 \neq 1$; $(X^i)^{++} \notin D^i_{22}$ because $\texttt{b}^i = 0 \neq 1$; $(X^i)^{++} \notin D^i_* \cap \{\texttt{mode}^i = 2\} \cap D^i_{20}$ because $\tau^i_{\text{trig}} = 0 < T^i_{\text{max}}$; $(X^i)^{++} \notin D^i_* \cap \{\texttt{mode}^i = 2\} \cap D^i_{23}$ because $\texttt{b}^i = 0 \neq 1$; and $(X^i)^{++} \notin D^i_* \cap \{\texttt{mode}^i = 2\} \cap D^i_{20} \cap D^i_{23}$ because $\tau^i_{\text{trig}} = 0 < T^i_{\text{max}}$.

  - If $(X^i)^{++} \in C^i_2 \setminus (D^i_{20} \cup D^i_{23})$, then there were two jumps in null-time.
  - If $(X^i)^{++} \in D^i_{20} \setminus D^i_{23}$, then according to the partial jump sets in (3–44) and the partial flow sets (3–36)–(3–39) $(X^i)^{++} \in \langle\!\langle \{0,1\}^N, \texttt{Plans}^i, \{2\}, \mathcal{F}^*_{\text{in}}, \mathcal{F}^*_{\text{in}}, \mathcal{F}^*_{\text{in}}, [\tau^i_o, \infty), \{0\}, [0,\infty), \{1\} \rangle\!\rangle$. If $(X^i)^{++} \in D^i_{20} \setminus D^i_{23}$, then the jump map in (3–45) yields $(X^i)^{+++} \in \langle\!\langle \{0,1\}^N, \{\texttt{rpl}^i\}, \{0\}, \mathcal{F}^*_{\text{in}}, \mathcal{F}^*_{\text{in}}, \mathcal{F}^*_{\text{in}}, \{0\}, \{0\}, \{0\}, \{1\} \rangle\!\rangle$. For an agent i with $\texttt{mode}^i = 0$, $(X^i)^{+++}$ can either be in $C^i_0 \setminus D^i_{01}$ or D^i_{01}.
    - If $(X^i)^{+++} \in C^i_0 \setminus D^i_{01}$, then there were three jumps in null-time.
    - If $(X^i)^{+++} \in D^i_{01}$, then according to the partial jump sets in (3–44) and the partial flow sets (3–36)–(3–39) $(X^i)^{+++} \langle\!\langle \{0,1\}^N, \{\texttt{rpl}^i\}, \{0\}, \{n\}, \{n\}, \{n\}, \{0\}, \{0\}, \{0\}, \{1\} \rangle\!\rangle$. If $(X^i)^{+++} \in D^i_{01}$, then the jump map in (3–45) yields $(X^i)^{++++} \in \langle\!\langle \{0,1\}^N, \{\texttt{rpl}^i\}, \{1\}, \{n\}, \{n\}, \{n\}, \{0\}, \{0\}, \{0\}, \{1\} \rangle\!\rangle$. Then according to the partial jump sets in (3–44) and the partial flow sets (3–36)–(3–39), $(X^i)^{++++}$ must be contained in C^i_1. Therefore, there were four jumps in null-time.
  - If $(X^i)^{++} \in D^i_{23} \setminus D^i_{20}$, then according to the partial jump sets in (3–44) and the partial flow sets (3–36)–(3–39) $(X^i)^{++} \in \langle\!\langle \{0,1\}^N, \texttt{Plans}^i, \{2\}, \mathbb{R}^2, \mathbb{R}^2, \mathbb{R}^2, [\tau^i_p, \infty), \{0\}, [0,\infty), \{1\} \rangle\!\rangle$. If $(X^i)^{++} \in D^i_{23} \setminus D^i_{20}$, then the jump map in (3–45) yields $(X^i)^{+++} = \langle\!\langle \{0,1\}^N, \texttt{Plans}^i, \{3\}, \mathcal{F}^{\complement}, \mathbb{R}^2, \mathbb{R}^2, [\tau^i_p, \infty), \{0\}, [0,\infty), \{1\} \rangle\!\rangle$. Since $\texttt{mode}^i = 3$ and $(X^i)^{+++} \notin D^i_{30}$, $(X^i)^{+++}$ must be contained in C^i_3. Since $(X^i)^{+++}$ must be in C^i_3, there were three jumps in null-time.
  - If $(X^i)^{++} \in D^i_{20} \cap D^i_{23}$, then according to the partial jump sets in (3–44) and the partial flow sets (3–36)–(3–39) $(X^i)^{++} \in \langle\!\langle \{0,1\}^N, \texttt{Plans}^i, \{2\}, \mathcal{F}^*_{\text{in}}, \mathbb{R}^2, \mathbb{R}^2, [\tau^i_p, \infty), \{0\}, [0,\infty), \{1\} \rangle\!\rangle$. If $(X^i)^{++} \in D^i_{23} \cap D^i_{20}$, then the jump map in (3–45) yields $(X^i)^{+++} \in \langle\!\langle \{0,1\}^N, \texttt{Plans}^i, \{3\}, \mathcal{F}^*_{\text{in}}, \mathbb{R}^2, \mathbb{R}^2, [\tau^i_p, \infty), \{0\}, [0,\infty), \{1\} \rangle\!\rangle \cup \langle\!\langle \{0,1\}^N, \{\texttt{rpl}^i\}, \{0\}, \mathcal{F}^*_{\text{in}}, \mathcal{F}^*_{\text{in}}, \mathcal{F}^*_{\text{in}}, \{0\}, \{0\}, \{0\}, \{1\} \rangle\!\rangle$.
    - If $(X^i)^{+++} \in \langle\!\langle \{0,1\}^N, \texttt{Plans}^i, \{3\}, \mathcal{F}^*_{\text{in}}, \mathbb{R}^2, \mathbb{R}^2, [\tau^i_p, \infty), \{0\}, [0,\infty), \{1\} \rangle\!\rangle$, then according to the partial jump sets in (3–44) and the partial

flow sets (3–36)–(3–39), $(X^i)^{+++}$ must be contained in D^i_{30}. Since $(X^i)^{+++} \in D^i_{30}$ then the jump map in (3–45) yields $(X^i)^{++++} \in \langle\!\langle \{0,1\}^N, \{\texttt{rpl}^i\}, \{0\}, \mathcal{F}^*_{\text{in}}, \mathcal{F}^*_{\text{in}}, \mathcal{F}^*_{\text{in}}, \{0\}, \{0\}, \{0\}, \{1\} \rangle\!\rangle$. For an agent i with $\texttt{mode}^i = 0$, $(X^i)^{++++}$ can either be in $C^i_0 \setminus D^i_{01}$ or D^i_{01}.

- If $(X^i)^{++++} \in C^i_0 \setminus D^i_{01}$, then there were four jumps in null-time.
- If $(X^i)^{++++} \in D^i_{01}$, then according to the partial jump sets in (3–44) and the partial flow sets (3–36)–(3–39) $(X^i)^{++++} \langle\!\langle \{0,1\}^N, \{\texttt{rpl}^i\}, \{0\}, \{n\}, \{n\}, \{n\}, \{0\}, \{0\}, \{0\}, \{1\} \rangle\!\rangle$. If $(X^i)^{++++} \in D^i_{01}$, then the jump map in (3–45) yields $(X^i)^{+++++} \in \langle\!\langle \{0,1\}^N, \{\texttt{rpl}^i\}, \{1\}, \{n\}, \{n\}, \{n\}, \{0\}, \{0\}, \{0\}, \{1\} \rangle\!\rangle$. Then according to the partial jump sets in (3–44) and the partial flow sets (3–36)–(3–39), $(X^i)^{+++++}$ must be contained in C^i_1. Therefore, there were five jumps in null-time.

* If $(X^i)^{+++} \in \langle\!\langle \{0,1\}^N, \{\texttt{rpl}^i\}, \{0\}, \mathcal{F}^*_{\text{in}}, \mathcal{F}^*_{\text{in}}, \mathcal{F}^*_{\text{in}}, \{0\}, \{0\}, \{0\}, \{1\} \rangle\!\rangle$, then for an agent i with $\texttt{mode}^i = 0$, $(X^i)^{+++}$ can either be in $C^i_0 \setminus D^i_{01}$ or D^i_{01}.

  - If $(X^i)^{+++} \in C^i_0 \setminus D^i_{01}$, then there were three jumps in null-time.
  - If $(X^i)^{+++} \in D^i_{01}$, then according to the partial jump sets in (3–44) and the partial flow sets (3–36)–(3–39) $(X^i)^{+++} \langle\!\langle \{0,1\}^N, \{\texttt{rpl}^i\}, \{0\}, \{n\}, \{n\}, \{n\}, \{0\}, \{0\}, \{0\}, \{1\} \rangle\!\rangle$. If $(X^i)^{+++} \in D^i_{01}$, then the jump map in (3–45) yields $(X^i)^{++++} \in \langle\!\langle \{0,1\}^N, \{\texttt{rpl}^i\}, \{1\}, \{n\}, \{n\}, \{n\}, \{0\}, \{0\}, \{0\}, \{1\} \rangle\!\rangle$. Then according to the partial jump sets in (3–44) and the partial flow sets (3–36)–(3–39), $(X^i)^{++++}$ must be contained in C^i_1. Therefore, there were four jumps in null-time.

The possible jump sequences can be visualized in the DAG in Figure A-4.

A.1.5 $X^i \in D^i_{12} \setminus D^i_*$

Suppose that there is a state X such that agent $i \in \mathcal{A}$ has the state $X^i \in D^i_{12} \setminus D^i_*$, then according to the partial jump sets in (3–44) and the partial flow sets (3–36)–(3–39), $X^i \in \langle\!\langle \{0,1\}^N, \texttt{Plans}^i, \{1\}, \mathbb{R}^2, \mathbb{R}^2, \mathbb{R}^2, [\tau^i_o, \infty), [0, T^i_{\text{max}}), [0, \infty), \{0\} \rangle\!\rangle$.

If $X^i \in D^i_{12} \setminus D^i_*$, then the jump map in (3–45) yields $(X^i)^+ \in \langle\!\langle \{0,1\}^N, \texttt{Plans}^i, \{2\}, \mathbb{R}^2, \mathbb{R}^2, \mathbb{R}^2, [\tau^i_o, \infty), [0, T^i_{\text{max}}), [0, \infty), \{0\} \rangle\!\rangle$. Then according to Table A-1, the partial jump sets in (3–44), and the partial flow sets (3–36)–(3–39), it is only possible for $(X^i)^+$ to be contained in $C^i_2 \setminus (D^i_{20} \cup D^i_{23})$, $D^i_{20} \setminus D^i_{23}$, $D^i_{23} \setminus D^i_{20}$, or $D^i_{20} \cap D^i_{23}$ since: $(X^i)^+ \notin D^i_*$ because $\tau^i_{\text{trig}} < T^i_{\text{max}}$; $(X^i)^+ \notin D^i_{\#2}$ because $\mathfrak{b}^i = 0 \neq 1$; $(X^i)^+ \notin D^i_{22}$

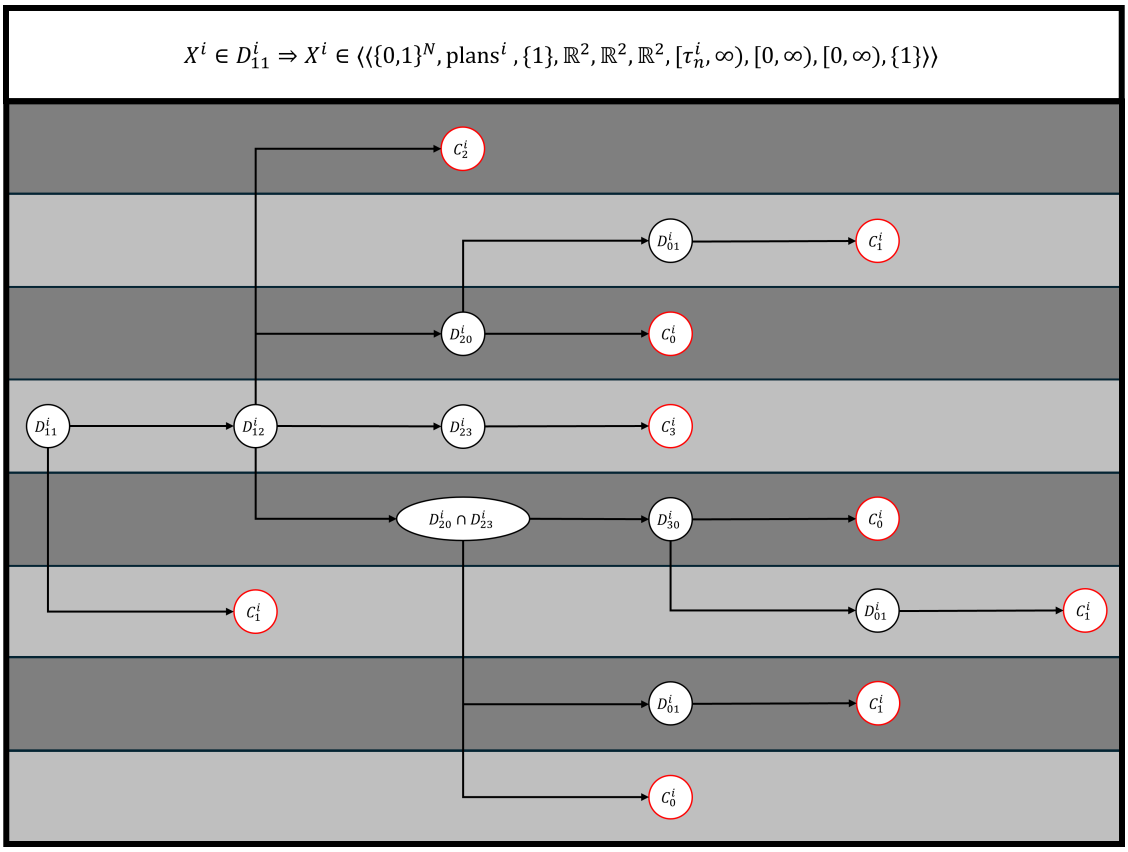

Figure A-4. Directed acyclic graph for $X^i \in D_{11}^i$.

because $\mathtt{b}^i = 0 \neq 1$; $(X^i)^+ \notin D^i_* \cap D^i_{20}$ because $\tau^i_{\mathsf{trig}} < T^i_{\mathsf{max}}$; $(X^i)^+ \notin D^i_* \cap D^i_{23}$ because $\tau^i_{\mathsf{trig}} < T^i_{\mathsf{max}}$; and $(X^i)^+ \notin D^i_* \cap D^i_{20} \cap D^i_{23}$ because $\tau^i_{\mathsf{trig}} < T^i_{\mathsf{max}}$.

- If $(X^i)^+ \in C^i_2 \setminus (D^i_{20} \cup D^i_{23})$, then there was one jump in null-time.
- If $(X^i)^+ \in D^i_{20} \setminus D^i_{23}$, then according to the partial jump sets in (3–44) and the partial flow sets (3–36)–(3–39) $(X^i)^+ \in \langle\!\langle \{0,1\}^N, \mathtt{Plans}^i, \{2\}, \mathcal{F}^*_{\mathsf{in}}, \mathcal{F}^*_{\mathsf{in}}, \mathcal{F}^*_{\mathsf{in}}, [\tau^i_o, \infty), [0, T^i_{\mathsf{max}}), [0, \infty), \{1\} \rangle\!\rangle$. If $(X^i)^+ \in D^i_{20} \setminus D^i_{23}$, then the jump map in (3–45) yields $(X^i)^{++} \in \langle\!\langle \{0,1\}^N, \{\mathtt{rpl}^i\}, \{0\}, \mathcal{F}^*_{\mathsf{in}}, \mathcal{F}^*_{\mathsf{in}}, \mathcal{F}^*_{\mathsf{in}}, \{0\}, \{0\}, \{0\}, \{1\} \rangle\!\rangle$. For an agent i with $\mathtt{mode}^i = 0$, $(X^i)^{++}$ can either be in $C^i_0 \setminus D^i_{01}$ or D^i_{01}.
  - If $(X^i)^{++} \in C^i_0 \setminus D^i_{01}$, then there were two jumps in null-time.
  - If $(X^i)^{++} \in D^i_{01}$, then according to the partial jump sets in (3–44) and the partial flow sets (3–36)–(3–39) $(X^i)^{++} \langle\!\langle \{0,1\}^N, \{\mathtt{rpl}^i\}, \{0\}, \{n\}, \{n\}, \{n\}, \{0\}, \{0\}, \{0\}, \{1\} \rangle\!\rangle$. If $(X^i)^{++} \in D^i_{01}$, then the jump map in (3–45) yields $(X^i)^{+++} \in \langle\!\langle \{0,1\}^N, \{\mathtt{rpl}^i\}, \{1\}, \{n\}, \{n\}, \{n\}, \{0\}, \{0\}, \{0\}, \{1\} \rangle\!\rangle$. Then according to the partial jump sets in (3–44) and the partial flow sets (3–36)–(3–39), $(X^i)^{+++}$ must be contained in C^i_1. Therefore, there were three jumps in null-time.
- If $(X^i)^+ \in D^i_{23} \setminus D^i_{20}$, then according to the partial jump sets in (3–44) and the partial flow sets (3–36)–(3–39) $(X^i)^+ \in \langle\!\langle \{0,1\}^N, \mathtt{Plans}^i, \{2\}, \mathbb{R}^2, \mathbb{R}^2, \mathbb{R}^2, [\tau^i_p, \infty), [0, T^i_{\mathsf{max}}), [0, \infty), \{1\} \rangle\!\rangle$. If $(X^i)^+ \in D^i_{23} \setminus D^i_{20}$, then the jump map in (3–45) yields $(X^i)^{++} = \langle\!\langle \{0,1\}^N, \mathtt{Plans}^i, \{3\}, \mathcal{F}^{\complement}, \mathbb{R}^2, \mathbb{R}^2, [\tau^i_p, \infty), [0, T^i_{\mathsf{max}}), [0, \infty), \{1\} \rangle\!\rangle$. Since $\mathtt{mode}^i = 3$ and $(X^i)^{++} \notin D^i_{30}$, $(X^i)^{++}$ must be contained in C^i_3. Since $(X^i)^{++}$ must be in C^i_3, there were two jumps in null-time.
- If $(X^i)^+ \in D^i_{20} \cap D^i_{23}$, then according to the partial jump sets in (3–44) and the partial flow sets (3–36)–(3–39) $(X^i)^+ \in \langle\!\langle \{0,1\}^N, \mathtt{Plans}^i, \{2\}, \mathcal{F}^*_{\mathsf{in}}, \mathbb{R}^2, \mathbb{R}^2, [\tau^i_p, \infty), [0, T^i_{\mathsf{max}}), [0, \infty), \{1\} \rangle\!\rangle$. If $(X^i)^+ \in D^i_{23} \cap D^i_{20}$, then the jump map in (3–45) yields $(X^i)^{++} \in \langle\!\langle \{0,1\}^N, \mathtt{Plans}^i, \{3\}, \mathcal{F}^*_{\mathsf{in}}, \mathbb{R}^2, \mathbb{R}^2, [\tau^i_p, \infty), [0, T^i_{\mathsf{max}}), [0, \infty), \{1\} \rangle\!\rangle \cup \langle\!\langle \{0,1\}^N, \{\mathtt{rpl}^i\}, \{0\}, \mathcal{F}^*_{\mathsf{in}}, \mathcal{F}^*_{\mathsf{in}}, \mathcal{F}^*_{\mathsf{in}}, \{0\}, \{0\}, \{0\}, \{1\} \rangle\!\rangle$.
  - If $(X^i)^{++} \in \langle\!\langle \{0,1\}^N, \mathtt{Plans}^i, \{3\}, \mathcal{F}^*_{\mathsf{in}}, \mathbb{R}^2, \mathbb{R}^2, [\tau^i_p, \infty), [0, T^i_{\mathsf{max}}), [0, \infty), \{1\} \rangle\!\rangle$, then according to the partial jump sets in (3–44) and the partial flow sets (3–36)–(3–39), $(X^i)^{++}$ must be contained in D^i_{30}. Since $(X^i)^{++} \in D^i_{30}$ then the jump map in (3–45) yields $(X^i)^{+++} \in \langle\!\langle \{0,1\}^N, \{\mathtt{rpl}^i\}, \{0\}, \mathcal{F}^*_{\mathsf{in}}, \mathcal{F}^*_{\mathsf{in}}, \mathcal{F}^*_{\mathsf{in}}, \{0\}, \{0\}, \{0\}, \{1\} \rangle\!\rangle$. For an agent i with $\mathtt{mode}^i = 0$, $(X^i)^{+++}$ can either be in $C^i_0 \setminus D^i_{01}$ or D^i_{01}.
    - If $(X^i)^{+++} \in C^i_0 \setminus D^i_{01}$, then there were three jumps in null-time.

* If $(X^i)^{+++} \in D^i_{01}$, then according to the partial jump sets in (3–44) and the partial flow sets (3–36)–(3–39) $(X^i)^{+++} \langle\!\langle \{0,1\}^N, \{\texttt{rpl}^i\}, \{0\}, \{n\}, \{n\}, \{n\}, \{0\}, \{0\}, \{0\}, \{1\} \rangle\!\rangle$. If $(X^i)^{+++} \in D^i_{01}$, then the jump map in (3–45) yields $(X^i)^{++++} \in \langle\!\langle \{0,1\}^N, \{\texttt{rpl}^i\}, \{1\}, \{n\}, \{n\}, \{n\}, \{0\}, \{0\}, \{0\}, \{1\} \rangle\!\rangle$. Then according to the partial jump sets in (3–44) and the partial flow sets (3–36)–(3–39), $(X^i)^{++++}$ must be contained in C^i_1. Therefore, there were four jumps in null-time.

– If $(X^i)^{++} \in \langle\!\langle \{0,1\}^N, \{\texttt{rpl}^i\}, \{0\}, \mathcal{F}^*_{\text{in}}, \mathcal{F}^*_{\text{in}}, \mathcal{F}^*_{\text{in}}, \{0\}, \{0\}, \{0\}, \{1\} \rangle\!\rangle$, then for an agent i with $\texttt{mode}^i = 0$, $(X^i)^{++}$ can either be in $C^i_0 \setminus D^i_{01}$ or D^i_{01}.

* If $(X^i)^{++} \in C^i_0 \setminus D^i_{01}$, then there were two jumps in null-time.

* If $(X^i)^{++} \in D^i_{01}$, then according to the partial jump sets in (3–44) and the partial flow sets (3–36)–(3–39) $(X^i)^{++} \langle\!\langle \{0,1\}^N, \{\texttt{rpl}^i\}, \{0\}, \{n\}, \{n\}, \{n\}, \{0\}, \{0\}, \{0\}, \{1\} \rangle\!\rangle$. If $(X^i)^{++} \in D^i_{01}$, then the jump map in (3–45) yields $(X^i)^{+++} \in \langle\!\langle \{0,1\}^N, \{\texttt{rpl}^i\}, \{1\}, \{n\}, \{n\}, \{n\}, \{0\}, \{0\}, \{0\}, \{1\} \rangle\!\rangle$. Then according to the partial jump sets in (3–44) and the partial flow sets (3–36)–(3–39), $(X^i)^{+++}$ must be contained in C^i_1. Therefore, there were three jumps in null-time.

The possible jump sequences can be visualized in the DAG in Figure A-5.

A.1.6 $X^i \in D^i_* \cap D^i_{12}$

Suppose that there is a state X such that agent $i \in \mathcal{A}$ has the state $X^i \in D^i_* \cap D^i_{12}$, then according to the partial jump sets in (3–44) and the partial flow sets (3–36)–(3–39), $X^i \in \langle\!\langle \{0,1\}^N, \texttt{Plans}^i, \{1\}, \mathbb{R}^2, \mathbb{R}^2, \mathbb{R}^2, [\tau^i_o, \infty), [T^i_{\text{max}}, \infty), [0, \infty), \{0\} \rangle\!\rangle$.

If $X^i \in D^i_* \cap D^i_{12}$, then the jump map in (3–45) yields

$(X^i)^+ \in \langle\!\langle \{0,1\}^N, \texttt{Plans}^i, \{1\}, \mathbb{R}^2, \mathbb{R}^2, \mathbb{R}^2, [\tau^i_o, \infty), \{0\}, [0, \infty), \{1\} \rangle\!\rangle \cup$

$\langle\!\langle \{0,1\}^N, \texttt{Plans}^i, \{2\}, \mathbb{R}^2, \mathbb{R}^2, \mathbb{R}^2, [\tau^i_o, \infty), [T^i_{\text{max}}, \infty), [0, \infty), \{0\} \rangle\!\rangle$.

- If $(X^i)^+ \in \langle\!\langle \{0,1\}^N, \texttt{Plans}^i, \{1\}, \mathbb{R}^2, \mathbb{R}^2, \mathbb{R}^2, [\tau^i_o, \infty), \{0\}, [0, \infty), \{1\} \rangle\!\rangle$, then according to the partial jump sets in (3–44) and the partial flow sets (3–36)–(3–39), $(X^i)^+$ must be contained in either $D^i_{\#1}$ or D^i_{11} since $\texttt{b}^i = 1$.

– If $X^i \in D^i_{\#1}$ then the jump map in (3–45) yields $(X^i)^{++} \in \langle\!\langle \{0,1\}^N, \texttt{Plans}^i, \{1\}, \mathbb{R}^2, \mathbb{R}^2, \mathbb{R}^2, [\tau^i_o, \infty), \{0\}, [0, \infty), \{1\} \rangle\!\rangle$. Then according to Table A-1, the partial jump sets in (3–44), and the partial flow sets (3–36)–(3–39), it is only possible for $(X^i)^{++}$ to be contained in D^i_{12} since: $(X^i)^{++} \notin D^i_* \cap \{\texttt{mode}^i = 1\}$ because $\tau^i_{\text{trig}} = 0 < T^i_{\text{max}}$; $(X^i)^{++} \notin D^i_{\#1}$ because $\texttt{b}^i = 0 \neq 1$;

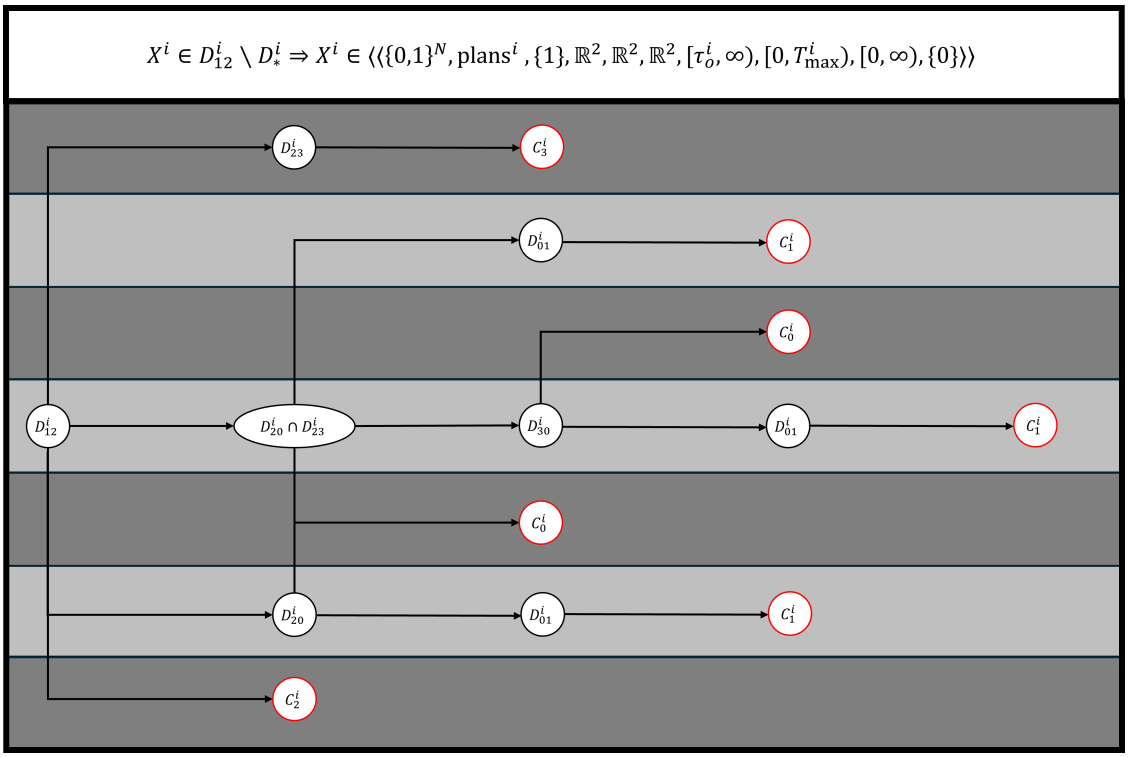

Figure A-5. Directed acyclic graph for $X^i \in D_{12}^i \setminus D_*^i$.

$(X^i)^{++} \notin D_{11}^i$ because $\texttt{b}^i = 0 \neq 1$; and $(X^i)^{++} \notin D_*^i \cap \{\texttt{mode}^i = 1\} \cap D_{12}^i$ because $\tau_{\text{trig}}^i = 0 < T_{\text{max}}^i$. If $(X^i)^{++} \in D_{12}^i$, then the jump map in (3–45) yields $(X^i)^{+++} \in \langle\langle \{0,1\}^N, \texttt{Plans}^i, \{2\}, \mathbb{R}^2, \mathbb{R}^2, \mathbb{R}^2, [\tau_o^i, \infty), \{0\}, [0, \infty), \{1\}\rangle\rangle$. Then according to Table A-2, the partial jump sets in (3–44), and the partial flow sets (3–36)–(3–39), it is only possible for $(X^i)^{+++}$ to be in: $C_2^i \setminus (D_{20}^i \cup D_{23}^i)$, $D_{20}^i \setminus D_{23}^i$, $D_{23}^i \setminus D_{20}^i$, or $D_{20}^i \cap D_{23}^i$ since: $(X^i)^{+++} \notin D_*^i \cap \{\texttt{mode}^i = 2\}$ because $\tau_{\text{trig}}^i = 0 < T_{\text{max}}^i$; $(X^i)^{+++} \notin D_{\#2}^i$ because $\texttt{b}^i = 0 \neq 1$; $(X^i)^{++} \notin D_{22}^i$ because $\texttt{b}^i = 0 \neq 1$; $(X^i)^{+++} \notin D_*^i \cap \{\texttt{mode}^i = 2\} \cap D_{20}^i$ because $\tau_{\text{trig}}^i = 0 < T_{\text{max}}^i$; $(X^i)^{+++} \notin D_*^i \cap \{\texttt{mode}^i = 2\} \cap D_{23}^i$ because $\texttt{b}^i = 0 \neq 1$; and $(X^i)^{+++} \notin D_*^i \cap \{\texttt{mode}^i = 2\} \cap D_{20}^i \cap D_{23}^i$ because $\tau_{\text{trig}}^i = 0 < T_{\text{max}}^i$.

* If $(X^i)^{+++} \in C_2^i \setminus (D_{20}^i \cup D_{23}^i)$, then there were three jumps in null-time.
* If $(X^i)^{+++} \in D_{20}^i \setminus D_{23}^i$, then according to the partial jump sets in (3–44) and the partial flow sets (3–36)–(3–39) $(X^i)^{+++} \in \langle\langle \{0,1\}^N, \texttt{Plans}^i, \{2\}, \mathcal{F}_{\text{in}}^*, \mathbb{R}^2, \mathbb{R}^2, [\tau_o^i, \infty), \{0\}, [0, \infty), \{1\}\rangle\rangle$. If $(X^i)^{+++} \in D_{20}^i \setminus D_{23}^i$, then the jump map in (3–45) yields $(X^i)^{++++} \in \langle\langle \{0,1\}^N, \{\texttt{rpl}^i\}, \{0\}, \mathcal{F}_{\text{in}}^*, \mathcal{F}_{\text{in}}^*, \mathcal{F}_{\text{in}}^*, \{0\}, \{0\}, \{0\}, \{1\}\rangle\rangle$. For an agent i with $\texttt{mode}^i = 0$, $(X^i)^{++++}$ can either be in $C_0^i \setminus D_{01}^i$ or D_{01}^i.
    - If $(X^i)^{++++} \in C_0^i \setminus D_{01}^i$, then there were four jumps in null-time.

- If $(X^i)^{++++} \in D^i_{01}$, then according to the partial jump sets in (3–44) and the partial flow sets (3–36)–(3–39) $(X^i)^{++++} \langle\!\langle \{0,1\}^N, \{\texttt{rpl}^i\}, \{0\}, \{n\}, \{n\}, \{n\}, \{0\}, \{0\}, \{0\}, \{1\} \rangle\!\rangle$. If $(X^i)^{++++} \in D^i_{01}$, then the jump map in (3–45) yields $(X^i)^{+++++} \in \langle\!\langle \{0,1\}^N, \{\texttt{rpl}^i\}, \{1\}, \{n\}, \{n\}, \{n\}, \{0\}, \{0\}, \{0\}, \{1\} \rangle\!\rangle$. Then according to the partial jump sets in (3–44) and the partial flow sets (3–36)–(3–39), $(X^i)^{+++++}$ must be contained in C^i_1. Therefore, there were five jumps in null-time.

* If $(X^i)^{+++} \in D^i_{23} \setminus D^i_{20}$, then according to the partial jump sets in (3–44) and the partial flow sets (3–36)–(3–39) $(X^i)^{+++} \in \langle\!\langle \{0,1\}^N, \texttt{Plans}^i, \{2\}, \mathbb{R}^2, \mathbb{R}^2, \mathbb{R}^2, [\tau^i_p, \infty), \{0\}, [0,\infty), \{1\} \rangle\!\rangle$. If $(X^i)^{+++} \in D^i_{23} \setminus D^i_{20}$, then the jump map in (3–45) yields $(X^i)^{++++} = \langle\!\langle \{0,1\}^N, \texttt{Plans}^i, \{3\}, \mathcal{F}^{\complement}, \mathbb{R}^2, \mathbb{R}^2, [\tau^i_p, \infty), \{0\}, [0,\infty), \{1\} \rangle\!\rangle$. Since $\texttt{mode}^i = 3$ and $(X^i)^{++++} \notin D^i_{30}$, $(X^i)^{+++}$ must be contained in C^i_3. Since $(X^i)^{++++}$ must be in C^i_3, there were four jumps in null-time.

* If $(X^i)^{+++} \in D^i_{20} \cap D^i_{23}$, then according to the partial jump sets in (3–44) and the partial flow sets (3–36)–(3–39) $(X^i)^{+++} \in \langle\!\langle \{0,1\}^N, \texttt{Plans}^i, \{2\}, \mathcal{F}^*_{\text{in}}, \mathbb{R}^2, \mathbb{R}^2, [\tau^i_p, \infty), \{0\}, [0,\infty), \{1\} \rangle\!\rangle$. If $(X^i)^{+++} \in D^i_{23} \cap D^i_{20}$, then the jump map in (3–45) yields $(X^i)^{++++} \in \langle\!\langle \{0,1\}^N, \texttt{Plans}^i, \{3\}, \mathcal{F}^*_{\text{in}}, \mathbb{R}^2, \mathbb{R}^2, [\tau^i_p, \infty), \{0\}, [0,\infty), \{1\} \rangle\!\rangle \cup \langle\!\langle \{0,1\}^N, \{\texttt{rpl}^i\}, \{0\}, \mathcal{F}^*_{\text{in}}, \mathcal{F}^*_{\text{in}}, \mathcal{F}^*_{\text{in}}, \{0\}, \{0\}, \{0\}, \{1\} \rangle\!\rangle$.

  - If $(X^i)^{++++} \in \langle\!\langle \{0,1\}^N, \texttt{Plans}^i, \{3\}, \mathcal{F}^*_{\text{in}}, \mathbb{R}^2, \mathbb{R}^2, [\tau^i_p, \infty), \{0\}, [0,\infty), \{1\} \rangle\!\rangle$, then according to the partial jump sets in (3–44) and the partial flow sets (3–36)–(3–39), $(X^i)^{++++}$ must be contained in D^i_{30}. Since $(X^i)^{++++} \in D^i_{30}$ then the jump map in (3–45) yields $(X^i)^{+++++} \in \langle\!\langle \{0,1\}^N, \{\texttt{rpl}^i\}, \{0\}, \mathcal{F}^*_{\text{in}}, \mathcal{F}^*_{\text{in}}, \mathcal{F}^*_{\text{in}}, \{0\}, \{0\}, \{0\}, \{1\} \rangle\!\rangle$. For an agent i with $\texttt{mode}^i = 0$, $(X^i)^{+++++}$ can either be in $C^i_0 \setminus D^i_{01}$ or D^i_{01}. 1) If $(X^i)^{+++++} \in C^i_0 \setminus D^i_{01}$, then there were five jumps in null-time. 2) If $(X^i)^{+++++} \in D^i_{01}$, then according to the partial jump sets in (3–44) and the partial flow sets (3–36)–(3–39) $(X^i)^{+++++} \langle\!\langle \{0,1\}^N, \{\texttt{rpl}^i\}, \{0\}, \{n\}, \{n\}, \{n\}, \{0\}, \{0\}, \{0\}, \{1\} \rangle\!\rangle$. If $(X^i)^{+++++} \in D^i_{01}$, then the jump map in (3–45) yields $(X^i)^{++++++} \in \langle\!\langle \{0,1\}^N, \{\texttt{rpl}^i\}, \{1\}, \{n\}, \{n\}, \{n\}, \{0\}, \{0\}, \{0\}, \{1\} \rangle\!\rangle$. Then according to the partial jump sets in (3–44) and the partial flow sets (3–36)–(3–39), $(X^i)^{++++++}$ must be contained in C^i_1. Therefore, there were six jumps in null-time.

* If $(X^i)^{++++} \in \langle\!\langle \{0,1\}^N, \{\texttt{rpl}^i\}, \{0\}, \mathcal{F}^*_{\text{in}}, \mathcal{F}^*_{\text{in}}, \mathcal{F}^*_{\text{in}}, \{0\}, \{0\}, \{0\}, \{1\} \rangle\!\rangle$, then for an agent i with $\texttt{mode}^i = 0$, $(X^i)^{++++}$ can either be in $C^i_0 \setminus D^i_{01}$ or D^i_{01}.

  - If $(X^i)^{++++} \in C^i_0 \setminus D^i_{01}$, then there were four jumps in null-time.

- If $(X^i)^{++++} \in D^i_{01}$, then according to the partial jump sets in (3–44) and the partial flow sets (3–36)–(3–39) $(X^i)^{++++} \langle\!\langle \{0,1\}^N, \{\texttt{rpl}^i\}, \{0\}, \{n\}, \{n\}, \{n\}, \{0\}, \{0\}, \{0\}, \{1\} \rangle\!\rangle$. If $(X^i)^{++++} \in D^i_{01}$, then the jump map in (3–45) yields $(X^i)^{+++++} \in \langle\!\langle \{0,1\}^N, \{\texttt{rpl}^i\}, \{1\}, \{n\}, \{n\}, \{n\}, \{0\}, \{0\}, \{0\}, \{1\} \rangle\!\rangle$. Then according to the partial jump sets in (3–44) and the partial flow sets (3–36)–(3–39), $(X^i)^{+++++}$ must be contained in C^i_1. Therefore, there were five jumps in null-time.

– If $X^i \in D^i_{11}$ then the jump map in (3–45) yields $(X^i)^{++} \in \langle\!\langle \{0,1\}^N, \texttt{Plans}^i, \{1\}, \mathbb{R}^2, \mathbb{R}^2, \mathbb{R}^2, [\tau^i_o, \infty), \{0\}, [0, \infty), \{1\} \rangle\!\rangle$. Then according to Table A-1, the partial jump sets in (3–44), and the partial flow sets (3–36)–(3–39), it is only possible for $(X^i)^{++}$ to be contained in D^i_{12} since: $(X^i)^{++} \notin D^i_* \cap \{\texttt{mode}^i = 1\}$ because $\tau^i_{\text{trig}} = 0 < T^i_{\text{max}}$; $(X^i)^{++} \notin D^i_{\#1}$ because $\texttt{b}^i = 0 \neq 1$; $(X^i)^{++} \notin D^i_{11}$ because $\texttt{b}^i = 0 \neq 1$; and $(X^i)^{++} \notin D^i_* \cap \{\texttt{mode}^i = 1\} \cap D^i_{12}$ because $\tau^i_{\text{trig}} = 0 < T^i_{\text{max}}$. If $(X^i)^{++} \in D^i_{12}$, then the jump map in (3–45) yields $(X^i)^{+++} \in \langle\!\langle \{0,1\}^N, \texttt{Plans}^i, \{2\}, \mathbb{R}^2, \mathbb{R}^2, \mathbb{R}^2, [\tau^i_o, \infty), \{0\}, [0, \infty), \{1\} \rangle\!\rangle$. Then according to Table A-2, the partial jump sets in (3–44), and the partial flow sets (3–36)–(3–39), it is only possible for $(X^i)^{+++}$ to be in: $C^i_2 \setminus (D^i_{20} \cup D^i_{23})$, $D^i_{20} \setminus D^i_{23}$, $D^i_{23} \setminus D^i_{20}$, or $D^i_{20} \cap D^i_{23}$ since: $(X^i)^{+++} \notin D^i_* \cap \{\texttt{mode}^i = 2\}$ because $\tau^i_{\text{trig}} = 0 < T^i_{\text{max}}$; $(X^i)^{+++} \notin D^i_{\#2}$ because $\texttt{b}^i = 0 \neq 1$; $(X^i)^{++} \notin D^i_{22}$ because $\texttt{b}^i = 0 \neq 1$; $(X^i)^{+++} \notin D^i_* \cap \{\texttt{mode}^i = 2\} \cap D^i_{20}$ because $\tau^i_{\text{trig}} = 0 < T^i_{\text{max}}$; $(X^i)^{+++} \notin D^i_* \cap \{\texttt{mode}^i = 2\} \cap D^i_{23}$ because $\texttt{b}^i = 0 \neq 1$; and $(X^i)^{+++} \notin D^i_* \cap \{\texttt{mode}^i = 2\} \cap D^i_{20} \cap D^i_{23}$ because $\tau^i_{\text{trig}} = 0 < T^i_{\text{max}}$.

* If $(X^i)^{+++} \in C^i_2 \setminus (D^i_{20} \cup D^i_{23})$, then there were three jumps in null-time.

* If $(X^i)^{+++} \in D^i_{20} \setminus D^i_{23}$, then according to the partial jump sets in (3–44) and the partial flow sets (3–36)–(3–39) $(X^i)^{+++} \in \langle\!\langle \{0,1\}^N, \texttt{Plans}^i, \{2\}, \mathcal{F}^*_{\text{in}}, \mathbb{R}^2, \mathbb{R}^2, [\tau^i_o, \infty), \{0\}, [0, \infty), \{1\} \rangle\!\rangle$. If $(X^i)^{+++} \in D^i_{20} \setminus D^i_{23}$, then the jump map in (3–45) yields $(X^i)^{++++} \in \langle\!\langle \{0,1\}^N, \{\texttt{rpl}^i\}, \{0\}, \mathcal{F}^*_{\text{in}}, \mathcal{F}^*_{\text{in}}, \mathcal{F}^*_{\text{in}}, \{0\}, \{0\}, \{0\}, \{1\} \rangle\!\rangle$. For an agent i with $\texttt{mode}^i = 0$, $(X^i)^{++++}$ can either be in $C^i_0 \setminus D^i_{01}$ or D^i_{01}.

  - If $(X^i)^{++++} \in C^i_0 \setminus D^i_{01}$, then there were four jumps in null-time.

  - If $(X^i)^{++++} \in D^i_{01}$, then according to the partial jump sets in (3–44) and the partial flow sets (3–36)–(3–39) $(X^i)^{++++} \langle\!\langle \{0,1\}^N, \{\texttt{rpl}^i\}, \{0\}, \{n\}, \{n\}, \{n\}, \{0\}, \{0\}, \{0\}, \{1\} \rangle\!\rangle$. If $(X^i)^{++++} \in D^i_{01}$, then the jump map in (3–45) yields $(X^i)^{+++++} \in \langle\!\langle \{0,1\}^N, \{\texttt{rpl}^i\}, \{1\}, \{n\}, \{n\}, \{n\}, \{0\}, \{0\}, \{0\}, \{1\} \rangle\!\rangle$. Then according to the partial jump sets in (3–44) and the partial flow sets (3–36)–(3–39), $(X^i)^{+++++}$ must be contained in C^i_1. Therefore, there were five jumps in null-time.

* If $(X^i)^{+++} \in D^i_{23} \setminus D^i_{20}$, then according to the partial jump sets in (3–44) and the partial flow sets (3–36)–(3–39) $(X^i)^{+++} \in \langle\!\langle \{0,1\}^N, \texttt{Plans}^i, \{2\}, \mathbb{R}^2, \mathbb{R}^2, \mathbb{R}^2, [\tau^i_p, \infty), \{0\}, [0,\infty), \{1\} \rangle\!\rangle$. If $(X^i)^{+++} \in D^i_{23} \setminus D^i_{20}$, then the jump map in (3–45) yields $(X^i)^{++++} = \langle\!\langle \{0,1\}^N, \texttt{Plans}^i, \{3\}, \mathcal{F}^{\complement}, \mathbb{R}^2, \mathbb{R}^2, [\tau^i_p, \infty), \{0\}, [0,\infty), \{1\} \rangle\!\rangle$. Since $\texttt{mode}^i = 3$ and $(X^i)^{++++} \notin D^i_{30}$, $(X^i)^{+++}$ must be contained in C^i_3. Since $(X^i)^{++++}$ must be in C^i_3, there were four jumps in null-time.

* If $(X^i)^{+++} \in D^i_{20} \cap D^i_{23}$, then according to the partial jump sets in (3–44) and the partial flow sets (3–36)–(3–39) $(X^i)^{+++} \in \langle\!\langle \{0,1\}^N, \texttt{Plans}^i, \{2\}, \mathcal{F}^*_{\text{in}}, \mathbb{R}^2, \mathbb{R}^2, [\tau^i_p, \infty), \{0\}, [0,\infty), \{1\} \rangle\!\rangle$. If $(X^i)^{+++} \in D^i_{23} \cap D^i_{20}$, then the jump map in (3–45) yields $(X^i)^{++++} \in \langle\!\langle \{0,1\}^N, \texttt{Plans}^i, \{3\}, \mathcal{F}^*_{\text{in}}, \mathbb{R}^2, \mathbb{R}^2, [\tau^i_p, \infty), \{0\}, [0,\infty), \{1\} \rangle\!\rangle \cup \langle\!\langle \{0,1\}^N, \{\texttt{rpl}^i\}, \{0\}, \mathcal{F}^*_{\text{in}}, \mathcal{F}^*_{\text{in}}, \mathcal{F}^*_{\text{in}}, \{0\}, \{0\}, \{0\}, \{1\} \rangle\!\rangle$.

  - If $(X^i)^{++++} \in \langle\!\langle \{0,1\}^N, \texttt{Plans}^i, \{3\}, \mathcal{F}^*_{\text{in}}, \mathbb{R}^2, \mathbb{R}^2, [\tau^i_p, \infty), \{0\}, [0,\infty), \{1\} \rangle\!\rangle$, then according to the partial jump sets in (3–44) and the partial flow sets (3–36)–(3–39), $(X^i)^{++++}$ must be contained in D^i_{30}. Since $(X^i)^{++++} \in D^i_{30}$ then the jump map in (3–45) yields $(X^i)^{+++++} \in \langle\!\langle \{0,1\}^N, \{\texttt{rpl}^i\}, \{0\}, \mathcal{F}^*_{\text{in}}, \mathcal{F}^*_{\text{in}}, \mathcal{F}^*_{\text{in}}, \{0\}, \{0\}, \{0\}, \{1\} \rangle\!\rangle$. For an agent i with $\texttt{mode}^i = 0$, $(X^i)^{+++++}$ can either be in $C^i_0 \setminus D^i_{01}$ or D^i_{01}.
    1) If $(X^i)^{+++++} \in C^i_0 \setminus D^i_{01}$, then there were five jumps in null-time.
    2) If $(X^i)^{+++++} \in D^i_{01}$, then according to the partial jump sets in (3–44) and the partial flow sets (3–36)–(3–39) $(X^i)^{+++++} \langle\!\langle \{0,1\}^N, \{\texttt{rpl}^i\}, \{0\}, \{n\}, \{n\}, \{n\}, \{0\}, \{0\}, \{0\}, \{1\} \rangle\!\rangle$. If $(X^i)^{+++++} \in D^i_{01}$, then the jump map in (3–45) yields $(X^i)^{++++++} \in \langle\!\langle \{0,1\}^N, \{\texttt{rpl}^i\}, \{1\}, \{n\}, \{n\}, \{n\}, \{0\}, \{0\}, \{0\}, \{1\} \rangle\!\rangle$. Then according to the partial jump sets in (3–44) and the partial flow sets (3–36)–(3–39), $(X^i)^{++++++}$ must be contained in C^i_1. Therefore, there were six jumps in null-time.

  - If $(X^i)^{++++} \in \langle\!\langle \{0,1\}^N, \{\texttt{rpl}^i\}, \{0\}, \mathcal{F}^*_{\text{in}}, \mathcal{F}^*_{\text{in}}, \mathcal{F}^*_{\text{in}}, \{0\}, \{0\}, \{0\}, \{1\} \rangle\!\rangle$, then for an agent i with $\texttt{mode}^i = 0$, $(X^i)^{++++}$ can either be in $C^i_0 \setminus D^i_{01}$ or D^i_{01}.
    1) If $(X^i)^{++++} \in C^i_0 \setminus D^i_{01}$, then there were four jumps in null-time.
    2) If $(X^i)^{++++} \in D^i_{01}$, then according to the partial jump sets in (3–44) and the partial flow sets (3–36)–(3–39) $(X^i)^{++++} \langle\!\langle \{0,1\}^N, \{\texttt{rpl}^i\}, \{0\}, \{n\}, \{n\}, \{n\}, \{0\}, \{0\}, \{0\}, \{1\} \rangle\!\rangle$. If $(X^i)^{++++} \in D^i_{01}$, then the jump map in (3–45) yields $(X^i)^{+++++} \in \langle\!\langle \{0,1\}^N, \{\texttt{rpl}^i\}, \{1\}, \{n\}, \{n\}, \{n\}, \{0\}, \{0\}, \{0\}, \{1\} \rangle\!\rangle$. Then according to the partial jump sets in (3–44) and the partial flow sets (3–36)–(3–39), $(X^i)^{+++++}$ must be contained in C^i_1. Therefore, there were five jumps in null-time.

- If $(X^i)^+ \in \langle\!\langle \{0,1\}^N, \texttt{Plans}^i, \{2\}, \mathbb{R}^2, \mathbb{R}^2, \mathbb{R}^2, [\tau_o^i, \infty), [T_{\text{max}}^i, \infty), [0, \infty), \{0\} \rangle\!\rangle$, then according to the partial jump sets in (3–44) and the partial flow sets (3–36)–(3–39), it is only possible for $(X^i)^+$ to be in: $D_*^i \setminus (D_{20}^i \cup D_{23}^i)$, $D_*^i \cap D_{20}^i \setminus D_{23}^i$, $D_*^i \cap D_{23}^i \setminus D_{20}^i$, or $D_*^i \cap D_{20}^i \cap D_{23}^i$ since: $(X^i)^+ \notin D_{\#2}^i$ because $\texttt{b}^i = 0 \neq 1$; $(X^i)^+ \notin D_{22}^i$ because $\texttt{b}^i = 0 \neq 1$; $(X^i)^+ \notin D_{20}^i \setminus (D_*^i \cup D_{23}^i)$ because $\tau_{\text{trig}}^i \geq T_{\text{max}}^i$; $(X^i)^+ \notin D_{23}^i \setminus (D_*^i \cup D_{20}^i)$ because $\tau_{\text{trig}}^i \geq T_{\text{max}}^i$; and $(X^i)^+ \notin (D_{20}^i \cap D_{23}^i) \setminus D_*^i$ because $\tau_{\text{trig}}^i \geq T_{\text{max}}^i$.

  – If $(X^i)^+ \in D_*^i \setminus (D_{20}^i \cup D_{23}^i)$, then according to the partial jump sets in (3–44) and the partial flow sets (3–36)–(3–39), $X^i \in \langle\!\langle \{0,1\}^N, \texttt{Plans}^i, \{2\}, \mathcal{F}^{\complement}, \mathbb{R}^2, \mathbb{R}^2, [\tau_o^i, \tau_p^i), [T_{\text{max}}^i, \infty), [0, \infty), \{0\} \rangle\!\rangle$. If $(X^i)^+ \in D_*^i \setminus (D_{20}^i \cup D_{23}^i)$, then the jump map in (3–45) yields $(X^i)^{++} \in \langle\!\langle \{0,1\}^N, \texttt{Plans}^i, \{2\}, \mathcal{F}^{\complement}, \mathbb{R}^2, \mathbb{R}^2, [\tau_o^i, \tau_p^i), [T_{\text{max}}^i, \infty), [0, \infty), \{1\} \rangle\!\rangle$. If $(X^i)^{++} \in \langle\!\langle \{0,1\}^N, \texttt{Plans}^i, \{2\}, \mathcal{F}^{\complement}, \mathbb{R}^2, \mathbb{R}^2, [\tau_o^i, \tau_p^i), [T_{\text{max}}^i, \infty), [0, \infty), \{1\} \rangle\!\rangle$, then according to the partial jump sets in (3–44) and the partial flow sets (3–36)–(3–39) implies that either $(X)^{++} \in D_{\#2}^i$ or $(X)^+ \in D_{22}^i$.

    * If $(X)^{++} \in D_{\#2}^i$ then the jump map in (3–45) yields $(X^i)^{+++} \in \langle\!\langle \{0,1\}^N, \texttt{Plans}^i, \{2\}, \mathcal{F}^{\complement}, \mathbb{R}^2, \mathbb{R}^2, [\tau_o^i, \tau_p^i), \{0\}, [0, \infty), \{1\} \rangle\!\rangle$. Then according to Table A-2, the partial jump sets in (3–44), and the partial flow sets (3–36)–(3–39), it is only possible for $(X^i)^{++}$ to be contained in C_2^i, since: $(X^i)^{+++} \notin D_*^i \cap \{\texttt{mode}^i = 2\} \setminus (D_{20}^i \cup D_{23}^i)$ because $\tau_{\text{trig}}^i = 0 < T_{\text{max}}^i$; $(X^i)^{+++} \notin D_{\#2}^i$ because $\texttt{b}^i = 0 \neq 1$; $(X^i)^{+++} \notin D_{22}^i$ because $\texttt{b}^i = 0 \neq 1$; $(X^i)^{+++} \notin D_{20}^i \setminus (D_*^i \cup D_{23}^i)$ because $x^i \in \mathcal{F}^{\complement}$; $(X^i)^{++} \notin D_{23}^i \setminus (D_*^i \cup D_{20}^i)$ because $\tau^i < \tau_p^i$; $(X^i)^{++} \notin (D_*^i \cap D_{20}^i) \setminus D_{23}^i$ because $\tau_{\text{trig}}^i = 0 < T_{\text{max}}^i$; $(X^i)^{+++} \notin (D_*^i \cap D_{23}^i) \setminus D_{20}^i$ because $\tau_{\text{trig}}^i = 0 < T_{\text{max}}^i$; $(X^i)^{+++} \notin D_{20}^i \cap D_{23}^i \setminus D_*^i$ because $x^i \in \mathcal{F}^{\complement}$; and $(X^i)^{+++} \notin D_*^i \cap D_{20}^i \cap D_{23}^i$ because $\tau_{\text{trig}}^i = 0 < T_{\text{max}}^i$. Since $(X^i)^{+++} \in C_2^i$, there were three jumps in null-time.

    * If $(X)^{++} \in D_{22}^i$ then the jump map in (3–45) yields $(X^i)^{+++} \in \langle\!\langle \{0,1\}^N, \texttt{Plans}^i, \{2\}, \mathcal{F}^{\complement}, \mathbb{R}^2, \mathbb{R}^2, [\tau_o^i, \tau_p^i), \{0\}, [0, \infty), \{1\} \rangle\!\rangle$. Then according to Table A-2, the partial jump sets in (3–44), and the partial flow sets (3–36)–(3–39), it is only possible for $(X^i)^{+++}$ to be contained in C_2^i, since: $(X^i)^{+++} \notin D_*^i \cap \{\texttt{mode}^i = 2\} \setminus (D_{20}^i \cup D_{23}^i)$ because $\tau_{\text{trig}}^i = 0 < T_{\text{max}}^i$; $(X^i)^{+++} \notin D_{\#2}^i$ because $\texttt{b}^i = 0 \neq 1$; $(X^i)^{+++} \notin D_{22}^i$ because $\texttt{b}^i = 0 \neq 1$; $(X^i)^{++} \notin D_{20}^i \setminus (D_*^i \cup D_{23}^i)$ because $x^i \in \mathcal{F}^{\complement}$; $(X^i)^{+++} \notin D_{23}^i \setminus (D_*^i \cup D_{20}^i)$ because $\tau^i < \tau_p^i$; $(X^i)^{+++} \notin (D_*^i \cap D_{20}^i) \setminus D_{23}^i$ because $\tau_{\text{trig}}^i = 0 < T_{\text{max}}^i$; $(X^i)^{+++} \notin (D_*^i \cap D_{23}^i) \setminus D_{20}^i$ because $\tau_{\text{trig}}^i = 0 < T_{\text{max}}^i$; $(X^i)^{++} \notin D_{20}^i \cap D_{23}^i \setminus D_*^i$ because $x^i \in \mathcal{F}^{\complement}$; and $(X^i)^{+++} \notin D_*^i \cap D_{20}^i \cap D_{23}^i$ because $\tau_{\text{trig}}^i = 0 < T_{\text{max}}^i$. Since $(X^i)^{+++} \in C_2^i$, there were three jumps in null-time.

  – If $(X^i)^+ \in D_*^i \cap D_{20}^i \setminus D_{23}^i$, then according to the partial jump sets in (3–44) and the partial flow sets (3–36)–(3–39), $(X^i)^+ \in$

$\langle\!\langle \{0,1\}^N, \texttt{Plans}^i, \{2\}, \mathcal{F}^*_{\text{in}}, \mathbb{R}^2, \mathbb{R}^2, [\tau^i_o, \tau^i_p), [T^i_{\text{max}}, \infty), [0,\infty), \{0\} \rangle\!\rangle$. If $(X^i)^+ \in (D^i_* \cap D^i_{20}) \setminus D^i_{23}$, then the jump map in (3–45) yields $(X^i)^{++} \in \langle\!\langle \{0,1\}^N, \texttt{Plans}^i, \{2\}, \mathcal{F}^*_{\text{in}}, \mathbb{R}^2, \mathbb{R}^2, [\tau^i_o, \tau^i_p), \{0\}, [0,\infty), \{1\} \rangle\!\rangle \cup \langle\!\langle \{0,1\}^N, \texttt{Plans}^i, \{0\}, \mathcal{F}^*_{\text{in}}, \mathcal{F}^*_{\text{in}}, \mathcal{F}^*_{\text{in}}, \{0\}, \{0\}, \{0\}, \{0\} \rangle\!\rangle$.

* If $(X^i)^{++} \in \langle\!\langle \{0,1\}^N, \texttt{Plans}^i, \{2\}, \mathcal{F}^*_{\text{in}}, \mathbb{R}^2, \mathbb{R}^2, [\tau^i_o, \tau^i_p), \{0\}, [0,\infty), \{1\} \rangle\!\rangle$, then according to the partial jump sets in (3–44) and the partial flow sets (3–36)–(3–39) implies that either $(X)^+ \in D^i_{\#2}$ or $(X)^+ \in D^i_{22}$.

  - If $(X)^{++} \in D^i_{\#2}$, then the jump map in (3–45) yields $(X^i)^{+++} \in \langle\!\langle \{0,1\}^N, \texttt{Plans}^i, \{2\}, \mathcal{F}^*_{\text{in}}, \mathbb{R}^2, \mathbb{R}^2, [\tau^i_o, \tau^i_p), \{0\}, [0,\infty), \{0\} \rangle\!\rangle$. Then according to Table A-2, the partial jump sets in (3–44), and the partial flow sets (3–36)–(3–39), it is only possible for $(X^i)^{+++}$ to be contained in D^i_{20}, since: $(X^i)^{+++} \notin D^i_* \cap \{\texttt{mode}^i = 2\} \setminus (D^i_{20} \cup D^i_{23})$ because $\tau^i_{\text{trig}} = 0 < T^i_{\text{max}}$; $(X^i)^{+++} \notin D^i_{\#2}$ because $\texttt{b}^i = 0 \neq 1$; $(X^i)^{+++} \notin D^i_{22}$ because $\texttt{b}^i = 0 \neq 1$; $(X^i)^{+++} \notin D^i_{23} \setminus (D^i_* \cup D^i_{20})$ because $\tau^i < \tau^i_p$; $(X^i)^{+++} \notin (D^i_* \cap D^i_{20}) \setminus D^i_{23}$ because $\tau^i_{\text{trig}} = 0 < T^i_{\text{max}}$; $(X^i)^{+++} \notin (D^i_* \cap D^i_{23}) \setminus D^i_{20}$ because $\tau^i_{\text{trig}} = 0 < T^i_{\text{max}}$; $(X^i)^{+++} \notin D^i_{20} \cap D^i_{23} \setminus D^i_*$ because $\tau^i < \tau^i_p$; and $(X^i)^{+++} \notin D^i_* \cap D^i_{20} \cap D^i_{23}$ because $\tau^i_{\text{trig}} = 0 < T^i_{\text{max}}$. If $(X^i)^{+++} \in D^i_{20}$, then the jump map in (3–45) yields $(X^i)^{++++} \in \langle\!\langle \{0,1\}^N, \texttt{rpl}^i, \{0\}, \mathcal{F}^*_{\text{in}}, \mathcal{F}^*_{\text{in}}, \mathcal{F}^*_{\text{in}}, \{0\}, \{0\}, \{0\}, \{0\} \rangle\!\rangle$. For an agent i with $\texttt{mode}^i = 0$, $(X^i)^{++++}$ can either be in $C^i_0 \setminus D^i_{01}$ or D^i_{01}.
    1) If $(X^i)^{++++} \in C^i_0 \setminus D^i_{01}$, then there were four jumps in null-time.
    2) If $(X^i)^{++++} \in D^i_{01}$, then according to the partial jump sets in (3–44) and the partial flow sets (3–36)–(3–39) $(X^i)^{++++} \langle\!\langle \{0,1\}^N, \{\texttt{rpl}^i\}, \{0\}, \{n\}, \{n\}, \{n\}, \{0\}, \{0\}, \{0\}, \{1\} \rangle\!\rangle$. If $(X^i)^{++++} \in D^i_{01}$, then the jump map in (3–45) yields $(X^i)^{+++++} \in \langle\!\langle \{0,1\}^N, \{\texttt{rpl}^i\}, \{1\}, \{n\}, \{n\}, \{n\}, \{0\}, \{0\}, \{0\}, \{1\} \rangle\!\rangle$. Then according to the partial jump sets in (3–44) and the partial flow sets (3–36)–(3–39), $(X^i)^{+++++}$ must be contained in C^i_1. Therefore, there were five jumps in null-time.

  - If $(X)^{++} \in D^i_{22}$, then the jump map in (3–45) yields $(X^i)^{+++} \in \langle\!\langle \{0,1\}^N, \texttt{Plans}^i, \{2\}, \mathcal{F}^*_{\text{in}}, \mathbb{R}^2, \mathbb{R}^2, [\tau^i_o, \tau^i_p), \{0\}, [0,\infty), \{0\} \rangle\!\rangle$. Then according to Table A-2, the partial jump sets in (3–44), and the partial flow sets (3–36)–(3–39), it is only possible for $(X^i)^{+++}$ to be contained in D^i_{20}, since: $(X^i)^{+++} \notin D^i_* \cap \{\texttt{mode}^i = 2\} \setminus (D^i_{20} \cup D^i_{23})$ because $\tau^i_{\text{trig}} = 0 < T^i_{\text{max}}$; $(X^i)^{+++} \notin D^i_{\#2}$ because $\texttt{b}^i = 0 \neq 1$; $(X^i)^{+++} \notin D^i_{22}$ because $\texttt{b}^i = 0 \neq 1$; $(X^i)^{+++} \notin D^i_{23} \setminus (D^i_* \cup D^i_{20})$ because $\tau^i < \tau^i_p$; $(X^i)^{+++} \notin (D^i_* \cap D^i_{20}) \setminus D^i_{23}$ because $\tau^i_{\text{trig}} = 0 < T^i_{\text{max}}$; $(X^i)^{+++} \notin (D^i_* \cap D^i_{23}) \setminus D^i_{20}$ because $\tau^i_{\text{trig}} = 0 < T^i_{\text{max}}$; $(X^i)^{+++} \notin D^i_{20} \cap D^i_{23} \setminus D^i_*$ because $\tau^i < \tau^i_p$; and $(X^i)^{+++} \notin D^i_* \cap D^i_{20} \cap D^i_{23}$ because $\tau^i_{\text{trig}} = 0 < T^i_{\text{max}}$. If $(X^i)^{+++} \in D^i_{20}$, then the jump map in (3–45) yields

$(X^i)^{++++} \in \langle\!\langle \{0,1\}^N, \texttt{rpl}^i, \{0\}, \mathcal{F}^*_{\text{in}}, \mathcal{F}^*_{\text{in}}, \mathcal{F}^*_{\text{in}}, \{0\}, \{0\}, \{0\}, \{0\} \rangle\!\rangle$. For an agent i with $\texttt{mode}^i = 0$, $(X^i)^{++++}$ can either be in $C^i_0 \setminus D^i_{01}$ or D^i_{01}.
1) If $(X^i)^{++++} \in C^i_0 \setminus D^i_{01}$, then there were four jumps in null-time.
2) If $(X^i)^{++++} \in D^i_{01}$, then according to the partial jump sets in (3–44) and the partial flow sets (3–36)–(3–39) $(X^i)^{++++} \langle\!\langle \{0,1\}^N, \{\texttt{rpl}^i\}, \{0\}, \{n\}, \{n\}, \{n\}, \{0\}, \{0\}, \{0\}, \{1\} \rangle\!\rangle$. If $(X^i)^{++++} \in D^i_{01}$, then the jump map in (3–45) yields $(X^i)^{+++++} \in \langle\!\langle \{0,1\}^N, \{\texttt{rpl}^i\}, \{1\}, \{n\}, \{n\}, \{n\}, \{0\}, \{0\}, \{0\}, \{1\} \rangle\!\rangle$. Then according to the partial jump sets in (3–44) and the partial flow sets (3–36)–(3–39), $(X^i)^{+++++}$ must be contained in C^i_1. Therefore, there were five jumps in null-time.

* If $(X^i)^{++} \in \langle\!\langle \{0,1\}^N, \texttt{Plans}^i, \{0\}, \mathcal{F}^*_{\text{in}}, \mathcal{F}^*_{\text{in}}, \mathcal{F}^*_{\text{in}}, \{0\}, \{0\}, \{0\}, \{0\} \rangle\!\rangle$, then according to the partial jump sets in (3–44) and the partial flow sets (3–36)–(3–39) implies that $(X)^{++} \in C^i_0 \setminus D^i_{01}$ or $(X)^{++} \in D^i_{01}$.

  · If $(X^i)^{++} \in C^i_0 \setminus D^i_{01}$, then there were two jumps in null-time.

  · If $(X^i)^{++} \in D^i_{01}$, then according to the partial jump sets in (3–44) and the partial flow sets (3–36)–(3–39) $(X^i)^{++} \langle\!\langle \{0,1\}^N, \{\texttt{rpl}^i\}, \{0\}, \{n\}, \{n\}, \{n\}, \{0\}, \{0\}, \{0\}, \{1\} \rangle\!\rangle$. If $(X^i)^{++} \in D^i_{01}$, then the jump map in (3–45) yields $(X^i)^{+++} \in \langle\!\langle \{0,1\}^N, \{\texttt{rpl}^i\}, \{1\}, \{n\}, \{n\}, \{n\}, \{0\}, \{0\}, \{0\}, \{1\} \rangle\!\rangle$. Then according to the partial jump sets in (3–44) and the partial flow sets (3–36)–(3–39), $(X^i)^{+++}$ must be contained in C^i_1. Therefore, there were three jumps in null-time.

– If $(X^i)^{+} \in D^i_* \cap D^i_{23} \setminus D^i_{20}$, then the jump map in (3–45) yields $(X^i)^{++} \in \langle\!\langle \{0,1\}^N, \texttt{Plans}^i, \{2\}, \mathcal{F}^{\complement}, \mathbb{R}^2, \mathbb{R}^2, [\tau^i_p, \infty), \{0\}, [0, \infty), \{1\} \rangle\!\rangle \cup \langle\!\langle \{0,1\}^N, \texttt{Plans}^i, \{3\}, \mathcal{F}^{\complement}, \mathbb{R}^2, \mathbb{R}^2, [\tau^i_p, \infty), [T^i_{\text{max}}, \infty), [0, \infty), \{0\} \rangle\!\rangle$.

  * If $(X^i)^{++} \in \langle\!\langle \{0,1\}^N, \texttt{Plans}^i, \{2\}, \mathcal{F}^{\complement}, \mathbb{R}^2, \mathbb{R}^2, [\tau^i_p, \infty), \{0\}, [0, \infty), \{1\} \rangle\!\rangle$, then according to the partial jump sets in (3–44) and the partial flow sets (3–36)–(3–39) implies that either $(X)^{++} \in D^i_{\#2}$ or $(X)^{++} \in D^i_{22}$.

    · If $(X)^{++} \in D^i_{\#2}$, then the jump map in (3–45) yields $(X^i)^{+++} \in \langle\!\langle \{0,1\}^N, \texttt{Plans}^i, \{2\}, \mathcal{F}^{\complement}, \mathbb{R}^2, \mathbb{R}^2, [\tau^i_p, \infty), \{0\}, [0, \infty), \{0\} \rangle\!\rangle$. Then according to Table A-2, the partial jump sets in (3–44), and the partial flow sets (3–36)–(3–39), it is only possible for $(X^i)^{+++}$ to be contained in $D^i_{23} \setminus (D^i_* \cup D^i_{20})$, since: $(X^i)^{+++} \notin D^i_* \cap \{\texttt{mode}^i = 2\} \setminus (D^i_{20} \cup D^i_{23})$ because $\tau^i_{\text{trig}} = 0 < T^i_{\text{max}}$; $(X^i)^{+++} \notin D^i_{\#2}$ because $\texttt{b}^i = 0 \neq 1$; $(X^i)^{+++} \notin D^i_{22}$ because $\texttt{b}^i = 0 \neq 1$; $(X^i)^{+++} \notin D^i_{20} \setminus (D^i_* \cup D^i_{23})$ because $x^i \in \mathcal{F}^{\complement}$; $(X^i)^{+++} \notin (D^i_* \cap D^i_{20}) \setminus D^i_{23}$ because $\tau^i_{\text{trig}} = 0 < T^i_{\text{max}}$; $(X^i)^{+++} \notin (D^i_* \cap D^i_{23}) \setminus D^i_{20}$ because $\tau^i_{\text{trig}} = 0 < T^i_{\text{max}}$; $(X^i)^{+++} \notin D^i_{20} \cap D^i_{23} \setminus D^i_*$ because $x^i \in \mathcal{F}^{\complement}$;

and $(X^i)^{+++} \notin D^i_* \cap D^i_{20} \cap D^i_{23}$ because $\tau^i_{\mathsf{trig}} = 0 < T^i_{\mathsf{max}}$. If $(X^i)^{+++} \in D^i_{23} \setminus (D^i_* \cup D^i_{20})$, then the jump map in (3–45) yields $(X^i)^{++++} \in \left\langle\!\left\langle \{0,1\}^N, \mathtt{Plans}^i, \{3\}, \mathcal{F}^{\complement}, \mathbb{R}^2, \mathbb{R}^2, [\tau^i_p, \infty), \{0\}, [0,\infty), \{0\} \right\rangle\!\right\rangle$. Then according to the partial jump sets in (3–44), and the partial flow sets (3–36)–(3–39), it is only possible for $(X^i)^{++++}$ to be contained in C^i_3 since $(X^i)^{++++} \notin D^i_{30}$ because $x^i \in \mathcal{F}^{\complement}$. Therefore, there were four jumps in null-time.

- If $(X)^{++} \in D^i_{22}$, then the jump map in (3–45) yields $(X^i)^{+++} \in \left\langle\!\left\langle \{0,1\}^N, \mathtt{Plans}^i, \{2\}, \mathcal{F}^{\complement}, \mathbb{R}^2, \mathbb{R}^2, [\tau^i_p, \infty), \{0\}, [0,\infty), \{0\} \right\rangle\!\right\rangle$. Then according to Table A-2, the partial jump sets in (3–44), and the partial flow sets (3–36)–(3–39), it is only possible for $(X^i)^{+++}$ to be contained in $D^i_{23} \setminus (D^i_* \cup D^i_{20})$, since: $(X^i)^{+++} \notin D^i_* \cap \{\mathtt{mode}^i = 2\} \setminus (D^i_{20} \cup D^i_{23})$ because $\tau^i_{\mathsf{trig}} = 0 < T^i_{\mathsf{max}}$; $(X^i)^{+++} \notin D^i_{\#2}$ because $\mathtt{b}^i = 0 \neq 1$; $(X^i)^{+++} \notin D^i_{22}$ because $\mathtt{b}^i = 0 \neq 1$; $(X^i)^{+++} \notin D^i_{20} \setminus (D^i_* \cup D^i_{23})$ because $x^i \in \mathcal{F}^{\complement}$; $(X^i)^{+++} \notin (D^i_* \cap D^i_{20}) \setminus D^i_{23}$ because $\tau^i_{\mathsf{trig}} = 0 < T^i_{\mathsf{max}}$; $(X^i)^{+++} \notin (D^i_* \cap D^i_{23}) \setminus D^i_{20}$ because $\tau^i_{\mathsf{trig}} = 0 < T^i_{\mathsf{max}}$; $(X^i)^{+++} \notin D^i_{20} \cap D^i_{23} \setminus D^i_*$ because $x^i \in \mathcal{F}^{\complement}$; and $(X^i)^{+++} \notin D^i_* \cap D^i_{20} \cap D^i_{23}$ because $\tau^i_{\mathsf{trig}} = 0 < T^i_{\mathsf{max}}$. If $(X^i)^{+++} \in D^i_{23} \setminus (D^i_* \cup D^i_{20})$, then the jump map in (3–45) yields $(X^i)^{++++} \in \left\langle\!\left\langle \{0,1\}^N, \mathtt{Plans}^i, \{3\}, \mathcal{F}^{\complement}, \mathbb{R}^2, \mathbb{R}^2, [\tau^i_p, \infty), \{0\}, [0,\infty), \{0\} \right\rangle\!\right\rangle$. Then according to the partial jump sets in (3–44), and the partial flow sets (3–36)–(3–39), it is only possible for $(X^i)^{++++}$ to be contained in C^i_3 since $(X^i)^{++++} \notin D^i_{30}$ because $x^i \in \mathcal{F}^{\complement}$. Therefore, there were four jumps in null-time.

  - If $(X^i)^{++} \in \left\langle\!\left\langle \{0,1\}^N, \mathtt{Plans}^i, \{3\}, \mathcal{F}^{\complement}, \mathbb{R}^2, \mathbb{R}^2, [\tau^i_p, \infty), [T^i_{\mathsf{max}}, \infty), [0,\infty), \{0\} \right\rangle\!\right\rangle$, then according to the partial jump sets in (3–44), and the partial flow sets (3–36)–(3–39), it is only possible for $(X^i)^{++}$ to be contained in C^i_3 since $(X^i)^{++} \notin D^i_{30}$ because $x^i \in \mathcal{F}^{\complement}$. Therefore, there were two jumps in null-time.

- If $(X^i)^{+} \in D^i_* \cap D^i_{20} \cap D^i_{23}$, then according to the partial jump sets in (3–44) and the partial flow sets (3–36)–(3–39), $(X^i)^{+} \in \left\langle\!\left\langle \{0,1\}^N, \mathtt{Plans}^i, \{2\}, \mathcal{F}^*_{\mathsf{in}}, \mathbb{R}^2, \mathbb{R}^2, [\tau^i_p, \infty), [T^i_{\mathsf{max}}, \infty), [0,\infty), \{0\} \right\rangle\!\right\rangle$. If $(X^i)^{+} \in D^i_* \cap D^i_{20} \cap D^i_{23}$, then the jump map in (3–45) yields $(X^i)^{++} \in \left\langle\!\left\langle \{0,1\}^N, \mathtt{Plans}^i, \{2\}, \mathcal{F}^*_{\mathsf{in}}, \mathbb{R}^2, \mathbb{R}^2, [\tau^i_p, \infty), \{0\}, [0,\infty), \{1\} \right\rangle\!\right\rangle \cup \left\langle\!\left\langle \{0,1\}^N, \mathtt{rpl}^i, \{0\}, \mathcal{F}^*_{\mathsf{in}}, \mathcal{F}^*_{\mathsf{in}}, \mathcal{F}^*_{\mathsf{in}}, \{0\}, \{0\}, \{0\}, \{0\} \right\rangle\!\right\rangle \cup \left\langle\!\left\langle \{0,1\}^N, \mathtt{Plans}^i, \{3\}, \mathcal{F}^*_{\mathsf{in}}, \mathbb{R}^2, \mathbb{R}^2, [\tau^i_p, \infty), [T^i_{\mathsf{max}}, \infty), [0,\infty), \{0\} \right\rangle\!\right\rangle$.

  - If $(X^i)^{++} \in \left\langle\!\left\langle \{0,1\}^N, \mathtt{Plans}^i, \{2\}, \mathcal{F}^*_{\mathsf{in}}, \mathbb{R}^2, \mathbb{R}^2, [\tau^i_p, \infty), \{0\}, [0,\infty), \{1\} \right\rangle\!\right\rangle$, then according to the partial jump sets in (3–44) and the partial flow sets (3–36)–(3–39) implies that either $(X)^{++} \in D^i_{\#2}$ or $(X)^{+} \in D^i_{22}$.

- If $(X)^{++} \in D^i_{\#2}$, then the jump map in (3–45) yields $(X^i)^{+++} \in \langle\!\langle \{0,1\}^N, \texttt{Plans}^i, \{2\}, \mathcal{F}^*_{\text{in}}, \mathbb{R}^2, \mathbb{R}^2, [\tau^i_p, \infty), \{0\}, [0,\infty), \{0\} \rangle\!\rangle$. Then according to Table A-2, the partial jump sets in (3–44), and the partial flow sets (3–36)–(3–39), it is only possible for $(X^i)^{+++}$ to be contained in $D^i_{20} \cap D_{23} \setminus D^i_*$, since: $(X^i)^{+++} \notin D^i_* \cap \{\texttt{mode}^i = 2\} \setminus (D^i_{20} \cup D^i_{23})$ because $\tau^i_{\text{trig}} = 0 < T^i_{\text{max}}$; $(X^i)^{++} \notin D^i_{\#2}$ because $\texttt{b}^i = 0 \neq 1$; $(X^i)^{+++} \notin D^i_{22}$ because $\texttt{b}^i = 0 \neq 1$; $(X^i)^{+++} \notin D^i_* \cap D^i_{20} \setminus D^i_{23}$ because $\tau^i_{\text{trig}} = 0 < T^i_{\text{max}}$; $(X^i)^{+++} \notin D^i_* \cap D^i_{23} \setminus D^i_{20}$ because $\tau^i_{\text{trig}} = 0 < T^i_{\text{max}}$; and $(X^i)^{+++} \notin D^i_* \cap D^i_{20} \cap D^i_{23}$ because $\tau^i_{\text{trig}} = 0 < T^i_{\text{max}}$.
  If $(X^i)^{+++} \in D^i_{20} \cap D_{23} \setminus D^i_*$, then the jump map in (3–45) yields $(X^i)^{+++} \in \langle\!\langle \{0,1\}^N, \texttt{upd}^i, \{0\}, \mathcal{F}^*_{\text{in}}, \mathcal{F}^*_{\text{in}}, \mathcal{F}^*_{\text{in}}, \{0\}, \{0\}, \{0\}, \{0\} \rangle\!\rangle \cup \langle\!\langle \{0,1\}^N, \texttt{Plans}^i, \{3\}, \mathcal{F}^*_{\text{in}}, \mathbb{R}^2, \mathbb{R}^2, [\tau^i_p, \infty), \{0\}, [0,\infty), \{0\} \rangle\!\rangle$.
  1) If $(X^i)^{+++} \in \langle\!\langle \{0,1\}^N, \texttt{upd}^i, \{0\}, \mathcal{F}^*_{\text{in}}, \mathcal{F}^*_{\text{in}}, \mathcal{F}^*_{\text{in}}, \{0\}, \{0\}, \{0\}, \{0\} \rangle\!\rangle$, then according to the partial jump sets in (3–44) and the partial flow sets (3–36)–(3–39) implies that $(X)^{+++} \in C^i_0 \setminus D^i_{01}$ or $(X)^{+++} \in D^i_{01}$.
  1a) If $(X^i)^{+++} \in C^i_0 \setminus D^i_{01}$, then there were three jumps in null-time.
  1b) If $(X^i)^{+++} \in D^i_{01}$, then according to the partial jump sets in (3–44) and the partial flow sets (3–36)–(3–39) $(X^i)^{+++} \langle\!\langle \{0,1\}^N, \{\texttt{rpl}^i\}, \{0\}, \{n\}, \{n\}, \{n\}, \{0\}, \{0\}, \{0\}, \{1\} \rangle\!\rangle$. If $(X^i)^{+++} \in D^i_{01}$, then the jump map in (3–45) yields $(X^i)^{++++} \in \langle\!\langle \{0,1\}^N, \{\texttt{rpl}^i\}, \{1\}, \{n\}, \{n\}, \{n\}, \{0\}, \{0\}, \{0\}, \{1\} \rangle\!\rangle$. Then according to the partial jump sets in (3–44) and the partial flow sets (3–36)–(3–39), $(X^i)^{++++}$ must be contained in C^i_1. Therefore, there were four jumps in null-time.
  2) If $(X^i)^{+++} \in \langle\!\langle \{0,1\}^N, \texttt{Plans}^i, \{3\}, \mathcal{F}^*_{\text{in}}, \mathbb{R}^2, \mathbb{R}^2, [\tau^i_p, \infty), \{0\}, [0,\infty), \{0\} \rangle\!\rangle$, then according to the partial jump sets in (3–44), and the partial flow sets (3–36)–(3–39), it is only possible for $(X^i)^{+++}$ to be contained in D^i_{30}. If $(X^i)^{+++} \in D^i_{30}$, then the jump map in (3–45) yields $(X^i)^{++++} \in \langle\!\langle \{0,1\}^N, \{\texttt{rpl}^i\}, \{1\}, \{n\}, \{n\}, \{n\}, \{0\}, \{0\}, \{0\}, \{1\} \rangle\!\rangle$. If $(X^i)^{++++} \in \langle\!\langle \{0,1\}^N, \texttt{upd}^i, \{0\}, \mathcal{F}^*_{\text{in}}, \mathcal{F}^*_{\text{in}}, \mathcal{F}^*_{\text{in}}, \{0\}, \{0\}, \{0\}, \{0\} \rangle\!\rangle$, then according to the partial jump sets in (3–44) and the partial flow sets (3–36)–(3–39) implies that $(X)^{++++} \in C^i_0 \setminus D^i_{01}$ or $(X)^{+} \in D^i_{01}$.
  2a) If $(X^i)^{++++} \in C^i_0 \setminus D^i_{01}$, then there were four jumps in null-time.
  2b) If $(X^i)^{++++} \in D^i_{01}$, then according to the partial jump sets in (3–44) and the partial flow sets (3–36)–(3–39) $(X^i)^{++++} \langle\!\langle \{0,1\}^N, \{\texttt{rpl}^i\}, \{0\}, \{n\}, \{n\}, \{n\}, \{0\}, \{0\}, \{0\}, \{1\} \rangle\!\rangle$. If $(X^i)^{++++} \in D^i_{01}$, then the jump map in (3–45) yields $(X^i)^{+++++} \in \langle\!\langle \{0,1\}^N, \{\texttt{rpl}^i\}, \{1\}, \{n\}, \{n\}, \{n\}, \{0\}, \{0\}, \{0\}, \{1\} \rangle\!\rangle$. Then according to the partial jump sets in (3–44) and the partial flow sets (3–36)–(3–39), $(X^i)^{+++++}$ must be contained in C^i_1. Therefore, there were five jumps in null-time.
- If $(X)^{++} \in D^i_{22}$, then the jump map in (3–45) yields $(X^i)^{+++} \in \langle\!\langle \{0,1\}^N, \texttt{Plans}^i, \{2\}, \mathcal{F}^*_{\text{in}}, \mathbb{R}^2, \mathbb{R}^2, [\tau^i_p, \infty), \{0\}, [0,\infty), \{0\} \rangle\!\rangle$. Then

according to Table A-2, the partial jump sets in (3–44), and the partial flow sets (3–36)–(3–39), it is only possible for $(X^i)^{+++}$ to be contained in $D^i_{20} \cap D_{23} \setminus D^i_*$, since: $(X^i)^{+++} \notin D^i_* \cap \{\texttt{mode}^i = 2\} \setminus (D^i_{20} \cup D^i_{23})$ because $\tau^i_{\text{trig}} = 0 < T^i_{\text{max}}$; $(X^i)^{+++} \notin D^i_{\#2}$ because $\texttt{b}^i = 0 \neq 1$; $(X^i)^{+++} \notin D^i_{22}$ because $\texttt{b}^i = 0 \neq 1$; $(X^i)^{+++} \notin D^i_* \cap D^i_{20} \setminus D^i_{23}$ because $\tau^i_{\text{trig}} = 0 < T^i_{\text{max}}$; $(X^i)^{+++} \notin D^i_* \cap D^i_{23} \setminus D^i_{20}$ because $\tau^i_{\text{trig}} = 0 < T^i_{\text{max}}$; and $(X^i)^{+++} \notin D^i_* \cap D^i_{20} \cap D^i_{23}$ because $\tau^i_{\text{trig}} = 0 < T^i_{\text{max}}$.
If $(X^i)^{+++} \in D^i_{20} \cap D_{23} \setminus D^i_*$, then the jump map in (3–45) yields $(X^i)^{+++} \in \left\langle\!\left\langle \{0,1\}^N, \texttt{upd}^i, \{0\}, \mathcal{F}^*_{\text{in}}, \mathcal{F}^*_{\text{in}}, \mathcal{F}^*_{\text{in}}, \{0\}, \{0\}, \{0\}, \{0\} \right\rangle\!\right\rangle \cup \left\langle\!\left\langle \{0,1\}^N, \texttt{Plans}^i, \{3\}, \mathcal{F}^*_{\text{in}}, \mathbb{R}^2, \mathbb{R}^2, [\tau^i_p, \infty), \{0\}, [0,\infty), \{0\} \right\rangle\!\right\rangle$.
1) If $(X^i)^{+++} \in \left\langle\!\left\langle \{0,1\}^N, \texttt{upd}^i, \{0\}, \mathcal{F}^*_{\text{in}}, \mathcal{F}^*_{\text{in}}, \mathcal{F}^*_{\text{in}}, \{0\}, \{0\}, \{0\}, \{0\} \right\rangle\!\right\rangle$, then according to the partial jump sets in (3–44) and the partial flow sets (3–36)–(3–39) implies that $(X)^{+++} \in C^i_0 \setminus D^i_{01}$ or $(X)^{+++} \in D^i_{01}$.
1a) If $(X^i)^{+++} \in C^i_0 \setminus D^i_{01}$, then there were three jumps in null-time.
1b) If $(X^i)^{+++} \in D^i_{01}$, then according to the partial jump sets in (3–44) and the partial flow sets (3–36)–(3–39) $(X^i)^{+++} \left\langle\!\left\langle \{0,1\}^N, \{\texttt{rpl}^i\}, \{0\}, \{n\}, \{n\}, \{n\}, \{0\}, \{0\}, \{0\}, \{1\} \right\rangle\!\right\rangle$. If $(X^i)^{+++} \in D^i_{01}$, then the jump map in (3–45) yields $(X^i)^{++++} \in \left\langle\!\left\langle \{0,1\}^N, \{\texttt{rpl}^i\}, \{1\}, \{n\}, \{n\}, \{n\}, \{0\}, \{0\}, \{0\}, \{1\} \right\rangle\!\right\rangle$. Then according to the partial jump sets in (3–44) and the partial flow sets (3–36)–(3–39), $(X^i)^{++++}$ must be contained in C^i_1. Therefore, there four two jumps in null-time.
2) If $(X^i)^{+++} \in \left\langle\!\left\langle \{0,1\}^N, \texttt{Plans}^i, \{3\}, \mathcal{F}^*_{\text{in}}, \mathbb{R}^2, \mathbb{R}^2, [\tau^i_p, \infty), \{0\}, [0,\infty), \{0\} \right\rangle\!\right\rangle$, then according to the partial jump sets in (3–44), and the partial flow sets (3–36)–(3–39), it is only possible for $(X^i)^{+++}$ to be contained in D^i_{30}. If $(X^i)^{+++} \in D^i_{30}$, then the jump map in (3–45) yields $(X^i)^{++++} \in \left\langle\!\left\langle \{0,1\}^N, \{\texttt{rpl}^i\}, \{1\}, \{n\}, \{n\}, \{n\}, \{0\}, \{0\}, \{0\}, \{1\} \right\rangle\!\right\rangle$. If $(X^i)^{++++} \in \left\langle\!\left\langle \{0,1\}^N, \texttt{upd}^i, \{0\}, \mathcal{F}^*_{\text{in}}, \mathcal{F}^*_{\text{in}}, \mathcal{F}^*_{\text{in}}, \{0\}, \{0\}, \{0\}, \{0\} \right\rangle\!\right\rangle$, then according to the partial jump sets in (3–44) and the partial flow sets (3–36)–(3–39) implies that $(X)^{++++} \in C^i_0 \setminus D^i_{01}$ or $(X)^{++++} \in D^i_{01}$.
2a) If $(X^i)^{++++} \in C^i_0 \setminus D^i_{01}$, then there were four jumps in null-time.
2b) If $(X^i)^{++++} \in D^i_{01}$, then according to the partial jump sets in (3–44) and the partial flow sets (3–36)–(3–39) $(X^i)^{++++} \left\langle\!\left\langle \{0,1\}^N, \{\texttt{rpl}^i\}, \{0\}, \{n\}, \{n\}, \{n\}, \{0\}, \{0\}, \{0\}, \{1\} \right\rangle\!\right\rangle$.
If $(X^i)^{++++} \in D^i_{01}$, then the jump map in (3–45) yields $(X^i)^{+++++} \in \left\langle\!\left\langle \{0,1\}^N, \{\texttt{rpl}^i\}, \{1\}, \{n\}, \{n\}, \{n\}, \{0\}, \{0\}, \{0\}, \{1\} \right\rangle\!\right\rangle$. Then according to the partial jump sets in (3–44) and the partial flow sets (3–36)–(3–39), $(X^i)^{+++++}$ must be contained in C^i_1. Therefore, there were five jumps in null-time.

* If $(X^i)^{++} \in \left\langle\!\left\langle \{0,1\}^N, \texttt{rpl}^i, \{0\}, \mathcal{F}^*_{\text{in}}, \mathcal{F}^*_{\text{in}}, \mathcal{F}^*_{\text{in}}, \{0\}, \{0\}, \{0\}, \{0\} \right\rangle\!\right\rangle$, then according to the partial jump sets in (3–44) and the partial flow sets (3–36)–(3–39) implies that $(X)^{++} \in C^i_0 \setminus D^i_{01}$ or $(X)^{++} \in D^i_{01}$.

- If $(X^i)^{++} \in C_0^i \setminus D_{01}^i$, then there were two jumps in null-time.
- If $(X^i)^{++} \in D_{01}^i$, then according to the partial jump sets in (3–44) and the partial flow sets (3–36)–(3–39) $(X^i)^{++} \left\langle\!\left\langle \{0,1\}^N, \{\texttt{rpl}^i\}, \{0\}, \{n\}, \{n\}, \{n\}, \{0\}, \{0\}, \{0\}, \{1\} \right\rangle\!\right\rangle$. If $(X^i)^{++} \in D_{01}^i$, then the jump map in (3–45) yields $(X^i)^{+++} \in \left\langle\!\left\langle \{0,1\}^N, \{\texttt{rpl}^i\}, \{1\}, \{n\}, \{n\}, \{n\}, \{0\}, \{0\}, \{0\}, \{1\} \right\rangle\!\right\rangle$. Then according to the partial jump sets in (3–44) and the partial flow sets (3–36)–(3–39), $(X^i)^{+++}$ must be contained in C_1^i. Therefore, there were three jumps in null-time.

* If $(X^i)^{++} \in \left\langle\!\left\langle \{0,1\}^N, \texttt{Plans}^i, \{3\}, \mathcal{F}_{\mathsf{in}}^*, \mathbb{R}^2, \mathbb{R}^2, [\tau_p^i, \infty), [T_{\mathsf{max}}^i, \infty), [0, \infty), \{0\} \right\rangle\!\right\rangle$, then according to the partial jump sets in (3–44), and the partial flow sets (3–36)–(3–39), it is only possible for $(X^i)^{++}$ to be contained in D_{30}^i. If $(X^i)^{++} \in D_{30}^i$, then the jump map in (3–45) yields $(X^i)^{+++} \in \left\langle\!\left\langle \{0,1\}^N, \{\texttt{rpl}^i\}, \{1\}, \{n\}, \{n\}, \{n\}, \{0\}, \{0\}, \{0\}, \{1\} \right\rangle\!\right\rangle$. If $(X^i)^{+++} \in \left\langle\!\left\langle \{0,1\}^N, \texttt{upd}^i, \{0\}, \mathcal{F}_{\mathsf{in}}^*, \mathcal{F}_{\mathsf{in}}^*, \mathcal{F}_{\mathsf{in}}^*, \{0\}, \{0\}, \{0\}, \{0\} \right\rangle\!\right\rangle$, then according to the partial jump sets in (3–44) and the partial flow sets (3–36)–(3–39) implies that $(X)^{+++} \in C_0^i \setminus D_{01}^i$ or $(X)^{+++} \in D_{01}^i$.
  - If $(X^i)^{+++} \in C_0^i \setminus D_{01}^i$, then there were three jumps in null-time.
  - If $(X^i)^{+++} \in D_{01}^i$, then according to the partial jump sets in (3–44) and the partial flow sets (3–36)–(3–39) $(X^i)^{+++} \left\langle\!\left\langle \{0,1\}^N, \{\texttt{rpl}^i\}, \{0\}, \{n\}, \{n\}, \{n\}, \{0\}, \{0\}, \{0\}, \{1\} \right\rangle\!\right\rangle$. If $(X^i)^{+++} \in D_{01}^i$, then the jump map in (3–45) yields $(X^i)^{++++} \in \left\langle\!\left\langle \{0,1\}^N, \{\texttt{rpl}^i\}, \{1\}, \{n\}, \{n\}, \{n\}, \{0\}, \{0\}, \{0\}, \{1\} \right\rangle\!\right\rangle$. Then according to the partial jump sets in (3–44) and the partial flow sets (3–36)–(3–39), $(X^i)^{++++}$ must be contained in C_1^i. Therefore, there were four jumps in null-time.

The possible jump sequences can be visualized in the DAGs in Figures A-6–A-14.

A.1.7 $X^i \in D_*^i \cap \{\texttt{mode}^i = 2\} \setminus (D_{20}^i \cup D_{23}^i)$

Suppose that there is a state X such that agent $i \in \mathcal{A}$ has the state $X^i \in D_*^i \cap \{\texttt{mode}^i = 2\} \setminus (D_{20}^i \cup D_{23}^i)$, then according to the partial jump sets in (3–44) and the partial flow sets (3–36)–(3–39), $X^i \in \left\langle\!\left\langle \{0,1\}^N, \texttt{Plans}^i, \{2\}, \mathcal{F}^{\complement}, \mathbb{R}^2, \mathbb{R}^2, [\tau_o^i, \tau_p^i), [T_{\mathsf{max}}^i, \infty), [0, \infty), \{0\} \right\rangle\!\right\rangle$. If $X^i \in D_*^i \cap \{\texttt{mode}^i = 2\} \setminus (D_{20}^i \cup D_{23}^i)$, then the jump map in (3–45) yields $(X^i)^+ \in \left\langle\!\left\langle \{0,1\}^N, \texttt{Plans}^i, \{2\}, \mathcal{F}^{\complement}, \mathbb{R}^2, \mathbb{R}^2, [\tau_o^i, \tau_p^i), [T_{\mathsf{max}}^i, \infty), [0, \infty), \{1\} \right\rangle\!\right\rangle$. If $(X^i)^+ \in$

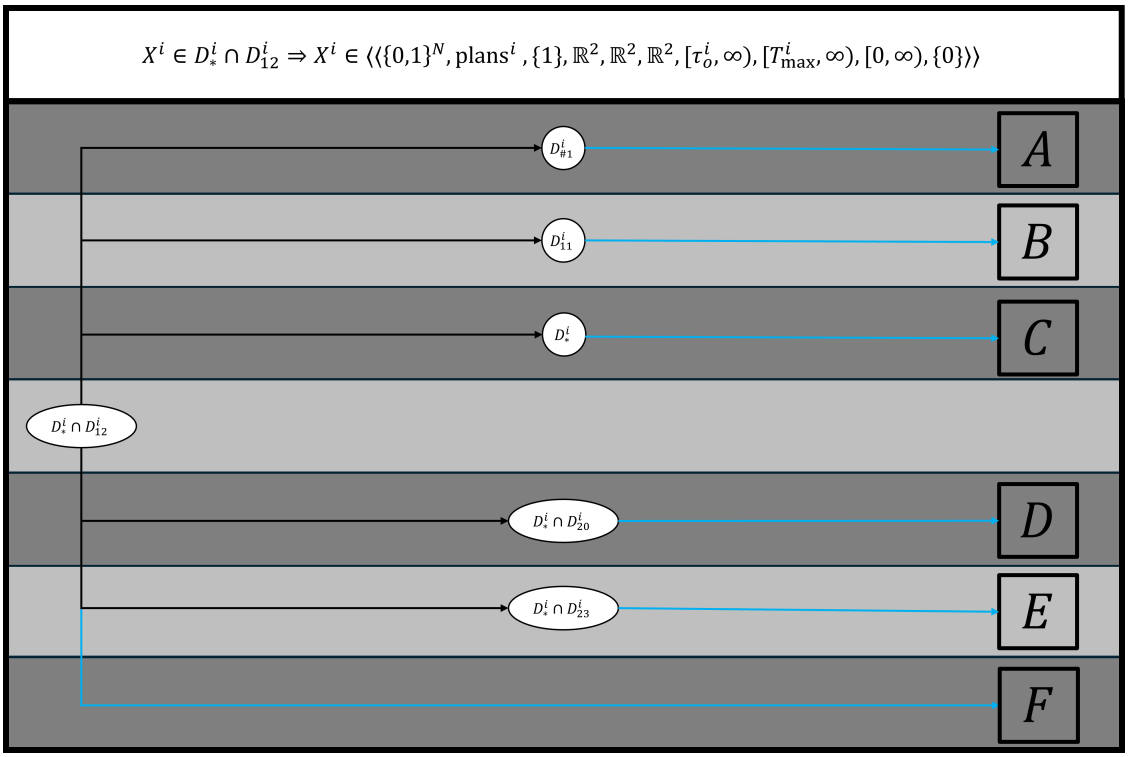

Figure A-6. Directed acyclic graph for $X^i \in D^i_* \cap D^i_{12}$. The graph continues to Figures A-7–A-14.

$\langle\!\langle \{0,1\}^N, \texttt{Plans}^i, \{2\}, \mathcal{F}^{\complement}, \mathbb{R}^2, \mathbb{R}^2, [\tau^i_o, \tau^i_p), [T^i_{\max}, \infty), [0, \infty), \{1\} \rangle\!\rangle$, then according to the partial jump sets in (3–44) and the partial flow sets (3–36)–(3–39) implies that either $(X)^+ \in D^i_{\#2}$ or $(X)^+ \in D^i_{22}$.

- If $(X)^+ \in D^i_{\#2}$ then the jump map in (3–45) yields $(X^i)^{++} \in \langle\!\langle \{0,1\}^N, \texttt{Plans}^i, \{2\}, \mathcal{F}^{\complement}, \mathbb{R}^2, \mathbb{R}^2, [\tau^i_o, \tau^i_p), \{0\}, [0, \infty), \{1\} \rangle\!\rangle$. Then according to Table A-2, the partial jump sets in (3–44), and the partial flow sets (3–36)–(3–39), it is only possible for $(X^i)^{++}$ to be contained in C^i_2, since: $(X^i)^{++} \notin D^i_* \cap \{\texttt{mode}^i = 2\} \setminus (D^i_{20} \cup D^i_{23})$ because $\tau^i_{\text{trig}} = 0 < T^i_{\max}$; $(X^i)^{++} \notin D^i_{\#2}$ because $\texttt{b}^i = 0 \neq 1$; $(X^i)^{++} \notin D^i_{22}$ because $\texttt{b}^i = 0 \neq 1$; $(X^i)^{++} \notin D^i_{20} \setminus (D^i_* \cup D^i_{23})$ because $x^i \in \mathcal{F}^{\complement}$; $(X^i)^{++} \notin D^i_{23} \setminus (D^i_* \cup D^i_{20})$ because $\tau^i < \tau^i_p$; $(X^i)^{++} \notin (D^i_* \cap D^i_{20}) \setminus D^i_{23}$ because $\tau^i_{\text{trig}} = 0 < T^i_{\max}$; $(X^i)^{++} \notin (D^i_* \cap D^i_{23}) \setminus D^i_{20}$ because $\tau^i_{\text{trig}} = 0 < T^i_{\max}$; $(X^i)^{++} \notin D^i_{20} \cap D^i_{23} \setminus D^i_*$ because $x^i \in \mathcal{F}^{\complement}$; and $(X^i)^{++} \notin D^i_* \cap D^i_{20} \cap D^i_{23}$ because $\tau^i_{\text{trig}} = 0 < T^i_{\max}$. Since $(X^i)^{++} \in C^i_2$, there were two jumps in null-time.

- If $(X)^+ \in D^i_{22}$ then the jump map in (3–45) yields $(X^i)^{++} \in \langle\!\langle \{0,1\}^N, \texttt{Plans}^i, \{2\}, \mathcal{F}^{\complement}, \mathbb{R}^2, \mathbb{R}^2, [\tau^i_o, \tau^i_p), \{0\}, [0, \infty), \{1\} \rangle\!\rangle$. Then according to Table A-2, the partial jump sets in (3–44), and the partial flow sets (3–36)–(3–39), it is only possible for $(X^i)^{++}$ to be contained in C^i_2, since:

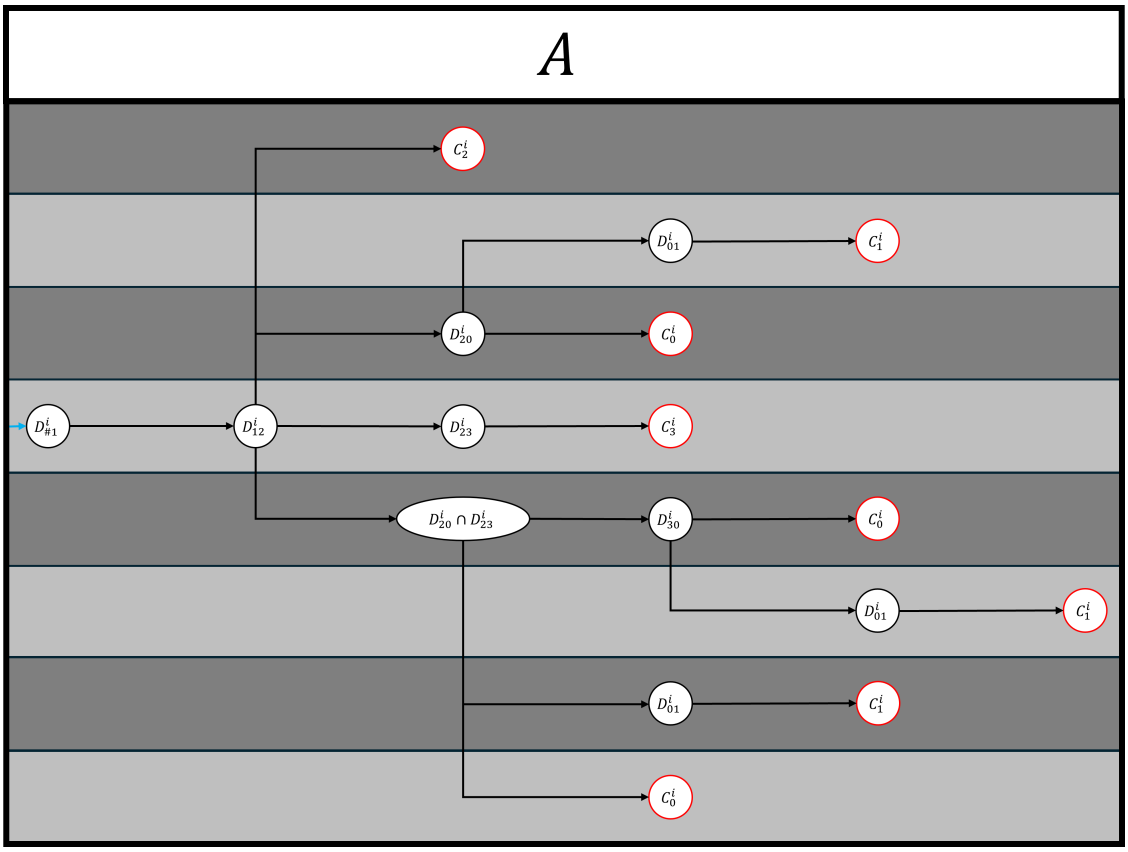

Figure A-7. Continuation of the directed acyclic graph for $X^i \in D_*^i \cap D_{12}^i$ in Figure A-6.

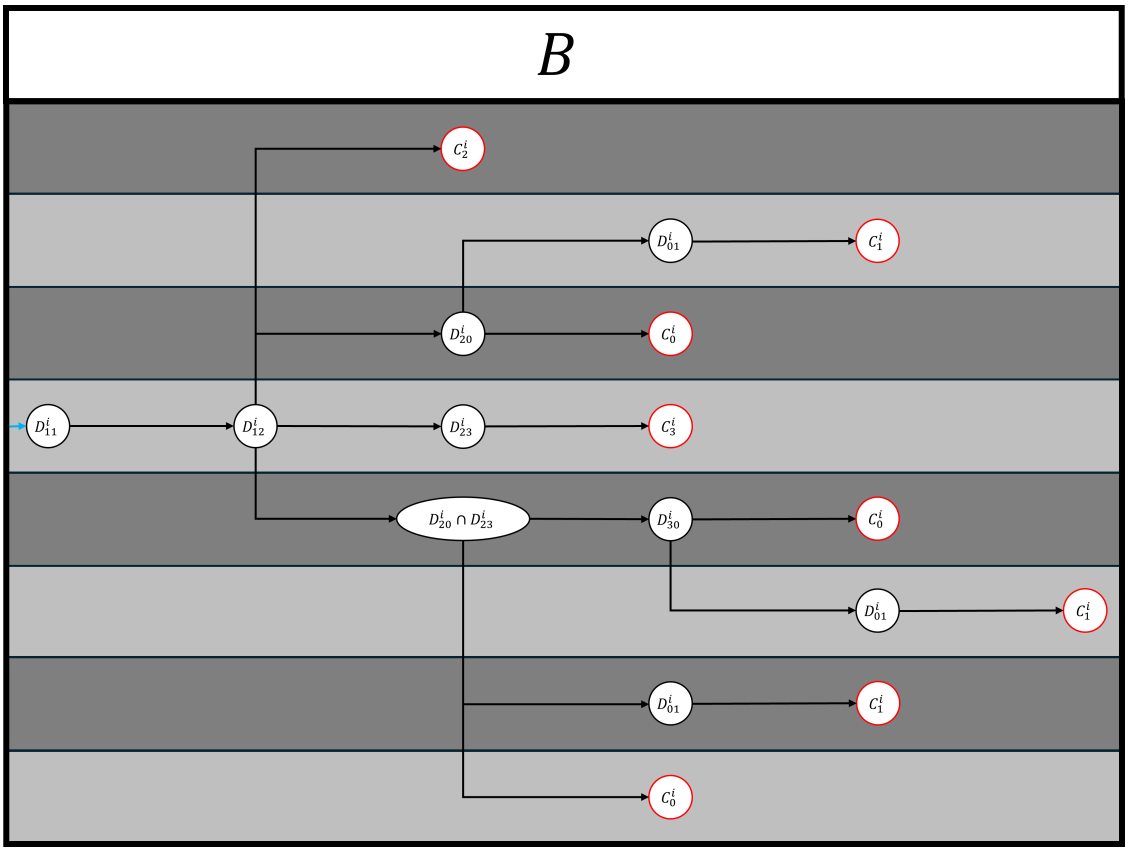

Figure A-8. Continuation of the directed acyclic graph for $X^i \in D_*^i \cap D_{12}^i$ in Figure A-6.

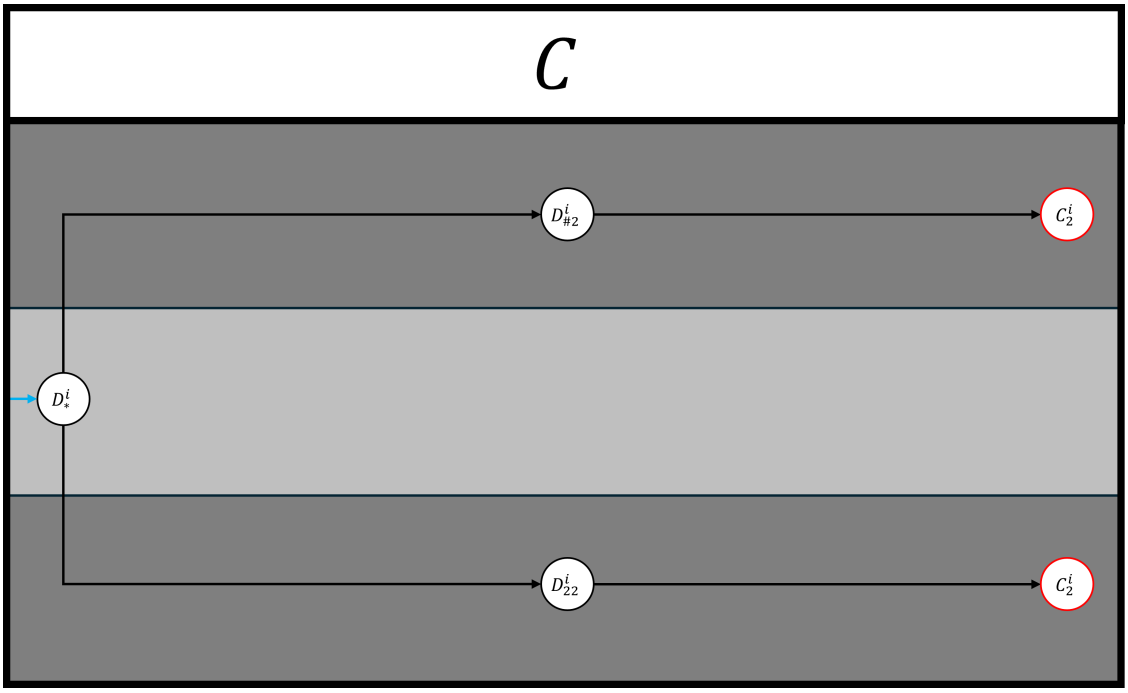

Figure A-9. Continuation of the directed acyclic graph for $X^i \in D_*^i \cap D_{12}^i$ in Figure A-6.

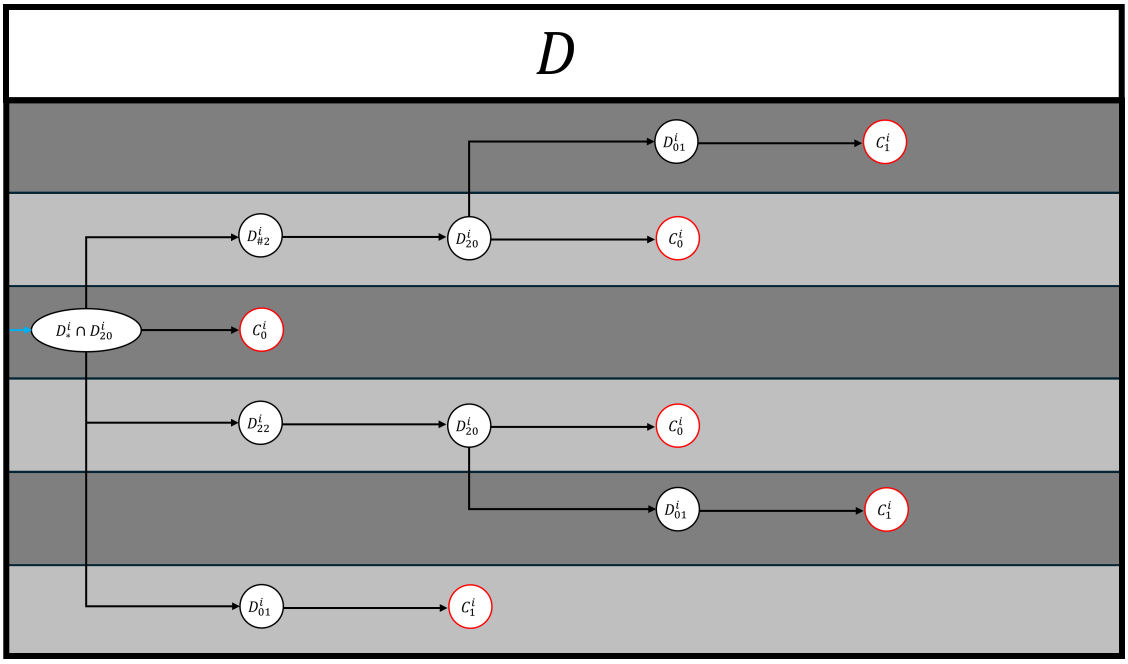

Figure A-10. Continuation of the directed acyclic graph for $X^i \in D^i_* \cap D^i_{12}$ in Figure A-6.

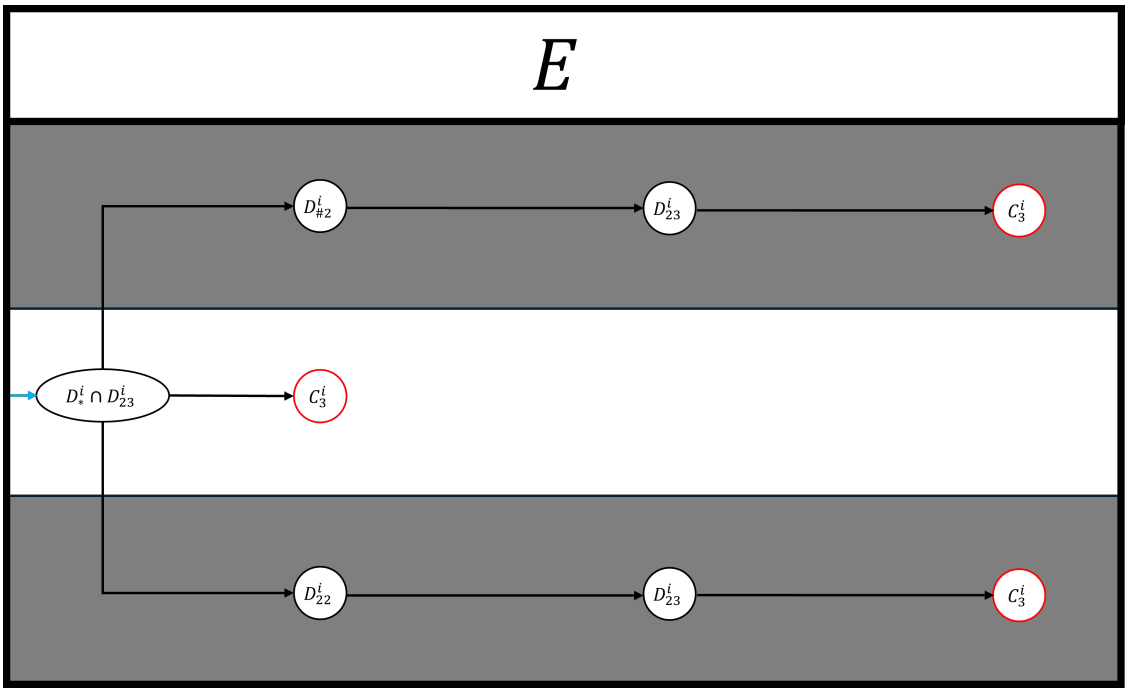

Figure A-11. Continuation of the directed acyclic graph for $X^i \in D^i_* \cap D^i_{12}$ in Figure A-6.

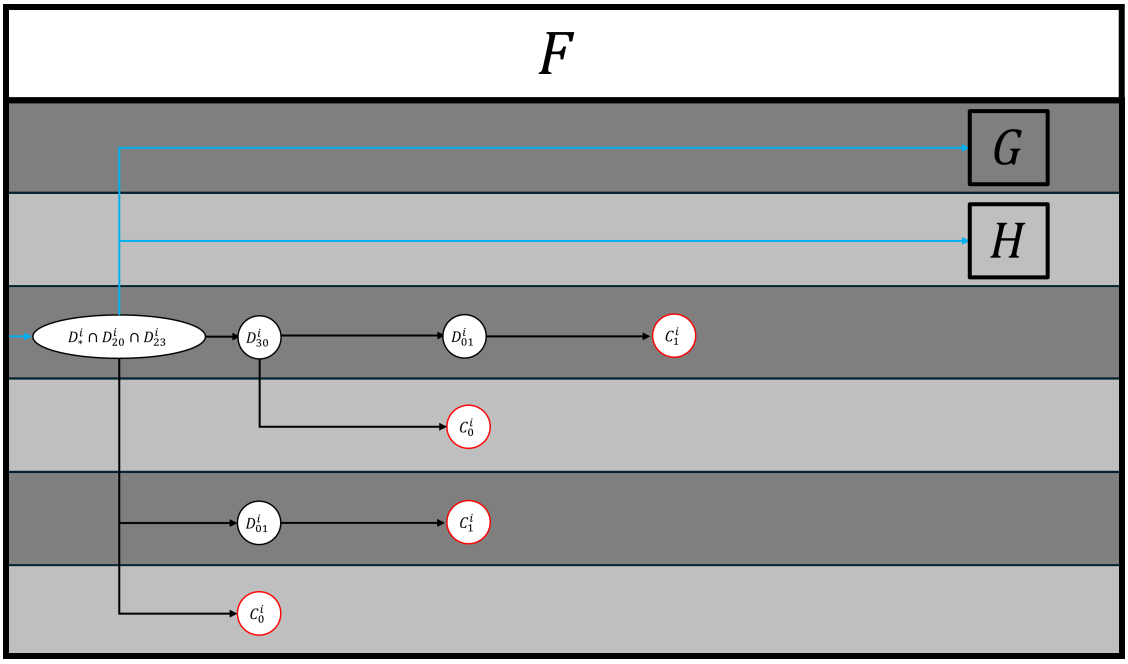

Figure A-12. Continuation of the directed acyclic graph for $X^i \in D^i_* \cap D^i_{12}$ in Figure A-6. This graph continues to Figures A-13 and A-14.

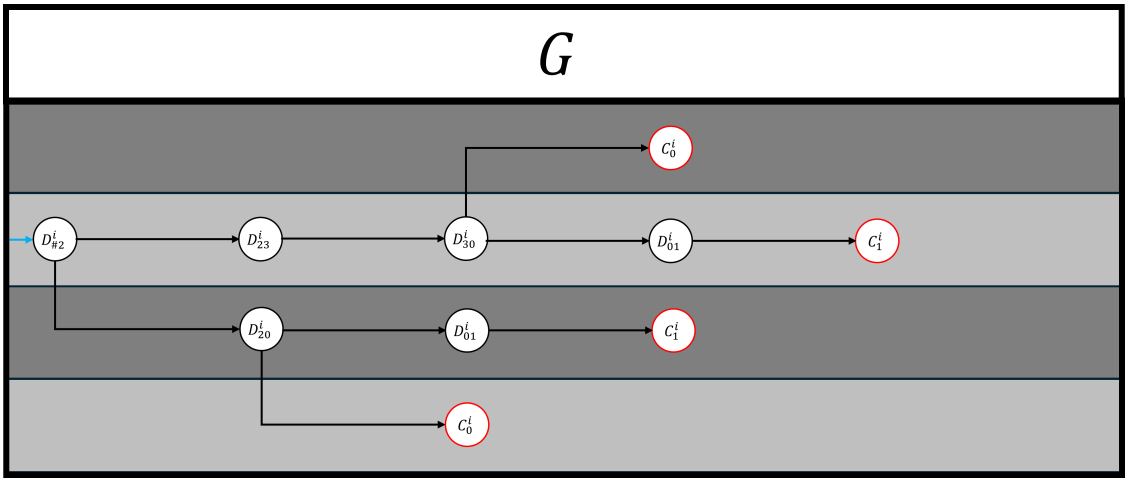

Figure A-13. Continuation of the directed acyclic graph for $X^i \in D^i_* \cap D^i_{12}$ in Figure A-12.

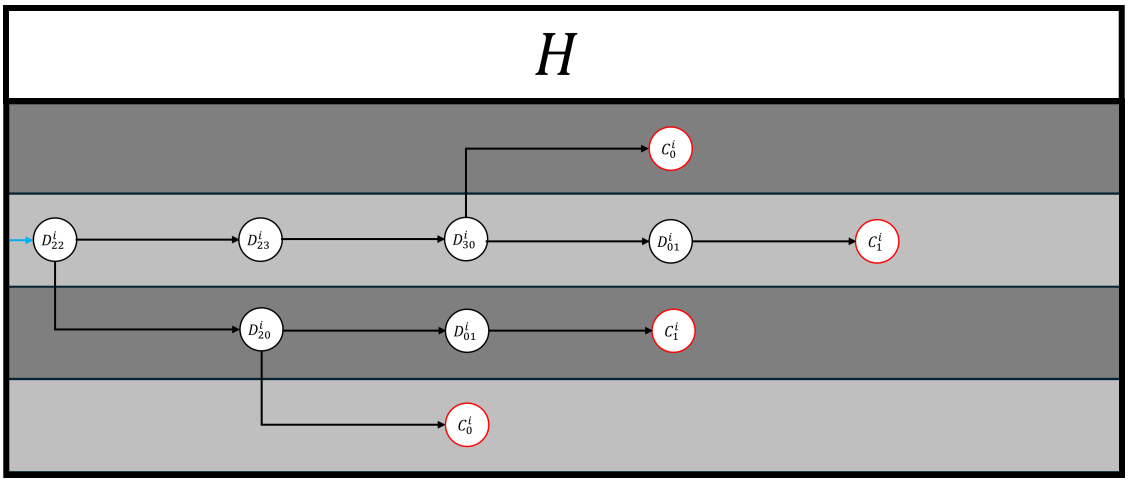

Figure A-14. Continuation of the directed acyclic graph for $X^i \in D_*^i \cap D_{12}^i$ in Figure A-12.

$(X^i)^{++} \notin D_*^i \cap \{\texttt{mode}^i = 2\} \setminus (D_{20}^i \cup D_{23}^i)$ because $\tau_{\text{trig}}^i = 0 < T_{\text{max}}^i$; $(X^i)^{++} \notin D_{\#2}^i$ because $\texttt{b}^i = 0 \neq 1$; $(X^i)^{++} \notin D_{22}^i$ because $\texttt{b}^i = 0 \neq 1$; $(X^i)^{++} \notin D_{20}^i \setminus (D_*^i \cup D_{23}^i)$ because $x^i \in \mathcal{F}^{\complement}$; $(X^i)^{++} \notin D_{23}^i \setminus (D_*^i \cup D_{20}^i)$ because $\tau^i < \tau_p^i$; $(X^i)^{++} \notin (D_*^i \cap D_{20}^i) \setminus D_{23}^i$ because $\tau_{\text{trig}}^i = 0 < T_{\text{max}}^i$; $(X^i)^{++} \notin (D_*^i \cap D_{23}^i) \setminus D_{20}^i$ because $\tau_{\text{trig}}^i = 0 < T_{\text{max}}^i$; $(X^i)^{++} \notin D_{20}^i \cap D_{23}^i \setminus D_*^i$ because $x^i \in \mathcal{F}^{\complement}$; and $(X^i)^{++} \notin D_*^i \cap D_{20}^i \cap D_{23}^i$ because $\tau_{\text{trig}}^i = 0 < T_{\text{max}}^i$. Since $(X^i)^{++} \in C_2^i$, there were two jumps in null-time.

The possible jump sequences can be visualized in the DAG in Figure A-15.

A.1.8 $X^i \in D_{\#2}^i$

Suppose that there is a state X such that agent $i \in \mathcal{A}$ has the state $X^i \in D_{\#2}^i$, then according to the partial jump sets in (3–44) and the partial flow sets (3–36)–(3–39), $X^i \in \langle\!\langle \{0,1\}^N, \texttt{Plans}^i, \{2\}, \mathbb{R}^2, \mathbb{R}^2, \mathbb{R}^2, [\tau_o^i, \infty), \{0\}, [0,\infty), \{0\} \rangle\!\rangle$. If $X^i \in D_{\#2}^i$, then the jump map in (3–45) yields $(X^i)^+ \in \langle\!\langle \{0,1\}^N, \texttt{Plans}^i, \{2\}, \mathbb{R}^2, \mathbb{R}^2, \mathbb{R}^2, [\tau_o^i, \infty), \{0\}, [0,\infty), \{0\} \rangle\!\rangle$. Then according to Table A-2, the partial jump sets in (3–44), and the partial flow sets (3–36)–(3–39), it is only possible for $(X^i)^+$ to be contained in either $D_{20}^i \setminus (D_{23}^i \cup D_*^i)$, $D_{23}^i \setminus (D_{20}^i \cup D_*^i)$, or $D_{20}^i \cap D_{23} \setminus D_*^i$, since: $(X^i)^+ \notin D_*^i \cap \{\texttt{mode}^i = 2\} \setminus (D_{20}^i \cup D_{23}^i)$ because $\tau_{\text{trig}}^i = 0 < T_{\text{max}}^i$; $(X^i)^+ \notin D_{\#2}^i$ because $\texttt{b}^i = 0 \neq 1$; $(X^i)^+ \notin D_{22}^i$ because $\texttt{b}^i = 0 \neq 1$; $(X^i)^+ \notin D_*^i \cap D_{20}^i \setminus D_{23}^i$ because $\tau_{\text{trig}}^i = 0 < T_{\text{max}}^i$; $(X^i)^+ \notin D_*^i \cap D_{23}^i \setminus D_{20}^i$ because $\tau_{\text{trig}}^i = 0 < T_{\text{max}}^i$; and $(X^i)^+ \notin D_*^i \cap D_{20}^i \cap D_{23}^i$ because $\tau_{\text{trig}}^i = 0 < T_{\text{max}}^i$.

- If $(X^i)^+ \in D_{20}^i \setminus (D_{23}^i \cup D_*^i)$, then according to the partial jump sets in (3–44) and the partial flow sets (3–36)–(3–39)

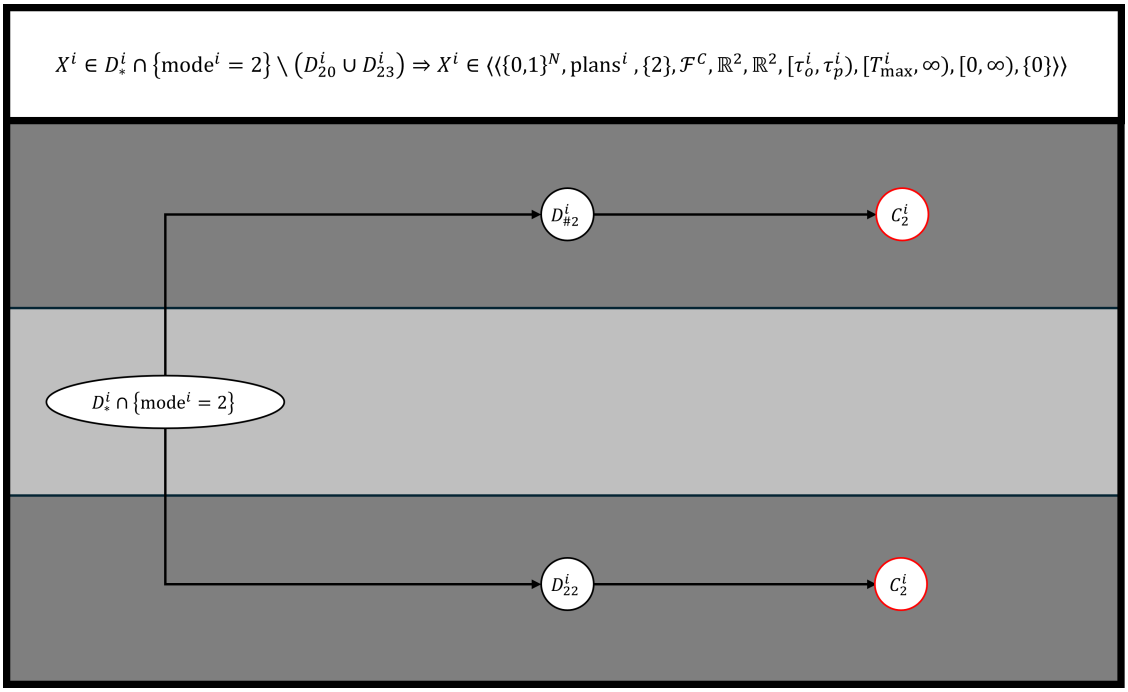

Figure A-15. Directed acyclic graph for $X^i \in D_*^i \cap \{\texttt{mode}^i = 2\} \setminus (D_{20}^i \cup D_{23}^i)$.

$(X^i)^+ \in \langle\!\langle \{0,1\}^N, \texttt{Plans}^i, \{2\}, \mathcal{F}_{\text{in}}^*, \mathbb{R}^2, \mathbb{R}^2, [\tau_o^i, \infty), \{0\}, [0,\infty), \{1\} \rangle\!\rangle$. If $(X^i)^+ \in D_{20}^i \setminus D_{23}^i$, then the jump map in (3–45) yields $(X^i)^{++} \in \langle\!\langle \{0,1\}^N, \{\texttt{rpl}^i\}, \{0\}, \mathcal{F}_{\text{in}}^*, \mathcal{F}_{\text{in}}^*, \mathcal{F}_{\text{in}}^*, \{0\}, \{0\}, \{0\}, \{1\} \rangle\!\rangle$. For an agent i with $\texttt{mode}^i = 0$, $(X^i)^{++}$ can either be in $C_0^i \setminus D_{01}^i$ or D_{01}^i.

- If $(X^i)^{++} \in C_0^i \setminus D_{01}^i$, then there were two jumps in null-time.
- If $(X^i)^{++} \in D_{01}^i$, then according to the partial jump sets in (3–44) and the partial flow sets (3–36)–(3–39) $(X^i)^{++} \langle\!\langle \{0,1\}^N, \{\texttt{rpl}^i\}, \{0\}, \{n\}, \{n\}, \{n\}, \{0\}, \{0\}, \{0\}, \{1\} \rangle\!\rangle$. If $(X^i)^{++} \in D_{01}^i$, then the jump map in (3–45) yields $(X^i)^{+++} \in \langle\!\langle \{0,1\}^N, \{\texttt{rpl}^i\}, \{1\}, \{n\}, \{n\}, \{n\}, \{0\}, \{0\}, \{0\}, \{1\} \rangle\!\rangle$. Then according to the partial jump sets in (3–44) and the partial flow sets (3–36)–(3–39), $(X^i)^{+++}$ must be contained in C_1^i. Therefore, there were three jumps in null-time.

- If $(X^i)^+ \in D_{23}^i \setminus (D_{20}^i \cup D_*^i)$, then according to the partial jump sets in (3–44), and the partial flow sets (3–36)–(3–39), it is only possible for $(X^i)^+$ to be contained in C_3^i since $(X^i)^+ \notin D_{30}^i$ because $x^i \in \mathcal{F}^{\complement}$. Therefore, there was one jump in null-time.

- If $(X^i)^+ \in D_{20}^i \cap D_{23} \setminus D_*^i$, then the jump map in (3–45) yields $(X^i)^{++} \in \langle\!\langle \{0,1\}^N, \texttt{upd}^i, \{0\}, \mathcal{F}_{\text{in}}^*, \mathcal{F}_{\text{in}}^*, \mathcal{F}_{\text{in}}^*, \{0\}, \{0\}, \{0\}, \{0\} \rangle\!\rangle \cup \langle\!\langle \{0,1\}^N, \texttt{Plans}^i, \{3\}, \mathcal{F}_{\text{in}}^*, \mathbb{R}^2, \mathbb{R}^2, [\tau_p^i, \infty), \{0\}, [0,\infty), \{0\} \rangle\!\rangle$.

– If $(X^i)^{++} \in \langle\!\langle \{0,1\}^N, \texttt{upd}^i, \{0\}, \mathcal{F}^*_{\text{in}}, \mathcal{F}^*_{\text{in}}, \mathcal{F}^*_{\text{in}}, \{0\}, \{0\}, \{0\}, \{0\} \rangle\!\rangle$, then according to the partial jump sets in (3–44) and the partial flow sets (3–36)–(3–39) implies that $(X)^{++} \in C^i_0 \setminus D^i_{01}$ or $(X)^{++} \in D^i_{01}$.

  * If $(X^i)^{++} \in C^i_0 \setminus D^i_{01}$, then there were two jumps in null-time.

    · If $(X^i)^{++} \in D^i_{01}$, then according to the partial jump sets in (3–44) and the partial flow sets (3–36)–(3–39) $(X^i)^{++} \langle\!\langle \{0,1\}^N, \{\texttt{rpl}^i\}, \{0\}, \{n\}, \{n\}, \{n\}, \{0\}, \{0\}, \{0\}, \{1\} \rangle\!\rangle$. If $(X^i)^{+} \in D^i_{01}$, then the jump map in (3–45) yields $(X^i)^{+++} \in \langle\!\langle \{0,1\}^N, \{\texttt{rpl}^i\}, \{1\}, \{n\}, \{n\}, \{n\}, \{0\}, \{0\}, \{0\}, \{1\} \rangle\!\rangle$. Then according to the partial jump sets in (3–44) and the partial flow sets (3–36)–(3–39), $(X^i)^{+++}$ must be contained in C^i_1. Therefore, there were three jumps in null-time.

– If $(X^i)^{++} \in \langle\!\langle \{0,1\}^N, \texttt{Plans}^i, \{3\}, \mathcal{F}^*_{\text{in}}, \mathbb{R}^2, \mathbb{R}^2, [\tau^i_p, \infty), \{0\}, [0,\infty), \{0\} \rangle\!\rangle$, then according to the partial jump sets in (3–44), and the partial flow sets (3–36)–(3–39), it is only possible for $(X^i)^{++}$ to be contained in D^i_{30}. If $(X^i)^{++} \in D^i_{30}$, then the jump map in (3–45) yields $(X^i)^{+++} \in \langle\!\langle \{0,1\}^N, \{\texttt{rpl}^i\}, \{1\}, \{n\}, \{n\}, \{n\}, \{0\}, \{0\}, \{0\}, \{1\} \rangle\!\rangle$. If $(X^i)^{+++} \in \langle\!\langle \{0,1\}^N, \texttt{upd}^i, \{0\}, \mathcal{F}^*_{\text{in}}, \mathcal{F}^*_{\text{in}}, \mathcal{F}^*_{\text{in}}, \{0\}, \{0\}, \{0\}, \{0\} \rangle\!\rangle$, then according to the partial jump sets in (3–44) and the partial flow sets (3–36)–(3–39) implies that $(X)^{+++} \in C^i_0 \setminus D^i_{01}$ or $(X)^{+} \in D^i_{01}$.

  * If $(X^i)^{+++} \in C^i_0 \setminus D^i_{01}$, then there were three jumps in null-time.

  * If $(X^i)^{+++} \in D^i_{01}$, then according to the partial jump sets in (3–44) and the partial flow sets (3–36)–(3–39) $(X^i)^{+++} \langle\!\langle \{0,1\}^N, \{\texttt{rpl}^i\}, \{0\}, \{n\}, \{n\}, \{n\}, \{0\}, \{0\}, \{0\}, \{1\} \rangle\!\rangle$. If $(X^i)^{+++} \in D^i_{01}$, then the jump map in (3–45) yields $(X^i)^{++++} \in \langle\!\langle \{0,1\}^N, \{\texttt{rpl}^i\}, \{1\}, \{n\}, \{n\}, \{n\}, \{0\}, \{0\}, \{0\}, \{1\} \rangle\!\rangle$. Then according to the partial jump sets in (3–44) and the partial flow sets (3–36)–(3–39), $(X^i)^{++++}$ must be contained in C^i_1. Therefore, there were four jumps in null-time.

The possible jump sequences can be visualized in the DAG in Figure A-16.

A.1.9 $X^i \in D^i_{22}$

Suppose that there is a state X such that agent $i \in \mathcal{A}$ has the state $X^i \in D^i_{22}$, then according to the partial jump sets in (3–44) and the partial flow sets (3–36)–(3–39), $X^i \in \langle\!\langle \{0,1\}^N, \texttt{Plans}^i, \{2\}, \mathbb{R}^2, \mathbb{R}^2, \mathbb{R}^2, [\tau^i_o, \infty), \{0\}, [0,\infty), \{0\} \rangle\!\rangle$. If $X^i \in D^i_{22}$, then the regularization of the jump map in (3–45) yields $(X^i)^{+} \in \langle\!\langle \{0,1\}^N, \texttt{Plans}^i, \{2\}, \mathbb{R}^2, \mathbb{R}^2, \mathbb{R}^2, [\tau^i_o, \infty), \{0\}, [0,\infty), \{0\} \rangle\!\rangle$. Then according to Table A-2,

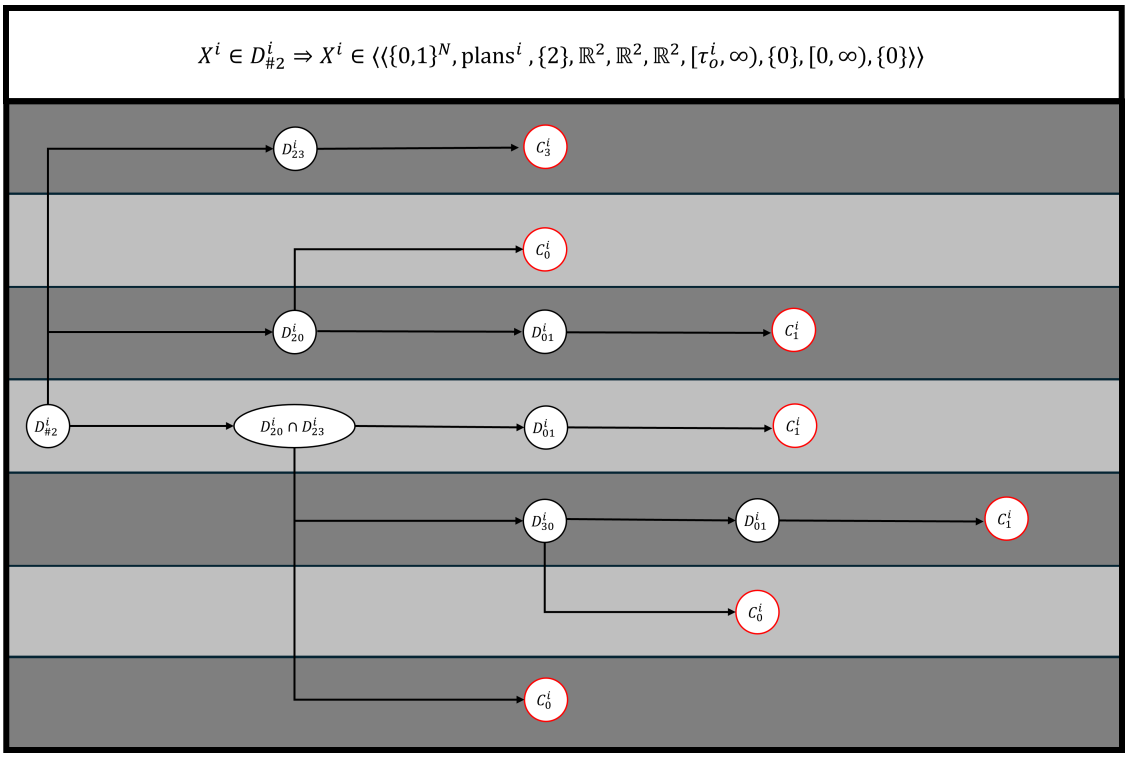

Figure A-16. Directed acyclic graph for $X^i \in D^i_{\#2}$.

the partial jump sets in (3–44), and the partial flow sets (3–36)–(3–39), it is only possible for $(X^i)^+$ to be contained in either $D^i_{20} \setminus (D^i_{23} \cup D^i_*)$, $D^i_{23} \setminus (D^i_{20} \cup D^i_*)$, or $D^i_{20} \cap D_{23} \setminus D^i_*$, since: $(X^i)^+ \notin D^i_* \cap \{\texttt{mode}^i = 2\} \setminus (D^i_{20} \cup D^i_{23})$ because $\tau^i_{\text{trig}} = 0 < T^i_{\text{max}}$; $(X^i)^+ \notin D^i_{\#2}$ because $\texttt{b}^i = 0 \neq 1$; $(X^i)^+ \notin D^i_{22}$ because $\texttt{b}^i = 0 \neq 1$; $(X^i)^+ \notin D^i_* \cap D^i_{20} \setminus D^i_{23}$ because $\tau^i_{\text{trig}} = 0 < T^i_{\text{max}}$; $(X^i)^+ \notin D^i_* \cap D^i_{23} \setminus D^i_{20}$ because $\tau^i_{\text{trig}} = 0 < T^i_{\text{max}}$; and $(X^i)^+ \notin D^i_* \cap D^i_{20} \cap D^i_{23}$ because $\tau^i_{\text{trig}} = 0 < T^i_{\text{max}}$.

- If $(X^i)^+ \in D^i_{20} \setminus (D^i_{23} \cup D^i_*)$, then according to the partial jump sets in (3–44) and the partial flow sets (3–36)–(3–39) $(X^i)^+ \in \langle\!\langle \{0,1\}^N, \texttt{Plans}^i, \{2\}, \mathcal{F}^*_{\text{in}}, \mathbb{R}^2, \mathbb{R}^2, [\tau^i_o, \infty), \{0\}, [0, \infty), \{1\}\rangle\!\rangle$. If $(X^i)^+ \in D^i_{20} \setminus D^i_{23}$, then the jump map in (3–45) yields $(X^i)^{++} \in \langle\!\langle \{0,1\}^N, \{\texttt{rpl}^i\}, \{0\}, \mathcal{F}^*_{\text{in}}, \mathcal{F}^*_{\text{in}}, \mathcal{F}^*_{\text{in}}, \{0\}, \{0\}, \{0\}, \{1\}\rangle\!\rangle$. For an agent i with $\texttt{mode}^i = 0$, $(X^i)^{++}$ can either be in $C^i_0 \setminus D^i_{01}$ or D^i_{01}.
  - If $(X^i)^{++} \in C^i_0 \setminus D^i_{01}$, then there were two jumps in null-time.
  - If $(X^i)^{++} \in D^i_{01}$, then according to the partial jump sets in (3–44) and the partial flow sets (3–36)–(3–39) $(X^i)^{++} \langle\!\langle \{0,1\}^N, \{\texttt{rpl}^i\}, \{0\}, \{n\}, \{n\}, \{n\}, \{0\}, \{0\}, \{0\}, \{1\}\rangle\!\rangle$. If

$(X^i)^{++} \in D^i_{01}$, then the jump map in (3–45) yields $(X^i)^{+++} \in \langle\!\langle \{0,1\}^N, \{\texttt{rpl}^i\}, \{1\}, \{n\}, \{n\}, \{n\}, \{0\}, \{0\}, \{0\}, \{1\} \rangle\!\rangle$. Then according to the partial jump sets in (3–44) and the partial flow sets (3–36)–(3–39), $(X^i)^{+++}$ must be contained in C^i_1. Therefore, there were three jumps in null-time.

- If $(X^i)^+ \in D^i_{23} \setminus (D^i_{20} \cup D^i_*)$, then according to the partial jump sets in (3–44), and the partial flow sets (3–36)–(3–39), it is only possible for $(X^i)^+$ to be contained in C^i_3 since $(X^i)^+ \notin D^i_{30}$ because $x^i \in \mathcal{F}^{\complement}$. Therefore, there was one jump in null-time.

- If $(X^i)^+ \in D^i_{20} \cap D_{23} \setminus D^i_*$, then the jump map in (3–45) yields $(X^i)^{++} \in \langle\!\langle \{0,1\}^N, \texttt{upd}^i, \{0\}, \mathcal{F}^*_{\text{in}}, \mathcal{F}^*_{\text{in}}, \mathcal{F}^*_{\text{in}}, \{0\}, \{0\}, \{0\}, \{0\} \rangle\!\rangle \cup \langle\!\langle \{0,1\}^N, \texttt{Plans}^i, \{3\}, \mathcal{F}^*_{\text{in}}, \mathbb{R}^2, \mathbb{R}^2, [\tau^i_p, \infty), \{0\}, [0,\infty), \{0\} \rangle\!\rangle$.

  – If $(X^i)^{++} \in \langle\!\langle \{0,1\}^N, \texttt{upd}^i, \{0\}, \mathcal{F}^*_{\text{in}}, \mathcal{F}^*_{\text{in}}, \mathcal{F}^*_{\text{in}}, \{0\}, \{0\}, \{0\}, \{0\} \rangle\!\rangle$, then according to the partial jump sets in (3–44) and the partial flow sets (3–36)–(3–39) implies that $(X)^{++} \in C^i_0 \setminus D^i_{01}$ or $(X)^{++} \in D^i_{01}$.

    * If $(X^i)^{++} \in C^i_0 \setminus D^i_{01}$, then there were two jumps in null-time.

      · If $(X^i)^{++} \in D^i_{01}$, then according to the partial jump sets in (3–44) and the partial flow sets (3–36)–(3–39) $(X^i)^{++} \langle\!\langle \{0,1\}^N, \{\texttt{rpl}^i\}, \{0\}, \{n\}, \{n\}, \{n\}, \{0\}, \{0\}, \{0\}, \{1\} \rangle\!\rangle$. If $(X^i)^+ \in D^i_{01}$, then the jump map in (3–45) yields $(X^i)^{+++} \in \langle\!\langle \{0,1\}^N, \{\texttt{rpl}^i\}, \{1\}, \{n\}, \{n\}, \{n\}, \{0\}, \{0\}, \{0\}, \{1\} \rangle\!\rangle$. Then according to the partial jump sets in (3–44) and the partial flow sets (3–36)–(3–39), $(X^i)^{+++}$ must be contained in C^i_1. Therefore, there were three jumps in null-time.

    * If $(X^i)^{++} \in \langle\!\langle \{0,1\}^N, \texttt{Plans}^i, \{3\}, \mathcal{F}^*_{\text{in}}, \mathbb{R}^2, \mathbb{R}^2, [\tau^i_p, \infty), \{0\}, [0,\infty), \{0\} \rangle\!\rangle$, then according to the partial jump sets in (3–44), and the partial flow sets (3–36)–(3–39), it is only possible for $(X^i)^{++}$ to be contained in D^i_{30}. If $(X^i)^{++} \in D^i_{30}$, then the jump map in (3–45) yields $(X^i)^{+++} \in \langle\!\langle \{0,1\}^N, \{\texttt{rpl}^i\}, \{1\}, \{n\}, \{n\}, \{n\}, \{0\}, \{0\}, \{0\}, \{1\} \rangle\!\rangle$. If $(X^i)^{+++} \in \langle\!\langle \{0,1\}^N, \texttt{upd}^i, \{0\}, \mathcal{F}^*_{\text{in}}, \mathcal{F}^*_{\text{in}}, \mathcal{F}^*_{\text{in}}, \{0\}, \{0\}, \{0\}, \{0\} \rangle\!\rangle$, then according to the partial jump sets in (3–44) and the partial flow sets (3–36)–(3–39) implies that $(X)^{+++} \in C^i_0 \setminus D^i_{01}$ or $(X)^+ \in D^i_{01}$.

      · If $(X^i)^{+++} \in C^i_0 \setminus D^i_{01}$, then there were three jumps in null-time.

      · If $(X^i)^{+++} \in D^i_{01}$, then according to the partial jump sets in (3–44) and the partial flow sets (3–36)–(3–39) $(X^i)^{+++} \langle\!\langle \{0,1\}^N, \{\texttt{rpl}^i\}, \{0\}, \{n\}, \{n\}, \{n\}, \{0\}, \{0\}, \{0\}, \{1\} \rangle\!\rangle$. If $(X^i)^{+++} \in D^i_{01}$, then the jump map in (3–45) yields $(X^i)^{++++} \in \langle\!\langle \{0,1\}^N, \{\texttt{rpl}^i\}, \{1\}, \{n\}, \{n\}, \{n\}, \{0\}, \{0\}, \{0\}, \{1\} \rangle\!\rangle$. Then according

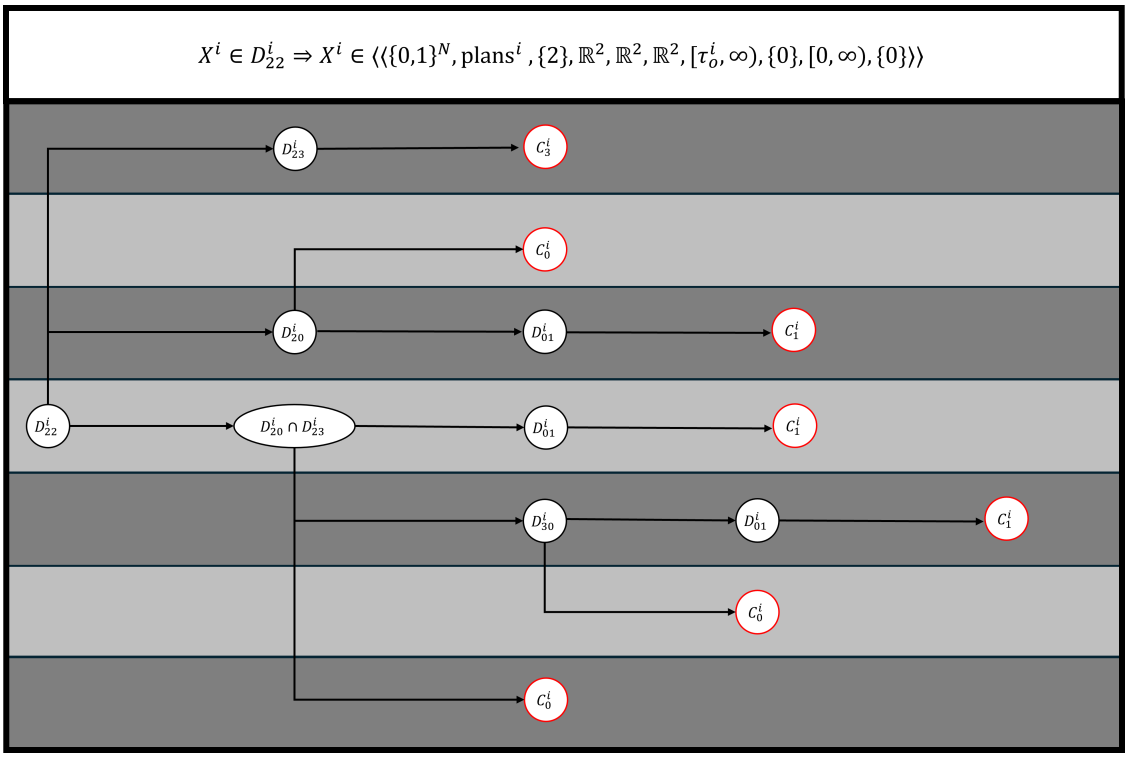

Figure A-17. Directed acyclic graph for $X^i \in D^i_{\#2}$.

to the partial jump sets in (3–44) and the partial flow sets (3–36)–(3–39), $(X^i)^{++++}$ must be contained in C^i_1. Therefore, there were four jumps in null-time.

The possible jump sequences can be visualized in the DAG in Figure A-17.

A.1.10 $X^i \in D^i_{20} \setminus (D^i_* \cup D^i_{23})$

Suppose that there is a state X such that agent $i \in \mathcal{A}$ has the state $X^i \in D^i_{20} \setminus (D^i_* \cup D^i_{23})$, then according to Table A-2, the partial jump sets in (3–44) and the partial flow sets (3–36)–(3–39), $X^i \in \langle\!\langle \{0,1\}^N, \texttt{Plans}^i, \{2\}, \mathcal{F}^*_{\text{in}}, \mathbb{R}^2, \mathbb{R}^2, [\tau^i_o, \tau^i_p), [0, T^i_{\text{max}}), [0, \infty), \{0\} \rangle\!\rangle$. If $X^i \in D^i_{20} \setminus (D^i_* \cup D^i_{23})$, then the jump map in (3–45) yields $(X^i)^+ \in \langle\!\langle \{0,1\}^N, \{\texttt{rpl}^i\}, \{1\}, \{n\}, \{n\}, \{n\}, \{0\}, \{0\}, \{0\}, \{1\} \rangle\!\rangle$. If $(X^i)^+ \in \langle\!\langle \{0,1\}^N, \texttt{upd}^i, \{0\}, \mathcal{F}^*_{\text{in}}, \mathcal{F}^*_{\text{in}}, \mathcal{F}^*_{\text{in}}, \{0\}, \{0\}, \{0\}, \{0\} \rangle\!\rangle$, then according to the partial jump sets in (3–44) and the partial flow sets (3–36)–(3–39) implies that $(X)^+ \in C^i_0 \setminus D^i_{01}$ or $(X)^+ \in D^i_{01}$.

- If $(X^i)^+ \in C^i_0 \setminus D^i_{01}$, then there was one jump in null-time.

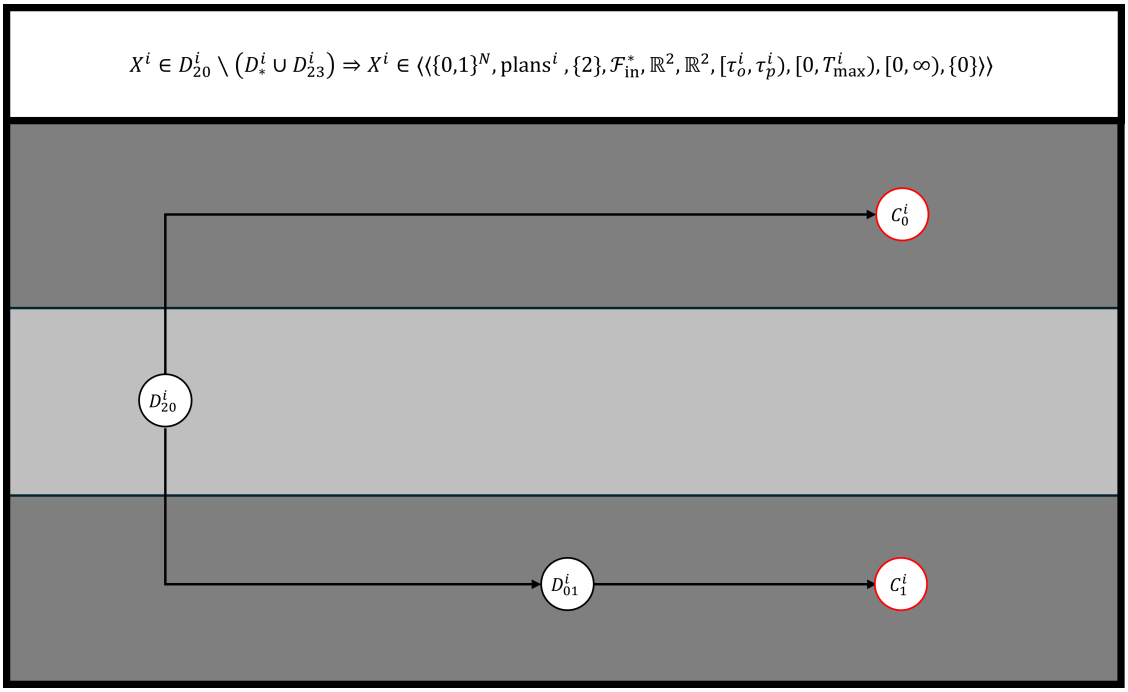

Figure A-18. Directed acyclic graph for $X^i \in D^i_{20} \setminus (D^i_* \cup D^i_{23})$.

– If $(X^i)^+ \in D^i_{01}$, then according to the partial jump sets in (3–44) and the partial flow sets (3–36)–(3–39) $(X^i)^+ \langle\!\langle \{0,1\}^N, \{\texttt{rpl}^i\}, \{0\}, \{n\}, \{n\}, \{n\}, \{0\}, \{0\}, \{0\}, \{1\} \rangle\!\rangle$. If $(X^i)^{+++} \in D^i_{01}$, then the jump map in (3–45) yields $(X^i)^{++} \in \langle\!\langle \{0,1\}^N, \{\texttt{rpl}^i\}, \{1\}, \{n\}, \{n\}, \{n\}, \{0\}, \{0\}, \{0\}, \{1\} \rangle\!\rangle$. Then according to the partial jump sets in (3–44) and the partial flow sets (3–36)–(3–39), $(X^i)^{++}$ must be contained in C^i_1. Therefore, there were two jumps in null-time.

The possible jump sequences can be visualized in the DAG in Figure A-18.

A.1.11 $X^i \in D^i_{23} \setminus (D^i_* \cup D^i_{20})$

Suppose that there is a state X such that agent $i \in \mathcal{A}$ has the state $X^i \in D^i_{23} \setminus (D^i_* \cup D^i_{20})$, then according to Table A-2, the partial jump sets in (3–44) and the partial flow sets (3–36)–(3–39), $X^i \in \langle\!\langle \{0,1\}^N, \texttt{Plans}^i, \{2\}, \mathcal{F}^{\complement}, \mathbb{R}^2, \mathbb{R}^2, [\tau^i_p, \infty), [0, T^i_{\max}), [0,\infty), \{0\} \rangle\!\rangle$. If $X^i \in D^i_{23}$, then the jump map in (3–45) yields $(X^i)^+ \in \langle\!\langle \{0,1\}^N, \texttt{Plans}^i, \{3\}, \mathcal{F}^{\complement}, \mathbb{R}^2, \mathbb{R}^2, [\tau^i_p, \infty), [0, T^i_{\max}), [0,\infty), \{0\} \rangle\!\rangle$. If $(X^i)^+ \in D^i_{23} \setminus (D^i_* \cup D^i_{20})$, then according to the partial jump sets in (3–44), and the partial flow sets (3–36)–(3–39), it is only possible for $(X^i)^+$ to be contained in C^i_3 since $(X^i)^+ \notin D^i_{30}$ because

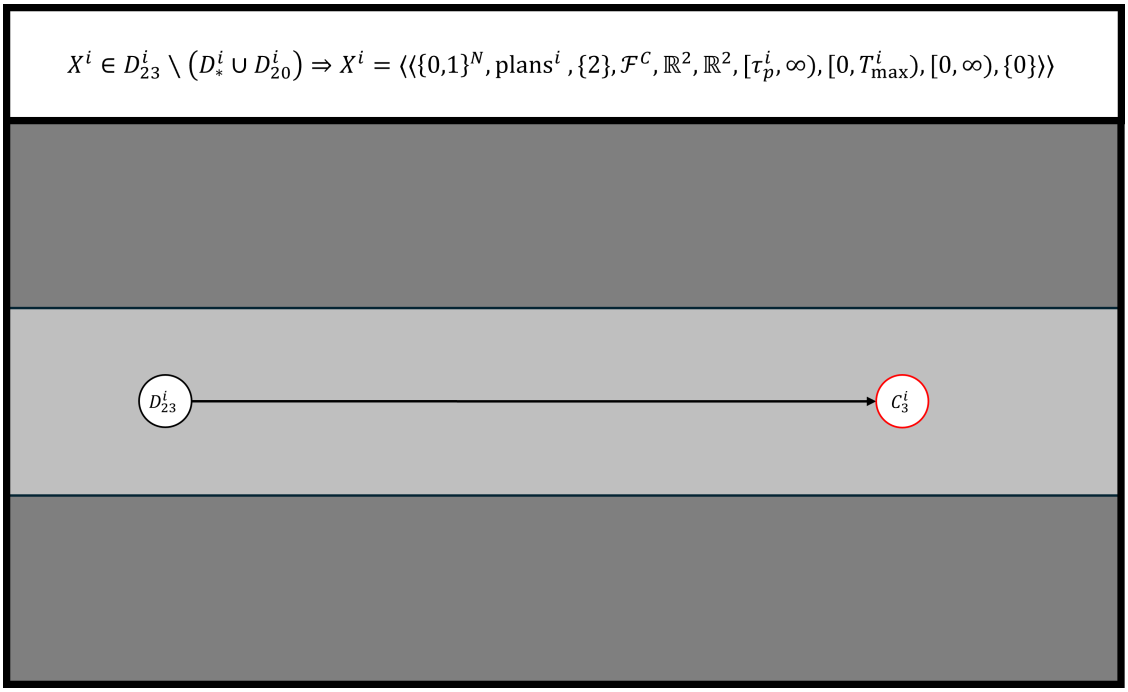

Figure A-19. Directed acyclic graph for $X^i \in D_*^i \cap \{\texttt{mode}^i = 2\} \setminus (D_{20}^i \cup D_{23}^i)$.

$x^i \in \mathcal{F}^{\texttt{C}}$. Therefore, there was one jump in null-time. The possible jump sequences can be visualized in the DAG in Figure A-19.

A.1.12 $X^i \in (D_*^i \cap D_{20}^i) \setminus D_{23}^i$

Suppose that there is a state X such that agent $i \in \mathcal{A}$ has the state $X^i \in (D_*^i \cap D_{20}^i) \setminus D_{23}^i$, then according to the partial jump sets in (3–44) and the partial flow sets (3–36)–(3–39), $X^i \in \left\langle\!\left\langle \{0,1\}^N, \texttt{Plans}^i, \{2\}, \mathcal{F}_{\text{in}}^*, \mathbb{R}^2, \mathbb{R}^2, [\tau_o^i, \tau_p^i), [T_{\max}^i, \infty), [0, \infty), \{0\} \right\rangle\!\right\rangle$. If $X^i \in (D_*^i \cap D_{20}^i) \setminus D_{23}^i$, then the jump map in (3–45) yields $(X^i)^+ \in \left\langle\!\left\langle \{0,1\}^N, \texttt{Plans}^i, \{2\}, \mathcal{F}_{\text{in}}^*, \mathbb{R}^2, \mathbb{R}^2, [\tau_o^i, \tau_p^i), \{0\}, [0, \infty), \{1\} \right\rangle\!\right\rangle \cup \left\langle\!\left\langle \{0,1\}^N, \texttt{Plans}^i, \{0\}, \mathcal{F}_{\text{in}}^*, \mathcal{F}_{\text{in}}^*, \mathcal{F}_{\text{in}}^*, \{0\}, \{0\}, \{0\}, \{0\} \right\rangle\!\right\rangle$.

- If $(X^i)^+ \in \left\langle\!\left\langle \{0,1\}^N, \texttt{Plans}^i, \{2\}, \mathcal{F}_{\text{in}}^*, \mathbb{R}^2, \mathbb{R}^2, [\tau_o^i, \tau_p^i), \{0\}, [0, \infty), \{1\} \right\rangle\!\right\rangle$, then according to the partial jump sets in (3–44) and the partial flow sets (3–36)–(3–39) implies that either $(X)^+ \in D_{\#2}^i$ or $(X)^+ \in D_{22}^i$.
  - If $(X)^+ \in D_{\#2}^i$, then the jump map in (3–45) yields $(X^i)^{++} \in \left\langle\!\left\langle \{0,1\}^N, \texttt{Plans}^i, \{2\}, \mathcal{F}_{\text{in}}^*, \mathbb{R}^2, \mathbb{R}^2, [\tau_o^i, \tau_p^i), \{0\}, [0, \infty), \{0\} \right\rangle\!\right\rangle$. Then according to Table A-2, the partial jump sets in (3–44), and the partial flow sets (3–36)–(3–39), it is only possible for $(X^i)^{++}$ to be contained in D_{20}^i, since:

$(X^i)^{++} \notin D^i_* \cap \{\texttt{mode}^i = 2\} \setminus (D^i_{20} \cup D^i_{23})$ because $\tau^i_{\text{trig}} = 0 < T^i_{\text{max}}$; $(X^i)^{++} \notin D^i_{\#2}$ because $\texttt{b}^i = 0 \neq 1$; $(X^i)^{++} \notin D^i_{22}$ because $\texttt{b}^i = 0 \neq 1$; $(X^i)^{++} \notin D^i_{23} \setminus (D^i_* \cup D^i_{20})$ because $\tau^i < \tau^i_p$; $(X^i)^{++} \notin (D^i_* \cap D^i_{20}) \setminus D^i_{23}$ because $\tau^i_{\text{trig}} = 0 < T^i_{\text{max}}$; $(X^i)^{++} \notin (D^i_* \cap D^i_{23}) \setminus D^i_{20}$ because $\tau^i_{\text{trig}} = 0 < T^i_{\text{max}}$; $(X^i)^{++} \notin D^i_{20} \cap D^i_{23} \setminus D^i_*$ because $\tau^i < \tau^i_p$; and $(X^i)^{++} \notin D^i_* \cap D^i_{20} \cap D^i_{23}$ because $\tau^i_{\text{trig}} = 0 < T^i_{\text{max}}$.

* If $(X^i)^{++} \in D^i_{20}$, then the jump map in (3–45) yields $(X^i)^{+++} \in \langle\!\langle \{0,1\}^N, \texttt{rpl}^i, \{0\}, \mathcal{F}^*_{\text{in}}, \mathcal{F}^*_{\text{in}}, \mathcal{F}^*_{\text{in}}, \{0\}, \{0\}, \{0\}, \{0\} \rangle\!\rangle$. For an agent i with $\texttt{mode}^i = 0$, $(X^i)^{+++}$ can either be in $C^i_0 \setminus D^i_{01}$ or D^i_{01}.

  · If $(X^i)^{+++} \in C^i_0 \setminus D^i_{01}$, then there were three jumps in null-time.

  · If $(X^i)^{+++} \in D^i_{01}$, then according to the partial jump sets in (3–44) and the partial flow sets (3–36)–(3–39) $(X^i)^{+++} \langle\!\langle \{0,1\}^N, \{\texttt{rpl}^i\}, \{0\}, \{n\}, \{n\}, \{n\}, \{0\}, \{0\}, \{0\}, \{1\} \rangle\!\rangle$. If $(X^i)^{+++} \in D^i_{01}$, then the jump map in (3–45) yields $(X^i)^{++++} \in \langle\!\langle \{0,1\}^N, \{\texttt{rpl}^i\}, \{1\}, \{n\}, \{n\}, \{n\}, \{0\}, \{0\}, \{0\}, \{1\} \rangle\!\rangle$. Then according to the partial jump sets in (3–44) and the partial flow sets (3–36)–(3–39), $(X^i)^{++++}$ must be contained in C^i_1. Therefore, there were four jumps in null-time.

– If $(X)^+ \in D^i_{22}$, then the jump map in (3–45) yields $(X^i)^{++} \in \langle\!\langle \{0,1\}^N, \texttt{Plans}^i, \{2\}, \mathcal{F}^*_{\text{in}}, \mathbb{R}^2, \mathbb{R}^2, [\tau^i_o, \tau^i_p), \{0\}, [0,\infty), \{0\} \rangle\!\rangle$. Then according to Table A-2, the partial jump sets in (3–44), and the partial flow sets (3–36)–(3–39), it is only possible for $(X^i)^{++}$ to be contained in D^i_{20}, since: $(X^i)^{++} \notin D^i_* \cap \{\texttt{mode}^i = 2\} \setminus (D^i_{20} \cup D^i_{23})$ because $\tau^i_{\text{trig}} = 0 < T^i_{\text{max}}$; $(X^i)^{++} \notin D^i_{\#2}$ because $\texttt{b}^i = 0 \neq 1$; $(X^i)^{++} \notin D^i_{22}$ because $\texttt{b}^i = 0 \neq 1$; $(X^i)^{++} \notin D^i_{23} \setminus (D^i_* \cup D^i_{20})$ because $\tau^i < \tau^i_p$; $(X^i)^{++} \notin (D^i_* \cap D^i_{20}) \setminus D^i_{23}$ because $\tau^i_{\text{trig}} = 0 < T^i_{\text{max}}$; $(X^i)^{++} \notin (D^i_* \cap D^i_{23}) \setminus D^i_{20}$ because $\tau^i_{\text{trig}} = 0 < T^i_{\text{max}}$; $(X^i)^{++} \notin D^i_{20} \cap D^i_{23} \setminus D^i_*$ because $\tau^i < \tau^i_p$; and $(X^i)^{++} \notin D^i_* \cap D^i_{20} \cap D^i_{23}$ because $\tau^i_{\text{trig}} = 0 < T^i_{\text{max}}$.

* If $(X^i)^{++} \in D^i_{20}$, then the jump map in (3–45) yields $(X^i)^{+++} \in \langle\!\langle \{0,1\}^N, \texttt{rpl}^i, \{0\}, \mathcal{F}^*_{\text{in}}, \mathcal{F}^*_{\text{in}}, \mathcal{F}^*_{\text{in}}, \{0\}, \{0\}, \{0\}, \{0\} \rangle\!\rangle$. For an agent i with $\texttt{mode}^i = 0$, $(X^i)^{+++}$ can either be in $C^i_0 \setminus D^i_{01}$ or D^i_{01}.

  · If $(X^i)^{+++} \in C^i_0 \setminus D^i_{01}$, then there were three jumps in null-time.

  · If $(X^i)^{+++} \in D^i_{01}$, then according to the partial jump sets in (3–44) and the partial flow sets (3–36)–(3–39) $(X^i)^{+++} \langle\!\langle \{0,1\}^N, \{\texttt{rpl}^i\}, \{0\}, \{n\}, \{n\}, \{n\}, \{0\}, \{0\}, \{0\}, \{1\} \rangle\!\rangle$. If $(X^i)^{+++} \in D^i_{01}$, then the jump map in (3–45) yields $(X^i)^{++++} \in \langle\!\langle \{0,1\}^N, \{\texttt{rpl}^i\}, \{1\}, \{n\}, \{n\}, \{n\}, \{0\}, \{0\}, \{0\}, \{1\} \rangle\!\rangle$. Then according

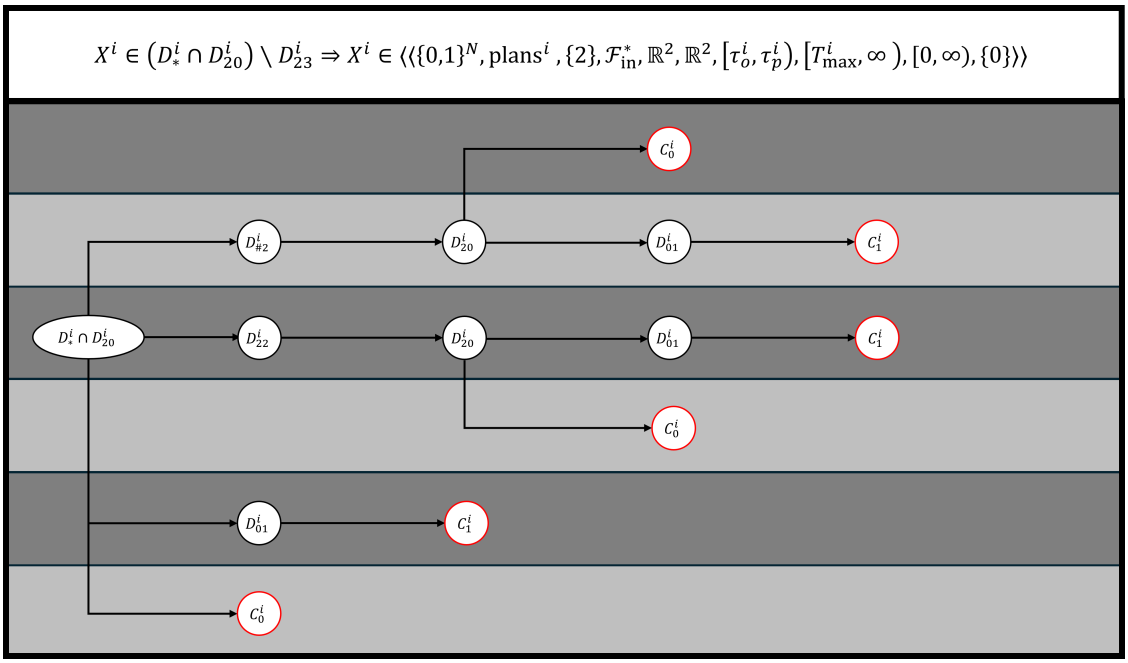

Figure A-20. Directed acyclic graph for $X^i \in (D^i_* \cap D^i_{20}) \setminus D^i_{23}$.

to the partial jump sets in (3–44) and the partial flow sets (3–36)–(3–39), $(X^i)^{++++}$ must be contained in C^i_1. Therefore, there were four jumps in null-time.

- If $(X^i)^+ \in \langle\!\langle \{0,1\}^N, \texttt{Plans}^i, \{0\}, \mathcal{F}^*_{\text{in}}, \mathcal{F}^*_{\text{in}}, \mathcal{F}^*_{\text{in}}, \{0\}, \{0\}, \{0\}, \{0\} \rangle\!\rangle$, then according to the partial jump sets in (3–44) and the partial flow sets (3–36)–(3–39) implies that $(X)^+ \in C^i_0 \setminus D^i_{01}$ or $(X)^+ \in D^i_{01}$.

  – If $(X^i)^+ \in C^i_0 \setminus D^i_{01}$, then there was one jump in null-time.

  – If $(X^i)^+ \in D^i_{01}$, then according to the partial jump sets in (3–44) and the partial flow sets (3–36)–(3–39) $(X^i)^+ \langle\!\langle \{0,1\}^N, \{\texttt{rpl}^i\}, \{0\}, \{n\}, \{n\}, \{n\}, \{0\}, \{0\}, \{0\}, \{1\} \rangle\!\rangle$. If $(X^i)^+ \in D^i_{01}$, then the jump map in (3–45) yields $(X^i)^{++} \in \langle\!\langle \{0,1\}^N, \{\texttt{rpl}^i\}, \{1\}, \{n\}, \{n\}, \{n\}, \{0\}, \{0\}, \{0\}, \{1\} \rangle\!\rangle$. Then according to the partial jump sets in (3–44) and the partial flow sets (3–36)–(3–39), $(X^i)^{++}$ must be contained in C^i_1. Therefore, there were two jumps in null-time.

The possible jump sequences can be visualized in the DAG in Figure A-20.

A.1.13 $X^i \in (D^i_* \cap D^i_{23}) \setminus D^i_{20}$

Suppose that there is a state X such that agent $i \in \mathcal{A}$ has the state $X^i \in (D^i_* \cap D^i_{23}) \setminus D^i_{20}$, then according to the partial jump sets in (3–44) and the partial flow sets (3–36)–(3–39), $X^i \in \langle\!\langle \{0,1\}^N, \texttt{Plans}^i, \{2\}, \mathcal{F}^{\complement}, \mathbb{R}^2, \mathbb{R}^2, [\tau^i_p, \infty), [T^i_{\max}, \infty), [0,\infty), \{0\} \rangle\!\rangle$.

If $X^i \in (D^i_* \cap D^i_{23}) \setminus D^i_{20}$, then the jump map in (3–45) yields

$(X^i)^+ \in \langle\!\langle \{0,1\}^N, \texttt{Plans}^i, \{2\}, \mathcal{F}^{\complement}, \mathbb{R}^2, \mathbb{R}^2, [\tau^i_p, \infty), \{0\}, [0,\infty), \{1\} \rangle\!\rangle \cup$

$\langle\!\langle \{0,1\}^N, \texttt{Plans}^i, \{3\}, \mathcal{F}^{\complement}, \mathbb{R}^2, \mathbb{R}^2, [\tau^i_p, \infty), [T^i_{\mathsf{max}}, \infty), [0,\infty), \{0\} \rangle\!\rangle$.

- If $(X^i)^+ \in \langle\!\langle \{0,1\}^N, \texttt{Plans}^i, \{2\}, \mathcal{F}^{\complement}, \mathbb{R}^2, \mathbb{R}^2, [\tau^i_p, \infty), \{0\}, [0,\infty), \{1\} \rangle\!\rangle$, then according to the partial jump sets in (3–44) and the partial flow sets (3–36)–(3–39) implies that either $(X)^+ \in D^i_{\#2}$ or $(X)^+ \in D^i_{22}$.

  – If $(X)^+ \in D^i_{\#2}$, then the jump map in (3–45) yields $(X^i)^{++} \in \langle\!\langle \{0,1\}^N, \texttt{Plans}^i, \{2\}, \mathcal{F}^{\complement}, \mathbb{R}^2, \mathbb{R}^2, [\tau^i_p, \infty), \{0\}, [0,\infty), \{0\} \rangle\!\rangle$. Then according to Table A-2, the partial jump sets in (3–44), and the partial flow sets (3–36)–(3–39), it is only possible for $(X^i)^{++}$ to be contained in $D^i_{23} \setminus (D^i_* \cup D^i_{20})$, since: $(X^i)^{++} \notin D^i_* \cap \{\texttt{mode}^i = 2\} \setminus (D^i_{20} \cup D^i_{23})$ because $\tau^i_{\mathsf{trig}} = 0 < T^i_{\mathsf{max}}$; $(X^i)^{++} \notin D^i_{\#2}$ because $\texttt{b}^i = 0 \neq 1$; $(X^i)^{++} \notin D^i_{22}$ because $\texttt{b}^i = 0 \neq 1$; $(X^i)^{++} \notin D^i_{20} \setminus (D^i_* \cup D^i_{23})$ because $x^i \in \mathcal{F}^{\complement}$; $(X^i)^{++} \notin (D^i_* \cap D^i_{20}) \setminus D^i_{23}$ because $\tau^i_{\mathsf{trig}} = 0 < T^i_{\mathsf{max}}$; $(X^i)^{++} \notin (D^i_* \cap D^i_{23}) \setminus D^i_{20}$ because $\tau^i_{\mathsf{trig}} = 0 < T^i_{\mathsf{max}}$; $(X^i)^{++} \notin D^i_{20} \cap D^i_{23} \setminus D^i_*$ because $x^i \in \mathcal{F}^{\complement}$; and $(X^i)^{++} \notin D^i_* \cap D^i_{20} \cap D^i_{23}$ because $\tau^i_{\mathsf{trig}} = 0 < T^i_{\mathsf{max}}$. If $(X^i)^{++} \in D^i_{23} \setminus (D^i_* \cup D^i_{20})$, then the jump map in (3–45) yields $(X^i)^{+++} \in \langle\!\langle \{0,1\}^N, \texttt{Plans}^i, \{3\}, \mathcal{F}^{\complement}, \mathbb{R}^2, \mathbb{R}^2, [\tau^i_p, \infty), \{0\}, [0,\infty), \{0\} \rangle\!\rangle$. Then according to the partial jump sets in (3–44), and the partial flow sets (3–36)–(3–39), it is only possible for $(X^i)^{+++}$ to be contained in C^i_3 since $(X^i)^{+++} \notin D^i_{30}$ because $x^i \in \mathcal{F}^{\complement}$. Therefore, there were three jumps in null-time.

  – If $(X)^+ \in D^i_{22}$, then the jump map in (3–45) yields $(X^i)^{++} \in \langle\!\langle \{0,1\}^N, \texttt{Plans}^i, \{2\}, \mathcal{F}^{\complement}, \mathbb{R}^2, \mathbb{R}^2, [\tau^i_p, \infty), \{0\}, [0,\infty), \{0\} \rangle\!\rangle$. Then according to Table A-2, the partial jump sets in (3–44), and the partial flow sets (3–36)–(3–39), it is only possible for $(X^i)^{++}$ to be contained in $D^i_{23} \setminus (D^i_* \cup D^i_{20})$, since: $(X^i)^{++} \notin D^i_* \cap \{\texttt{mode}^i = 2\} \setminus (D^i_{20} \cup D^i_{23})$ because $\tau^i_{\mathsf{trig}} = 0 < T^i_{\mathsf{max}}$; $(X^i)^{++} \notin D^i_{\#2}$ because $\texttt{b}^i = 0 \neq 1$; $(X^i)^{++} \notin D^i_{22}$ because $\texttt{b}^i = 0 \neq 1$; $(X^i)^{++} \notin D^i_{20} \setminus (D^i_* \cup D^i_{23})$ because $x^i \in \mathcal{F}^{\complement}$; $(X^i)^{++} \notin (D^i_* \cap D^i_{20}) \setminus D^i_{23}$ because $\tau^i_{\mathsf{trig}} = 0 < T^i_{\mathsf{max}}$; $(X^i)^{++} \notin (D^i_* \cap D^i_{23}) \setminus D^i_{20}$ because $\tau^i_{\mathsf{trig}} = 0 < T^i_{\mathsf{max}}$; $(X^i)^{++} \notin D^i_{20} \cap D^i_{23} \setminus D^i_*$ because $x^i \in \mathcal{F}^{\complement}$; and $(X^i)^{++} \notin D^i_* \cap D^i_{20} \cap D^i_{23}$ because $\tau^i_{\mathsf{trig}} = 0 < T^i_{\mathsf{max}}$. If $(X^i)^{++} \in D^i_{23} \setminus (D^i_* \cup D^i_{20})$, then the jump map in (3–45) yields $(X^i)^{+++} \in \langle\!\langle \{0,1\}^N, \texttt{Plans}^i, \{3\}, \mathcal{F}^{\complement}, \mathbb{R}^2, \mathbb{R}^2, [\tau^i_p, \infty), \{0\}, [0,\infty), \{0\} \rangle\!\rangle$. Then according to the partial jump sets in (3–44), and the partial flow sets (3–36)–(3–39), it is only possible for $(X^i)^{+++}$ to be contained in C^i_3 since $(X^i)^{+++} \notin D^i_{30}$ because $x^i \in \mathcal{F}^{\complement}$. Therefore, there were three jumps in null-time.

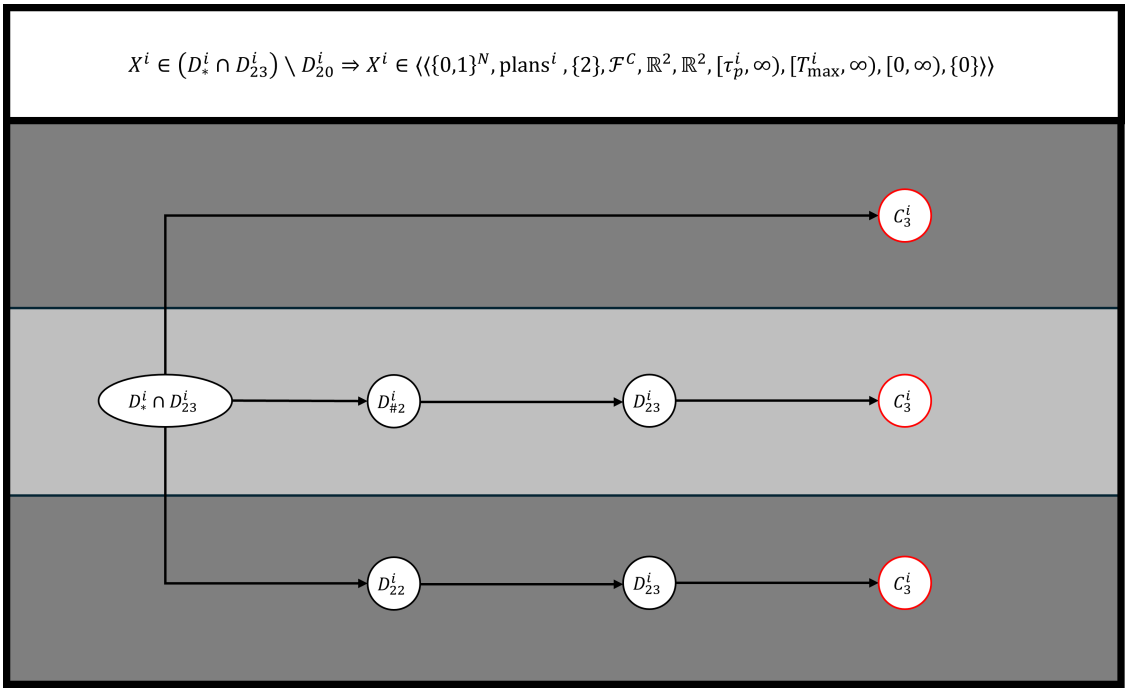

Figure A-21. Directed acyclic graph for $X^i \in (D_*^i \cap D_{23}^i) \setminus D_{20}^i$

- If $(X^i)^+ \in \left\langle\!\left\langle \{0,1\}^N, \texttt{Plans}^i, \{3\}, \mathcal{F}^{\complement}, \mathbb{R}^2, \mathbb{R}^2, [\tau_p^i, \infty), [T_{\max}^i, \infty), [0, \infty), \{0\} \right\rangle\!\right\rangle$, then according to the partial jump sets in (3–44), and the partial flow sets (3–36)–(3–39), it is only possible for $(X^i)^+$ to be contained in C_3^i since $(X^i)^+ \notin D_{30}^i$ because $x^i \in \mathcal{F}^{\complement}$. Therefore, there was one jump in null-time.

The possible jump sequences can be visualized in the DAG in Figure A-21.

A.1.14 $X^i \in D_{20}^i \cap D_{23}^i \setminus D_*^i$

Suppose that there is a state X such that agent $i \in \mathcal{A}$ has the state $X^i \in D_{20}^i \cap D_{23}^i \setminus D_*^i$, then according to the partial jump sets in (3–44) and the partial flow sets (3–36)–(3–39), $X^i \in \left\langle\!\left\langle \{0,1\}^N, \texttt{Plans}^i, \{2\}, \mathcal{F}_{\text{in}}^*, \mathbb{R}^2, \mathbb{R}^2, [\tau_p^i, \infty), [0, T_{\max}^i), [0, \infty), \{0\} \right\rangle\!\right\rangle$. If $X^i \in (D_*^i \cap D_{23}^i) \setminus D_{20}^i$, then the jump map in (3–45) yields

$$(X^i)^+ \in \left\langle\!\left\langle \{0,1\}^N, \texttt{upd}^i, \{0\}, \mathcal{F}_{\text{in}}^*, \mathcal{F}_{\text{in}}^*, \mathcal{F}_{\text{in}}^*, \{0\}, \{0\}, \{0\}, \{0\} \right\rangle\!\right\rangle \cup$$
$$\left\langle\!\left\langle \{0,1\}^N, \texttt{Plans}^i, \{3\}, \mathcal{F}_{\text{in}}^*, \mathbb{R}^2, \mathbb{R}^2, [\tau_p^i, \infty), [0, T_{\max}^i), [0, \infty), \{0\} \right\rangle\!\right\rangle.$$

- If $(X^i)^+ \in \left\langle\!\left\langle \{0,1\}^N, \texttt{upd}^i, \{0\}, \mathcal{F}_{\text{in}}^*, \mathcal{F}_{\text{in}}^*, \mathcal{F}_{\text{in}}^*, \{0\}, \{0\}, \{0\}, \{0\} \right\rangle\!\right\rangle$, then according to the partial jump sets in (3–44) and the partial flow sets (3–36)–(3–39) implies that $(X)^+ \in C_0^i \setminus D_{01}^i$ or $(X)^+ \in D_{01}^i$.
  - If $(X^i)^+ \in C_0^i \setminus D_{01}^i$, then there was one jump in null-time.

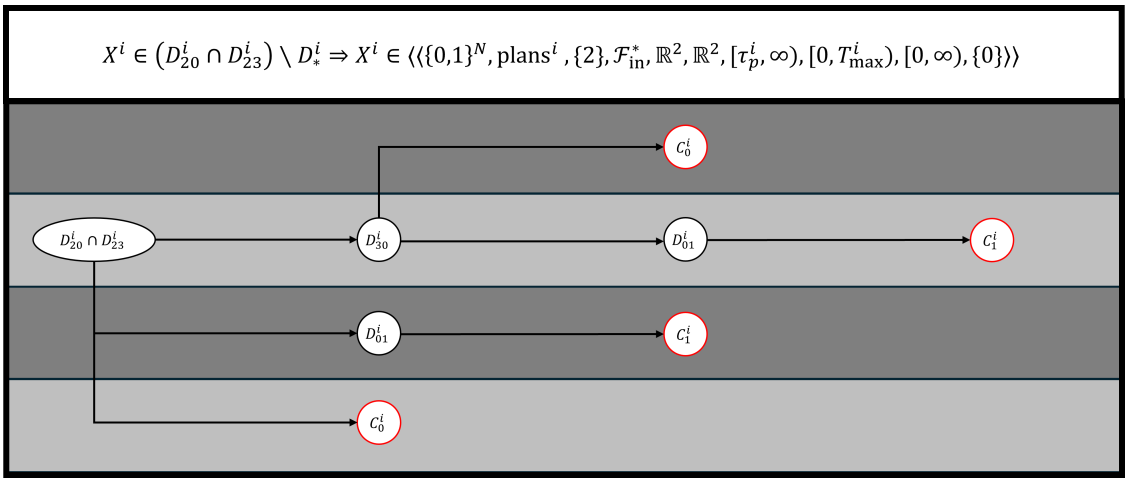

Figure A-22. Directed acyclic graph for $X^i \in D^i_{20} \cap D^i_{23} \setminus D^i_*$.

* If $(X^i)^+ \in D^i_{01}$, then according to the partial jump sets in (3–44) and the partial flow sets (3–36)–(3–39) $(X^i)^+ \left\langle\!\!\left\langle \{0,1\}^N, \{\texttt{rpl}^i\}, \{0\}, \{n\}, \{n\}, \{n\}, \{0\}, \{0\}, \{0\}, \{1\} \right\rangle\!\!\right\rangle$. If $(X^i)^+ \in D^i_{01}$, then the jump map in (3–45) yields $(X^i)^{++} \in \left\langle\!\!\left\langle \{0,1\}^N, \{\texttt{rpl}^i\}, \{1\}, \{n\}, \{n\}, \{n\}, \{0\}, \{0\}, \{0\}, \{1\} \right\rangle\!\!\right\rangle$. Then according to the partial jump sets in (3–44) and the partial flow sets (3–36)–(3–39), $(X^i)^{++}$ must be contained in C^i_1. Therefore, there were two jumps in null-time.

– If $(X^i)^+ \in \left\langle\!\!\left\langle \{0,1\}^N, \texttt{Plans}^i, \{3\}, \mathcal{F}^*_{\text{in}}, \mathbb{R}^2, \mathbb{R}^2, [\tau^i_p, \infty), \{0\}, [0, \infty), \{0\} \right\rangle\!\!\right\rangle$, then according to the partial jump sets in (3–44), and the partial flow sets (3–36)–(3–39), it is only possible for $(X^i)^+$ to be contained in D^i_{30}. If $(X^i)^+ \in D^i_{30}$, then the jump map in (3–45) yields $(X^i)^{++} \in \left\langle\!\!\left\langle \{0,1\}^N, \{\texttt{rpl}^i\}, \{1\}, \{n\}, \{n\}, \{n\}, \{0\}, \{0\}, \{0\}, \{1\} \right\rangle\!\!\right\rangle$. If $(X^i)^{++} \in \left\langle\!\!\left\langle \{0,1\}^N, \texttt{upd}^i, \{0\}, \mathcal{F}^*_{\text{in}}, \mathcal{F}^*_{\text{in}}, \mathcal{F}^*_{\text{in}}, \{0\}, \{0\}, \{0\}, \{0\} \right\rangle\!\!\right\rangle$, then according to the partial jump sets in (3–44) and the partial flow sets (3–36)–(3–39) implies that $(X)^{++} \in C^i_0 \setminus D^i_{01}$ or $(X)^+ \in D^i_{01}$.

* If $(X^i)^{++} \in C^i_0 \setminus D^i_{01}$, then there were two jumps in null-time.

  · If $(X^i)^{++} \in D^i_{01}$, then according to the partial jump sets in (3–44) and the partial flow sets (3–36)–(3–39) $(X^i)^{++} \left\langle\!\!\left\langle \{0,1\}^N, \{\texttt{rpl}^i\}, \{0\}, \{n\}, \{n\}, \{n\}, \{0\}, \{0\}, \{0\}, \{1\} \right\rangle\!\!\right\rangle$. If $(X^i)^{++} \in D^i_{01}$, then the jump map in (3–45) yields $(X^i)^{+++} \in \left\langle\!\!\left\langle \{0,1\}^N, \{\texttt{rpl}^i\}, \{1\}, \{n\}, \{n\}, \{n\}, \{0\}, \{0\}, \{0\}, \{1\} \right\rangle\!\!\right\rangle$. Then according to the partial jump sets in (3–44) and the partial flow sets (3–36)–(3–39), $(X^i)^{+++}$ must be contained in C^i_1. Therefore, there were three jumps in null-time.

The possible jump sequences can be visualized in the DAG in Figure A-22.

A.1.15 $X^i \in D^i_* \cap D^i_{20} \cap D^i_{23}$

Suppose that there is a state X such that agent $i \in \mathcal{A}$ has the state $X^i \in D^i_* \cap D^i_{20} \cap D^i_{23}$, then according to the partial jump sets in (3–44) and the partial flow sets (3–36)–(3–39), $X^i \in \langle\!\langle \{0,1\}^N, \texttt{Plans}^i, \{2\}, \mathcal{F}^*_{\text{in}}, \mathbb{R}^2, \mathbb{R}^2, [\tau^i_p, \infty), [T^i_{\text{max}}, \infty), [0,\infty), \{0\} \rangle\!\rangle$. If $X^i \in D^i_* \cap D^i_{20} \cap D^i_{23}$, then the jump map in (3–45) yields

$(X^i)^+ \in \langle\!\langle \{0,1\}^N, \texttt{Plans}^i, \{2\}, \mathcal{F}^*_{\text{in}}, \mathbb{R}^2, \mathbb{R}^2, [\tau^i_p, \infty), \{0\}, [0,\infty), \{1\} \rangle\!\rangle \cup$

$\langle\!\langle \{0,1\}^N, \texttt{rpl}^i, \{0\}, \mathcal{F}^*_{\text{in}}, \mathcal{F}^*_{\text{in}}, \mathcal{F}^*_{\text{in}}, \{0\}, \{0\}, \{0\}, \{0\} \rangle\!\rangle \cup$

$\langle\!\langle \{0,1\}^N, \texttt{Plans}^i, \{3\}, \mathcal{F}^*_{\text{in}}, \mathbb{R}^2, \mathbb{R}^2, [\tau^i_p, \infty), [T^i_{\text{max}}, \infty), [0,\infty), \{0\} \rangle\!\rangle$.

- If $(X^i)^+ \in \langle\!\langle \{0,1\}^N, \texttt{Plans}^i, \{2\}, \mathcal{F}^*_{\text{in}}, \mathbb{R}^2, \mathbb{R}^2, [\tau^i_p, \infty), \{0\}, [0,\infty), \{1\} \rangle\!\rangle$, then according to the partial jump sets in (3–44) and the partial flow sets (3–36)–(3–39) implies that either $(X)^+ \in D^i_{\#2}$ or $(X)^+ \in D^i_{22}$.

  – If $(X)^+ \in D^i_{\#2}$, then the jump map in (3–45) yields $(X^i)^{++} \in \langle\!\langle \{0,1\}^N, \texttt{Plans}^i, \{2\}, \mathcal{F}^*_{\text{in}}, \mathbb{R}^2, \mathbb{R}^2, [\tau^i_p, \infty), \{0\}, [0,\infty), \{0\} \rangle\!\rangle$. Then according to Table A-2, the partial jump sets in (3–44), and the partial flow sets (3–36)–(3–39), it is only possible for $(X^i)^{++}$ to be contained in $D^i_{20} \cap D_{23} \setminus D^i_*$, since: $(X^i)^{++} \notin D^i_* \cap \{\texttt{mode}^i = 2\} \setminus (D^i_{20} \cup D^i_{23})$ because $\tau^i_{\text{trig}} = 0 < T^i_{\text{max}}$; $(X^i)^{++} \notin D^i_{\#2}$ because $\texttt{b}^i = 0 \neq 1$; $(X^i)^{++} \notin D^i_{22}$ because $\texttt{b}^i = 0 \neq 1$; $(X^i)^{++} \notin D^i_* \cap D^i_{20} \setminus D^i_{23}$ because $\tau^i_{\text{trig}} = 0 < T^i_{\text{max}}$; $(X^i)^{++} \notin D^i_* \cap D^i_{23} \setminus D^i_{20}$ because $\tau^i_{\text{trig}} = 0 < T^i_{\text{max}}$; and $(X^i)^{++} \notin D^i_* \cap D^i_{20} \cap D^i_{23}$ because $\tau^i_{\text{trig}} = 0 < T^i_{\text{max}}$. If $(X^i)^{++} \in D^i_{20} \cap D_{23} \setminus D^i_*$, then the jump map in (3–45) yields $(X^i)^{+++} \in \langle\!\langle \{0,1\}^N, \texttt{upd}^i, \{0\}, \mathcal{F}^*_{\text{in}}, \mathcal{F}^*_{\text{in}}, \mathcal{F}^*_{\text{in}}, \{0\}, \{0\}, \{0\}, \{0\} \rangle\!\rangle \cup \langle\!\langle \{0,1\}^N, \texttt{Plans}^i, \{3\}, \mathcal{F}^*_{\text{in}}, \mathbb{R}^2, \mathbb{R}^2, [\tau^i_p, \infty), \{0\}, [0,\infty), \{0\} \rangle\!\rangle$.

    * If $(X^i)^{+++} \in \langle\!\langle \{0,1\}^N, \texttt{upd}^i, \{0\}, \mathcal{F}^*_{\text{in}}, \mathcal{F}^*_{\text{in}}, \mathcal{F}^*_{\text{in}}, \{0\}, \{0\}, \{0\}, \{0\} \rangle\!\rangle$, then according to the partial jump sets in (3–44) and the partial flow sets (3–36)–(3–39) implies that $(X)^{+++} \in C^i_0 \setminus D^i_{01}$ or $(X)^{++} \in D^i_{01}$.

      · If $(X^i)^{+++} \in C^i_0 \setminus D^i_{01}$, then there were three jumps in null-time.

      · If $(X^i)^{+++} \in D^i_{01}$, then according to the partial jump sets in (3–44) and the partial flow sets (3–36)–(3–39) $(X^i)^{+++} \langle\!\langle \{0,1\}^N, \{\texttt{rpl}^i\}, \{0\}, \{n\}, \{n\}, \{n\}, \{0\}, \{0\}, \{0\}, \{1\} \rangle\!\rangle$. If $(X^i)^{+++} \in D^i_{01}$, then the jump map in (3–45) yields $(X^i)^{+++}+ \in \langle\!\langle \{0,1\}^N, \{\texttt{rpl}^i\}, \{1\}, \{n\}, \{n\}, \{n\}, \{0\}, \{0\}, \{0\}, \{1\} \rangle\!\rangle$. Then according to the partial jump sets in (3–44) and the partial flow sets (3–36)–(3–39), $(X^i)^{++++}$ must be contained in C^i_1. Therefore, there were four jumps in null-time.

* If $(X^i)^{+++} \in \langle\!\langle \{0,1\}^N, \texttt{Plans}^i, \{3\}, \mathcal{F}^*_{\text{in}}, \mathbb{R}^2, \mathbb{R}^2, [\tau^i_p, \infty), \{0\}, [0,\infty), \{0\} \rangle\!\rangle$, then according to the partial jump sets in (3–44), and the partial flow sets (3–36)–(3–39), it is only possible for $(X^i)^{+++}$ to be contained in D^i_{30}. If $(X^i)^{+++} \in D^i_{30}$, then the jump map in (3–45) yields $(X^i)^{++++} \in \langle\!\langle \{0,1\}^N, \{\texttt{rpl}^i\}, \{1\}, \{n\}, \{n\}, \{n\}, \{0\}, \{0\}, \{0\}, \{1\} \rangle\!\rangle$. If $(X^i)^{+++}{+} \in \langle\!\langle \{0,1\}^N, \texttt{upd}^i, \{0\}, \mathcal{F}^*_{\text{in}}, \mathcal{F}^*_{\text{in}}, \mathcal{F}^*_{\text{in}}, \{0\}, \{0\}, \{0\}, \{0\} \rangle\!\rangle$, then according to the partial jump sets in (3–44) and the partial flow sets (3–36)–(3–39) implies that $(X)^{++++} \in C^i_0 \setminus D^i_{01}$ or $(X)^{+} \in D^i_{01}$.

  · If $(X^i)^{++++} \in C^i_0 \setminus D^i_{01}$, then there were four jumps in null-time.

  · If $(X^i)^{++++} \in D^i_{01}$, then according to the partial jump sets in (3–44) and the partial flow sets (3–36)–(3–39) $(X^i)^{++++} \langle\!\langle \{0,1\}^N, \{\texttt{rpl}^i\}, \{0\}, \{n\}, \{n\}, \{n\}, \{0\}, \{0\}, \{0\}, \{1\} \rangle\!\rangle$. If $(X^i)^{++++} \in D^i_{01}$, then the jump map in (3–45) yields $(X^i)^{+++++} \in \langle\!\langle \{0,1\}^N, \{\texttt{rpl}^i\}, \{1\}, \{n\}, \{n\}, \{n\}, \{0\}, \{0\}, \{0\}, \{1\} \rangle\!\rangle$. Then according to the partial jump sets in (3–44) and the partial flow sets (3–36)–(3–39), $(X^i)^{+++++}$ must be contained in C^i_1. Therefore, there were five jumps in null-time.

– If $(X)^{+} \in D^i_{22}$, then the regularization of the jump map in (3–45) yields $(X^i)^{++} \in \langle\!\langle \{0,1\}^N, \texttt{Plans}^i, \{2\}, \mathcal{F}^*_{\text{in}}, \mathbb{R}^2, \mathbb{R}^2, [\tau^i_p, \infty), \{0\}, [0,\infty), \{0\} \rangle\!\rangle$. Then according to Table A-2, the partial jump sets in (3–44), and the partial flow sets (3–36)–(3–39), it is only possible for $(X^i)^{++}$ to be contained in $D^i_{20} \cap D_{23} \setminus D^i_*$, since: $(X^i)^{++} \notin D^i_* \cap \{\texttt{mode}^i = 2\} \setminus (D^i_{20} \cup D^i_{23})$ because $\tau^i_{\text{trig}} = 0 < T^i_{\text{max}}$; $(X^i)^{++} \notin D^i_{\#2}$ because $\texttt{b}^i = 0 \neq 1$; $(X^i)^{++} \notin D^i_{22}$ because $\texttt{b}^i = 0 \neq 1$; $(X^i)^{++} \notin D^i_* \cap D^i_{20} \setminus D^i_{23}$ because $\tau^i_{\text{trig}} = 0 < T^i_{\text{max}}$; $(X^i)^{++} \notin D^i_* \cap D^i_{23} \setminus D^i_{20}$ because $\tau^i_{\text{trig}} = 0 < T^i_{\text{max}}$; and $(X^i)^{++} \notin D^i_* \cap D^i_{20} \cap D^i_{23}$ because $\tau^i_{\text{trig}} = 0 < T^i_{\text{max}}$. If $(X^i)^{++} \in D^i_{20} \cap D_{23} \setminus D^i_*$, then the jump map in (3–45) yields $(X^i)^{+++} \in \langle\!\langle \{0,1\}^N, \texttt{upd}^i, \{0\}, \mathcal{F}^*_{\text{in}}, \mathcal{F}^*_{\text{in}}, \mathcal{F}^*_{\text{in}}, \{0\}, \{0\}, \{0\}, \{0\} \rangle\!\rangle \cup \langle\!\langle \{0,1\}^N, \texttt{Plans}^i, \{3\}, \mathcal{F}^*_{\text{in}}, \mathbb{R}^2, \mathbb{R}^2, [\tau^i_p, \infty), \{0\}, [0,\infty), \{0\} \rangle\!\rangle$.

  * If $(X^i)^{+++} \in \langle\!\langle \{0,1\}^N, \texttt{upd}^i, \{0\}, \mathcal{F}^*_{\text{in}}, \mathcal{F}^*_{\text{in}}, \mathcal{F}^*_{\text{in}}, \{0\}, \{0\}, \{0\}, \{0\} \rangle\!\rangle$, then according to the partial jump sets in (3–44) and the partial flow sets (3–36)–(3–39) implies that $(X)^{+++} \in C^i_0 \setminus D^i_{01}$ or $(X)^{++} \in D^i_{01}$.

    · If $(X^i)^{+++} \in C^i_0 \setminus D^i_{01}$, then there were three jumps in null-time.

    · If $(X^i)^{+++} \in D^i_{01}$, then according to the partial jump sets in (3–44) and the partial flow sets (3–36)–(3–39) $(X^i)^{+++} \langle\!\langle \{0,1\}^N, \{\texttt{rpl}^i\}, \{0\}, \{n\}, \{n\}, \{n\}, \{0\}, \{0\}, \{0\}, \{1\} \rangle\!\rangle$. If $(X^i)^{+++} \in D^i_{01}$, then the jump map in (3–45) yields $(X^i)^{+++}{+} \in \langle\!\langle \{0,1\}^N, \{\texttt{rpl}^i\}, \{1\}, \{n\}, \{n\}, \{n\}, \{0\}, \{0\}, \{0\}, \{1\} \rangle\!\rangle$. Then according to the partial jump sets in (3–44) and the partial flow sets (3–36)–(3–39), $(X^i)^{++++}$ must be contained in C^i_1. Therefore, there were four jumps in null-time.

* If $(X^i)^{+++} \in \langle\!\langle \{0,1\}^N, \texttt{Plans}^i, \{3\}, \mathcal{F}^*_{\text{in}}, \mathbb{R}^2, \mathbb{R}^2, [\tau^i_p, \infty), \{0\}, [0,\infty), \{0\} \rangle\!\rangle$, then according to the partial jump sets in (3–44), and the partial flow sets (3–36)–(3–39), it is only possible for $(X^i)^{+++}$ to be contained in D^i_{30}. If $(X^i)^{+++} \in D^i_{30}$, then the jump map in (3–45) yields $(X^i)^{++++} \in \langle\!\langle \{0,1\}^N, \{\texttt{rpl}^i\}, \{1\}, \{n\}, \{n\}, \{n\}, \{0\}, \{0\}, \{0\}, \{1\} \rangle\!\rangle$. If $(X^i)^{+++}{+} \in \langle\!\langle \{0,1\}^N, \texttt{upd}^i, \{0\}, \mathcal{F}^*_{\text{in}}, \mathcal{F}^*_{\text{in}}, \mathcal{F}^*_{\text{in}}, \{0\}, \{0\}, \{0\}, \{0\} \rangle\!\rangle$, then according to the partial jump sets in (3–44) and the partial flow sets (3–36)–(3–39) implies that $(X)^{++++} \in C^i_0 \setminus D^i_{01}$ or $(X)^+ \in D^i_{01}$.

  · If $(X^i)^{++++} \in C^i_0 \setminus D^i_{01}$, then there were four jumps in null-time.

  · If $(X^i)^{++++} \in D^i_{01}$, then according to the partial jump sets in (3–44) and the partial flow sets (3–36)–(3–39) $(X^i)^{++++} \langle\!\langle \{0,1\}^N, \{\texttt{rpl}^i\}, \{0\}, \{n\}, \{n\}, \{n\}, \{0\}, \{0\}, \{0\}, \{1\} \rangle\!\rangle$. If $(X^i)^{++++} \in D^i_{01}$, then the jump map in (3–45) yields $(X^i)^{+++++} \in \langle\!\langle \{0,1\}^N, \{\texttt{rpl}^i\}, \{1\}, \{n\}, \{n\}, \{n\}, \{0\}, \{0\}, \{0\}, \{1\} \rangle\!\rangle$. Then according to the partial jump sets in (3–44) and the partial flow sets (3–36)–(3–39), $(X^i)^{+++++}$ must be contained in C^i_1. Therefore, there were five jumps in null-time.

- If $(X^i)^+ \in \langle\!\langle \{0,1\}^N, \texttt{rpl}^i, \{0\}, \mathcal{F}^*_{\text{in}}, \mathcal{F}^*_{\text{in}}, \mathcal{F}^*_{\text{in}}, \{0\}, \{0\}, \{0\}, \{0\} \rangle\!\rangle$, then according to the partial jump sets in (3–44) and the partial flow sets (3–36)–(3–39) implies that $(X)^+ \in C^i_0 \setminus D^i_{01}$ or $(X)^+ \in D^i_{01}$.

  – If $(X^i)^+ \in C^i_0 \setminus D^i_{01}$, then there was one jump in null-time.

  – If $(X^i)^+ \in D^i_{01}$, then according to the partial jump sets in (3–44) and the partial flow sets (3–36)–(3–39) $(X^i)^+ \langle\!\langle \{0,1\}^N, \{\texttt{rpl}^i\}, \{0\}, \{n\}, \{n\}, \{n\}, \{0\}, \{0\}, \{0\}, \{1\} \rangle\!\rangle$. If $(X^i)^+ \in D^i_{01}$, then the jump map in (3–45) yields $(X^i)^{++} \in \langle\!\langle \{0,1\}^N, \{\texttt{rpl}^i\}, \{1\}, \{n\}, \{n\}, \{n\}, \{0\}, \{0\}, \{0\}, \{1\} \rangle\!\rangle$. Then according to the partial jump sets in (3–44) and the partial flow sets (3–36)–(3–39), $(X^i)^{++}$ must be contained in C^i_1. Therefore, there were two jumps in null-time.

- If $(X^i)^+ \in \langle\!\langle \{0,1\}^N, \texttt{Plans}^i, \{3\}, \mathcal{F}^*_{\text{in}}, \mathbb{R}^2, \mathbb{R}^2, [\tau^i_p, \infty), [T^i_{\text{max}}, \infty), [0,\infty), \{0\} \rangle\!\rangle$, then according to the partial jump sets in (3–44), and the partial flow sets (3–36)–(3–39), it is only possible for $(X^i)^+$ to be contained in D^i_{30}. If $(X^i)^+ \in D^i_{30}$, then the jump map in (3–45) yields $(X^i)^{++} \in \langle\!\langle \{0,1\}^N, \{\texttt{rpl}^i\}, \{1\}, \{n\}, \{n\}, \{n\}, \{0\}, \{0\}, \{0\}, \{1\} \rangle\!\rangle$. If $(X^i)^{++} \in \langle\!\langle \{0,1\}^N, \texttt{upd}^i, \{0\}, \mathcal{F}^*_{\text{in}}, \mathcal{F}^*_{\text{in}}, \mathcal{F}^*_{\text{in}}, \{0\}, \{0\}, \{0\}, \{0\} \rangle\!\rangle$, then according to the partial jump sets in (3–44) and the partial flow sets (3–36)–(3–39) implies that $(X)^{++} \in C^i_0 \setminus D^i_{01}$ or $(X)^+ \in D^i_{01}$.

  – If $(X^i)^{++} \in C^i_0 \setminus D^i_{01}$, then there were two jumps in null-time.

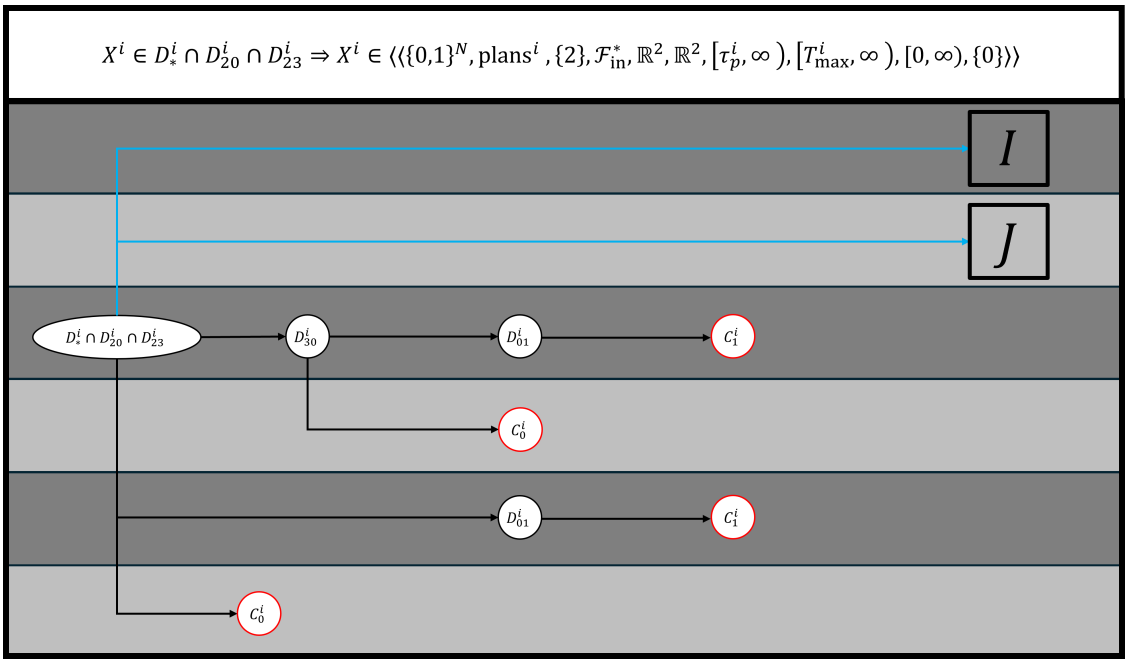

Figure A-23. Directed acyclic graph for $X^i \in D^i_* \cap D^i_{20} \cap D^i_{23}$. This graph continues to Figures A-24–A-25.

* If $(X^i)^{++} \in D^i_{01}$, then according to the partial jump sets in (3–44) and the partial flow sets (3–36)–(3–39) $(X^i)^{++} \langle\!\langle \{0,1\}^N, \{\texttt{rpl}^i\}, \{0\}, \{n\}, \{n\}, \{n\}, \{0\}, \{0\}, \{0\}, \{1\} \rangle\!\rangle$. If $(X^i)^{++} \in D^i_{01}$, then the jump map in (3–45) yields $(X^i)^{+++} \in \langle\!\langle \{0,1\}^N, \{\texttt{rpl}^i\}, \{1\}, \{n\}, \{n\}, \{n\}, \{0\}, \{0\}, \{0\}, \{1\} \rangle\!\rangle$. Then according to the partial jump sets in (3–44) and the partial flow sets (3–36)–(3–39), $(X^i)^{+++}$ must be contained in C^i_1. Therefore, there were three jumps in null-time.

The possible jump sequences can be visualized in the DAGs in Figures A-23–A-25.

A.1.16 $X^i \in D^i_{30}$

Suppose that there is a state X such that agent $i \in \mathcal{A}$ has the state $X^i \in D^i_{30}$, then according to the partial jump sets in (3–44) and the partial flow sets (3–36)–(3–39), $X^i \in \langle\!\langle \{0,1\}^N, \texttt{Plans}^i, \{3\}, \mathcal{F}^*_{\text{in}}, \mathbb{R}^2, \mathbb{R}^2, [\tau^i_p, \infty), [0,\infty), [0,\infty), \{0\} \rangle\!\rangle$. If $X^i \in D^i_{30}$, then the jump map in (3–45) yields $(X^i)^+ \in \langle\!\langle \{0,1\}^N, \{\texttt{rpl}^i\}, \{1\}, \{n\}, \{n\}, \{n\}, \{0\}, \{0\}, \{0\}, \{1\} \rangle\!\rangle$. If $(X^i)^+ \in \langle\!\langle \{0,1\}^N, \texttt{upd}^i, \{0\}, \mathcal{F}^*_{\text{in}}, \mathcal{F}^*_{\text{in}}, \mathcal{F}^*_{\text{in}}, \{0\}, \{0\}, \{0\}, \{0\} \rangle\!\rangle$, then according to the partial jump sets in (3–44) and the partial flow sets (3–36)–(3–39) implies that $(X)^+ \in C^i_0 \setminus D^i_{01}$ or $(X)^+ \in D^i_{01}$.

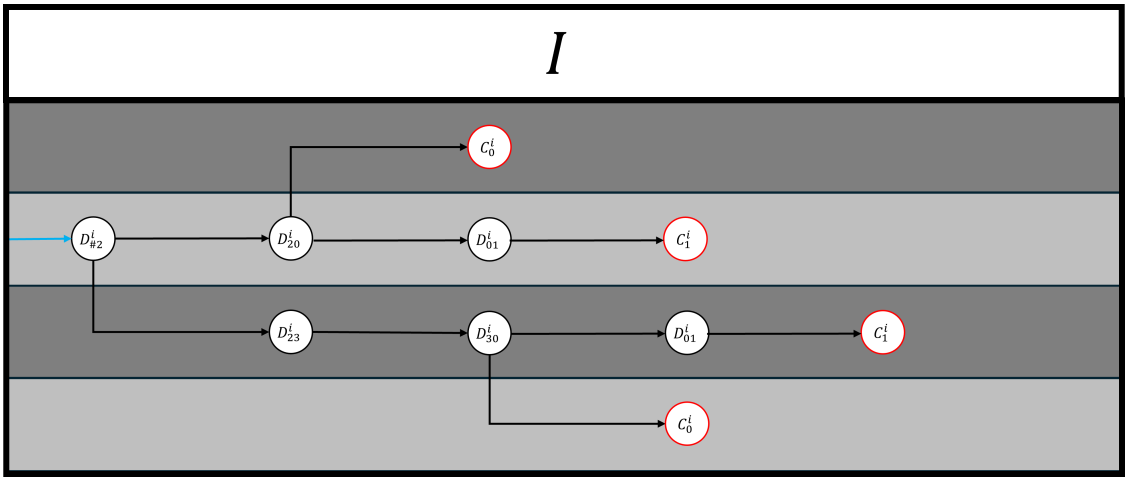

Figure A-24. Continuation of the directed acyclic graph in Figure A-23.

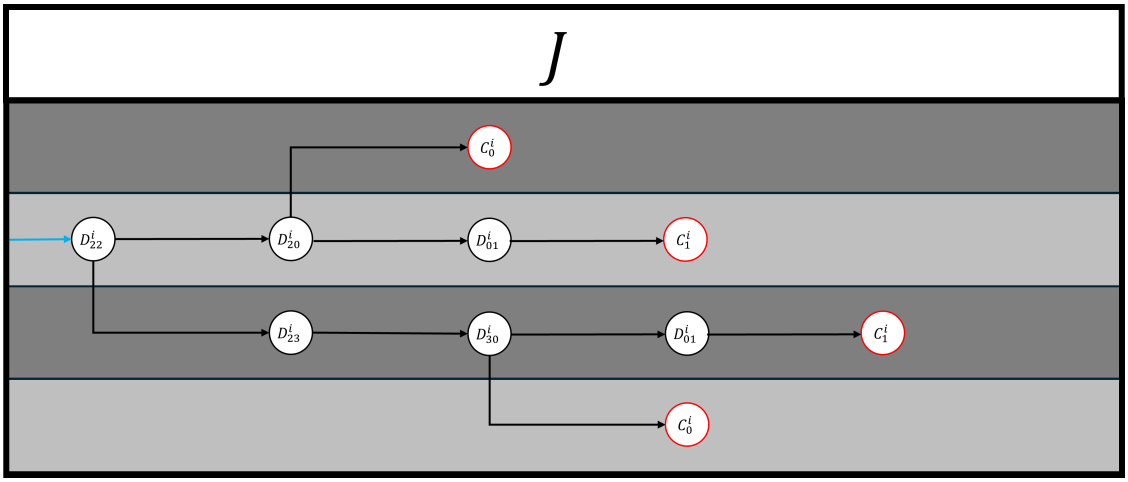

Figure A-25. Continuation of the directed acyclic graph in Figure A-23.

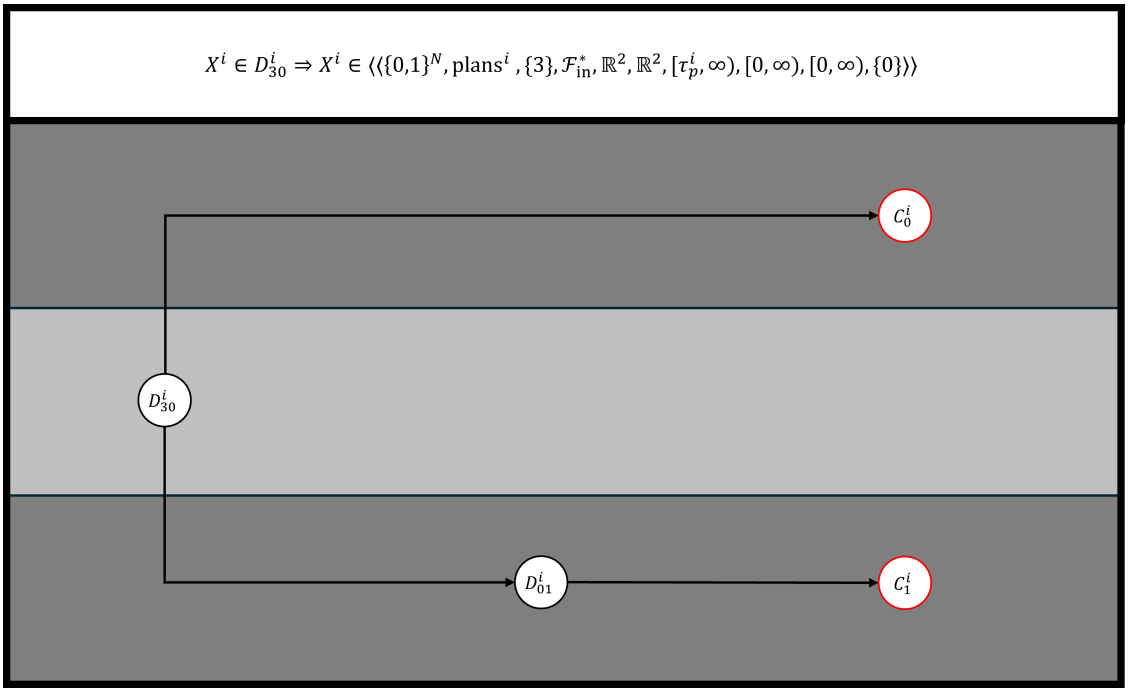

Figure A-26. Directed acyclic graph for $X^i \in D_{30}^i$.

- If $(X^i)^+ \in C_0^i \setminus D_{01}^i$, then there was one jump in null-time.

  – If $(X^i)^+ \in D_{01}^i$, then according to the partial jump sets in (3–44) and the partial flow sets (3–36)–(3–39) $(X^i)^+ \left\langle\!\left\langle \{0,1\}^N, \{\texttt{rpl}^i\}, \{0\}, \{n\}, \{n\}, \{n\}, \{0\}, \{0\}, \{0\}, \{1\} \right\rangle\!\right\rangle$. If $(X^i)^{+++} \in D_{01}^i$, then the jump map in (3–45) yields $(X^i)^{++} \in \left\langle\!\left\langle \{0,1\}^N, \{\texttt{rpl}^i\}, \{1\}, \{n\}, \{n\}, \{n\}, \{0\}, \{0\}, \{0\}, \{1\} \right\rangle\!\right\rangle$. Then according to the partial jump sets in (3–44) and the partial flow sets (3–36)–(3–39), $(X^i)^{++}$ must be contained in C_1^i. Therefore, there were two jumps in null-time.

The possible jump sequences can be visualized in the DAG in Figure A-26.

APPENDIX B
MATLAB® IMPLEMENTATION OF TARGETREGION

The TargetRegion function can be implemented in MATLAB®, specifically using the operations for PolyShape objects (i.e., isinterior, convhull, intersect, subtract, union, and regions) from MATLAB®'s Computational Geometry library. In addition to this, findPoint(R) is a generic function that takes a polyShape object, representing a polygon $R \subset \mathbb{R}^2$, as an input, and outputs a double, represnting a point $p \in \mathbb{R}^2$ that is contained within R. The MATLAB® implimentation and desciption is now given: TargetRegion $=$ MakeTargetRegion$($BoundingRegion, FeedbackRegion, Uinit$)$ returns the target region for a given bounding region R, feedback region $\mathcal{F}$, and initial region of uncertainty $U(t_j^u, t)$, according to Algorithm 4.1. TargetRegion, BoundingRegion, and FeedbackRegion are polyshape objects, whereas Uinit (the initial region of uncertainty) can either be a polyshape object or a double (i.e., when the region of uncertainity is defined by a single point).

```
function TargetRegion = MakeTargetRegion(BoundingRegion,
   FeedbackRegion,Uinit)
        if isa(Uinit,'double')
                B = subtract(BoundingRegion,FeedbackRegion);
                BRegions = regions(B);
                [Blength,~] = size(BRegions);
                TargetRegion = BoundingRegion;
                for i = 1:Blength
                        if isinterior(BRegions(j),Uinit)
                                TargetRegion = subtract(
                                   TargetRegion,BRegions(j));
                        end
                end
```

```
        else
                A = subtract(Uinit,FeedbackRegion);
                B = subtract(BoundingRegion,FeedbackRegion);
                ARegions = regions(A);
                BRegions = regions(B);
                [Alength,~] = size(ARegions);
                [Blength,~] = size(BRegions);
                TargetRegion = BoundingRegion;
                for i = 1:Alength
                        [px,py] = findPoint(ARegions(i));
                        for j = 1:Blength
                                if isinterior(BRegions(j),[px,
                                   py])
                                        TargetRegion = subtract
                                           (TargetRegion,
                                           BRegions(j));
                                end
                        end
                end
        end
end
```

REFERENCES

[1] K. Okamoto and P. Tsiotras, "Optimal stochastic vehicle path planning using covariance steering," *IEEE Robot. Autom. Lett.*, vol. 4, no. 3, pp. 2276–2281, 2019.

[2] B. T. Demoz Gebre-Egziabher, "Impact and mitigation of gps-unavailability onsmall uav navigation, guidance and control," 2012. [Online]. Available: https://conservancy.umn.edu/bitstream/handle/11299/170849/White_Paper_UAV_Operation_in_GPS_Denied_Environment_Nov_19_2012.pdf?isAllowed=y&sequence=21

[3] K. A. F. Base, "Joint navigation warfare center," 2022. [Online]. Available: https://www.kirtland.af.mil/Units/Joint-Navigation-Warfare-Center/

[4] T. T. Patterson, "Bridging the gap: How an airborne mobile mesh network can overcome space vulnerabilities in tomorrow's fight," 2018.

[5] K. McCaney, "DoD puts emphasis on Navigation Warfare, accurate GPS signals," 2015. [Online]. Available: https://defensesystems.com/it-infrastructure/2015/02/dod-puts-emphasis-on-navigation-warfare-accurate-gps-signals/190637/

[6] USASMDC/ARSTRAT, "Navigation warfare," 2016. [Online]. Available: https://www.army.mil/standto/archive/2016/09/07/

[7] M. Gilday, "Cybersecurity: More than a buzzword," 2019. [Online]. Available: https://www.navy.mil/Resources/Blogs/Detail/Article/2268199/cybersecurity-more-than-a-buzzword/

[8] S. Waterman, "Nasa seeks wider use of gps: Not from space, but in space," 2019. [Online]. Available: https://www.satellitetoday.com/government-military/2019/06/21/nasa-seeks-wider-use-of-gps-not-from-space-but-in-space/

[9] Smithsonian, "Time and navigation: Navigating in deep space," 2022. [Online]. Available: https://timeandnavigation.si.edu/navigating-space/deep-space

[10] G. Awesomeness, 2014. [Online]. Available: https://geoawesomeness.com/wp-content/uploads/2014/01/urbancanyon.jpg

[11] S. Hutchinson, G. Hager, and P. Corke, "A tutorial on visual servo control," *IEEE Trans. Robot. Autom.*, vol. 12, no. 5, pp. 651–670, Oct. 1996.

[12] G. Hu, N. Gans, N. Fitz-Coy, and W. E. Dixon, "Adaptive homography-based visual servo tracking control via a quaternion formulation," *IEEE Trans. Control Syst. Technol.*, vol. 18, no. 1, pp. 128–135, 2010. [Online]. Available: http://ncr.mae.ufl.edu/papers/CST10.pdf

[13] J. Chen, D. M. Dawson, W. E. Dixon, and V. Chitrakaran, "Navigation function based visual servo control," *Automatica*, vol. 43, pp. 1165–1177, 2007. [Online]. Available: http://ncr.mae.ufl.edu/papers/auto07.pdf

[14] G. Palmieri, M. Palpacelli, M. Battistelli, and M. Callegari, “A comparison between position-based and image-based dynamic visual servoings in the control of a translating parallel manipulator,” *J. Robot.*, vol. 2012, 2012.

[15] S. S. Mehta, G. Hu, A. P. Dani, and W. E. Dixon, “Multi-reference visual servo control of an unmanned ground vehicle,” in *Proc. AIAA Guid. Navig. Control Conf.*, Honolulu, Hawaii, Aug. 2008.

[16] B. Jia and S. Liu, “Switched visual servo control of nonholonomic mobile robots with field-of-view constraints based on homography,” *Control Theory Technol.*, vol. 13, no. 4, pp. 311–320, 2015.

[17] G. Klein and D. Murray, “Parallel tracking and mapping for small ar workspaces,” in *IEEE ACM Int. Symp. Mixed Augment. Real.*, 2007, pp. 225–234.

[18] A. J. Davison, I. D. Reid, N. D. Molton, and O. Stasse, “MonoSLAM: Real-time single camera SLAM,” *IEEE Trans. Pattern Anal. Mach. Intell.*, vol. 29, no. 6, pp. 1052–1067, Jun. 2007.

[19] D. Cremers, “Direct methods for 3d reconstruction and visual slam,” in *IEEE IAPR Int. Conf. Mach. Vis. Appl.*, 2017, pp. 34–38.

[20] B. Williams, M. Cummins, J. Neira, P. Newman, I. Reid, and J. Tardós, “A comparison of loop closing techniques in monocular SLAM,” *Robot. Auton. Syst.*, vol. 57, no. 12, pp. 1188–1197, 2009.

[21] C. Cadena, L. Carlone, H. Carrillo, Y. Latif, D. Scaramuzza, J. Neira, I. Reid, and J. Leonard, “Past, present, and future of simultaneous localization and mapping: Towards the robust-perception age,” *IEEE Trans. Robot.*, vol. 32, no. 6, pp. 1309–1332, 2016.

[22] H.-Y. Chen, Z. I. Bell, P. Deptula, and W. E. Dixon, “A switched systems framework for path following with intermittent state feedback,” *IEEE Control Syst. Lett.*, vol. 2, no. 4, pp. 749–754, Oct. 2018.

[23] R. Sun, C. Harris, Z. Bell, and W. E. Dixon, “Relay-explorer approach for multi-agent exploration of an unknown environment with intermittent communication,” in *Proc. IEEE Conf. Decis. Control*, 2020, pp. 5218–5223.

[24] R. Sun, Z. Bell, F. Zegers, and W. E. Dixon, “A switched systems approach to unknown environment exploration with intermittent state feedback for nonholonomic systems,” in *Proc. Am. Control Conf.*, 2020, pp. 5275–5280.

[25] D. Le, H.-Y. Chen, A. R. Teel, and W. E. Dixon, “Path following with stable and unstable modes subject to time-varying dwell-time conditions,” in *IFAC World Congr.*, 2020.

[26] D. Le, A. R. Teel, and W. E. Dixon, “A switched system dwell-time update mechanism for path following with intermittent state feedback constraints,” *IEEE Trans. Autom. Control*, 2024.

[27] S. Edwards, D. Le, D. Guralnik, and W. E. Dixon, “A topologically inspired path-following method with intermittent state feedback,” *IEEE Robot. Automat. Lett.*, vol. 6, no. 3, pp. 4449–4456, 2021.

[28] F. Zegers, H.-Y. Chen, P. Deptula, and W. E. Dixon, “Distributed coordination of a multi-agent system with intermittent communication: A switched systems approach,” in *Proc. ASME Dyn. Syst. Control Conf.*, 2018.

[29] C. J. Taylor and J. Spletzer, “A bounded uncertainty approach to cooperative localization using relative bearing constraints,” in *Int. Conf. Intell. Robot. Sys.*, 2007, pp. 2500–2506.

[30] M. Z. W. Henk Wymeersch, Jaime Lien, “Cooperative localization in wireless networks,” *Proc. IEEE*, 2009.

[31] J. P. H. Prabir Barooah, Wm. Joshua Russell, “Approximate distributed kalman filtering for cooperative multi-agent localization,” *Springer Berlin Heidelberg*, 2010.

[32] M. Wei, R. Aragues, C. Sagues, and G. C. Calafiore, “Noisy range network localization based on distributed multidimensional scaling,” *IEEE Sens. J.*, 2015.

[33] N. Gans, G. Hu, K. Nagarajan, and W. E. Dixon, “Keeping multiple moving targets in the field of view of a mobile camera,” *IEEE Trans. Robot. Autom.*, vol. 27, no. 4, pp. 822–828, 2011. [Online]. Available: http://ncr.mae.ufl.edu/papers/TRO11.pdf

[34] L. Wren, J. Thornton, D. White, and J. Dale, “Autonomous target reacquisition after image disturbance,” in *Acquisition, Tracking, and Pointing XX*, vol. 6238. SPIE, 2006, pp. 41–50.

[35] W. E. Dixon, *Encyclopedia of Systems and Control*. Springer, 2020, ch. Intermittent Image-Based Estimation, pp. 1–4.

[36] G. P. Huang, A. I. Mourikis, and S. I. Roumeliotis, “A quadratic-complexity observability-constrained unscented Kalman filter for SLAM,” *IEEE Trans. Robot.*, vol. 29, no. 5, pp. 1226–1243, Oct. 2013.

[37] N. Wang, Y. Gao, H. Zhao, and C. K. Ahn, “Reinforcement learning-based optimal tracking control of an unknown unmanned surface vehicle,” *IEEE Trans. Neural Netw. Learn. Syst.*, vol. 32, no. 7, pp. 3034–3045, 2020.

[38] M. Montemerlo, S. Thrun, D. Koller, and B. Wegbreit, “FastSLAM 2.0: An improved particle filtering algorithm for simultaneous localization and mapping that provably converges,” in *Proc. Int. Joint Conf. Artif. Intell.*, 2003, pp. 1151–1156.

[39] A. Pulido, K. Volle, K. Waters, Z. I. Bell, P. Ganesh, and J. Shin, "Uncertainty-aware guidance for target tracking subject to intermittent measurements using motion model learning," *arXiv preprint arXiv:2402.00671*, 2024.

[40] J. Sola, A. Monin, M. Devy, and T. Vidal-Calleja, "Fusing monocular information in multicamera SLAM," *IEEE Trans. Robot.*, vol. 24, no. 5, pp. 958–968, Oct. 2008.

[41] A. Parikh, T.-H. Cheng, H.-Y. Chen, and W. E. Dixon, "A switched systems framework for guaranteed convergence of image-based observers with intermittent measurements," *IEEE Trans. Robot.*, vol. 33, no. 2, pp. 266–280, April 2017.

[42] A. Parikh, R. Kamalapurkar, and W. E. Dixon, "Target tracking in the presence of intermittent measurements via motion model learning," *IEEE Trans. Robot.*, vol. 34, no. 3, pp. 805–819, 2018.

[43] A. Parikh, T.-H. Cheng, R. Licitra, and W. E. Dixon, "A switched systems approach to image-based localization of targets that temporarily leave the camera field of view," *IEEE Trans. Control Syst. Technol.*, vol. 26, no. 6, pp. 2149–2156, 2018.

[44] L. Zhang, S. Wang, B. Cai, T. Liu, and Y. Cheng, "Switching control of a mecanum wheeled mobile robot for vision-based tracking with intermittent image losses," in *IEEE Int. Conf. Syst., Man and Cybern.*, 2019, pp. 493–499.

[45] M. J. McCourt, Z. I. Bell, and S. A. Nivison, "Passivity-based target tracking robust to intermittent measurements," in *Am. Control Conf.*, 2022, pp. 1626–1631.

[46] Y. Liang, J. Yang, L. Zhang, S. Baldi, and B. De Schutter, "Switched control design for quadrotor in target tracking with complex intermittent measurements," *Journal Guid., Control, and Dyn.*, vol. 46, no. 1, pp. 206–214, 2023.

[47] Z. Bell, R. Sun, K. Volle, P. Ganesh, S. Nivison, and W. E. Dixon, "Target tracking subject to intermittent measurements using attention deep neural networks," *IEEE Control Syst. Lett.*, vol. 7, pp. 379–384, 2023.

[48] D. Liberzon, *Switching in Systems and Control*. Birkhauser, 2003.

[49] R. Goebel, R. G. Sanfelice, and A. R. Teel, *Hybrid Dynamical Systems*. Princeton University Press, 2012.

[50] D. S. Bernstein, *Matrix Mathematics*. Princeton university press, 2009.

[51] J. Gallier and D. Xu, *A Guide to the Classification Theorem for Compact Surfaces*. Springer, 2012, ch. Appendix E, pp. 157–163.

[52] A. Hatcher, *Algebraic Topology*. Cambridge University Press, Cambridge, 2002, 2002. [Online]. Available: http://www.math.cornell.edu/~hatcher/AT/ATpage.html

[53] M. Brown, "A proof of the generalized Schoenflies theorem," *Bull. Am. Math. Soc.*, vol. 66, no. 2, pp. 74–76, 1960.

[54] R. Burns, B. Dubrovin, A. Fomenko, and S. Novikov, *Modern Geometry–Methods and Applications: Part II: The Geometry and Topology of Manifolds*. Springer, 2012.

[55] E. Moulay and W. Perruquett, "Finite time stability and stabilization of a class of continuous systems," *J. Math. Anal. Appl.*, 2006.

[56] R. Kamalapurkar, J. A. Rosenfeld, A. Parikh, A. R. Teel, and W. E. Dixon, "Invariance-like results for nonautonomous switched systems," *IEEE Trans. Autom. Control*, vol. 64, no. 2, pp. 614–627, Feb. 2019.

[57] F. Clarke, *Optimization and Nonsmooth Analysis*. Reading, MA: Addison-Wesley, 1983.

[58] T. C. Project, *CGAL User and Reference Manual*. CGAL Editorial Board, 2013.

[59] M.-S. K. Gill Barequet, Gershon Elber, "Computing the minimum enclosing circle of a set of planar curves," *Comput. Des. Appl.*, 2005.

[60] G. B. Ramanathan Muthuganapathy, Gershon Elber and M.-S. Kim, "Computing the minimum enclosing sphere of free-form hypersurfaces in arbitrary dimensions," *Comput. Des.*, 2011.

[61] E. Welzl, *Smallest enclosing disks (balls and ellipsoids)*, H. Maurer, Ed. Springer Berlin Heidelberg, 1991.

[62] T. Cormen, *Introduction to algorithms*. The MIT press, 2001.

[63] P. Casau, R. G. Sanfelice, and C. Silvestre, "On the robustness of nominally well-posed event-triggered controllers," *IEEE Control Syst. Lett.*, vol. 6, pp. 415–420, 2022.

[64] V. Isler and R. Bajcsy, "The sensor selection problem for bounded uncertainty sensing models," in *Int. Symp. Inf. Process. Sens. Netw.*, 2005, pp. 151–158.

[65] P. Kidger and T. Lyons, "Universal approximation with deep narrow networks," in *Conf. Learn. Theory*, 2020, pp. 2306–2327.

[66] O. Patil, D. Le, M. Greene, and W. E. Dixon, "Lyapunov-derived control and adaptive update laws for inner and outer layer weights of a deep neural network," *IEEE Control Syst Lett.*, vol. 6, pp. 1855–1860, 2022.

[67] O. S. Patil, D. M. Le, E. Griffis, and W. E. Dixon, "Deep residual neural network (ResNet)-based adaptive control: A Lyapunov-based approach," in *Proc. IEEE Conf. Decis. Control*, 2022.

[68] E. Griffis, O. Patil, Z. Bell, and W. E. Dixon, "Lyapunov-based long short-term memory (Lb-LSTM) neural network-based control," *IEEE Control Syst. Lett.*, vol. 7, pp. 2976–2981, 2023.

[69] R. Hart, E. Griffis, O. Patil, and W. E. Dixon, "Lyapunov-based physics-informed long short-term memory (LSTM) neural network-based adaptive control," *IEEE Control Syst. Lett.*, vol. 8, pp. 13–18, 2024.

[70] S. Akbari, E. J. Griffis, O. S. Patil, and W. E. Dixon, "Lyapunov-based dropout deep neural network (lb-ddnn) controller," *arXiv preprint arXiv:2310.19938*, 2023.

[71] J. P. Aubin and H. Frankowska, *Set-valued analysis*. Birkhäuser, 2008.

[72] A. F. Filippov, "Differential equations with discontinuous right-hand side," in *Fifteen papers on differential equations*, ser. American Mathematical Society Translations - Series 2. American Mathematical Society, 1964, vol. 42, pp. 199–231.

[73] H. Schaub and J. Junkins, *Analytical Mechanics of Space Systems*, AIAA, Ed. New York: AIAA Education Series, 2003.

[74] F. L. Lewis, R. Selmic, and J. Campos, *Neuro-Fuzzy Control of Industrial Systems with Actuator Nonlinearities*. Philadelphia, PA, USA: Society for Industrial and Applied Mathematics, 2002.

[75] H. T. Dinh, R. Kamalapurkar, S. Bhasin, and W. E. Dixon, "Dynamic neural network-based robust observers for uncertain nonlinear systems," *Neural Netw.*, vol. 60, pp. 44–52, Dec. 2014.

[76] B. Xian, M. S. de Queiroz, D. M. Dawson, and M. McIntyre, "A discontinuous output feedback controller and velocity observer for nonlinear mechanical systems," *Automatica*, vol. 40, no. 4, pp. 695–700, 2004.

[77] M. Krstic, I. Kanellakopoulos, and P. V. Kokotovic, *Nonlinear and Adaptive Control Design*. New York: John Wiley & Sons, 1995.

[78] O. Patil, A. Isaly, B. Xian, and W. E. Dixon, "Exponential stability with RISE controllers," *IEEE Control Syst. Lett.*, vol. 6, pp. 1592–1597, 2022.

[79] F. H. Clarke, *Optimization and nonsmooth analysis*. SIAM, 1990.

[80] B. E. Paden and S. S. Sastry, "A calculus for computing Filippov's differential inclusion with application to the variable structure control of robot manipulators," *IEEE Trans. Circuits Syst.*, vol. 34, no. 1, pp. 73–82, Jan. 1987.

[81] N. Fischer, R. Kamalapurkar, and W. E. Dixon, "LaSalle-Yoshizawa corollaries for nonsmooth systems," *IEEE Trans. Autom. Control*, vol. 58, no. 9, pp. 2333–2338, Sep. 2013.

[82] A. D. Ames, S. Coogan, M. Egerstedt, G. Notomista, K. Sreenath, and P. Tabuada, "Control barrier functions: Theory and applications," in *Proc. Eur. Control Conf.* IEEE, 2019, pp. 3420–3431.

[83] A. Isaly, “Safe control design for uncertain nonlinear systems using multiple control barrier functions,” Ph.D. dissertation, University of Florida, 2023.

[84] M. Marley, R. Skjetne, and A. R. Teel, “Hybrid control barrier functions for continuous-time systems,” *Trans. Autom. Control*, 2024.

[85] P. Glotfelter, J. Cortés, and M. Egerstedt, “Nonsmooth barrier functions with applications to multi-robot systems,” *IEEE Control Syst. Lett.*, vol. 1, no. 2, pp. 310–315, 2017.

[86] J. Knaup, K. Okamoto, and P. Tsiotras, “Safe high-performance autonomous off-road driving using covariance steering stochastic model predictive control,” *IEEE Trans. Control Sys. Technol.*, 2023.

[87] J. Pilipovsky and P. Tsiotras, “Data-driven covariance steering control design,” in *2023 62nd IEEE Conf Decis. Control*, 2023, pp. 2610–2615.

[88] F. Liu and P. Tsiotras, “Optimal covariance steering for continuous-time linear stochastic systems with martingale additive noise.”

[89] Wikipedia contributors, “Standard deviation — Wikipedia, the free encyclopedia,” [Online; accessed 11-March-2024]. [Online]. Available: https://en.wikipedia.org/wiki/Standard_deviation

[90] P. Masters and S. Sardina, “Deceptive path-planning.” in *IJCAI*, 2017, pp. 4368–4375.

[91] C. Dwork, “Differential privacy,” in *Int. colloq, autom., lang., progr.*, 2006, pp. 1–12.

BIOGRAPHICAL SKETCH

Sage Christian Edwards was born in 1996, in Youngstown Ohio. He received his bachelor's degrees in mechanical engineering and physics in the Spring of 2019 from Youngstown University, Youngstown OH. In 2019, Sage joined the Nonlinear Controls and Robotics (NCR) group under the guidance of Dr. Warren E. Dixon to pursue his doctoral studies. During this time he developed theoretical frameworks for path planning, estimation, and control in the presence of intermittent state feedback, deploying Lyapunov and topological-based techniques. He was also awarded the SMART fellowship where he will continue his research at his sponsoring facility within the Air Force.